

Geophysics and Ore Deposits

by

Stanley H. Ward**

Gerald W. Hohmann**

William E. Glenn+

William R. Sill**

Phillip M. Wright**

*Department of Geology and Geophysics, University of Utah

+Earth Science Laboratory, University of Utah Research Institute

TABLE OF CONTENTS

SECTION 1 - INTRODUCTION

SECTION 2 - ELECTRICAL METHODS

Introduction

- Basic principles
- Electrical properties of rocks
- Applications
- Interpretation

Resistivity and Induced Polarization Methods

- Basic principles
- In-situ measurements and rock models
- Problems

- Overburden masking:
- Electromagnetic coupling:
- Natural fields:
- Geologic noise:
- Culture:
- Topography:

Interpretation

- Models:
- Electric field patterns in the earth:
- Prism responses:

Applications

- Deep sulfide mineralization:
- Low resistivity cover:

Electromagnetic Methods

Introduction

- Induction and current gathering
- Separating the elements in the geoelectric section
- Depth of exploration
- Time and frequency domains

Interpretation

- Introduction:
- Thin sheet and ribbon models:
- Sphere models:
- TEM modeling:
- Two and three dimensional modeling:

Field configurations, natural field methods

- Introduction:
- The magnetotelluric method:
- AFMAG:
- VLF:

Field configurations, controlled source, ground methods

- Introduction:
- Two loop, roving coil pairs, fixed-orientation:
- Two loop, roving coil pairs, rotatable orientation:

- Large loop source:
- Single loop:
- CSAMT:
- Field configurations, controlled source, airborne
 - Introduction:
 - Rigid boom systems:
 - Towed bird systems:
 - Semi-airborne system:
 - Unicoil:
- Sources of noise in electromagnetic surveys
- Applications
 - Airborne electromagnetics in areas of conductive overburden:
 - Ground electromagnetics in deeply-weathered areas:
 - Detecting a sulfide body by current channeling:
 - Detecting ore adjacent to disseminated sulfides in conductive terrain:
 - Airborne detection of conductors beneath deep resistive cover:
 - Uses of airborne electromagnetic systems:
- Basis for selecting a particular electromagnetic system
 - Ground systems, transmitting loop size:
 - Ground systems, domain of acquisition:
 - Ground systems, decades of spectrum:
 - Ground systems, signal-to-noise ratio:
 - Ground systems, lateral resolution:
 - Ground systems, coil configurations:
 - Airborne systems, transmitting coil size:
 - Airborne systems, domain of acquisition and decades of spectrum:
 - Airborne systems, signal-to-noise ratio:
 - Airborne systems, lateral resolution, swath width, and depth of exploration:
 - Airborne systems, coil configurations:
- Self Potential Method
 - Principles
 - Instrumentation and Measurements
 - Problems
 - Applications
 - Interpretation
- References
- Figure Captions
- List of Tables

SECTION 3 - GRAVITY AND MAGNETIC METHODS

- Introduction
- Principles of Gravity Method
 - Instrumentation
 - Surveying and Data Reduction
 - Applications
- Principles of the Magnetic Method
 - Instrumentation
 - Surveying and Data Reduction

- Applications
- Gravity and Magnetic Interpretation
- References
- Figure Captions
- List of Tables

SECTION 4 - GAMMA-RAY SPECTROMETRY

- Introduction
- Natural Radioactive Decay Processes
 - Elementary Particles
 - Energies of α , β , and γ
 - The decay equation
- The Gamma-ray Spectrum
- Equilibrium and Disequilibrium
- Scattering and Absorption of Gamma-rays
 - Scattering
 - Absorption
- Gamma-ray Detector Systems
 - Introduction
 - Principles of Scintillation
 - Selection and Design of NaI(Tl) Crystals and PMT Detectors
 - Stability of NaI(Tl) Crystals and PMT Detectors
 - Volume of crystal
- Operational Considerations
 - Background
 - Meteorological effects
 - Atmospheric Bismuth 214:
 - Rainfall:
- Calibration of Gamma-ray Spectrometers
 - Introduction
 - Ground level calibration of airborne and ground systems
 - Compton stripping:
 - Airborne level calibration of airborne systems
 - Introduction:
 - Effects of temperature and pressure:
 - Correction of spectral stripping coefficients for aircraft altitude:
 - Sequence of corrections, airborne surveys
- Statistical errors in count rates
- Fields of view of airborne gamma-ray detectors
 - Introduction
 - The effect of topography
 - Deposit detection
 - Hand specimens
- The Effect of Overburden
- Applications
 - Geological mapping
 - Deposit detection
- References
- Figure Captions

List of Tables

SECTION 5 - WELL LOGGING AND BOREHOLE GEOPHYSICS

- Introduction
- Caliper and Temperature Logging
- Electrical Logging
 - Introduction
 - Spontaneous polarization
 - Resistivity/IP logging
 - Electromagnetic logging
- Radioactivity Logging
 - Introduction
 - Passive radioactive methods
 - Active radioactive methods
 - Gamma-ray density logging:
 - Gamma-ray assaying:
 - Neutron density logging:
 - Neutron assaying:
- Acoustic Logging
- Gravity Logging
- Magnetic Logging
- Cross Plots
- The Outlook for Borehole Assaying
- References
- Figure Captions
- List of Tables

SECTION 6 - SEISMIC METHODS

- Introduction
- Principles
- The Seismic Reflection Method
- The Seismic Refraction Method
- Problems in Mineral Application
- Applications
- References
- Figure Captions
- List of Tables

ABSTRACT

The principles, practice, applications, and limitations of the resistivity, induced polarization, electromagnetic, self-potential, gravity, magnetic, gamma-ray spectrometric, well logging, borehole geophysics, and seismic exploration methods are reviewed in relation to the search for ore deposits.

The resistivity, induced polarization, and electromagnetic methods are each benefitting from increased bandwidth, higher signal-to-noise ratio achievable with in-field digital processing, improved transmitter-receiver geometries, and improved methods of interpretation obtained mostly by expensive and sophisticated numerical modeling. The self-potential method has benefitted from improved electrode preparation coupled with improved understanding of the principles underlying the method. The gravity and magnetic methods have benefitted mostly from higher instrumental sensitivity but also from improved methods of numerical modeling.

The full spectrum, fully-calibrated, approach to gamma-ray spectrometry has led to capabilities for airborne geological mapping and airborne equivalent chemical assaying for uranium and thorium to an accuracy of order 1 ppm and for potassium to an accuracy of order 1 percent.

Borehole logging via passive and active radioactive methods permits down-hole chemical assaying without sample retrieval. Electrical, magnetic, porosity, and density logging is proving extremely useful in downhole lithologic and ore deposit identification. The use of borehole

geophysics can expand the useful radius of a borehole to 100 m or more.

High resolution seismic methods, only just entering ore deposits search, are capable of mapping ore horizons, faults, and structure.

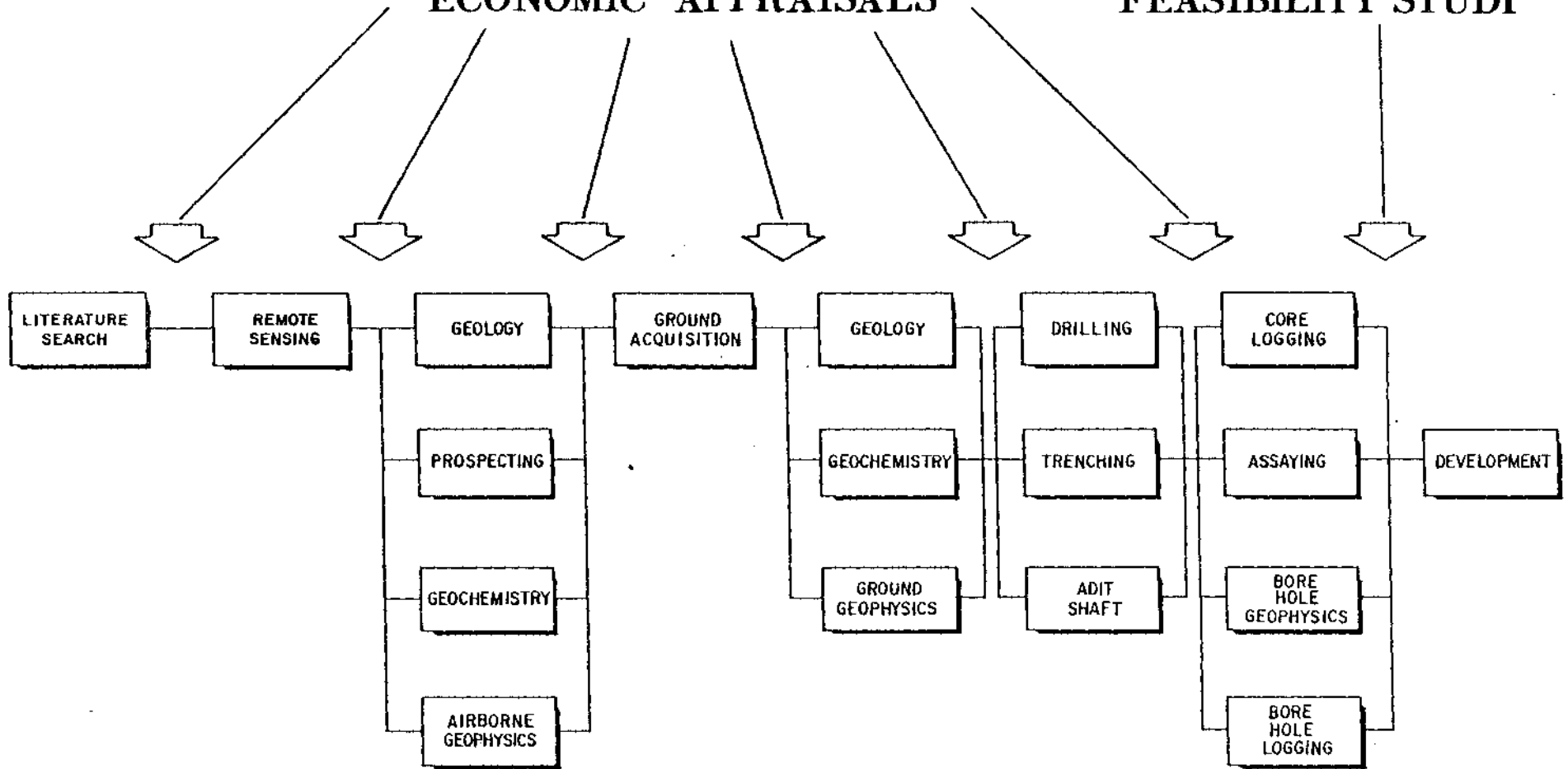
SECTION 1 - INTRODUCTION

"For any new development in geophysical methodology to impact an exploration system, it must be made within a framework of improving efficiency or cost-effectiveness of that system" (Ward, 1972). An exploration *system* is a rational integration of the various geological, geochemical, geophysical, econometric, and pilot plant mining and metallurgical activities which culminate in a feasibility study which triggers a decision to drop or to develop the prospect. Figure 1-1 is a schematic presentation of a generalized exploration sequence or *exploration architecture*. Usually, the least expensive methodologies are used first, and the most expensive methodologies used last in the exploration architecture. At any given time, the ability of a particular geological, geochemical, or geophysical methodology to provide information in a cost-effective manner will dictate its inclusion in, or exclusion from, the architecture suited to a particular exploration problem. Usually, but not always, specific architecture is designed to find a particular ore generic type, but the architecture must also take into account physiographic, weathering, logistical, political, legal, economical, and other factors.

In ore deposits exploration in Australia, the great depth of weathering is of paramount importance in developing exploration architecture almost regardless of generic metallic mineral type; iron ore is an exception. In exploration for uranium either in the Athabasca basin in Canada or in the Pine Creek Geosyncline in Australia, a great depth of inert overlying sandstone dictates the approach used to exploration architecture. As exploration for ore deposits trends toward deeper and/or

ECONOMIC APPRAISALS

FEASIBILITY STUDY



lower grade targets, sophistication in exploration methodology becomes necessary. Thus, today, one finds micro-computers in the field for data acquisition, processing, and first-cut interpretation for most geophysical methodologies.

Despite the sophistication of geophysical methods used in today's search for ore deposits, many problems face the practitioners of these methods. In the ensuing pages we have attempted to describe the geophysical methods currently used in the search for ore deposits, to identify problems currently encountered in use of them, to indicate via case histories the nature of these problems, to indicate current state-of-the art means of attacking these problems, and finally, to forecast the future direction of solutions to these problems. Throughout the following discourse, the authors have directed their comments to those most often responsible for exploration decisions, the economic geologists.

At the December, 1976 NSF workshop on "Geophysics Applied to Detection and Delineation of Non-energy Non-renewable Resources" (Ward et al., 1977), the participants concluded that seven research items warranted highest priorities:

- 1) establish several geoscience test sites where research can be carried out and where new equipment may be evaluated,
- 2) expand research on modeling of resistivity, induced polarization, and electromagnetic methods,
- 3) expand development of broadband induced polarization and electromagnetic methods,
- 4) expand development of nuclear borehole technology,
- 5) investigate applications of high-resolution seismic methods in

mining exploration and exploitation,

- 6) investigate a systems approach to application of multiple borehole methods in mining exploration, and
- 7) disseminate more a) case histories, b) translations of pertinent foreign literature, and c) computer programs relating to forward and inverse algorithms especially for electrical methods.

The authors of the present article can find no reason to differ with these research priorities; the number of pages herein devoted to each of the methods more or less reflects them.

References:

Ward, S. H., 1972, Mining geophysics - new techniques and concepts,

Mining Congress Journal, v. 58, p. 58-68.

Ward, S. H.; Campbell, R. E., Corbett, J. D., Hohmann, G. W., Moss, C. K.,
and Wright, P. M., 1977, The frontiers of mining geophysics,

Geophysics, v. 42(4), p. 878-886.

SECTION 2 -ELECTRICAL METHODS

Introduction

Basic principles

All electrical geophysical methods involve the measurement of an impedance, with subsequent interpretation in terms of the subsurface electrical properties and, in turn, the subsurface geology. Basically an impedance is the ratio of the response or anomaly (output) to the excitation (input). In resistivity and induced polarization (IP) the input is a current injected into the ground between two electrodes, while the output is a voltage measured between two other electrodes. In electromagnetics (EM) the input might be a current through a coil of wire and the output is the voltage induced in another coil of wire.

In *frequency domain* impedance measurements, the input current is a sine wave at a particular frequency. The output also is a sine wave, as shown in Figure 2-1; its amplitude (A) and phase (ϕ) depend upon the earth. The frequency (f) of the sine wave is the inverse of the period (T). In general, the output is delayed by $\phi \times T/2\pi$ seconds. Often it is convenient to decompose the output wave into *in-phase* (real) and *quadrature* (imaginary) components, as shown in Figure 2-1. If we denote their peak amplitudes as R and I, respectively, then the amplitude and phase of the output waveform are given by

$$A = \sqrt{R^2 + I^2}, \quad 2-1$$

and

$$\phi = \text{Arctan} (I/R). \quad 2-2$$

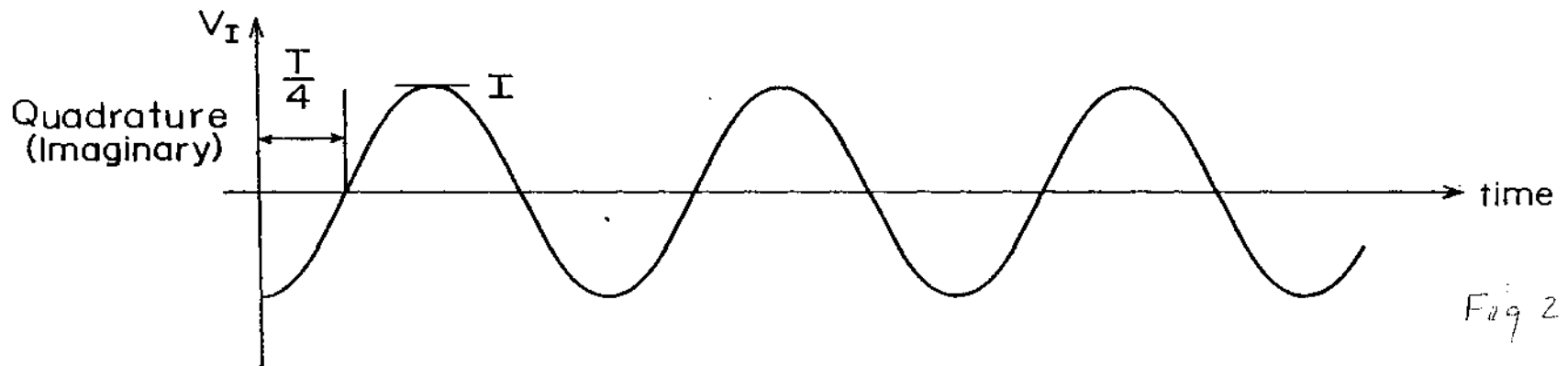
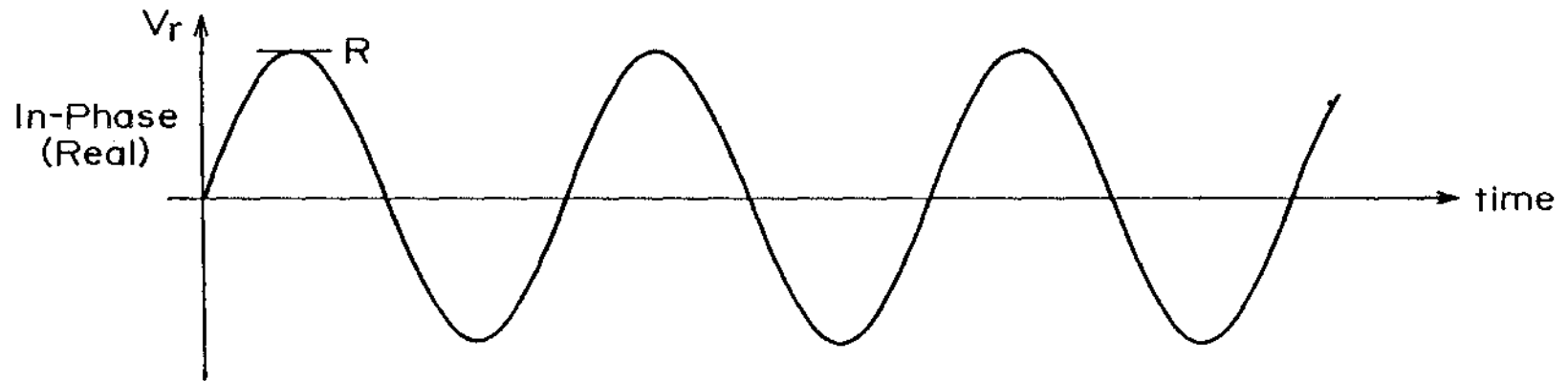
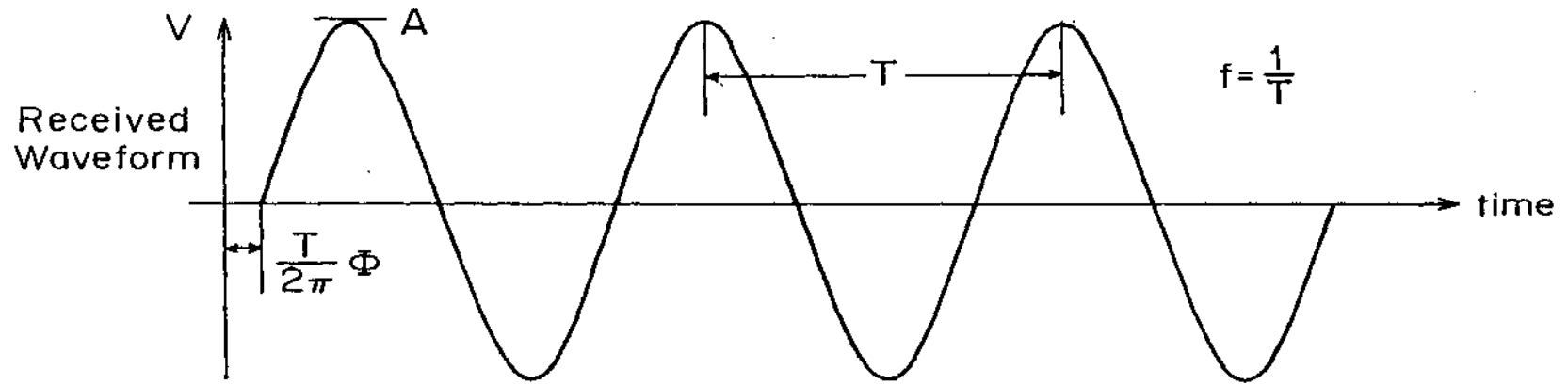
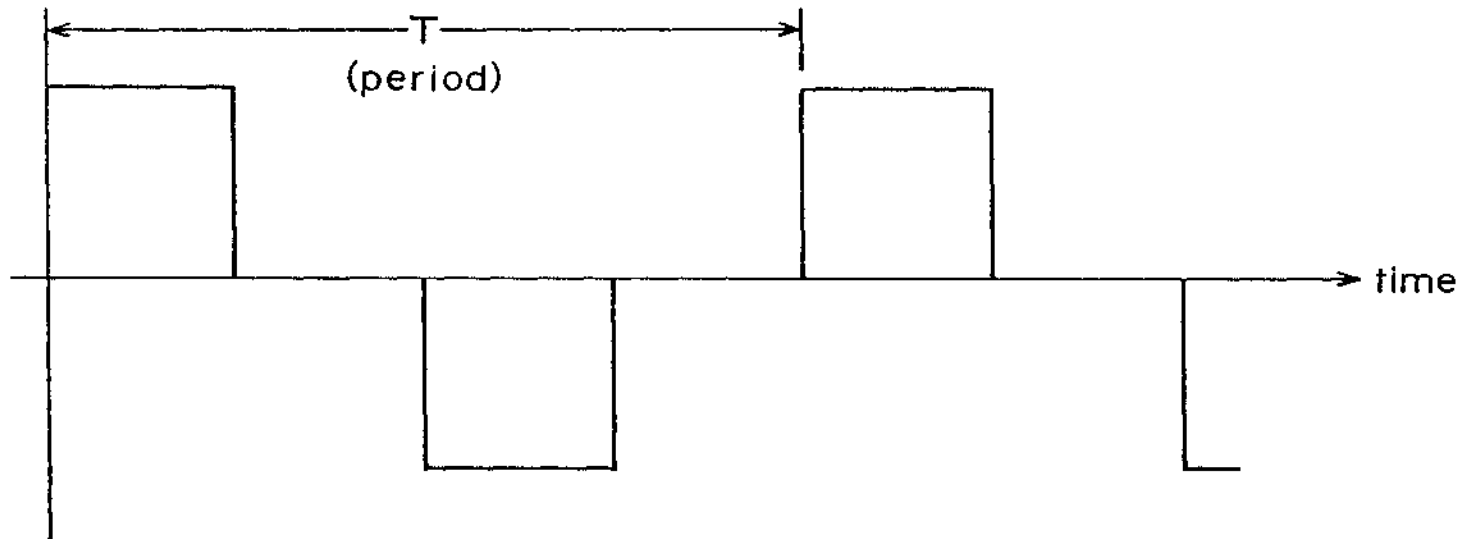


Fig 2-1

TRANSMITTER CURRENT



RECEIVED SIGNAL

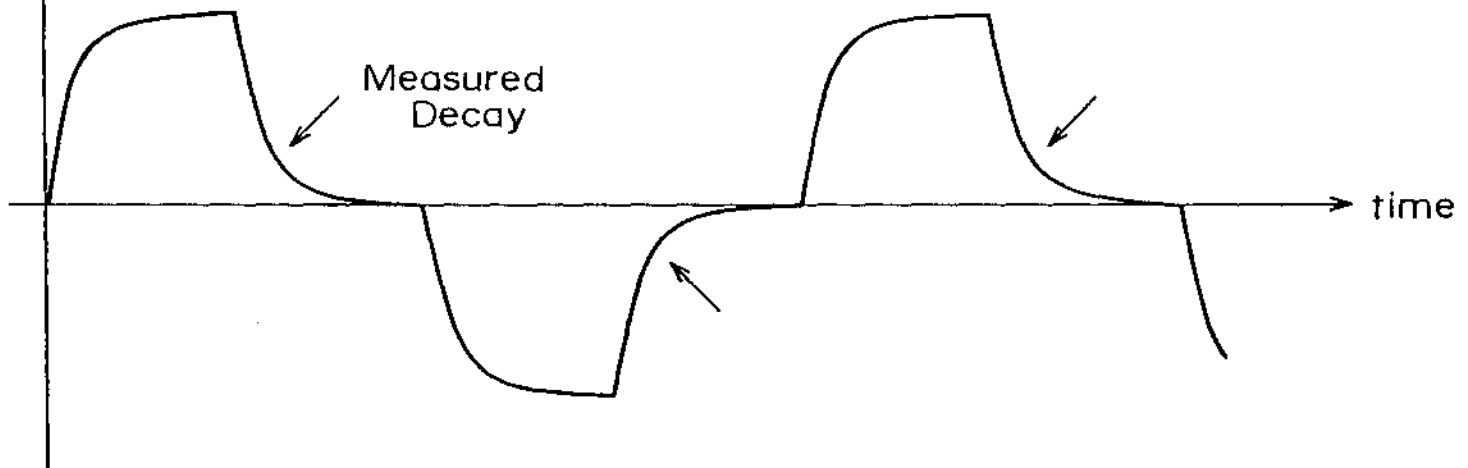


Fig 2-2

Impedance also can be measured in the *time domain*, in which case the current is periodically turned on and off. As shown in Figure 2-2, the output is the voltage measured at various times when the transmitter current is off. Note that the input again is periodic, because measurements must be made for several periods and added together to eliminate noise. Time and frequency domain measurements are directly related through the Fourier transform, and in that sense, are equivalent. However, in practice, each system has advantages and disadvantages, which will be elucidated later.

There are three basic modes of operation for any electrical method: (1) sounding, (2) profiling, and (3) sounding-profiling. In sounding, the transmitter-receiver separation is changed, or the frequency is changed, and the results are interpreted in terms of a layered earth. Because the earth usually is not layered in mineral prospecting, sounding has little application. In profiling, the transmitter or receiver, or both, are moved along the earth to detect anomalies. The most useful method is a combination of sounding and profiling, which delineates structures with both lateral and vertical variations.

Electrical methods have become more useful in recent years through advances in both interpretation and instrumentation. Modern field instruments are based on micro-computers. Processing the signals digitally greatly increases the accuracy and, in fact, makes possible new types of measurements. Further, data reduction in the field results in more reliable results and more cost-effective surveys. While the state-of-the-art of digital instrumentation is an interesting and important topic, because of the interests of readers of this journal, we will concentrate on applications and on recent advances in interpretation.

Electrical properties of rocks

Crustal rocks conduct electricity primarily via the movement of ions through pore water, although semiconduction in minerals such as sulfides and graphite sometimes contributes significantly. Semiconduction in silicate minerals becomes important in the mantle due to the increased temperature and partial melting.

An electrical current, I , is a flow of charge, measured by the rate at which charge passes through a surface. The current density, \vec{J} , is a vector having the direction of the flow of positive charge, and magnitude equal to the current per unit area through a surface normal to the current flow.

Ohm's law,

$$\vec{J} = \sigma \vec{E}, \quad (2-3)$$

relates the current density \vec{J} and electric field \vec{E} through the conductivity σ which, basically, is a measure of the ability of rock to conduct electricity. Assuming the current is conducted by N different ionic species, the conductivity of water in the pore of a rock is given by

$$\sigma_w = \sum_{i=1}^N n_i q_i \mu_i, \quad (2-4)$$

where n_i is the density of ion species i , q_i its charge, and μ_i its mobility. The relation between the pore water conductivity (σ_w) and the rock conductivity (σ_r) is given by Archie's Law,

$$\sigma_r = \sigma_w \phi^m, \quad (2-5)$$

where ϕ is the fractional porosity and m is between 1.5 and 2.5. Ionic conduction in rocks increases with increasing porosity, increasing salinity, or increasing amounts of minerals exhibiting cation exchange. Higher temperature increases ionic mobility up to a certain point, and

hence increases conductivity.

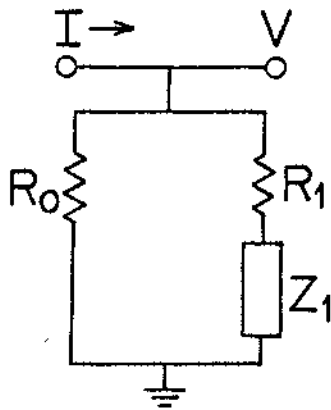
Electrical methods are important in mineral exploration because measurements are directly affected by the high conductivity of concentrations of semiconducting sulfide minerals.

Resistivity, ρ , is the reciprocal of conductivity, σ ; it provides a measure of resistance to current flow. In the MKS system, the unit of ρ is ohm-meter ($\Omega\text{-m}$), while the unit of σ is mho/meter (U/m).

Induced polarization in rocks is due to the accumulation of charge and the generation of diffusion gradients (1) where ionic conduction in pore water changes to semi conduction in metallic minerals, and (2) where exchange cations, excess positive ions often from clays, alter the relative currents carried by the positive and negative ions. The former is called interfacial or electrode polarization, and the latter is called membrane polarization.

A simple equivalent circuit for a small portion of a rock with these effects is given in Figure 2-3. Although useful, the following interpretation should not be taken too literally: R_0 represents the resistivity of pores in the rock not involved with polarizable materials, R_1 represents pores leading to polarizable zones, and Z_1 represents the complex and frequency-dependent impedance of the polarizable zones. For simple charge separation effects the polarization would be capacitive ($Z_1 = 1/i\omega C$), and for simple diffusion effects the impedance is given by a Warburg element ($Z_1 = A/\sqrt{i\omega}$). In most rocks the polarizable zones can be represented by $Z_1 = (i\omega X)^{-c}$, with c in the range .2 to .6. The resistivity of a rock is also frequency dependent and complex and is represented by either its real and imaginary parts or more commonly by its amplitude and

EQUIVALENT CIRCUIT AND RESPONSE FOR IP EFFECTS IN ROCKS



$$Z(\omega) = \frac{V}{I} = \frac{R_0}{1 + R_0/(R_1 + Z_1)}, \quad Z_1 = (i\omega\chi)^{-c}$$

$$= R_\infty + \frac{\Delta R}{1 + (i\omega\tau)^c}$$

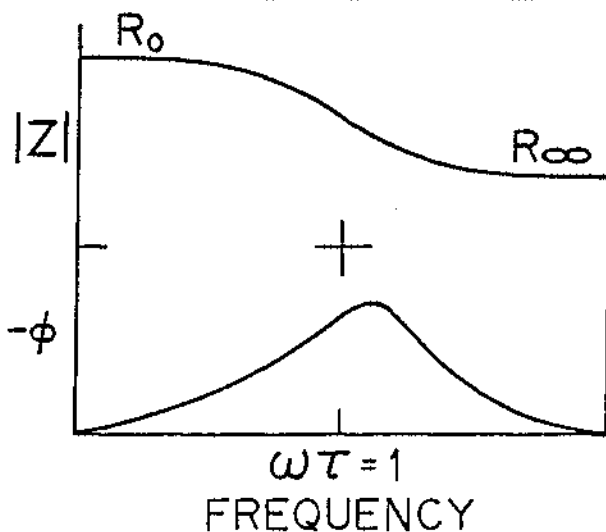
$$i = \sqrt{-1}$$

= 90° Phase Rotation

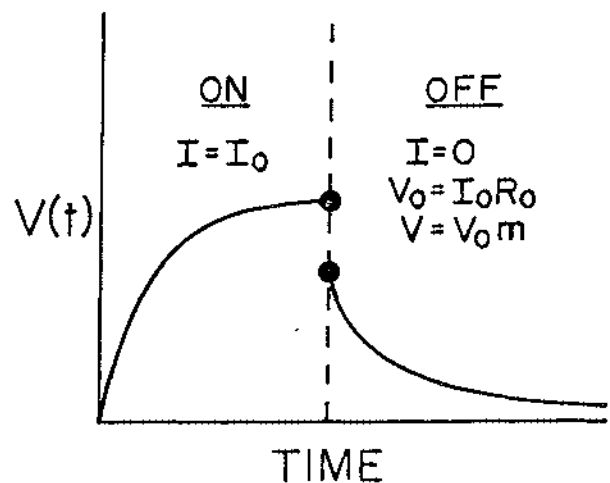
$$R_\infty = \frac{R_0 R_1}{R_0 + R_1}, \quad \Delta R = R_0 - R_\infty$$

$$m = \frac{\Delta R}{R_0} \quad \tau = \chi (R_0 + R_1)^{1/c} \quad Z^2 = Z_r^2 + Z_i^2 \quad \tan\phi = Z_i/Z_r$$

FREQUENCY RESPONSE



TIME RESPONSE



phase. Under these conditions, current flow in a rock will generate voltage components in quadrature with the current.

Applications

The introduction of IP in the late 1950's represented a major advance in mining geophysics. For the first time it was possible to detect *disseminated* sulfides directly, in concentrations less than 5 or 6 percent by weight. Such low percentages of sulfides do not appreciably alter the resistivity, in view of the large variation in resistivity due to porosity and salinity changes, but they do produce the induced polarization phenomenon.

EM methods respond only to large changes in resistivity. Hence their primary domain is the detection of *massive* sulfides, which are highly conductive, at least when they have been metamorphosed and the sulfides remobilized and interconnected as in Precambrian rocks. Because grounded electrodes are not required, EM surveys generally are less expensive than IP surveys. Furthermore, they can be carried out from the air. Many massive sulfide ore bodies have been found by airborne EM since its introduction in the early 1950's.

Interpretation

Interpretation of data is accomplished by estimating the parameters of simplified *models* of the earth. The earth is far too complex for its electrical response to be evaluated exactly, but the simplified model, if it is close enough to reality, achieves the economic goal of identifying a target for drilling.

The three basic types of simple interpretation models are illustrated

in Figure 2-4: one dimensional (1D-layered); two dimensional (2D-body infinitely long in one direction); and three dimensional (3D). Resistivity is denoted by ρ and IP response by ϕ . Models can be made more complex by including more layers in the 1D case and more bodies in the 2D and 3D cases. Solutions for layered models have been available for many years; they are *analytic*, consisting of integrals or summations. Evaluating the response of a 2D or 3D model is much more difficult, requiring sophisticated mathematics. Such solutions have become possible only in the last ten years, with the availability of large computers. Solutions are achieved by approximating the relevant differential or integral equation.

There are four basic methods of interpreting data:

- intuition,
- comparison with simple numerical or scale models,
- trial-and-error data fitting with complex numerical models, and
- inversion.

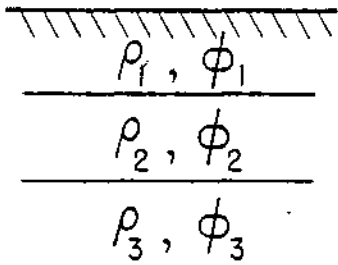
Rudimentary interpretation by intuition is not sufficient for the subtle signatures of the ore deposits that remain to be found. Catalogs of simple numerical models are essential for proper survey design, for rough field interpretations, and for insight into more sophisticated interpretation schemes. Trial and error data fitting with complex models is very useful, but those who have used it for 2D and 3D structures recognize the following difficulties:

- many options in selecting the initial model,
- many time-consuming iterations,
- many options in selecting the next model, and
- no generation of a range of acceptable models.

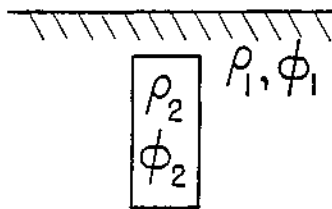
Inversion, i.e., programming a computer to calculate a model based on the data, has significantly enhanced the science of interpretation. It is doubtful, however, that strictly automated inversion can be applied to complete earths because of non-uniqueness, geological noise, and the large computer time involved. Furthermore, good initial estimates of model parameters are crucial for the success of inversion, but they are difficult to obtain for complex geology. Probably some combination of trial-and-error fitting and inversion, call it interactive inversion, is optimum.

INTERPRETATION MODELS

1D



2D



3D

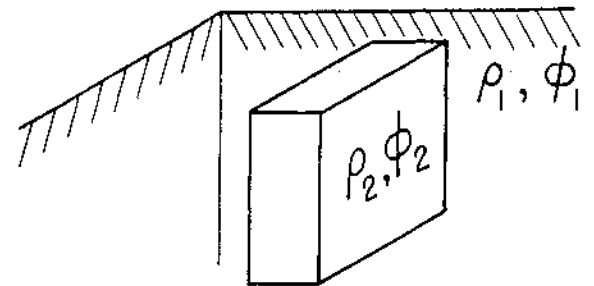


Fig 2-4

Resistivity and Induced Polarization Methods

Basic principles

The resistivity and induced polarization methods are based on the response of earth materials to the flow of current at low frequencies. Strictly speaking the resistivity method is based on *potential theory* which requires direct current, i.e. zero frequency, but noise and measurement problems quickly lead to the use of low frequency alternating currents. The induced polarization method on the other hand requires the use of alternating current, because it is based on changes in resistivity as a function of frequency. As the frequency increases to some critical frequency f_c , determined by the resistivity (ρ) of the materials and the scale size L of the measurement, electromagnetic coupling between transmitting and receiving circuits violates potential theory so that *electromagnetic theory* is required.

For low frequencies where potential theory is applicable the voltage (V) produced by a point source of current (I) on a homogeneous half-space of resistivity ρ is

$$V = \frac{\rho I}{2\pi r}, \quad (2-6)$$

where r is the distance from the point current source. For a given voltage and current measurement, (2-6) can be solved for the resistivity. In actual practice, current is introduced through a pair of electrodes, and the voltage difference (ΔV) is measured between another pair. For a homogeneous earth the resistivity is given by

$$\rho = K \frac{\Delta V}{I}, \quad (2-7)$$

where K is a geometric factor, which depends on the electrode configuration. The geometric factors for a number of common electrode arrangements are given in Figure 2-5. When the ground is not homogeneous, the voltage and current data are reduced in the same fashion using (2-7), but the resistivity is called the apparent resistivity ρ_a . It is the resistivity a homogeneous earth would have to produce the same measurement.

When polarizable materials are present, the voltage will have a component in quadrature with the transmitter current. The apparent resistivity is then complex and can be represented by its real, or in phase, and imaginary, or quadrature, components or by its magnitude and phase angle.

The parameters measured depend on whether the system makes use of a time domain or frequency domain current wave form (Figures 2-1 and 2-2). The time domain response can be understood with reference to Figure 2-3. During the on cycle the impedance Z_1 will store charge (for simplicity, it may be thought of as a capacitor), and the voltage will saturate at $V_0 = IR_0$ given enough time. When the current is turned off, the voltage will drop to $V_0 R_0 / (R_0 + R_1)$ and then decay exponentially with a time constant $(R_1 + R_0)C_1$. The maximum value of the voltage during the on cycle, along with the current, can be used to calculate the apparent resistivity. The transient during the off cycle contains the basic time domain IP information. This transient is specified by its normalized value just after the current is turned off ($m = R_0 / (R_0 + R_1)$) and by the form and rate of decay. For frequency domain measurements the basic data are the magnitude and phase angle of the resistivity, as functions of frequency.

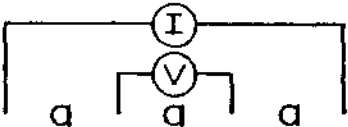
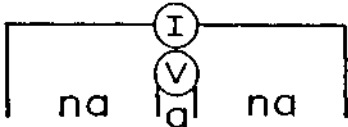


<u>ARRAY</u>	<u>GEOMETRY</u>	<u>K</u>	<u>DISPLAY</u>	<u>USE</u>
WENNER		$2\pi a$	$\rho_a \text{ vs } a$	SOUNDING
SCHLUMBERGER		$\pi n(n+1)a$	$\rho_a \text{ vs } (n+1/2)a$	SOUNDING
POLE-DIPOLE		$2\pi n(n+1)a$	$\rho_a \text{ vs } n$	SOUNDING- PROFILING
DIPOLE-DIPOLE		$\pi n(n+1)(n+2)a$	$\rho_a \text{ vs } n$	SOUNDING- PROFILING

Fig 2.5

Older analogue time domain receivers integrate one or several intervals under the decay curve, at sampling times ranging from around 0.05 sec. to 2.0 sec after current shut-off. When the integrated voltage is normalized by the primary voltage (V_0) and the integration time (Δt), the unit of the measurement is given as mV/V and is called the chargeability (M). As the integration time becomes short and as the sampling time approaches the current shut-off time, $M \times 10^{-3}$ approaches m as defined for the equivalent circuit of Figure 2-3. Another definition of chargeability, the Newmont Standard, does not normalize by the integration time; the units are (mV-sec)/V or m-sec. Since the equivalent integration time of the Newmont Standard is one sec, normalization by the integration time does not change the numerical value of the chargeability.

Analogue frequency domain receivers often use two to five frequencies, and many have no current waveform reference, so that phase information is lost. The basic data are then the magnitudes of the apparent resistivity, ρ_1 and ρ_2 at two frequencies, f_1 and f_2 , which can be used to calculate percent frequency effect (PFE):

$$PFE = 100 \frac{\rho_1 - \rho_2}{\rho_1} \quad (2-8)$$

In this expression, ρ_1 is the resistivity at the lower frequency. Modern digital receivers sample the waveform at discrete points in time, and store the samples as numbers in the computer memory. Manipulation of the data stored in memory is under program control, and in principle either time or frequency domain processing can be done. To increase the ratio of signal to noise, multiple cycles are stored and averaged, or stacked, in the memory. Phase information is obtained by using a pair of very accurate, synchronized oscillators at the receiver and

transmitter or by using a cable link between the receiver and transmitter.

A simple relation between time and frequency domain parameters is provided through the model of Figure 2-3, where

$$10^{-3}M_{zm} = \frac{R_0}{R_0 + R_1} = \frac{R_0 - R_\infty}{R_0} \approx \frac{\text{PFE}}{100}.$$

Because M is hardly ever measured a) over a sufficiently short interval and b) at times close enough to the switching instant, and because the measured PFE hardly ever span the whole range of the change in resistivity, the above relations are only conceptually useful. For the Newmont Standard of chargeability, practical relations between time domain and frequency domain units are

$$M \approx 6.8 \text{ PFE/Decade}, \quad (2-9)$$

and

$$M \approx -\phi (\text{mrad}).$$

Relations between phase and PFE can be derived, under certain assumptions, through the Hilbert transform relations, giving

$$\phi (\text{mrad}) \approx 6.8(\text{PFE/Decade}) . \quad (2-10)$$

In-situ measurements and rock models

Pelton et al. (1978) present in-situ data from a number of different types of mineralization. Typical phase spectra from porphyry copper, massive sulfide, and graphite deposits are shown in Figure 2-6. These curves are chosen to illustrate the ranges in magnitudes and forms of the curves obtained. Pelton et al. found that the spectra could be fitted with a Cole-Cole dispersion model, which is the same type of dispersion as that

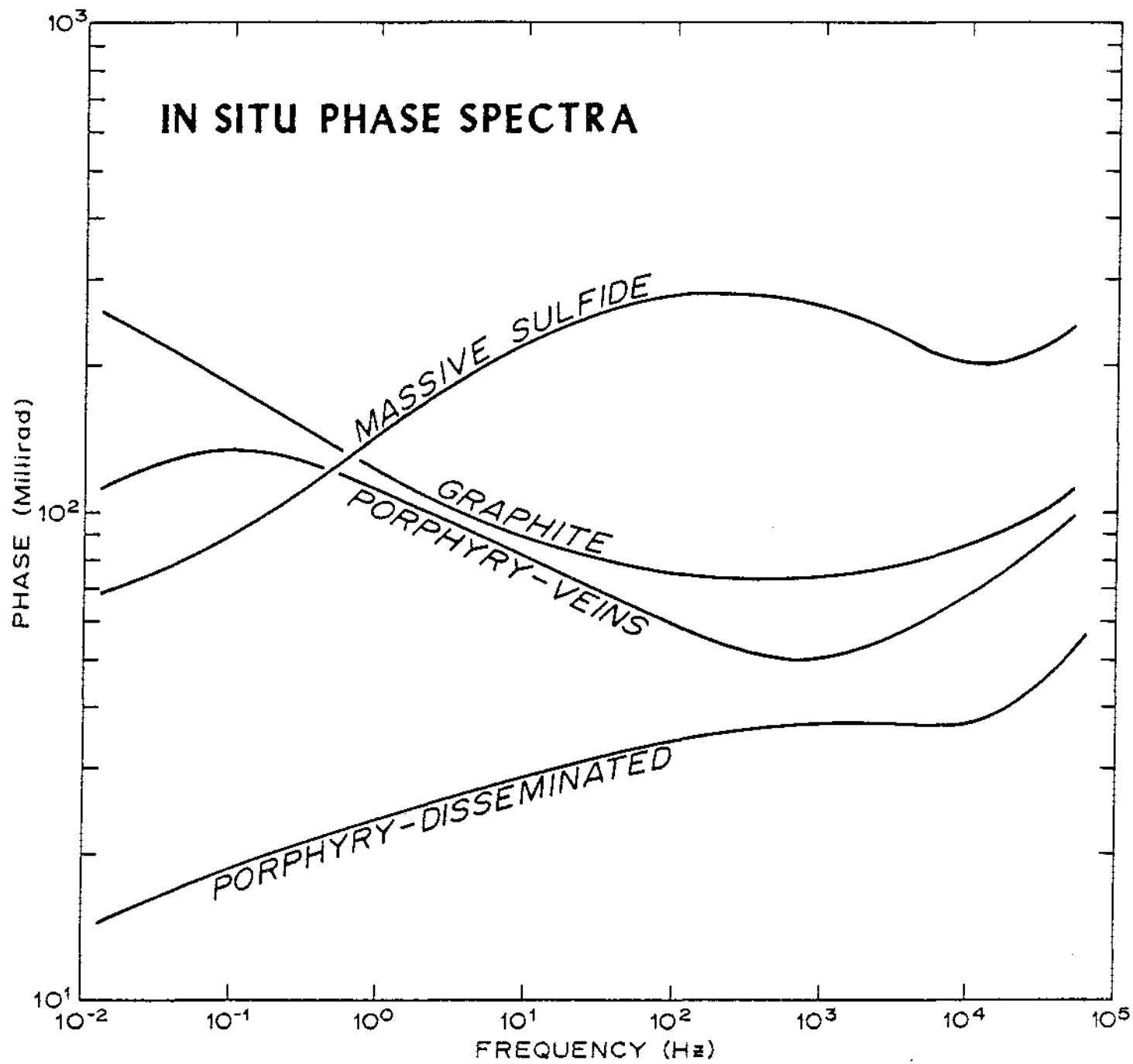


Fig 2-6

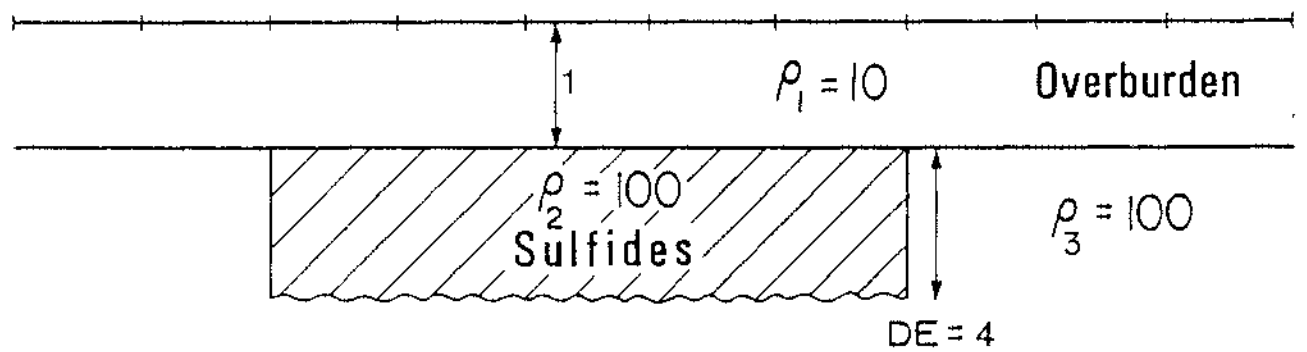
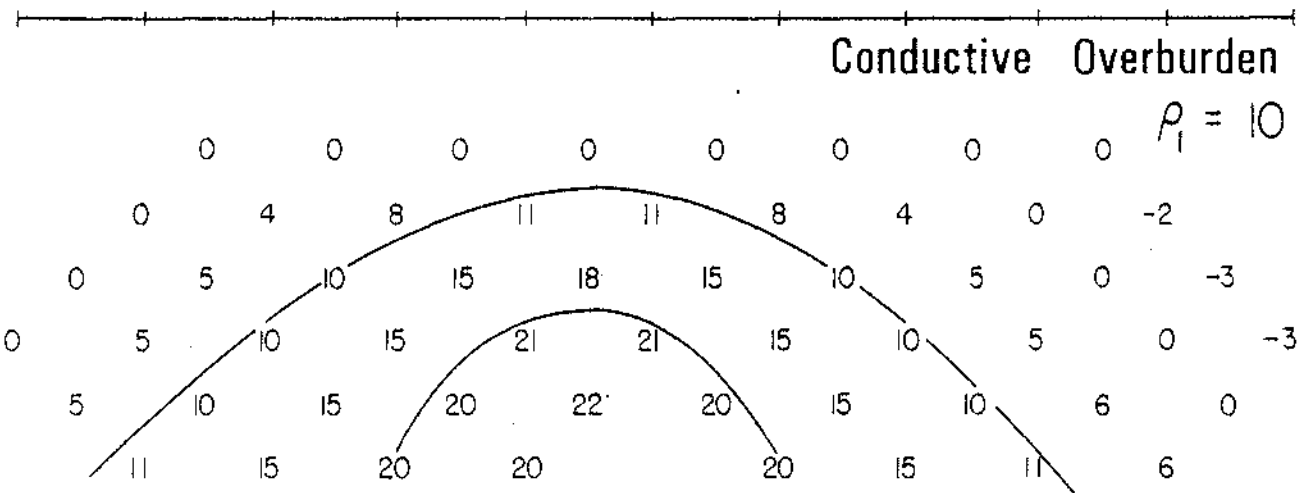
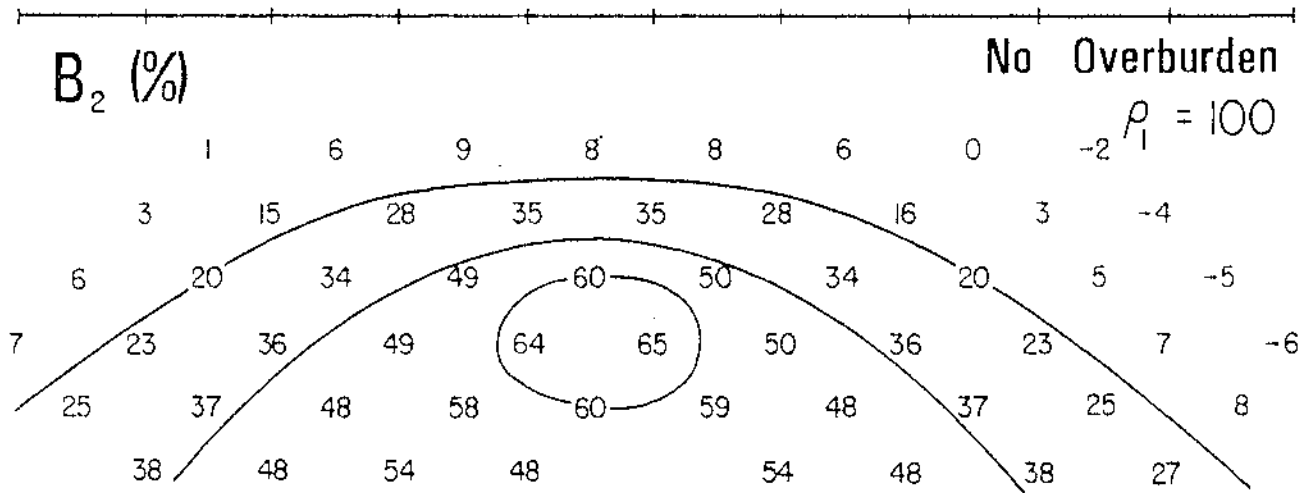
given by the equivalent circuit of Figure 2-3. The peaks in the phase angle as a function of frequency are determined largely by the time constant ($\tau = X(R_0/m)^{1/c}$) of the equivalent circuit and the magnitude by the factor $m = R_0/(R_0 + R_1)$. As can be seen, there are *observable* changes in the parameters for the various types of deposits.

VanVoorhis et al. (1973) on the other hand found in their studies of porphyry copper deposits simpler spectra characterized by essentially constant phase angles. This type of spectrum can be produced by the equivalent circuit of Figure 2-3 if $R_1 \rightarrow 0$ and $R_0 \rightarrow \infty$ (or $R_1 \ll Z$ and $R_0 \gg Z_1$ in the frequency range of interest). Wynn and Zonge (1975) reported three basic types of responses when the real and imaginary components of resistivity are plotted in the complex plane as functions of frequency. The form of the spectra in this display are then used for specific mineral identification as well as discriminating between host rock and economic mineral.

In any of the methods using the spectral character of either the phase or the real and imaginary parts, problems arise when electromagnetic coupling is superposed on the ore and rock IP response. Various schemes are used to remove electromagnetic coupling, but there is always the possibility that the coupling removal will generate false results.

Problems

Because resistivity is less important than IP in mineral exploration, we will concentrate on problems with IP. Since its inception, IP has been plagued by a number of problems; some have been overcome, some will benefit from future research and some represent fundamental limitations. We have



already discussed one problem that has been solved: because IP effects are small, accurate measurements have been possible only since the introduction of digital receivers and transmitters with accurate current control. In the following we discuss the other major problems.

Overburden masking: Conductive overburden, generally in the form of porous alluvium or weathered bedrock, prevents current from penetrating to sulfides in the more resistive bedrock. Hence the sulfides influence the measurements less than they would if the overburden were absent. Figure 2-7 illustrates the effect of conductive overburden on the theoretical IP response of a 2D body. The upper pseudosection shows the IP response without overburden, while the lower one shows the IP response with overburden 10 times as conductive as the bedrock. In this realistic example, overburden reduces the IP response by roughly a factor of 3.

For surface electrode arrays, conductive overburden represents a fundamental limitation. However, one way of combatting it is to force current into the bedrock by placing an electrode in a drill hole. In another approach, Seigel (1974) claims that measuring the magnetic field due to a polarizable body is superior to measuring the electric field, as in conventional IP, in areas of conductive overburden.

Electromagnetic coupling: Electromagnetic (EM) coupling presents a serious problem for IP surveys, particularly when large electrode separations are used in areas of low resistivity. The EM eddy currents vary with frequency, and their effects are similar to those of sulfide mineralization.

The first step in combatting EM coupling is to use an appropriate

electrode array. Arrays such as the Schlumberger and Wenner, where measurements are made between widely spaced current electrodes, generate large EM coupling and must not be used. If a long current line is necessary to increase the signal, measurements must be made perpendicular to the current wire near one of the electrodes, as in the three-array or the perpendicular pole-dipole array. If the earth is homogeneous, there is no EM coupling for a perpendicular array. But lateral or vertical resistivity changes can produce large, and sometimes negative, EM coupling. The commonly used in-line dipole-dipole array offers both high earth resolution and lower EM coupling, at the expense of low receiver voltage levels.

Even if an optimum array is used, however, EM coupling poses a serious problem. Figure 2-8, for example, shows the theoretical EM coupling phase over a 2000 ft (610 m) wide by 3000 ft (915 m) depth extent by 6000 ft (1830 m) long prism at a depth of 1000 ft (305 m). Its resistivity is 1 Ω -m, and the background resistivity is 100 Ω -m. The dipole length is 1000 ft (305 m). Results are shown for the three frequencies 1 Hz, 0.5 Hz, and 0.1 Hz. For comparison, EM coupling values for a homogeneous half-space of resistivity 100 ohm-m are shown at the right. EM coupling is greater than the half-space coupling when the transmitter and receiver straddle the body at large separations. However, there are areas in the pseudosection where EM coupling over the prism is less than half-space coupling. In fact, negative EM coupling often is seen in field data taken over very conductive bodies.

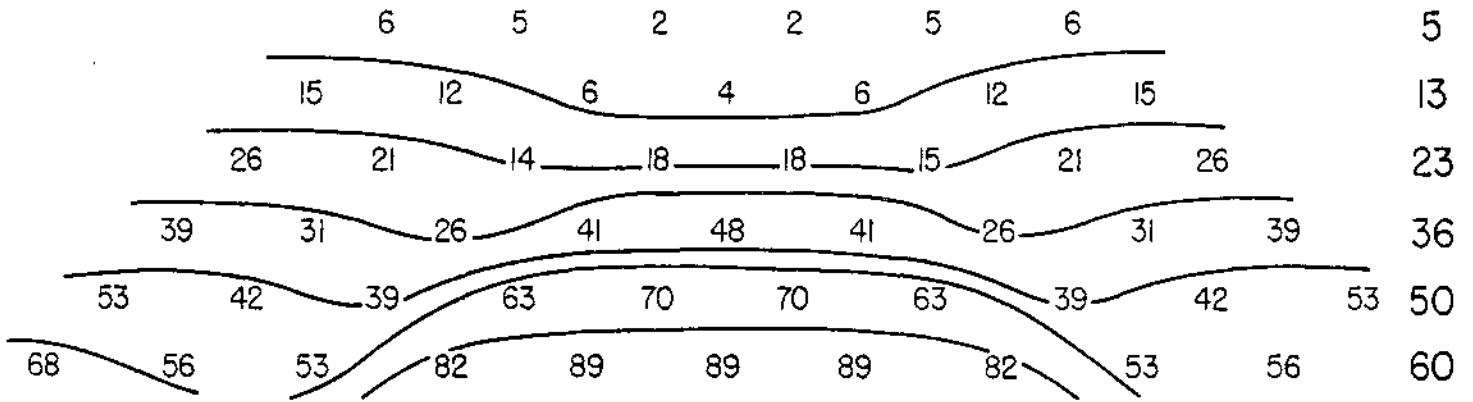
The level of EM coupling shown in Figure 2-8 is unacceptable, even at 0.1 Hz, for an IP anomaly of interest may be as low as 10 mrad or less.

EM COUPLING

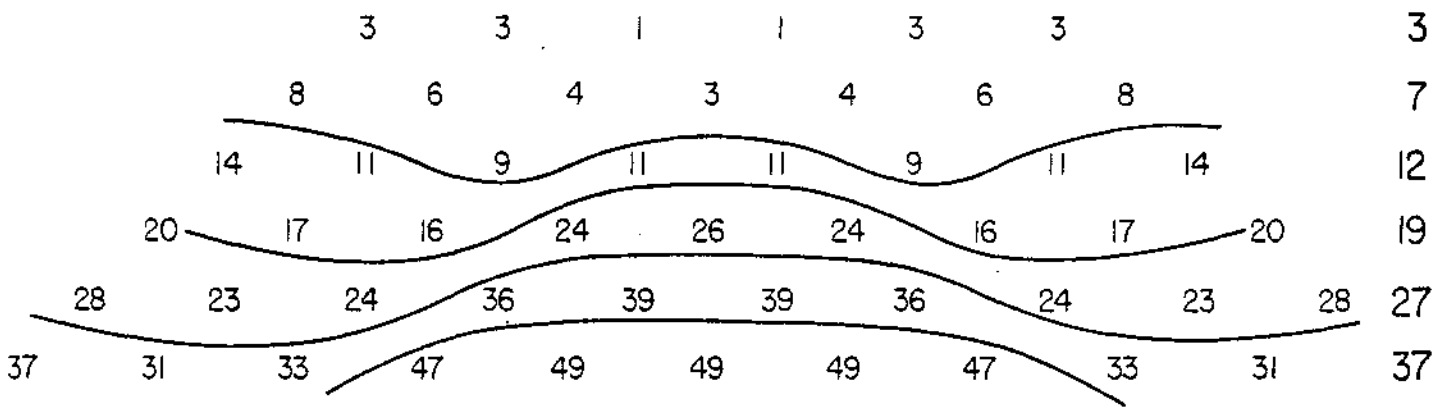
Phase (mrad)

$f = 1.0 \text{ hz}$

Half-space Value



$f = 0.5 \text{ hz}$



$f = 0.1 \text{ hz}$

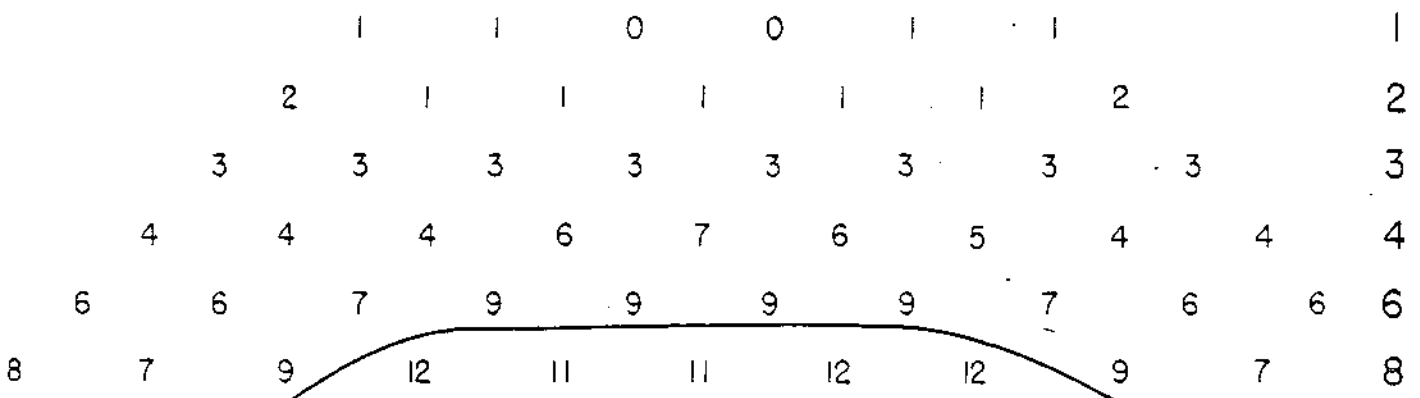


Fig 2-8

Furthermore, background resistivities below 100 Ω -m are common, and would result in much greater phase angles. Hence, some means must be devised to eliminate EM coupling. The EM effects would decrease at lower frequencies, but due to increasing natural electric fields, reliable measurements often cannot be made below about 0.1 Hz. Time domain practitioners reduce the problem by using high currents and large, perpendicular arrays, and by allowing a large time interval between current shut-off and voltage measurement. This technique is successful because the EM coupling decays more rapidly than the IP response.

However, in situ IP measurements with short electrode spacings show that the IP phenomenon persists to frequencies below .01 Hz, and that the IP phase angle is approximately constant between .01 Hz and 10 Hz (VanVoorhis, et al., 1973). Based on these results, VanVoorhis devised a simple, effective technique for eliminating EM coupling; a similar technique was published by Hallof (1974). The method is illustrated in Figure 2-9. The phase is the sum of two components: (1) caused by IP, which is constant with frequency and persists to very low frequencies; and (2) due to EM coupling, which varies with frequency and is negligible at very low frequencies. By fitting the IP data to a polynomial and extrapolating to zero frequency, as shown in Figure 2-9, EM coupling is eliminated. Generally, a second-degree polynomial is required; linear extrapolation is not sufficient.

Techniques for removing EM coupling over a broad frequency range and retaining the spectral character of IP have been proposed by Wynn and Zonge (1975) and Pelton, et al. (1978). However, their validity remains to be demonstrated.

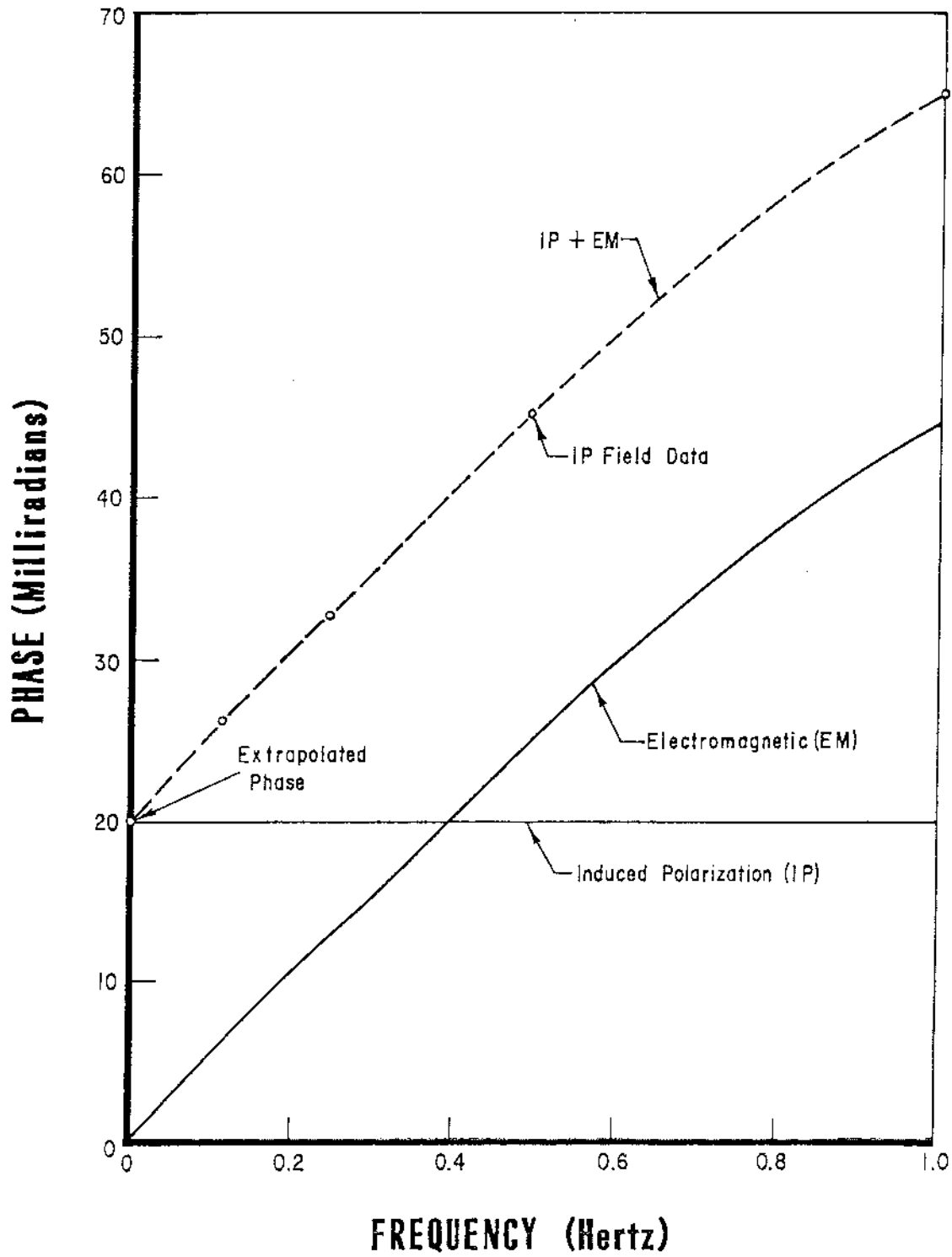


Fig 2-9

Natural fields: Natural electric and magnetic fields below 1 Hz are due mainly to the interaction of fields and particles from the sun with the earth's magnetic field, and hence their magnitude depends on solar activity. Above 1 Hz they are primarily due to worldwide thunderstorms. Their amplitude increases rapidly with decreasing frequency below 1 Hz, as shown in Figure 2-10, and effectively prevents IP measurements below about 0.1 Hz. EM coupling is too high above 10 Hz. Hence, IP measurements with large arrays are limited to the range 0.1 to 10 Hz. Even in that range, sophisticated digital signal processing is required to make accurate measurements, because of the natural field noise. Coherent detection and digital high-pass filtering are required. Stacking, i.e. adding successive transients, is necessary to reduce noise in time domain measurements, but noise rejection is not as good as for coherent detection in the frequency domain.

Another promising method, suggested by Halverson (1977) utilizes multiple receiver dipoles to reduce telluric noise. Natural fields are more uniform than the artificial fields of interest, so that they can be cancelled by making simultaneous measurements at a location that is not affected by the transmitter current.

Geologic noise: Any response from a body or zone that is not of interest, and that interferes with the target response, is termed geologic noise. Geologic noise always is high in resistivity surveys because of the large variations of resistivity due to changes in porosity and water saturation. In effect, it prevents resistivity from being much more than an accessory to IP in most mineral exploration.

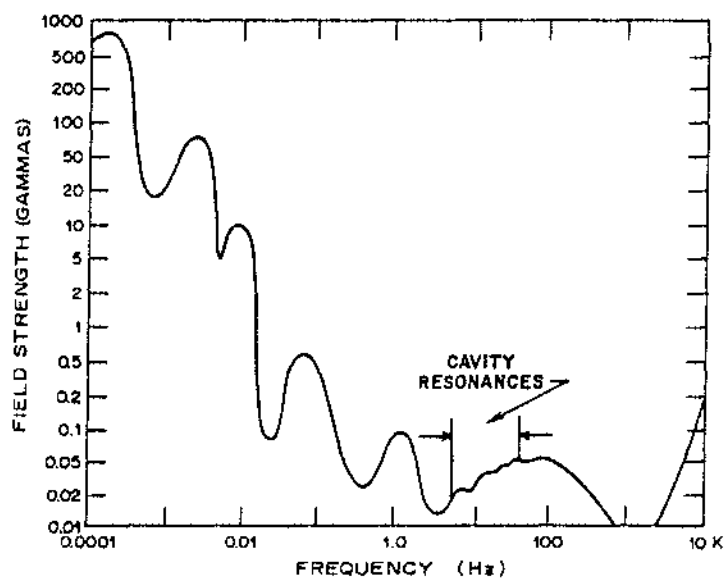


Fig 2-10

However, magnetometric resistivity (MMR) is a promising new method designed to delineate resistivity boundaries beneath conductive overburden. In this resistivity method the magnetic field rather than the electric field is measured in the vicinity of grounded electrodes. Because it is an integral over a volume distribution of current, the magnetic field is much less distorted than the electric field by surficial inhomogeneities. Edwards and Howell (1975) show a field example of delineation of a fault beneath a considerable thickness of variably conductive overburden using MMR. Standard resistivity methods would have been useless due to large geologic noise from the overburden.

Geologic noise in IP is due to uneconomic sulfide mineralization, clay and zeolites, carbonaceous sedimentary rocks, magnetite, and possibly other sources. There are some indications (Pelton, et. al, 1978) that it may be possible to distinguish among clay, sulfide, and graphite responses on the basis of their spectral characteristics, using broad-band measurements with short electrode spacings. Basically, clay response has a rapid decay or short time constant, very conductive graphite has a slow decay or large time constant, and most sulfide mineralization has an intermediate time constant. However, it is doubtful that this discrimination can be achieved in typical field surveys, where large electrode spacings lead to high EM coupling and averaging of many kinds of IP responses. Because geologic noise is so detrimental in IP surveys, much current research is concentrated on this problem.

Culture: Grounded structures such as fences, powerlines, and pipelines redistribute current from the IP transmitter so that part of the current flows through the cultural feature. The complex grounding impedance causes an IP response that is virtually indistinguishable from a sulfide response. In a definitive analysis of the problem, Nelson (1977) finds that the only certain means of eliminating such spurious IP responses is to keep IP transmitting and receiving lines away from grounded structures.

Cultural features also can introduce noise into IP measurements by providing a path for the travel of various interfering signals. Of course strong noise voltages are present in the vicinity of powerlines, requiring filtering at the front end of the receiver. Pipelines, furthermore, often carry electrical current for cathodic protection and this current is a source of noise.

Topography: Much mineral exploration is done in mountainous terrain where topography can produce spurious resistivity anomalies. For example, when a hill occurs between the transmitter and receiver dipoles of a dipole-dipole array, current focusing causes an erroneous apparent resistivity high. When there is a valley between transmitter and receiver dipoles, current dispersion produces an apparent resistivity low.

Because IP is a normalized measurement, current focusing and dispersion produced by an irregular terrain surface do not significantly affect basic IP data. Thus if the earth were homogeneous and polarizable, irregular terrain would produce no significant spurious IP response. However, second-order topographic effects in IP surveys are introduced by variations in distances between surface electrodes and a polarizable body

relative to a flat earth.

In a recent study Fox, et. al (1980) have systematically analyzed the effects of topography for the dipole-dipole array using a 2D numerical solution. Figure 2-11 shows the apparent resistivity anomaly produced by a valley with 30 degree slopes. The pseudosection is characterized by a central apparent resistivity low flanked by zones of high apparent resistivity. The low is most pronounced when the transmitter and receiver dipoles are on extreme opposite sides of the valley. This example shows that a valley can produce a large, spurious low in resistivity which could easily be misinterpreted as evidence for a buried conductor.

The effect of a ridge is shown in Figure 2-12. Its resistivity anomaly is opposite that of a valley; a central apparent resistivity high is flanked by zones of low apparent resistivity. Again, the well-defined zones of low resistivity on either side of the diagonal could be mistaken as indicative of buried conductive bodies. On the other hand the terrain-effect high could mask the expression of an actual conductive zone below the ridge.

The significance of an IP anomaly often depends upon its associated resistivity anomaly. For example, an IP anomaly due to sulfide mineralization may have a corresponding resistivity low associated with hydrothermally altered host rock. The resistivity high caused by a ridge could mask an actual zone of low resistivity associated with an IP anomaly, suggesting a source in fresh rather than altered host rock. A moderately anomalous IP response associated with the resistivity low caused by a valley could be interpreted as positive evidence for significant sulfide mineralization, when in reality the IP anomaly would be due to high

inherent IP response in a rock of high resistivity.

In general, topographic effects are important where slope angles are 10 degrees or more for slope lengths of one dipole or more. The solution to the problem is to include the topographic surface in numerical models used for interpretation, as illustrated by examples in Fox et al. (1980).

Interpretation

Models: One dimensional interpretation, i.e. use of layered earth models, has reached an advanced state. Efficient computer inverse algorithms produce reliable solutions, and, furthermore, provide estimates of the attainable resolution. Unfortunately, such techniques only occasionally are useful in mineral exploration, where the target usually has finite lateral extent. Hence we will emphasize practical interpretation with inhomogeneous models.

Before about 1970 resistivity/IP interpretation in mineral exploration was rudimentary and unsatisfactory because of a lack of forward solutions. Since then, however, computer programs that calculate the responses of assumed 2D and 3D models have been developed. Hence it is now possible to compute catalogs of simple, realistic models for comparison with field data. More detailed interpretation can be carried out by trial-and-error matching of data with theoretical responses for complex models. However, practical inversion techniques for 2D and 3D models do not yet exist, although they are the subject of much current research.

We show representative results from a catalog of simple 3D models. We consider only IP responses and only the dipole-dipole array because of their importance in mineral exploration. They were computed using the

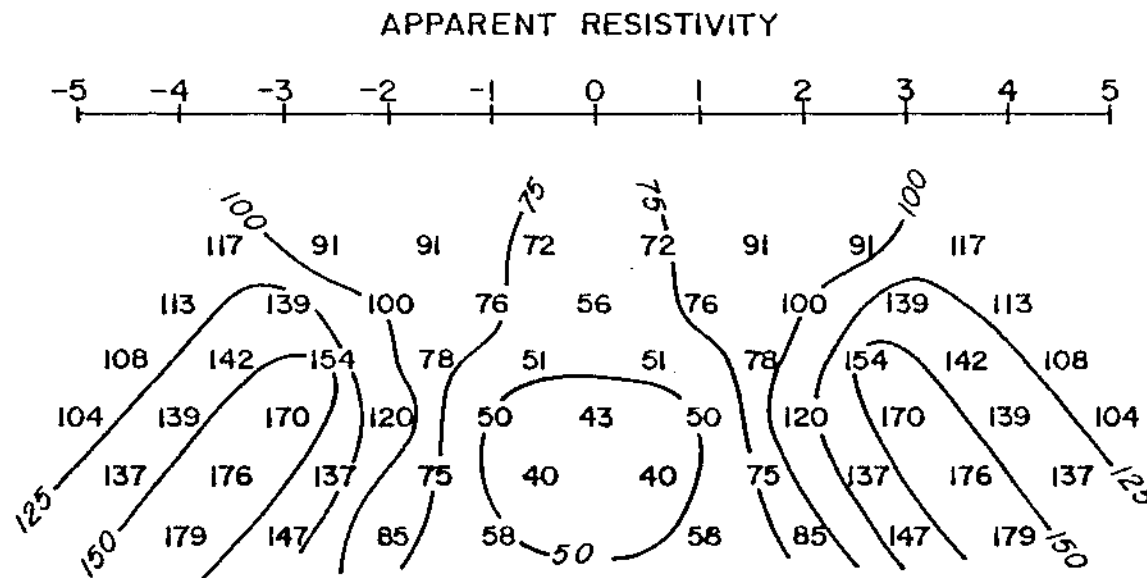
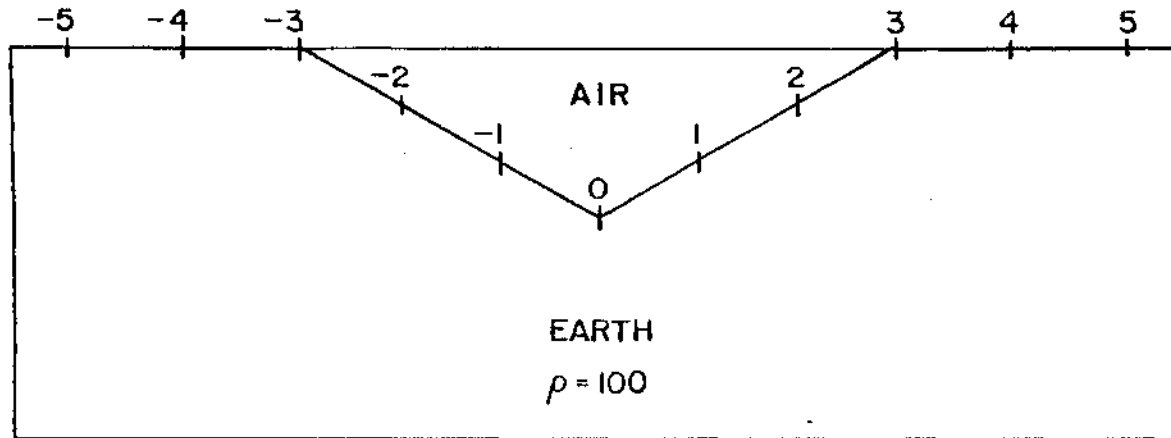


Fig 2-11

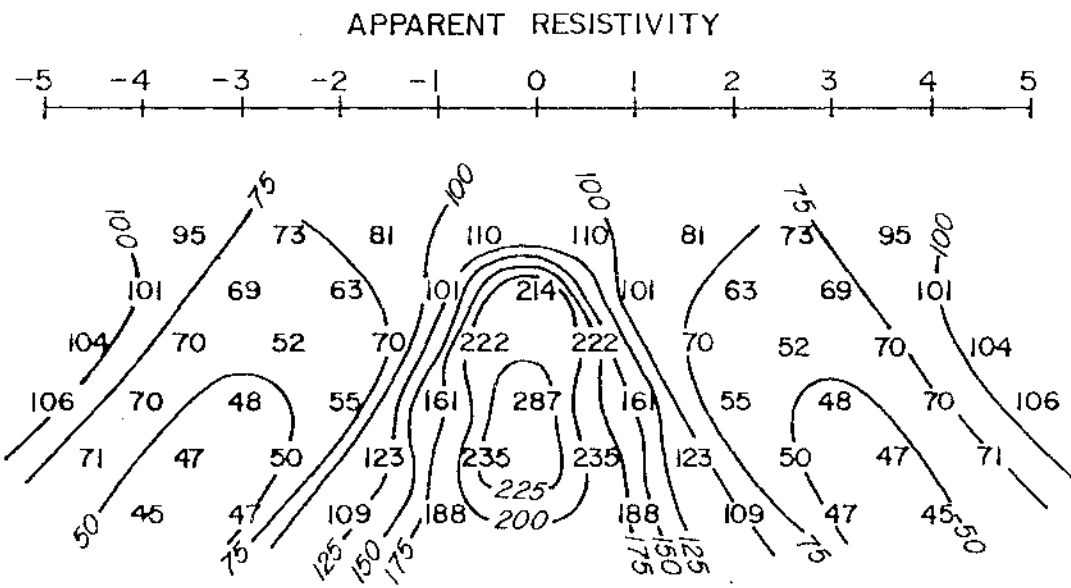
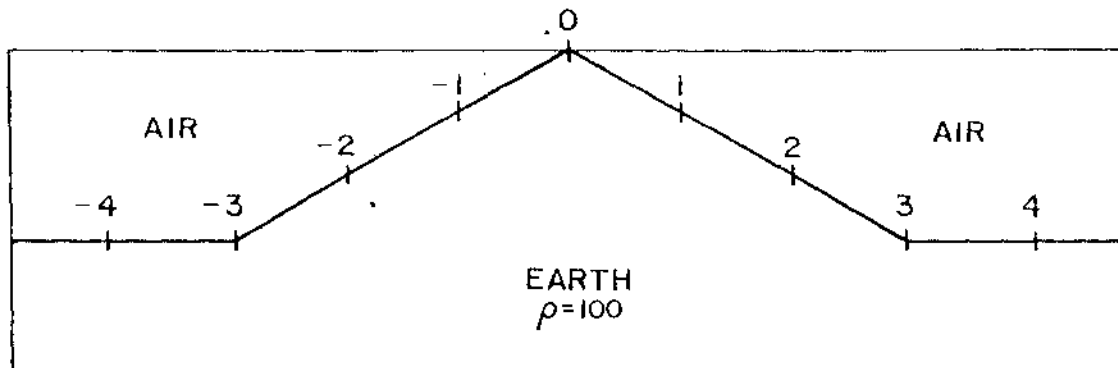
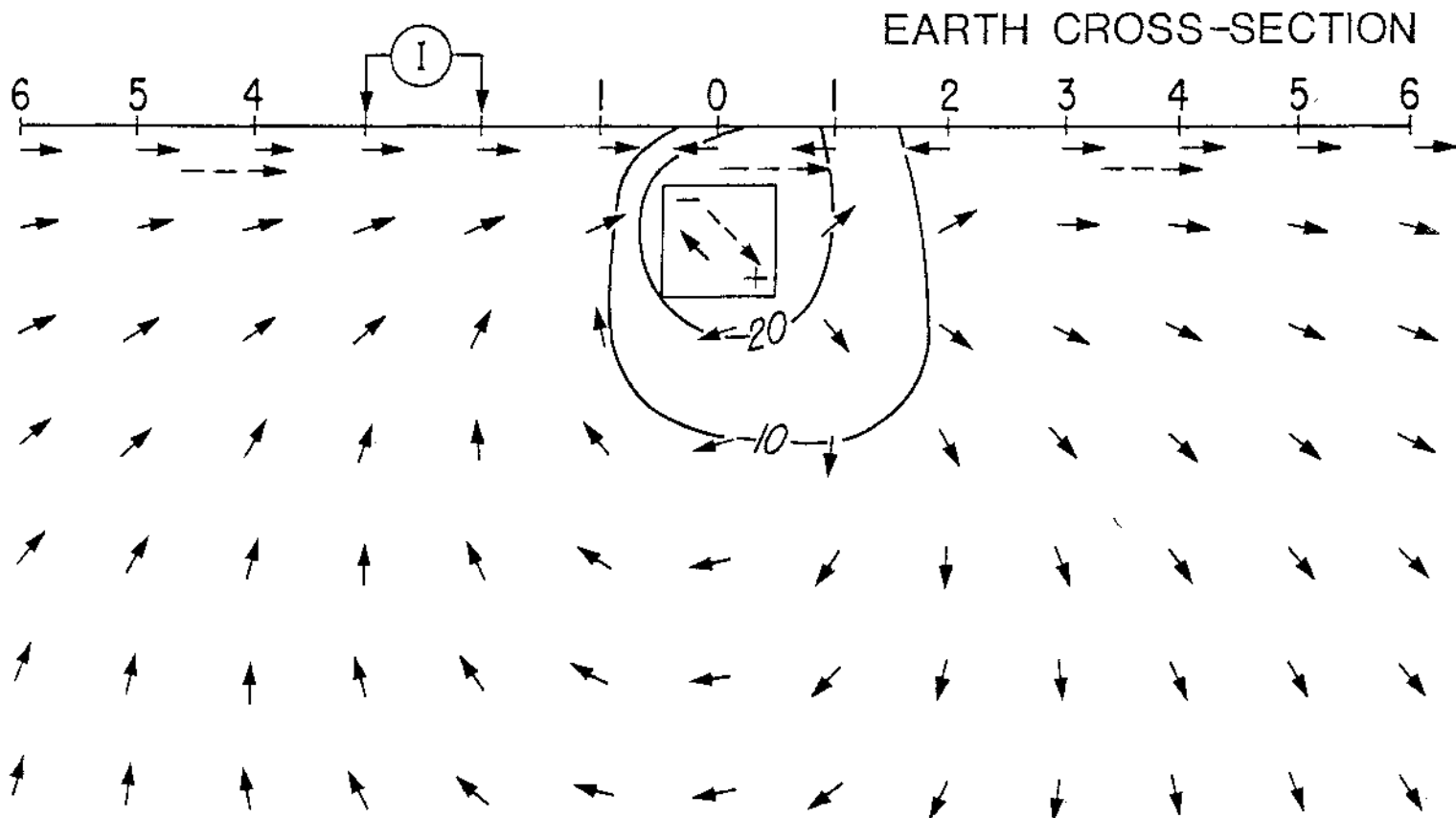
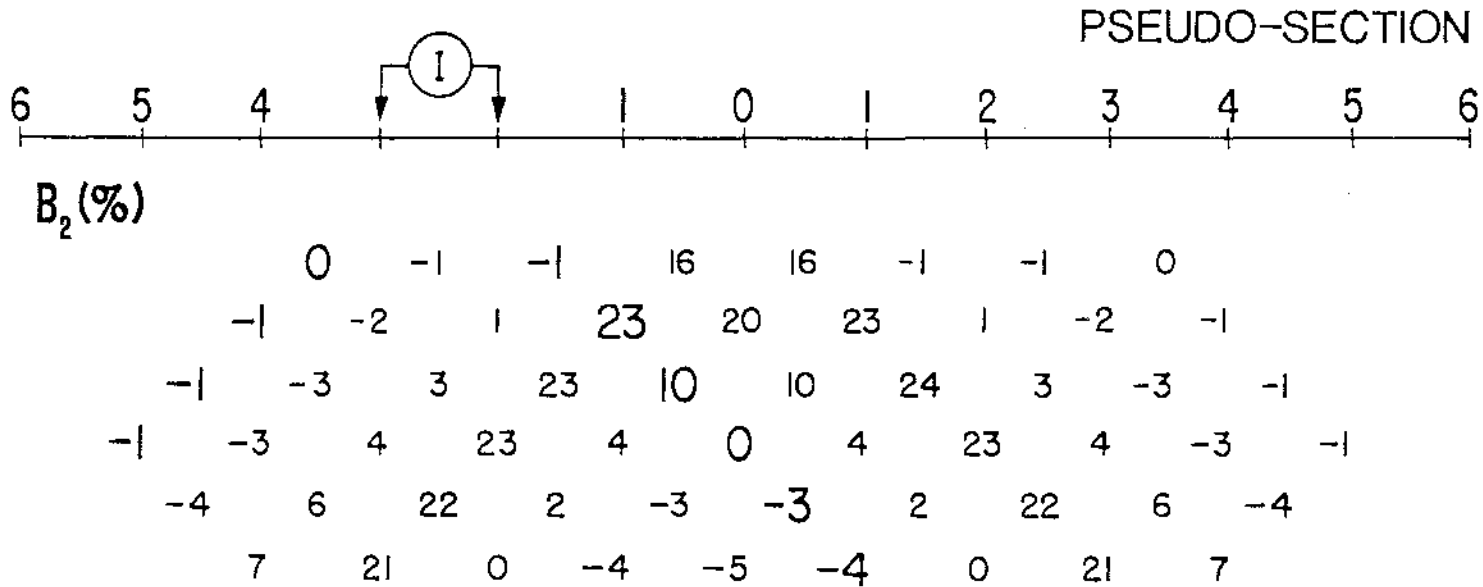


Fig 2-12

integral equation technique described by Hohmann (1975). IP responses are given as a percentage of the intrinsic response in the body ($B_2\%$), so that they apply to any IP parameter such as phase, PFE, or chargeability.

Electric field patterns in the earth: Looking at IP in terms of the mathematical modeling technique provides an intuitive feeling for IP behavior. The measured potential is the sum of the primary and secondary potentials. The former is what would be measured over a homogeneous earth of resistivity ρ_1 , while the latter represents the contribution from the inhomogeneity. The secondary potential consists of in-phase and quadrature components; they originate at polarization dipoles distributed throughout the body, or, equivalently, at surface charges on the body. The quadrature dipoles, as well as the in-phase dipoles for a conductive body, are oriented in roughly the same direction as the incident field. For a resistive body, the in-phase dipoles are oriented in the opposite direction.

To illustrate, Figure 2-13 shows the quadrature (IP) current pattern in a cross-section of the earth through the center of a body which is 1 unit wide by 0.5 unit deep by 5 units long. A corresponding pseudo-section is shown; the bold numbers correspond to the particular transmitter dipole to which the electric field pattern pertains. The contoured numbers in the cross-section are the phase of the total electric field, i.e., total quadrature field divided by total in-phase field. In this case the in-phase field is the field of a homogeneous earth, because there is no resistivity contrast. Because the intrinsic IP response of the body is 100 milliradians (mrad), the numbers as given are percent of the intrinsic



response, called $B_2(\%)$. The solid arrows show the quadrature field direction, while the broken arrows show the in-phase field direction.

The dipole-dipole array measures the component of electric field along the line. By convention, the IP response is positive when the quadrature, or polarization, and in-phase fields are in opposite directions, and negative when they are in the same direction. IP response is negative to the left of the transmitter dipole of Figure 2-13, and there are two changes in sign to the right. Comparing the pseudo-section and the cross-section, we see how negative IP responses arise when both transmitter and receiver are on one side of a body, and when they are on opposite sides of a body at large separations. Note the positions of positive and negative surface charges, from which the quadrature field originates.

Prism responses: The effects of changes in the parameters of a simple 3D prism are shown in Figures 2-15 through 2-24. A good appreciation of these effects is crucial for interpreting both simple and complex IP responses observed in the field.

Figure 2-14 shows the prism model with the dipole-dipole electrode array. The basic model parameters are: strike length (L), width (W), depth (D), depth extent (DE), and resistivity contrast (ρ_2/ρ_1). As usual, all dimensions are in units of a , the dipole length.

Strike length: Figure 2-15 shows how strike length affects the response of a body that is two units in width and four units in depth extent. The depth to the top of the body is one unit, and there is no resistivity contrast. There is a large increase in IP response as the strike length increases from two to five units, but only a small change when the strike

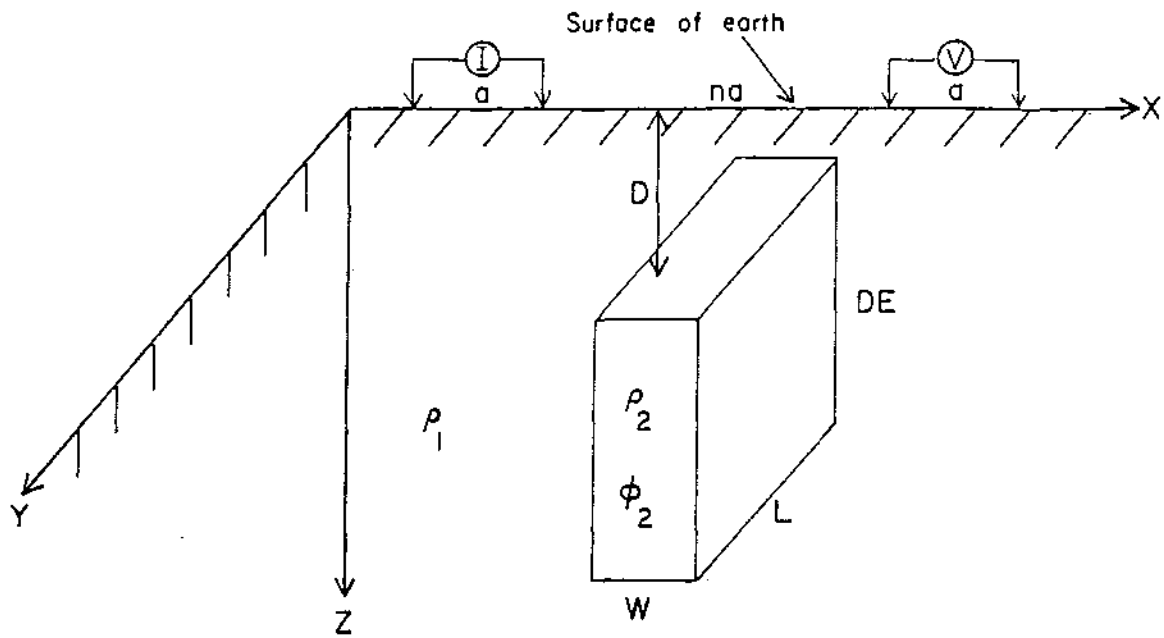


Fig 2-14

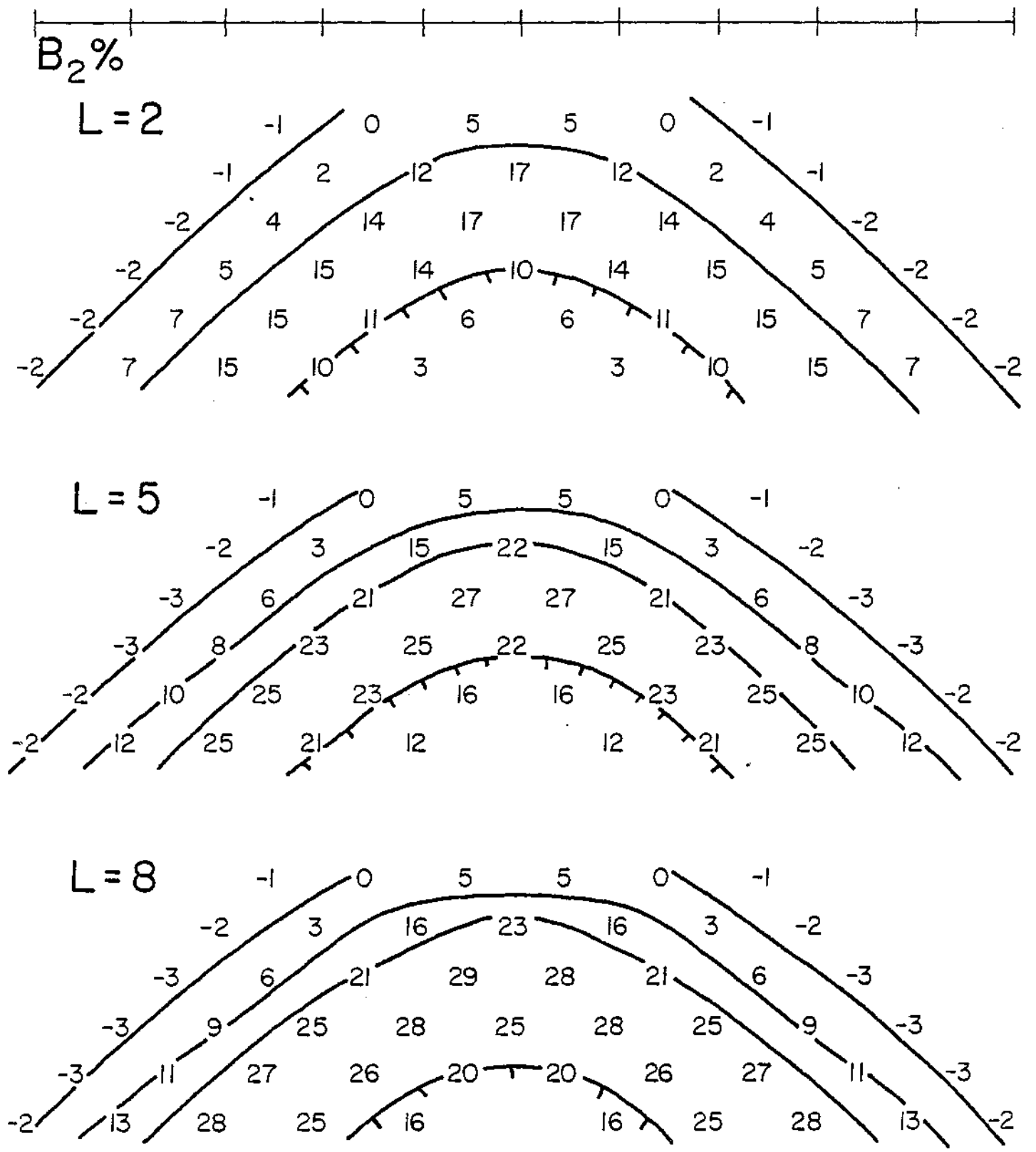


Fig 2-15

length increases further. In fact, the values for $L = 8$ are all within 2 of those for a 2D body (C. M. Swift, personal communication). For all practical purposes the IP response of a body five or so units long is equivalent to that of a 2D body unless the body is very conductive. This observation is important, because it is much less expensive to model a large, complex body by use of a 2D technique, such as that given by Coggon (1971, 1973).

Depth: One of the most important source parameters to determine in exploration is the depth of a polarizable body. Fortunately, dipole-dipole data are very diagnostic. Figure 2-16 compares the IP responses of a prism at depths of 0.5, 1, and 2 units. IP response varies with body depth differently for different points in the pseudosection. Hence, the pattern of the response is important for depth interpretation. In general, deeper bodies give rise to broader, lower-amplitude anomalies.

Width: IP responses of prisms for widths of 1, 2, and 4 units are shown in Figure 2-17. Again, the resistivity of the prism is the same as that of its surroundings; in this case its strike length is 5 and depth extent 4. Note that the IP response for $W = 2$ is about twice that for $W = 1$ at most points in the pseudo-section. Hence, the IP response of a thin body ($W=2$) is a function of its IP-width product, and the two parameters cannot be determined separately. The response pattern changes when the width increases to 4, with the anomaly becoming broader and larger in amplitude.

Results for a polarizable layer ($W = \infty$, $DE = 4$, $L = \infty$) are shown on the right in the lower pseudo-section for comparison. The three layer earth values for separations less than 4 are almost the same as those directly

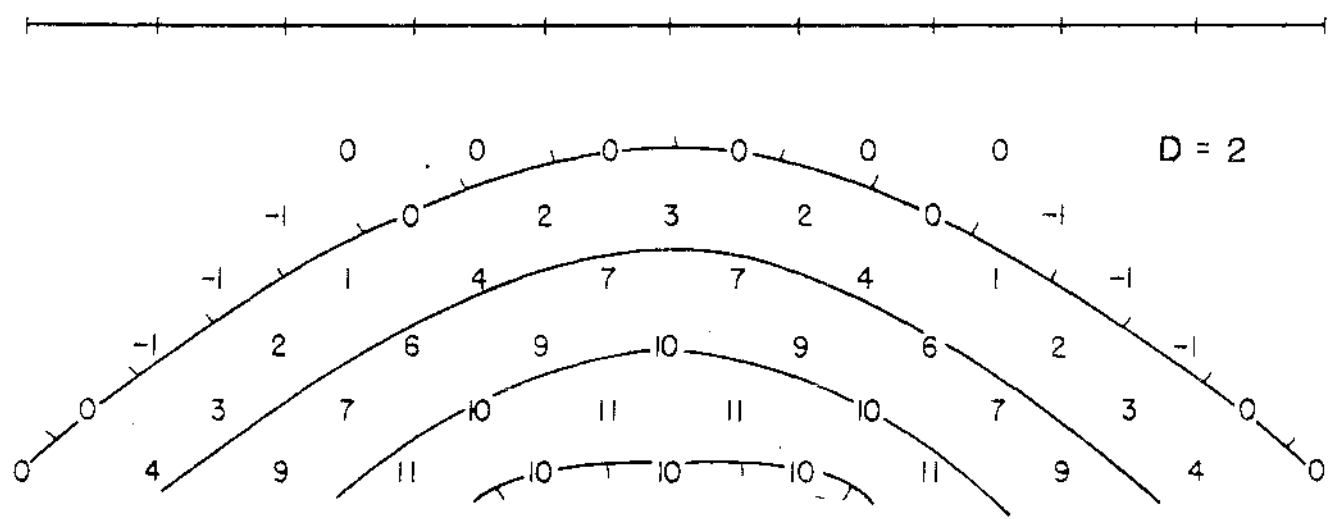
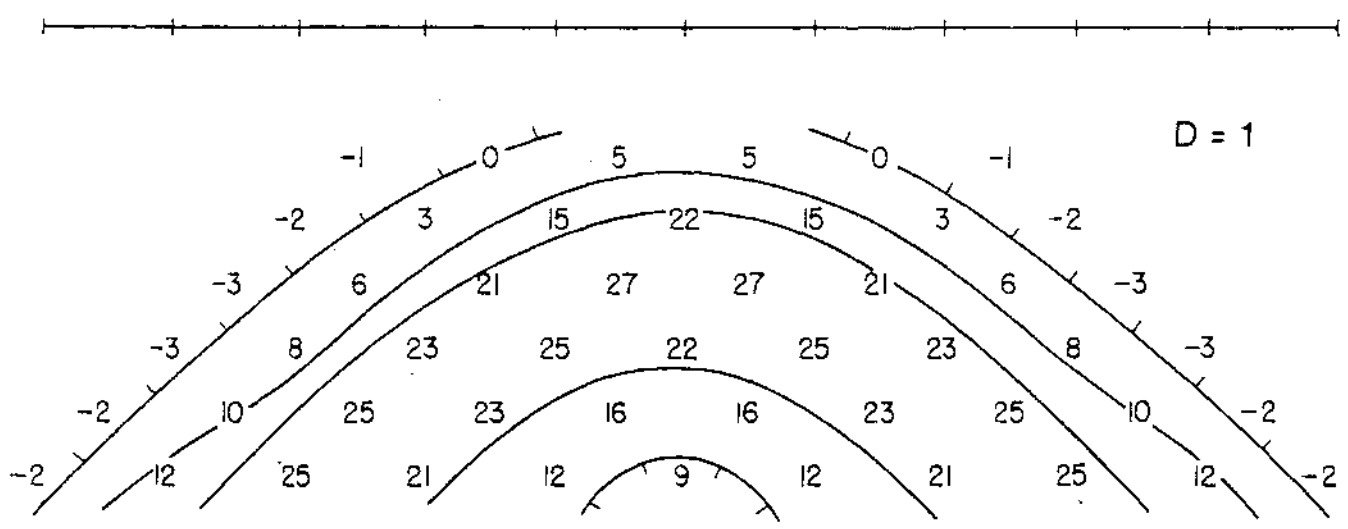
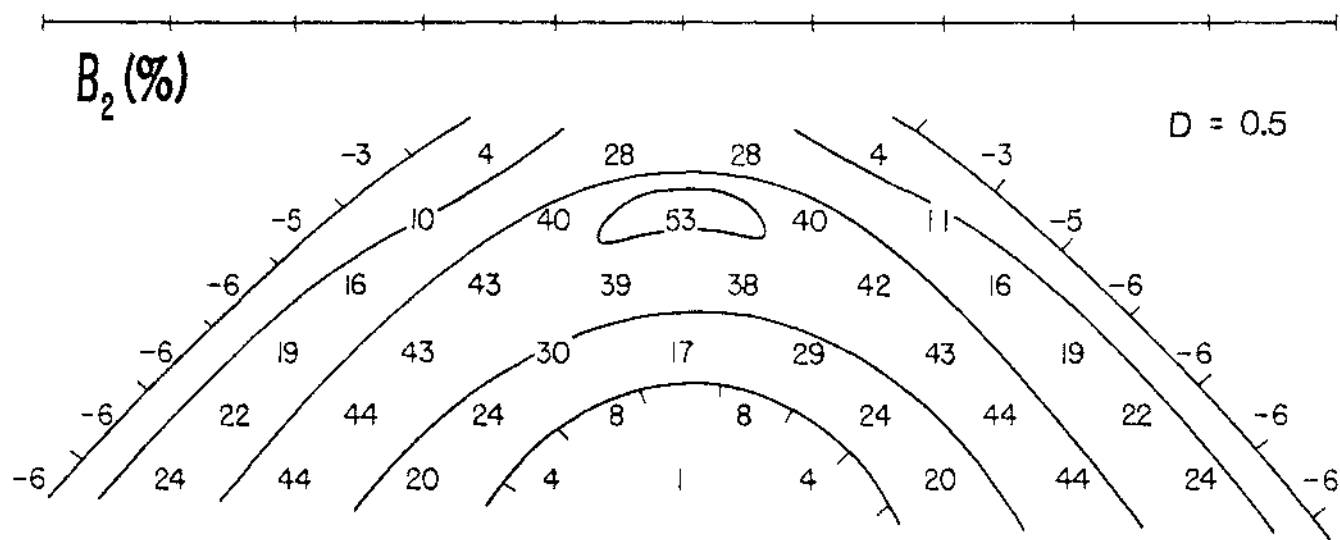


Fig. 2-16

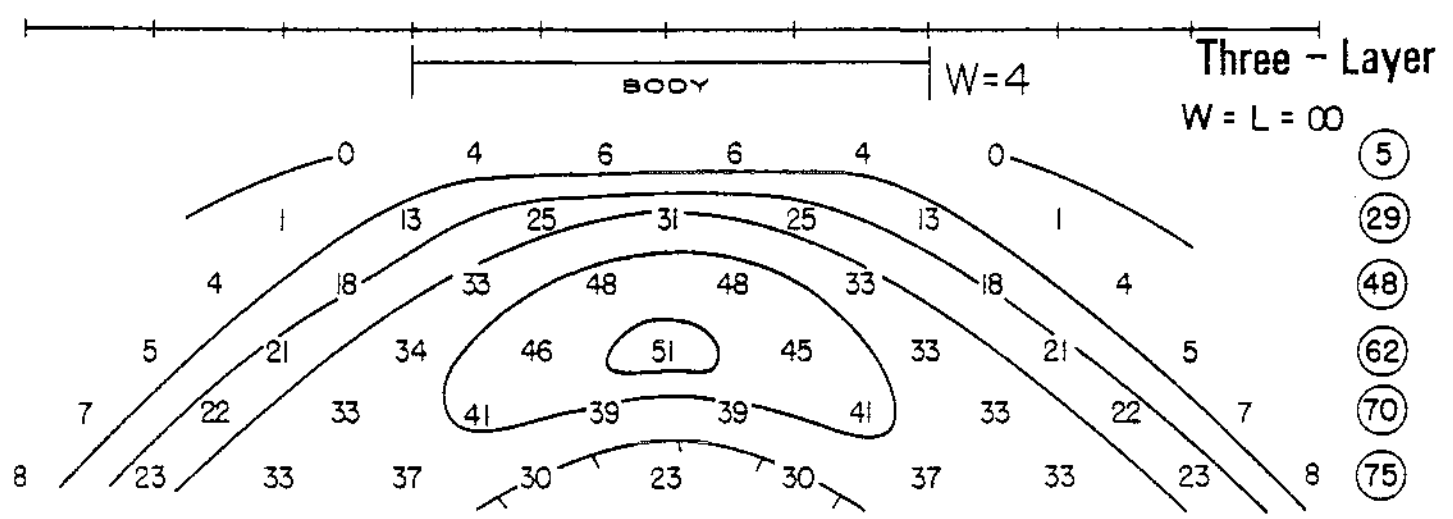
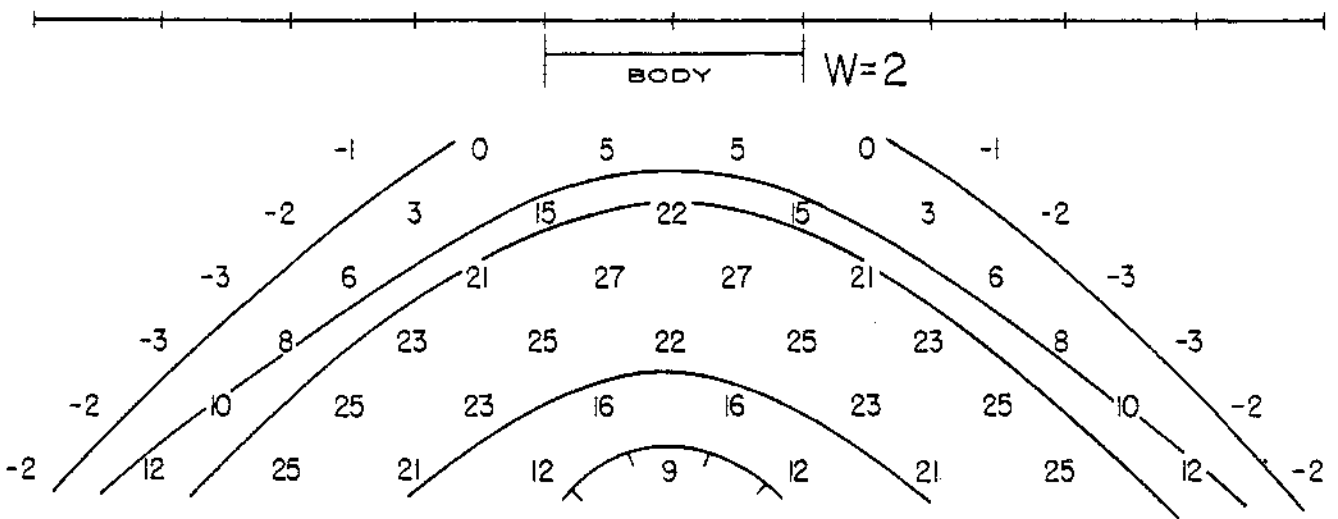
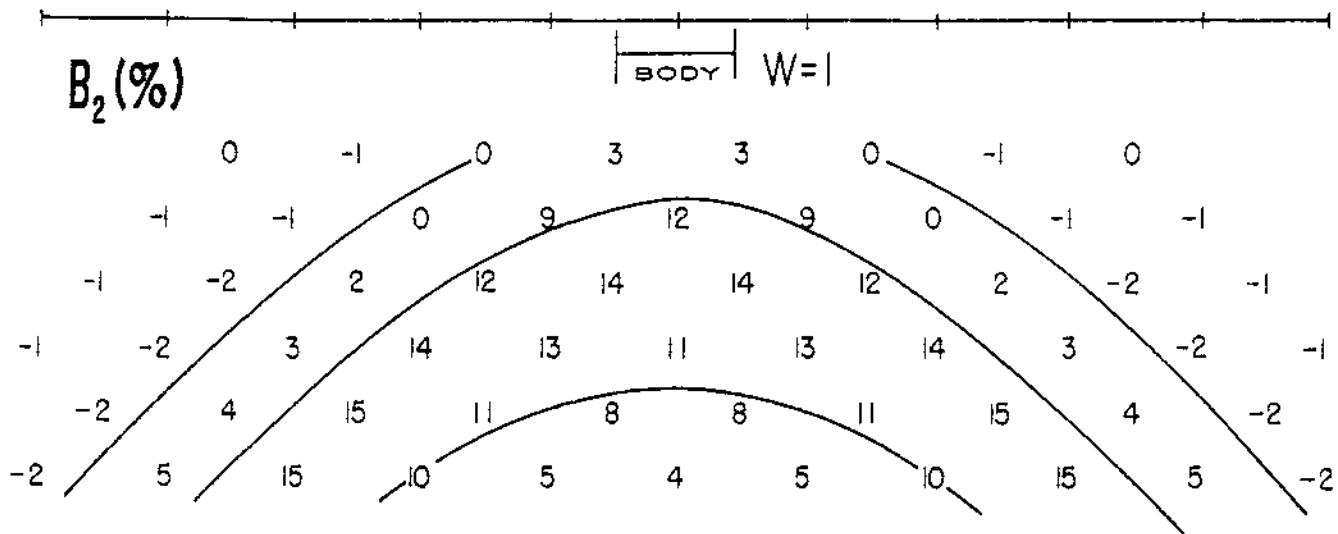


Fig 2-17

over the wide prism, but they diverge elsewhere. Hence, a body must be much larger than 4 by 5 in plan for layered-earth interpretation to be applicable.

Depth extent: Figure 2-18 compares IP responses for depth extents of 1, 2, and 4. The only important depth-extent effects occur when the transmitter and receiver dipoles straddle the body at large separations, i.e., for points at the bottom center of the pseudosection. For practical purposes, there is very little difference between results for DE = 2 and those for DE = 4. The differences between the DE = 1 and DE = 2 responses are more definitive, for this simple model. However, because of background response, complex geology, and uncertainty in intrinsic response, it generally would be impossible to distinguish between depth extents of 1 and 4 from field data. Depth extent is very difficult to resolve, because most of the IP response is due to the upper part of the body.

Resistivity contrast: IP response is highly dependent on the ratio of polarizable body resistivity (ρ_2) to host rock resistivity (ρ_1). The response peaks at intermediate contrasts and decreases for very resistive and for very conductive bodies. To summarize this behavior, we have plotted in Figure 2-19 the peak dipole-dipole IP response as a function of resistivity contrast for a sphere of radius one, a 3D body of 2 units width, 4 units depth extent, and 5 units strike length, and a couple of 2D bodies. All are at one unit depth.

For a small sphere, the integral equation solution for the secondary potential due to a polarizable body reduces to

$$V_S = \frac{\rho_2 I}{2\pi} P \cdot G, \quad (2-11)$$

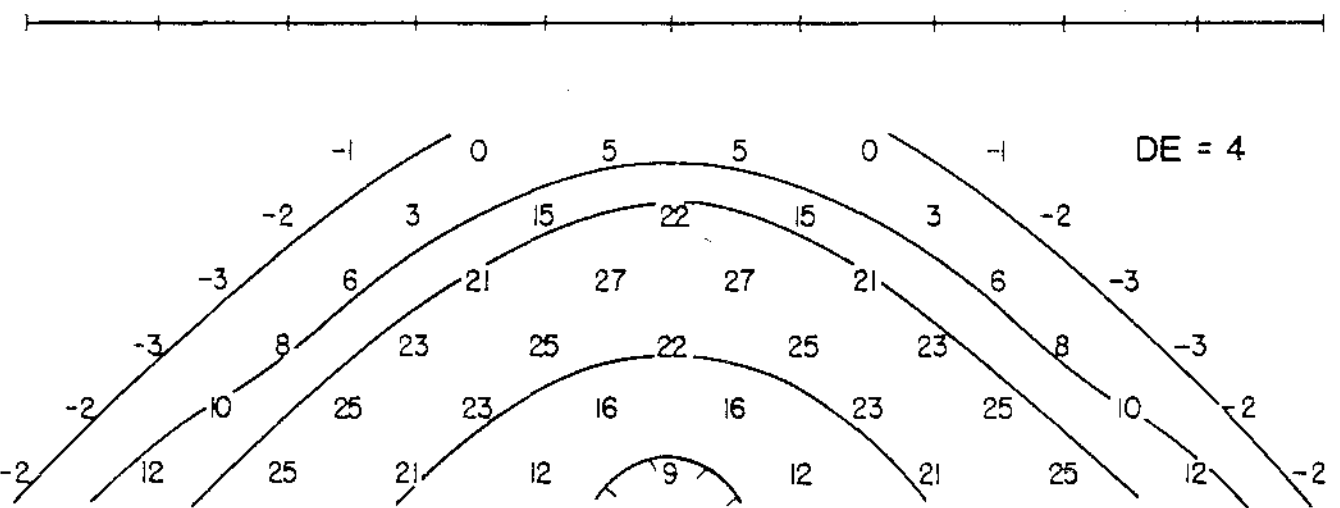
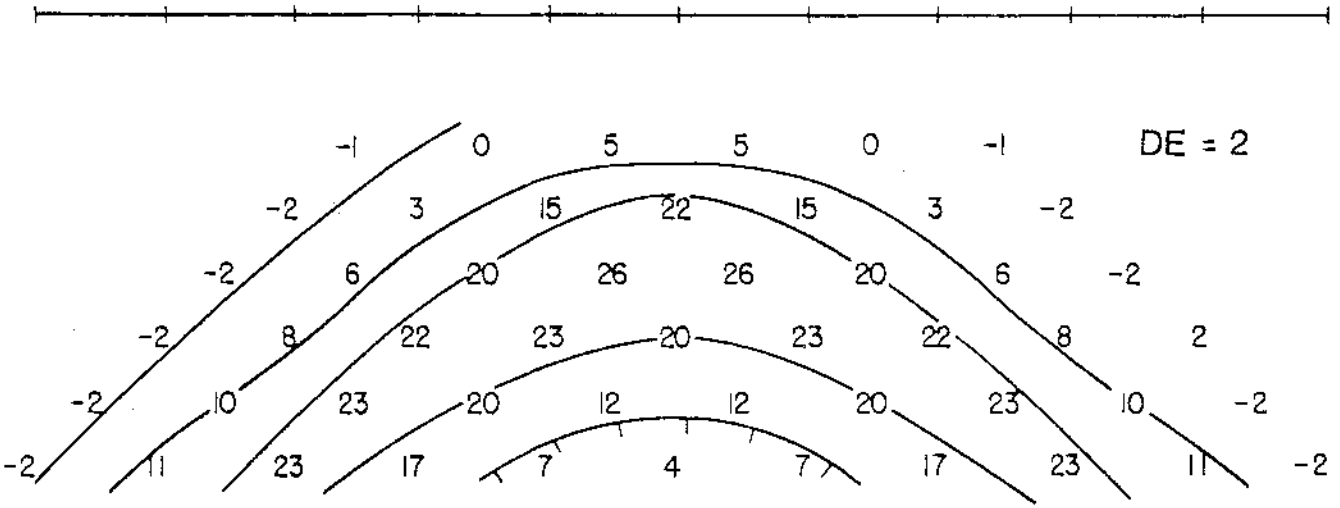
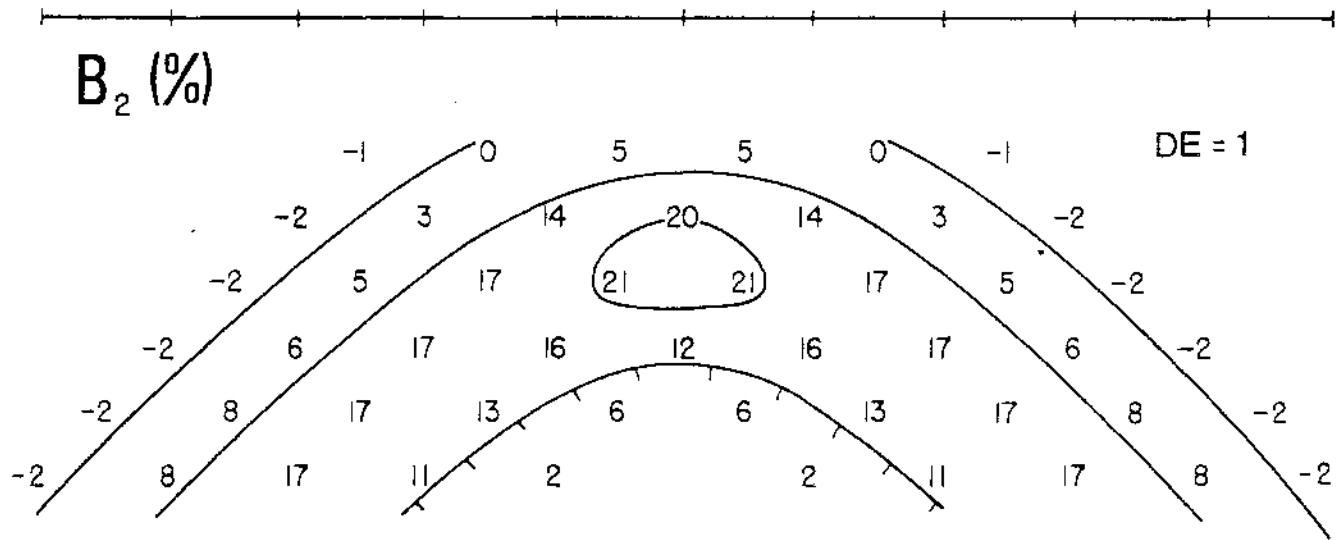


Fig 2-13

where G depends only on geometry, and where P , which contains the effects of the resistivities, is given by

$$P = 3 \frac{1 - \rho_2/\rho_1}{1 + 2\rho_2/\rho_1} + i 9 \phi^2 \frac{\rho_2/\rho_1}{(1 + 2\rho_2/\rho_1)^2} \quad (2-12)$$

The real term controls the apparent resistivity, while the imaginary or quadrature term controls the IP response. The real part asymptotes to 3 and to $-3/2$ for small and for large values of ρ_2/ρ_1 , respectively. That is, the sphere becomes saturated, so that further decreases or increases in ρ_2/ρ_1 have no effect on apparent resistivity. The quadrature part, upon which IP response depends, peaks at $\rho_2/\rho_1 = 0.5$, and goes to zero for both low and high resistivity contrasts. However, because IP response is given by phase, the magnitude of the IP response also depends on the in-phase potential. For most geometries the scattered in-phase potential, due to a conductive body subtracts from the incident potential, which serves to increase the phase; the opposite occurs for a resistive body.

Indeed, the calculated response for the sphere in Figure 2-19 peaks at $\rho_2/\rho_1 = 0.5$, and that for the $2 \times 4 \times 5$ body peaks at $\rho_2/\rho_1 = 0.3$. However, response curves for 2D bodies are different; they peak at $\rho_2/\rho_1 < 0.1$. The position of the peak seems to be controlled by body thickness; the peak occurs at lower values of ρ_2/ρ_1 for thinner bodies.

Hence, the correspondence between 3D and 2D bodies that we noted previously is not valid for ρ_2/ρ_1 less than about 0.3. For example, the IP response of a very conductive (say $\rho_2/\rho_1 = .02$) 3D body is negligible, while that for a 2D body of the same contrast is substantial. Thus a long massive sulfide body, even though it is very conductive, can produce a large IP anomaly.

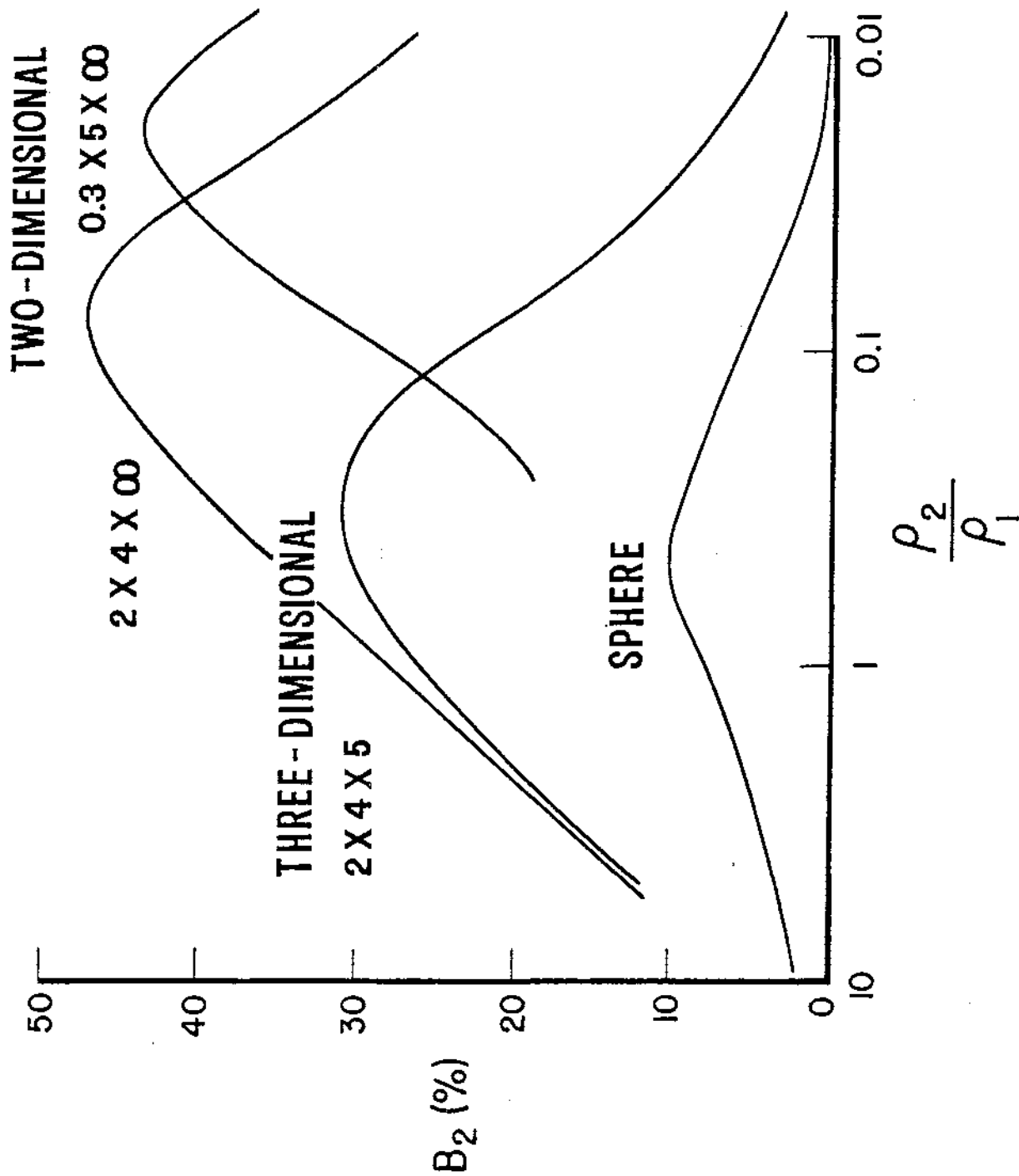
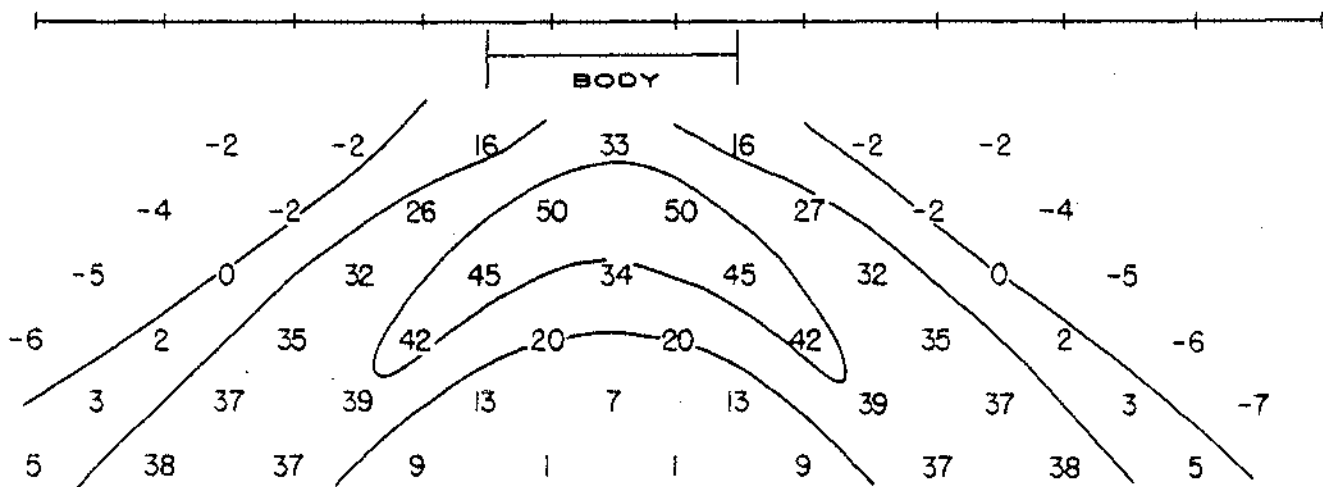
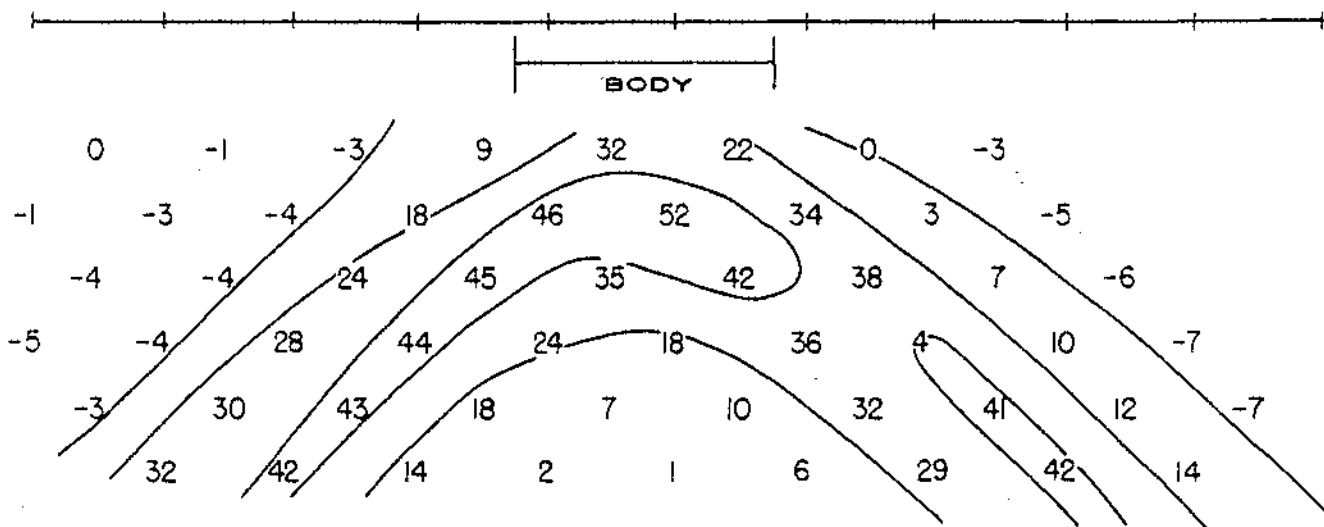
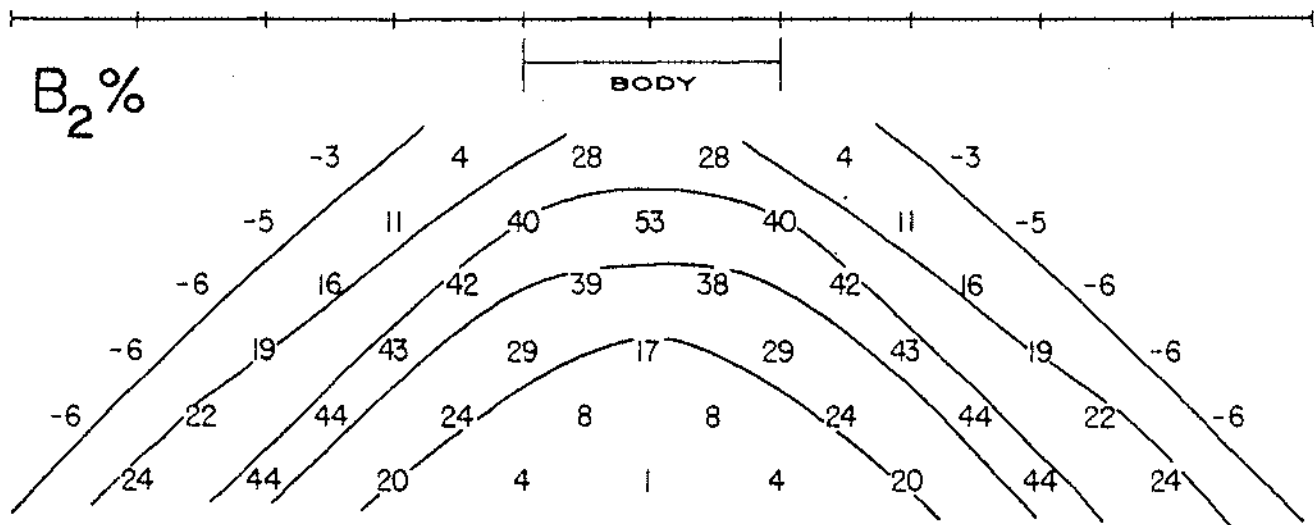


Fig 2-19

Furthermore, these types of models, which assume only a volume distribution of polarizable material, do not tell the whole story for very conductive bodies. If they did, there would be no IP response from a grounded pipeline. Nelson (1977) shows that IP effects from grounded conductors, such as pipelines, powerlines, or fences, can be calculated by assuming that the grounding points act as point sources of secondary field. It is necessary to use a similar approach to calculate the IP effect from very conductive massive sulfide or graphite bodies. Most of the IP response probably originates at the surface of the body where current enters and leaves, rather than at polarization dipoles throughout the body. IP response from good conductors, then, can be much larger than would be predicted by techniques which model a polarizable volume of material.

Electrode position along strike: Figure 2-20 shows the effect of moving the IP line along strike. Results are shown for three positions: the center of the body, the end of the body, and one unit off the end of the body. Moving the line away from the center produces an effect similar to that of increasing the depth of the body. Roughly speaking, moving the line from the center to the end of the body cuts the IP response almost in half, because the amount of polarizable material contributing to the response is halved. Then moving the line one unit off the end of the body further reduces the anomaly by about a factor of two for this resistivity contrast.

Electrode position across strike: In each of the above cases, the polarizable prism was centered at the center electrode on the IP line. Figure 2-21 compares the response of a centered shallow ($D = 0.5$) body with those for two other body positions. The magnitudes are about the same, but

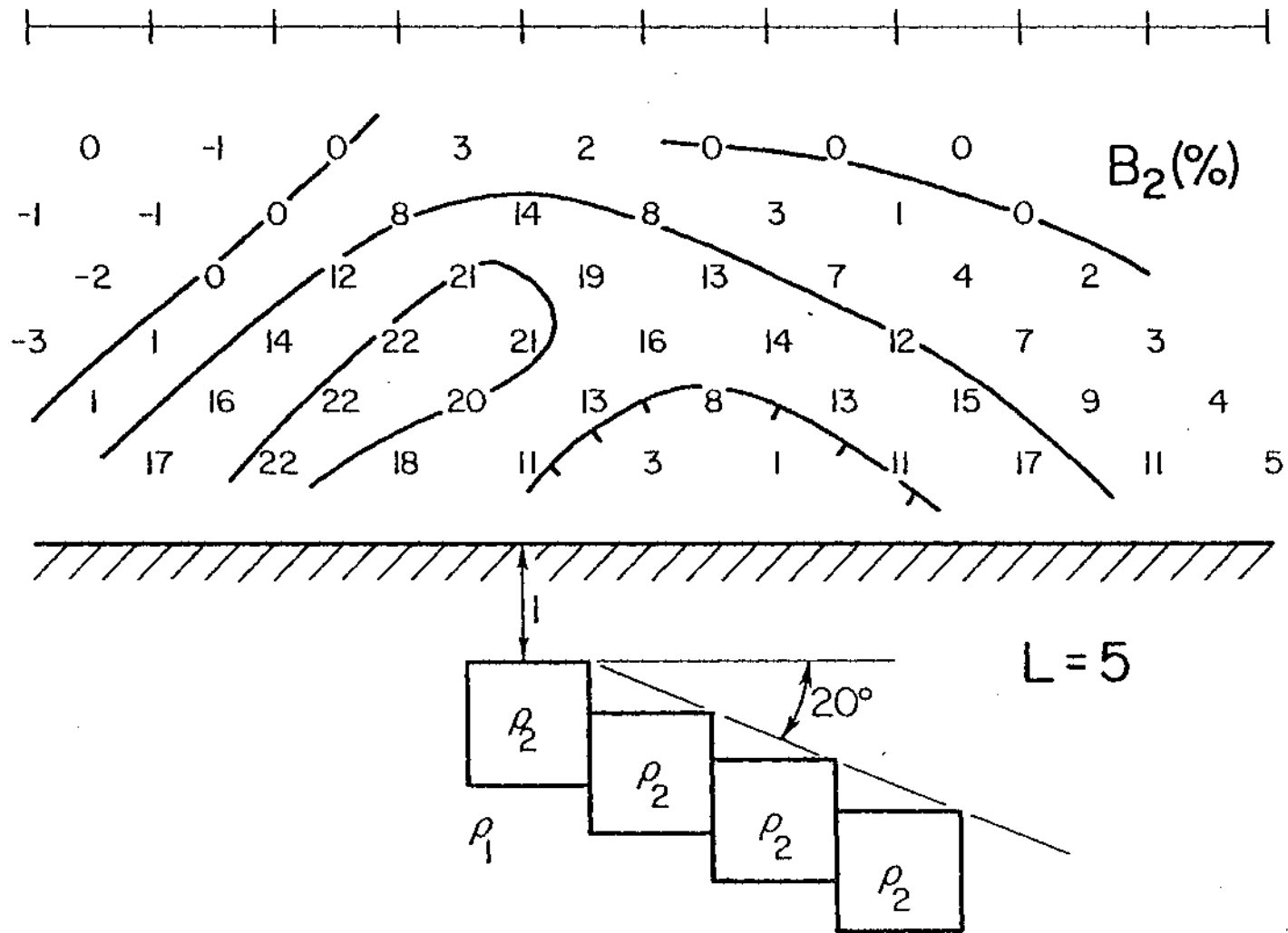


the patterns are slightly different. Asymmetric response patterns, such as that shown in the center of Figure 2-21, can be due to electrode-body geometry rather than to dip or to complex geology.

Dip: It is easy to model a dipping body by displacing the cubic cells into which it is divided. Figures 2-22 and 2-23 illustrate the effect of dip on the IP responses of conductive and resistive bodies, respectively. Each cell is one unit on a side, and the strike length is five units. For the conductive body, the highest IP response occurs on the side opposite the direction of dip, while for the resistive body the highest response is in the direction of dip.

In general, however, particularly for dips greater than 30 degrees, it is difficult to distinguish a dipping body from a vertical body on the basis of dipole-dipole data. Interfering bodies, resistivity changes, and electrode positioning can produce similar asymmetric effects. Coggon (1971, 1973) noted the same lack of dip resolution for the dipole-dipole array for 2D bodies. He showed that the gradient array is more definitive.

Multiple bodies: Superposition of IP responses from two or more bodies can be confusing. Figure 2-24 shows how the IP responses of two prisms superpose as they are moved closer together. Each prism is conductive ($\rho_2/\rho_1 = 0.2$), has dimensions 1 x 4 x 5 (W x DE x L), and occurs at depth 1. This case dramatically illustrates the need for sophisticated interpretation of IP anomalies: a pseudo-section should not be construed as a cross-section of the earth. Drilling would be unsuccessful if the hole were spotted over the IP high in the pseudo-section in the two cases where the bodies are separated. "Bullseye" pseudo-section anomalies such as these usually are caused by superposition. When the bodies join, their



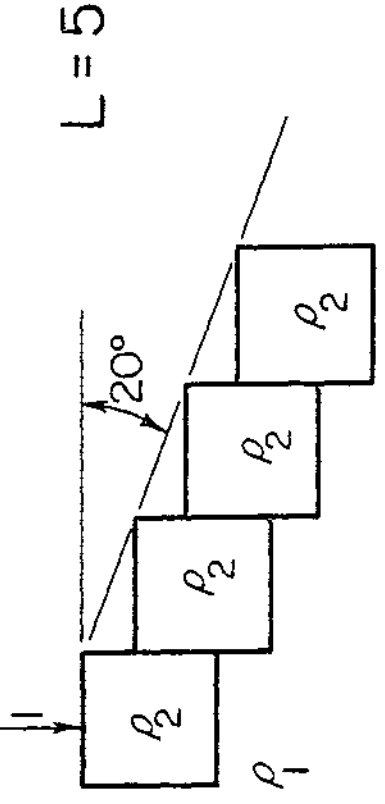
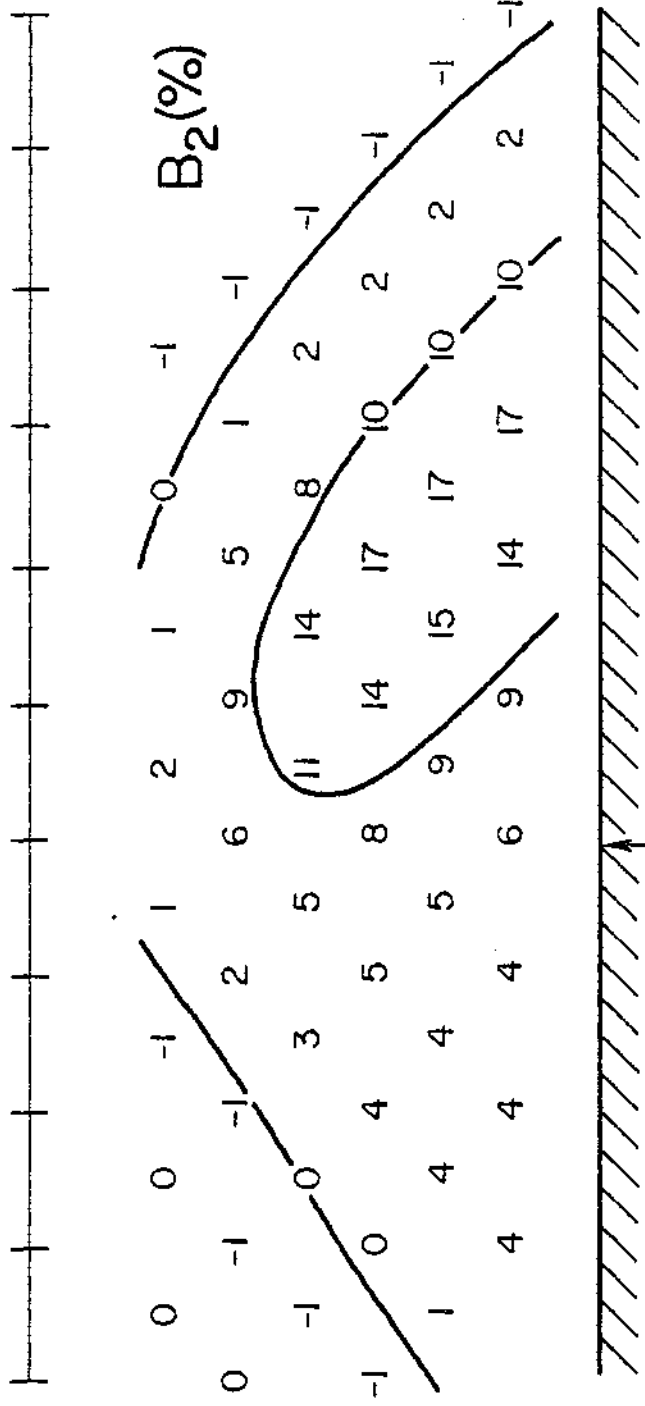
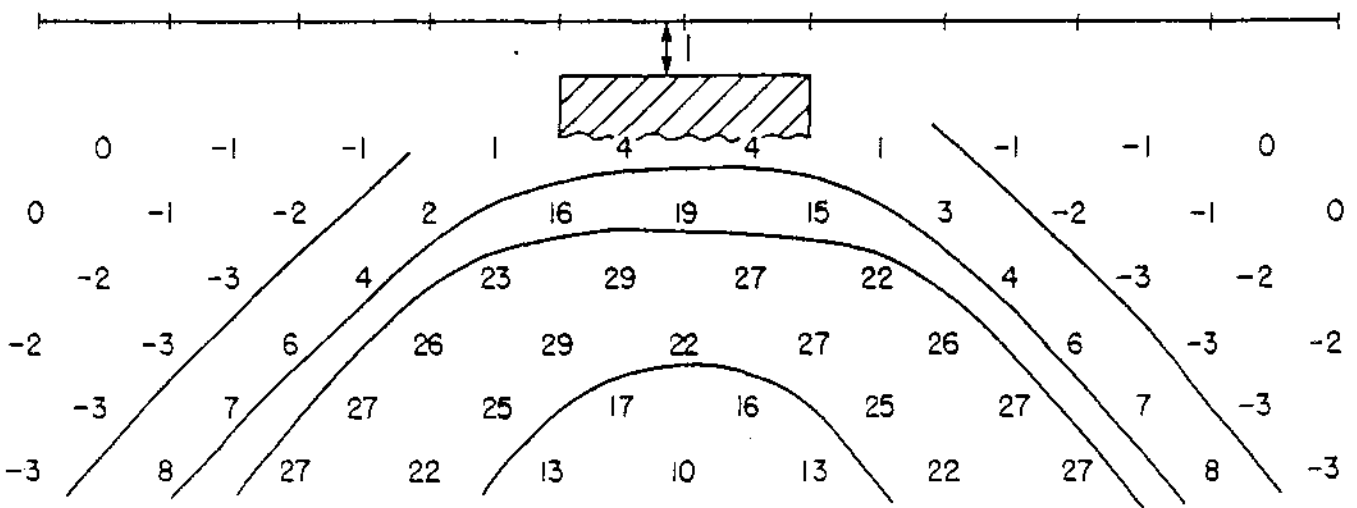
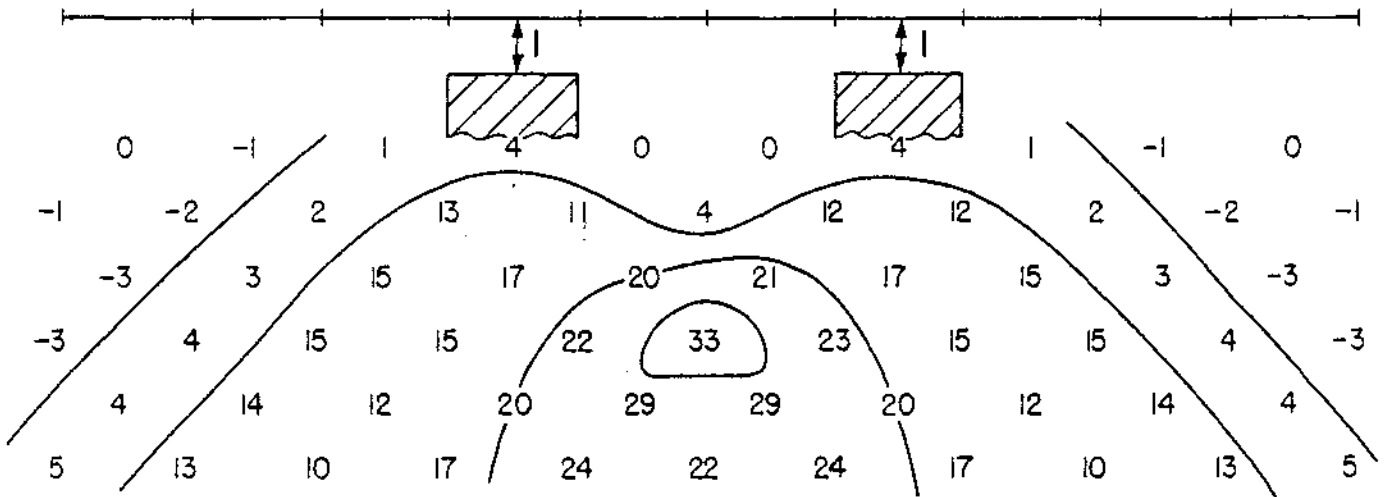
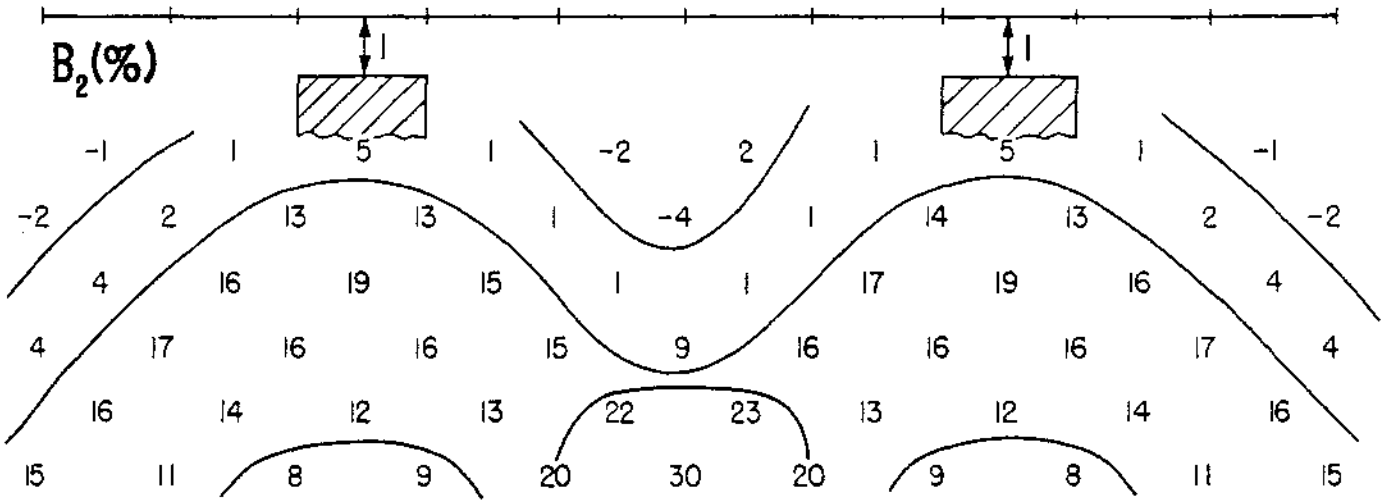


Fig 2-23

$B_2(\%)$

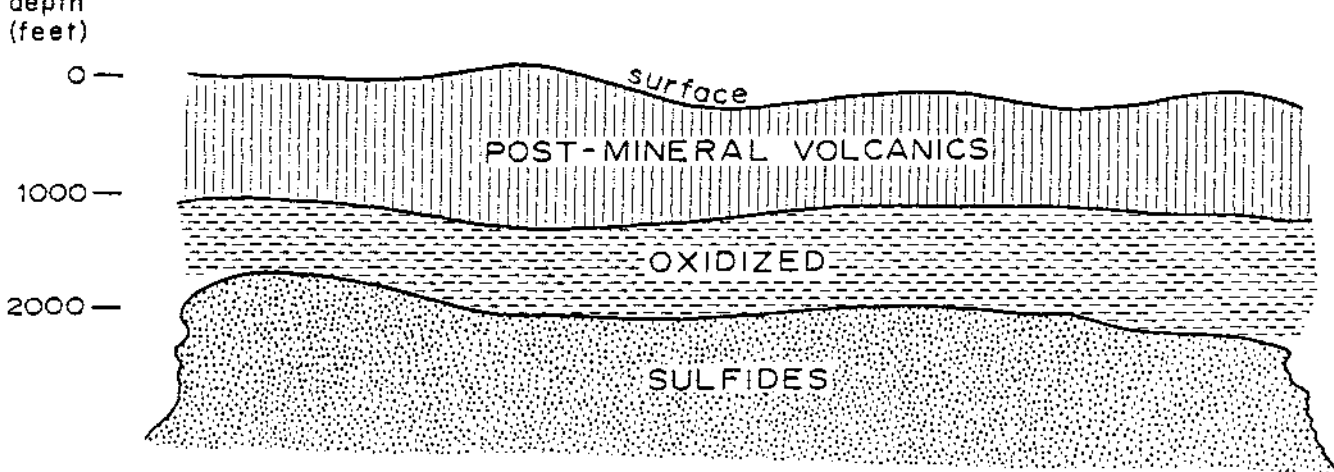
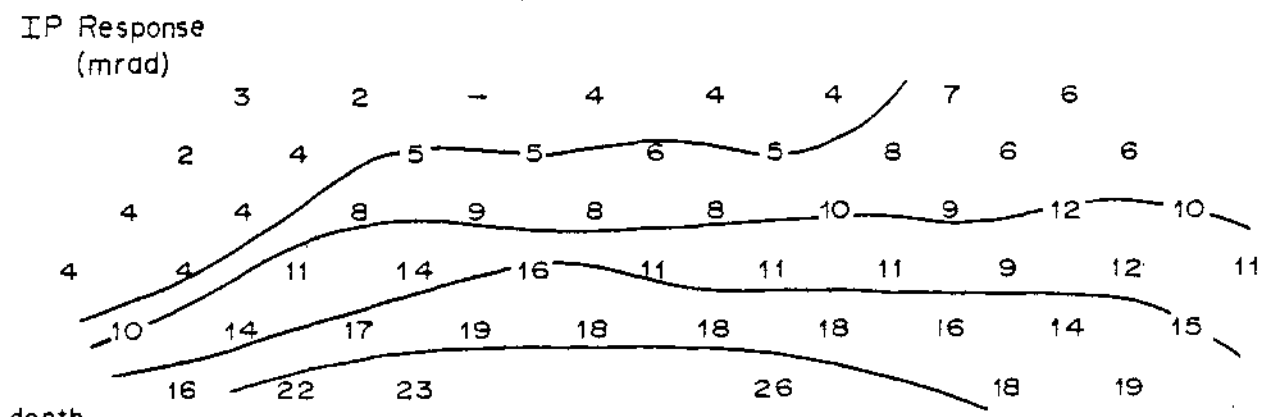
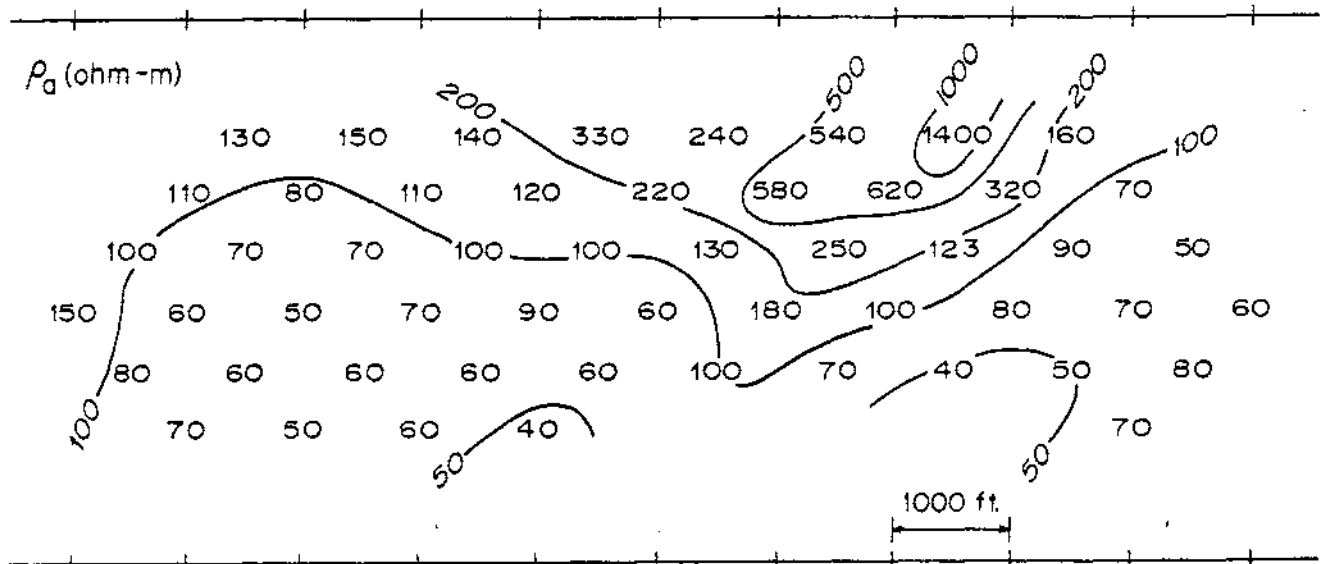


responses merge into that for a single wide body, as shown in the lower pseudo-section of Figure 2-24.

Applications

Deep sulfide mineralization: One of the main applications of IP is in porphyry copper exploration, because it provides a means of directly detecting disseminated sulfides, which do not appreciably affect the resistivity of the host rock. Now that digital receivers can provide very accurate IP data and EM coupling can be minimized by the phase extrapolation technique described above, IP is indispensable in searching for disseminated sulfides beneath post-mineral cover.

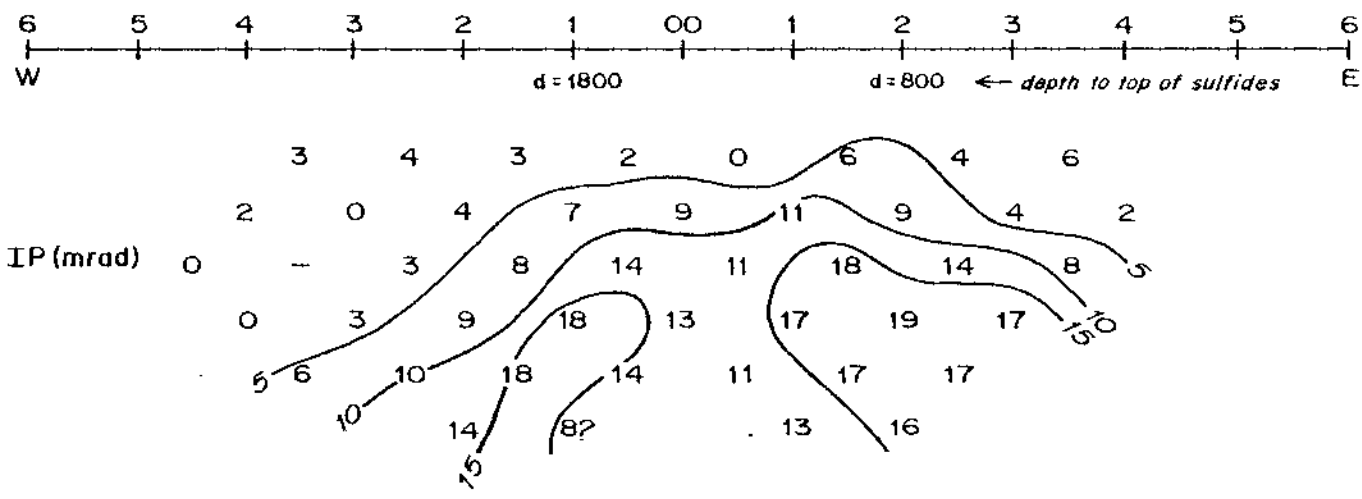
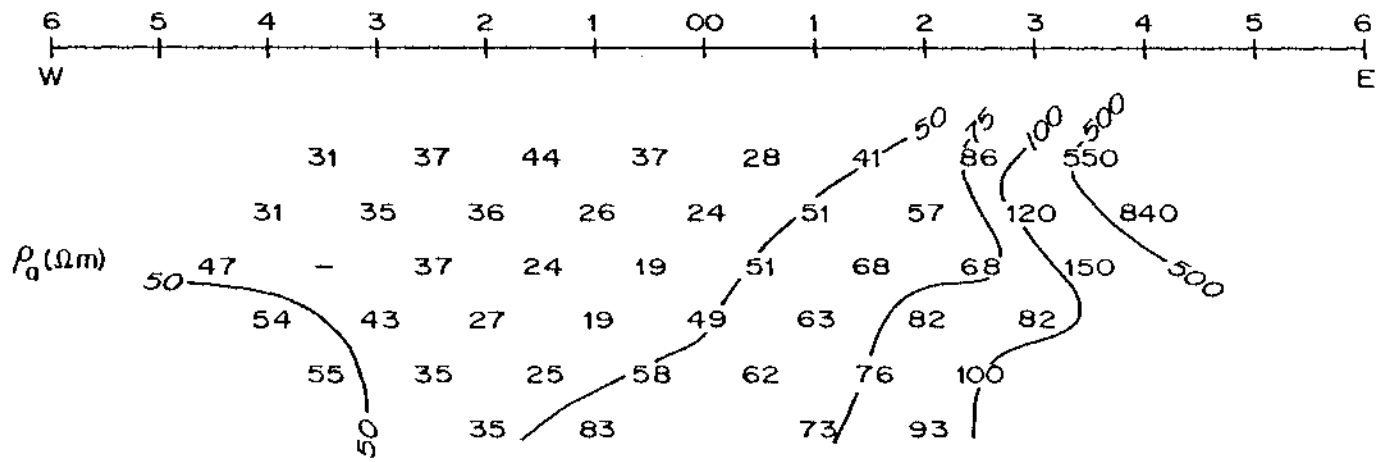
Figure 2-25, an IP line from the Kennecott, Safford, Arizona, porphyry copper deposit shows that sulfides can be detected at great depths beneath overburden of high resistivity cover. These data were collected in 1969 by G. D. VanVoorhis with the Kennecott Mk 3 phase-measuring IP gear. The overburden in this case consists of 1000 ft (305 m) of post-mineral volcanics plus 500 to 1000 ft (152 to 305 m) of oxidized host rock. The dipole length is 1000 ft (305 m); the sulfide body is detected by electrode separations of 3000 ft (915 m) or more. Accurate data and EM coupling removal are necessary, because the IP response is only about 0 to 20 mrad above a general background response of 5 mrad.



Low-resistivity cover

Figure 2-26 shows phase IP data over the Lakeshore porphyry copper deposit in Arizona. This example illustrates the use of IP in searching for disseminated sulfides beneath alluvium of low resistivity on a pediment adjacent to slightly mineralized outcrop.

The low apparent resistivities on the west end of the line are due to alluvium, while outcropping bedrock produces the high apparent resistivities on the east end of the line. The sulfide body producing the IP response lies at depths on the order of 800 ft (244 m) to the east and 1800 ft (549 m) to the west. Again accurate data and elimination of EM coupling are necessary to define the 15 mrad anomaly in a 3 mrad background. Computer modeling of the data indicates that the drilled sulfides account for the observed anomaly if the sulfide system has a bulk intrinsic response of 60 mrad.



2-16

Electromagnetic Methods

Introduction

Electromagnetic (EM) methods are capable of yielding information on the distribution of electrical conductivity in the shallow subsurface. Frequencies in the range 10 Hz to 100 kHz are most commonly used for EM probing of the earth's shallow crust. Anomalies obtained in EM profiling are interpreted in terms of a range of expected geologic occurrence. Mathematical and scaled physical models are used to produce catalogues of the predicted anomaly profiles with which to compare the observed anomaly profiles. Electromagnetic sounding is either parametric, in which case the frequency is varied while the transmitter-receiver separation is held constant, or geometric, in which case the reverse is true. Mathematical models are most commonly used to produce catalogues of predicted EM field descriptor versus frequency or versus separation with which to compare the observed field descriptor.

For the complex earths typically encountered in economic geology, sounding-profiling may be performed to obtain the maximum amount of information about the geoelectric section. This approach to delineating a complex earth shall be stressed in the ensuing.

Induction and current gathering

The EM methods of geophysical exploration depend upon the fundamental relationship between electricity and magnetism. An alternating current flowing in a wire at or above the earth's surface will cause an associated *primary* alternating magnetic field to pervade the space adjacent to the wire. If the space is partly or wholly occupied by conducting materials

such as rocks and ores, then *secondary* currents will be induced in these conductive materials by the primary field. The secondary currents in the rocks and ores will have associated with them *secondary* alternating magnetic fields. These secondary fields will react with the primary field to produce a *resultant* field. It is expected, then, that the resultant field will contain information on the geometrical and electrical properties of the distribution of rocks and ores.

Figure 2-27 portrays a generalized model of the earth in which a massive sulfide body is the object of search for the EM method. An alternating current flows through a *transmitting coil* creating an alternating magnetic field in its vicinity. This latter field, we shall assume for simplicity at the outset, induces alternating currents to flow in the massive sulfide body. These currents will circulate in closed loops only within the massive sulfide body under this assumption as shown by the arrows in Figure 2-28a. The actual configuration of these circulating currents will be determined by the geometry and location of both the transmitting coil and the massive sulfide body, and by the frequency of the field transmitted.

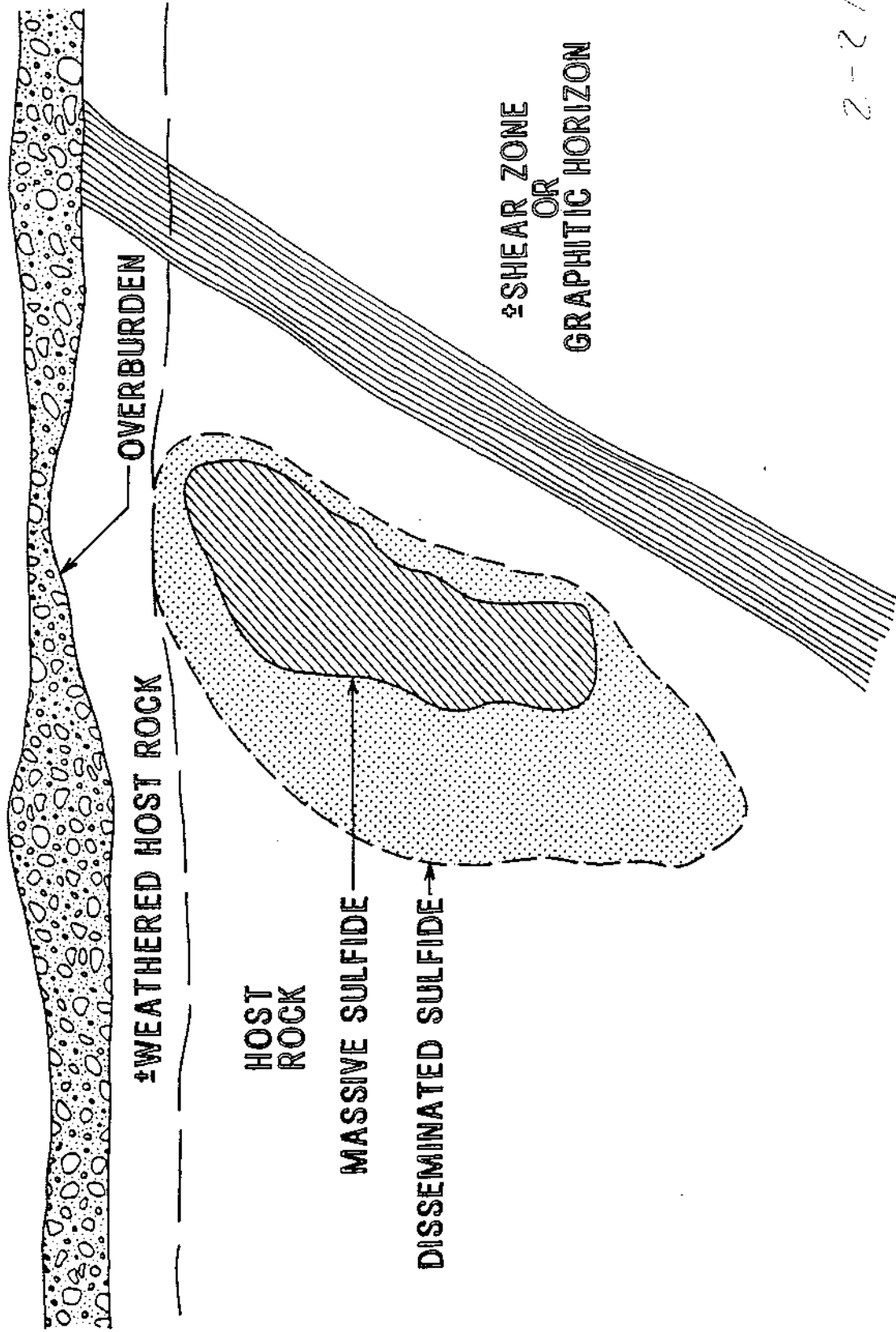
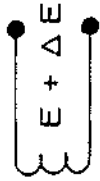
Let us now make a different assumption; induced currents flow in an assumed homogeneous earth, perhaps as depicted by the arrows in Figure 2-28b. The configuration of currents in Figure 2-28b is dictated only by the geometry and location of the transmitting coil and by the frequency of the transmitted field provided the surface topography is reasonably flat.

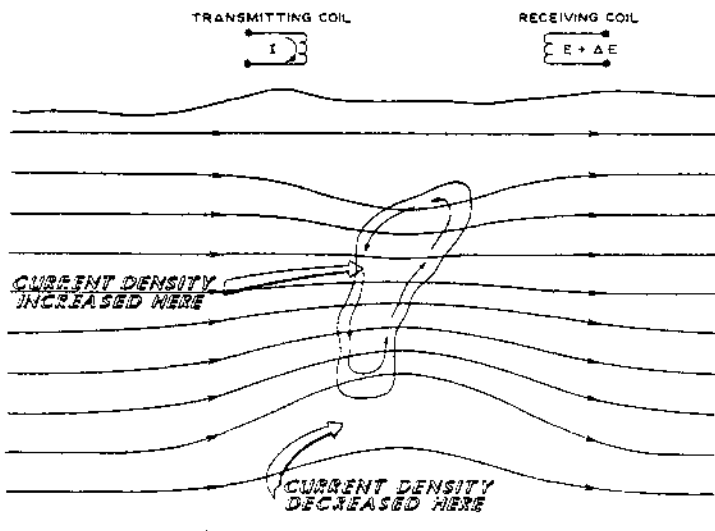
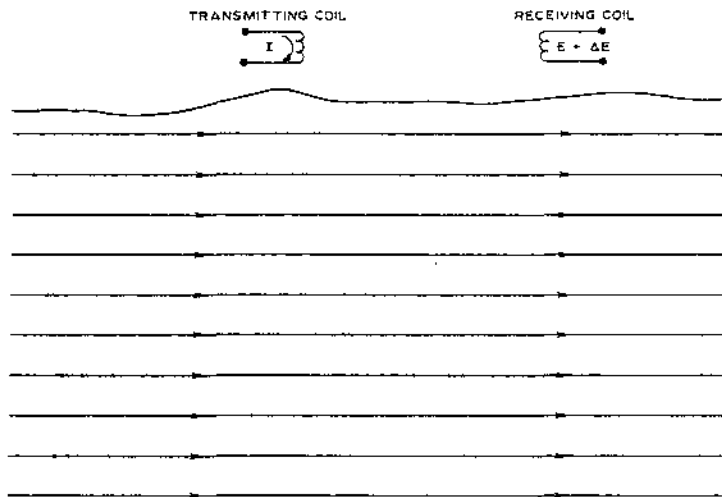
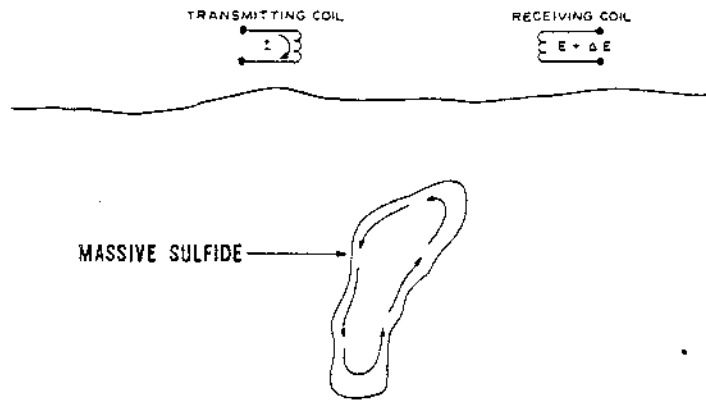
In the early days of EM prospecting one customarily attempted to eliminate currents of the type portrayed in Figure 2-28b and to allow only currents of the type portrayed in Figure 2-28a. In that manner one could

TRANSMITTING COIL



RECEIVING COIL





concentrate on the geometrical and electrical information about the massive sulfide body contained in the resultant field. Unfortunately, experience revealed that one could not ignore the currents induced in the host rock (Figure 2-28b) or, for that matter, currents induced in the overburden, the weathered layer, the graphitic shear, or the disseminated sulfides of the model of Figure 2-27. In fact, if one discarded the overburden, the weathered layer, the graphitic shear, and the disseminated sulfide halo, he still had to be content with the fact that the resultant magnetic field reflected the presumably superimposed effects of the two quite different current distributions of Figures 2-28a and 2-28b. Could one then still separate the effects of the two? For some time explorationists assumed that they could. Then it was realized that currents induced in a homogeneous half-space as in Figure 2-28b would be deflected, or gathered, into the massive sulfide body and intensified once that body was added to the geologic picture. Thus the resultant magnetic field contains information about the *total currents* which are a superposition of the *induced* circulating currents and *gathered* currents (Fig. 2-28c). Present day electromagnetic methods recognize interactions, not mere superpositions of currents initially induced in each of the six distinct elements of the geoelectric section depicted in Figure 2-27.

Separating the elements in the geoelectric section

Although not an objective in the past, we currently have as a main objective of the EM method an ability to detect and evaluate each element of the geoelectric section so that the resistivity environment surrounding the assumed one may be assessed. In this fashion, for example, we may hope

to recognize the massive sulfide ore from disseminated non-economic mineralization in a volcanogenic environment.

The EM exploration problem then may be described as a search for procedures to separate the geologic signal due to a massive or concentrated sulfide deposit from the geologic noise arising in the other elements of the geoelectric section (Fig. 2-27). The procedures must be sought with the realization that each noise source may shift the phase, alter the amplitude, and change the spatial spectrum of each component of the secondary fields scattered by the concentrated or massive sulfide deposit. If we are to solve this problem completely, we will need to (a) obtain precise data over several decades of frequency, (b) avoid spatial aliasing of data, (c) consider employing several configurations of the transmitter and receiver, and (d) use 3D complex models to simulate the real earth. Trade offs between complete solutions and economical or practical solutions are to be expected within this framework.

Ward (1979) reviewed recent papers which address the problems encountered by the EM method when faced with a real earth in which overburden, host rock, surface topography, buried topography, all elements of the geoelectric section of Figure 2-27, are included. He summarized their conclusions in Table 2-1.

Interpretation of EM data obtained over a model such as shown in Figure 2-27 can be accomplished by either forward or inverse methods. With the forward method, a catalogue of signatures is prepared to which observed signatures are compared by visual inspection or are matched with computed signatures by trial and error. The catalogues may be developed by scaled physical modeling, by analytic solution, or by numerical approximation.

Table 2-1 Summary of Effects of Extraneous Features in Electromagnetic Search for Massive Sulfides

<u>Feature</u>	<u>Effect</u>	<u>Interpretation problem re massive sulfide body</u>
Overburden	rotates phase decreases amplitude	depth estimates invalidated conductivity and thickness estimates invalidated
Host rock	rotates phase increases amplitude for shallow conductors increases or decreases amplitude for deep conductors changes shape of profiles fall-off laws changed	depth estimates invalidated conductivity and thickness estimates invalidated dip estimates invalidated
Surface and buried topography	introduces geologic noise	depth estimates invalidated conductivity and thickness estimates invalidated dip estimates invalidated may obscure sulfide anomalies
Halo	rotates phase increases amplitude	depth estimates invalidated conductivity and thickness estimates invalidated dip estimates invalidated
Weathered host rock	introduces geologic noise	may obscure sulfide anomalies may invalidate all quantitative interpretation
Faults, shears, graphitic structures	introduces geologic noise	may invalidate all quantitative interpretation may obscure sulfide anomalies

With the inverse method, observed signatures are automatically compared with numerically derived signatures via computer; the difference between the two is minimized in a least-squares sense and the ambiguity of interpretation is assessed statistically. Clearly the 3D models employed to interpret field data ideally must include all of the elements of the real earth, as in Figure 2-27. This task of modeling is a formidable one, the absence of which has led for example, to the drilling of overburden anomalies (Fountain, 1972, Scott and Fraser, 1973).

Depth of exploration

When a plane electromagnetic wave travels through earth materials, the amplitudes of its electric and magnetic vectors are attenuated exponentially as

$$\begin{Bmatrix} \vec{E} \\ \vec{H} \end{Bmatrix} \propto e^{-\beta d} \quad , \quad 2-1$$

in which d is distance travelled and β is the attenuation coefficient given by

$$\beta = \frac{\sigma\mu\omega}{2} \quad , \quad 2-2$$

in which σ is electrical conductivity in mhos/m, μ is magnetic permeability in henry/m, $\omega = 2\pi f$ is angular frequency, while f is frequency in Hz.

At a depth $d = 1/\beta$, the intensity of the incident electric or magnetic field has fallen off to $1/e$ of its value at the surface of the earth; this depth is called the skin depth or depth of penetration and is denoted by δ where

$$\delta = \sqrt{\frac{2}{\sigma\mu\omega}}$$

Assuming the magnetic permeability is that of free space in m.k.s, rationalized units, i.e. $\mu = \mu_0 = 4\pi \times 10^{-7}$ henry/m, then the skin depth is very closely approximated by

$$\delta = 500\sqrt{\rho/f} \quad 2-4$$

where ρ is the resistivity in Ω -m. At very large distances from a source of electromagnetic waves attenuation of this type would control the *depth of exploration*. Depth of exploration is defined as the maximum depth a body can be buried and still produce a signal recognizable above the noise. The depth of exploration for a sphere is much less than the depth of exploration for an infinitely extended buried horizontal interface. Hence both the ratio of signal to noise and the shape of the body influence the depth of exploration. The matter is even more complicated because the *geometrical decay* of magnetic field amplitude is $1/R^3$ for a loop source and $1/R$ for a line source where R is the distance from the source to a point of interest in the earth. To visualize the relative importance of attenuation and geometrical decay, we have computed each at a depth of 100 m beneath a loop and a line source on the surface of the earth for three frequencies and earth resistivities (Table 2-2). As one can see, attenuation is insignificant relative to geometrical decay. This fact is not often recognized in EM prospecting. Pridmore et al. (1979) have described it in more detail for a horizontal loop source.

Given that depth of exploration is such a difficult number to define, it is not surprising that only general rules of thumb have arisen in practice. For example, typical depth of exploration statements are: "a

TABLE 2-2 Attenuation and Geometrical Decay

	$\rho = 1000, f = 1000$	$\rho = 100, f = 10,000$	$\rho = 1000, f = 10$
Attenuation	$H_{100m}/H_{om} = 0.8$	$H_{100m}/H_{om} = 0.14$	$H_{100m}/H_{om} = 0.98$
Geometrical Decay Loop source	$H_{100m}/H_{om} = 10^{-6}$	$H_{100m}/H_{om} = 10^{-6}$	$H_{100m}/H_{om} = 10^{-6}$
Geometrical Decay Line source	$H_{100m}/H_{om} = 10^{-2}$	$H_{100m}/H_{om} = 10^{-2}$	$H_{100m}/H_{om} = 10^{-2}$

conductive interface can be detected at about 0.3 to 0.5 of the separation between transmitter and receiver," or "the depth of exploration of the EM method is 100 m to 200 m". This is unfortunate for the geologist who must utilize the method. In most instances, the depth of exploration can be determined by numerical modeling if knowledge of it is vital.

Time and frequency domains

Most EM surveys in the past were carried out in the frequency domain (FEM), i.e., measurements of the mutual impedance of two loops were made at one or more frequencies. However, time domain (TEM) methods have increased in popularity in recent years as exploration emphasis has shifted to the more difficult problems which involve conductive overburden and deep targets. In the time domain, one measures the decay of the secondary field after the transmitter current is shut off, as illustrated in Figure 2-2.

The difficult exploration problems of today require broadband measurements, which partly accounts for the increased use of TEM: information equivalent to that of a range of frequencies can be obtained without time lost in changing the transmitter frequency. Hence, surveys can be carried out more efficiently, particularly with a fixed source method, because a transmitter operator is not required and the data are acquired faster.

Figure 2-29 shows how FEM and TEM systems discriminate between good conductors and poor conductors. We assume that the conductor is a sphere with radius R and conductivity σ . The time domain response can be approximated by a single exponential decay:

$$h(t) = e^{-t/\tau} \quad 2-5$$

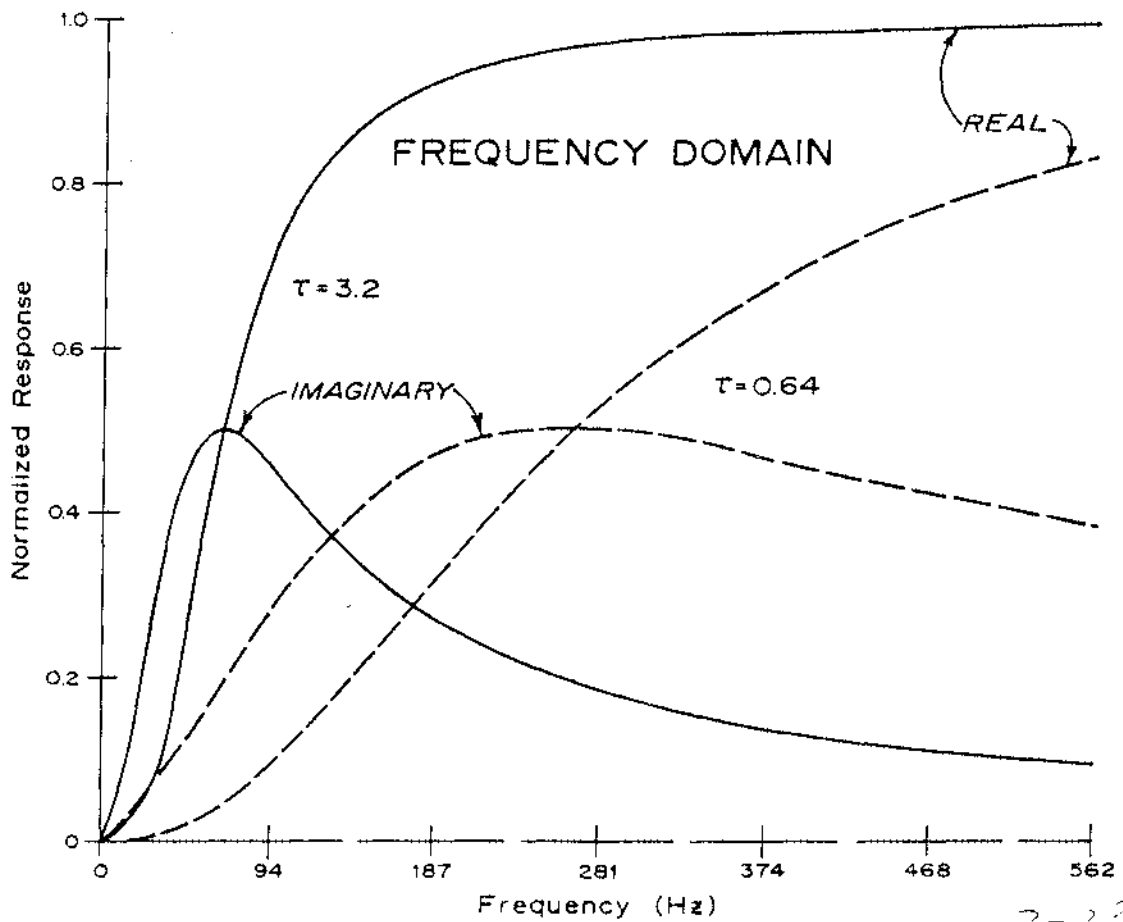
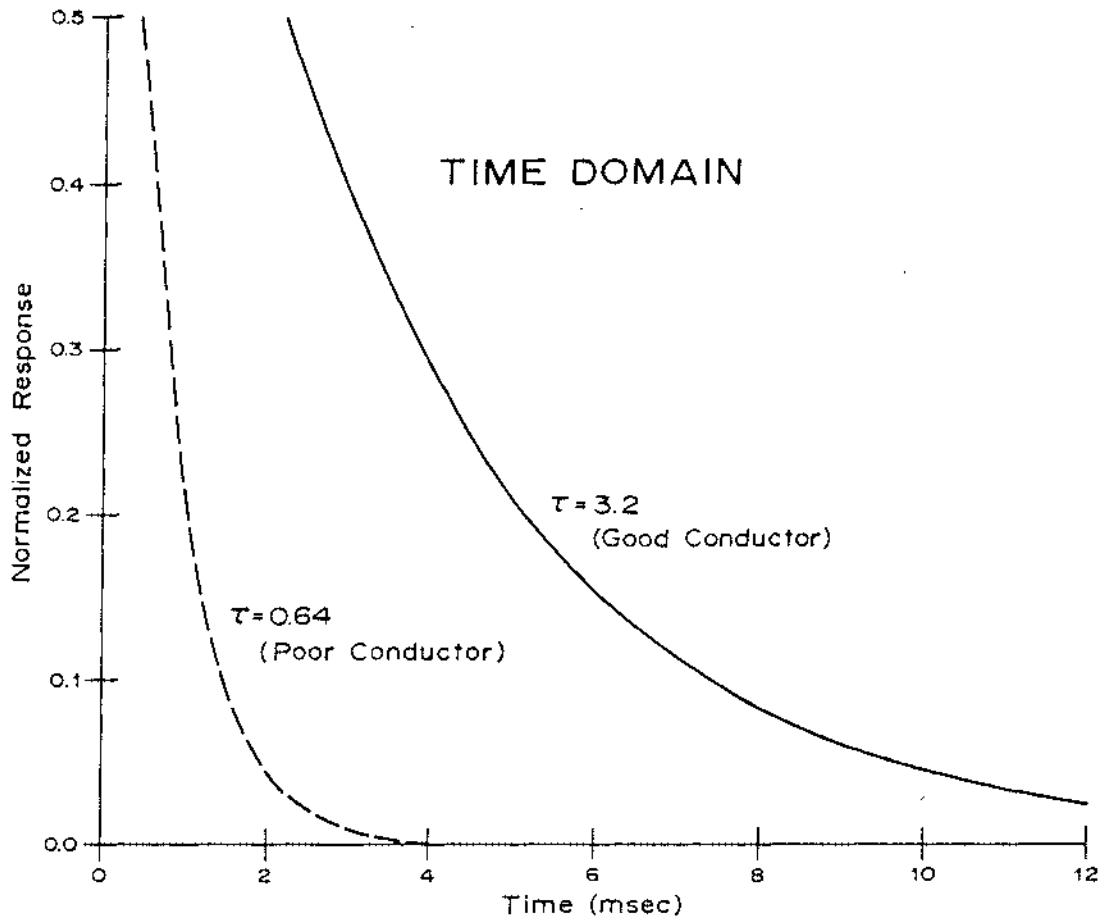
where the time constant, τ is given by

$$\tau = \frac{\sigma \mu_0 R^2}{\pi^2} \quad 2-6$$

where $\mu_0 = 1.26 \times 10^{-6}$ henry/m is the magnetic permeability of free space.

The equivalent FEM response is:

$$H(f) = \frac{(1/\tau)^2}{\left(\frac{1}{\tau}\right)^2 + 4\pi^2 f^2} + j \frac{2\pi \frac{f}{\tau}}{\left(\frac{1}{\tau}\right)^2 + 4\pi^2 f^2} \quad 2-7$$



Larger time constants, then, correspond to larger σR^2 products.

In Figure 2-29, we compare FEM and TEM responses of a good conductor ($\tau=3.2$ msec) and a poor conductor ($\tau=0.64$ msec). For spheres of radii 50 m and 100 m, respectively, these time constants correspond to conductivities of 10 and 0.5 mho/m, respectively. In the time domain, the poor conductor is characterized by a more rapid decay, while in the frequency domain the peak quadrature response and maximum slope of the in-phase response occur at a higher frequency for the poor conductor.

As Oristaglio, et al. (1979) show, there are certain theoretical advantages to TEM, in addition to the increased efficiency mentioned above. For example, noise due to topography, location errors, and coil orientation errors can seriously contaminate in-phase FEM measurements with certain coil configurations but are minimal with TEM, because measurements are made with the transmitter current turned off. Furthermore, TEM measurements at late times can eliminate geologic noise more effectively than can FEM measurements at low frequencies (Oristaglio et al., 1979).

FEM systems provide better rejection of natural EM field noise, but that advantage is negated by the TEM capability for much greater transmitter current with the same size generator if low duty cycles are used. For example, the Newmont EMP TEM system drives 100 amperes through the transmitter loop with only a 2 kv generator because the duty cycle is low.

Hence, even though FEM measurements are related to and derivable from, TEM measurements through the Fourier transform:

$$V_{FEM}(f) = \int_{-\infty}^{\infty} V_{TEM}(t)e^{-i2\pi ft}dt \quad 2-8$$

it would appear that there are both practical and theoretical advantages to TEM systems. However, at present, TEM systems are limited to about two decades of spectrum whereas FEM systems can accommodate four decades of spectrum; field examples will be presented later which will illustrate the advantage to be gained by use of a broader spectrum.

Interpretation

Introduction: Most early interpretation of EM prospecting data was based on scaled model results for thin-sheet conductors in air; the conductivity of overburden and host rock was ignored. While this type of interpretation yields reasonable results for appropriately shaped conductors in resistive shield areas (Grant and West, 1965; Ward, 1967), there are many cases where more sophisticated models are needed. Predicted EM anomalies can also be computed using the analytic solution for a sphere to represent a thick body (Best and Shamma, 1979). The present trend, however, is to use the power of computers to calculate EM response of the typical complex geoelectric section.

Electromagnetic scaled modeling is based on the similitude relations:

$$\sigma_f f_f L_f^2 = \sigma_m f_m L_m^2, \quad (\text{frequency domain}) \quad 2-9$$

and

$$\frac{\sigma_f L_f^2}{t_f} = \frac{\sigma_m L_m^2}{t_m}, \quad (\text{time domain}) \quad 2-10$$

where σ is conductivity, f is frequency, t is time, and L is length. The subscript f refers to the field parameters, and the subscript m denotes model parameters. If these dimensionless products are the same for the field and the model, i.e., if the model conductivity and/or frequency are increased to correct for the decreased lengths, then the geometry of the electromagnetic field in the scaled model will be the same as that in actual field work.

This *geometric scale modeling* works for EM systems which measure dimensionless quantities such as the mutual impedance between loops

normalized by their mutual impedance in free space, or the tilt angle of the magnetic field polarization ellipse. However, TEM systems measure V/I , the decay voltage in the receiver normalized by the transmitter current. Since V/I is not dimensionless, *absolute scale modeling* is required (Spies, 1976). The voltages measured in the scale model must be corrected by the factor

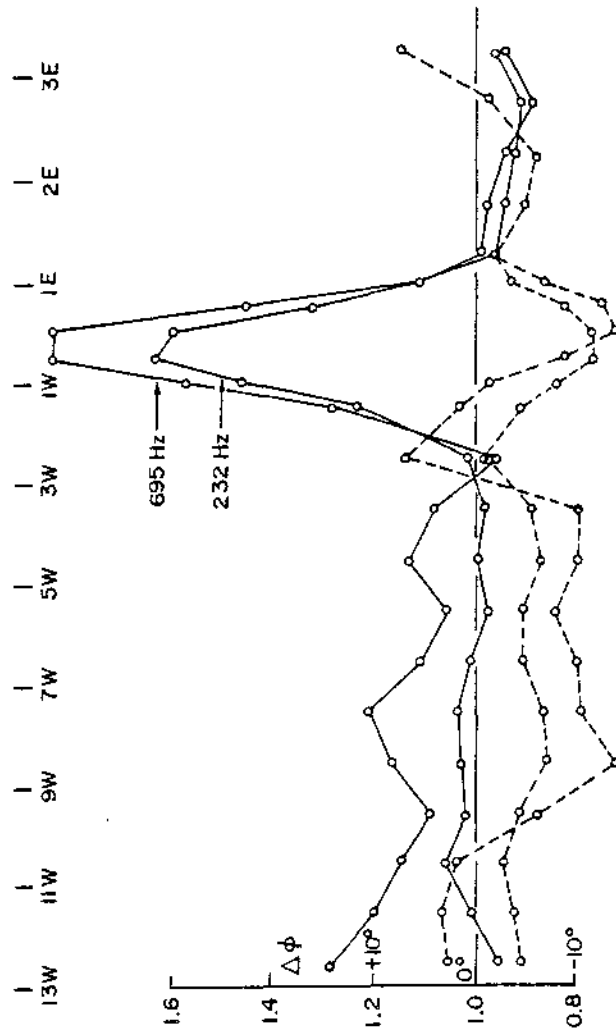
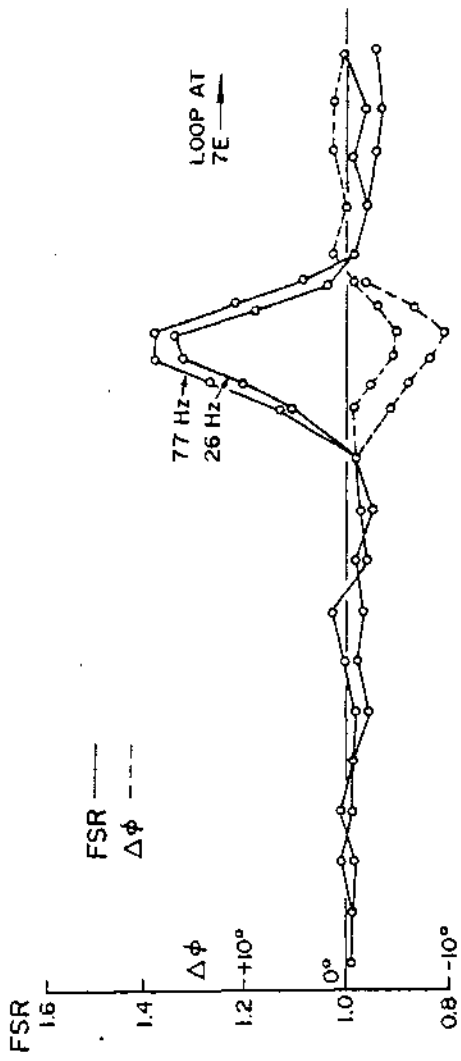
$$\frac{V_f}{V_m} = \frac{L_f t_m}{L_m t_f}$$

2-11

Several papers have been published recently on airborne electromagnetic (AEM) interpretation using scaled model results. Particularly important are those by Ghosh (1972), and Palacky and West (1973), Palacky (1975), Palacky (1978). A recent innovation is to use computers to interpret and classify AEM anomalies through a response diagram obtained by scaled modeling (e.g., Fraser, 1979).

Interpretation always must be based on a simplified model of the relatively complex earth. Fortunately, simplified models often are adequate if they are a reasonable representation of the earth. However, interpretation is bound to be erroneous if based on an inappropriate model. Hence thin-sheet model results cannot be used to interpret EM anomalies over thick or equidimensional conductors (Palacky, 1978).

Thin sheet and ribbon models: For example, Figure 2-30 shows Turam data over a *thick* conductor. Vertical loop EM results for the same conductor are illustrated by Hohmann, et al. (1978). Interpretation based on free-space, thin sheet models yields estimates of conductivity-thickness product (σt) of 500, 200, 70, and 25 mhos at 26, 77, 232, and 695 Hz,



2-35

respectively. Hence, the thin-sheet model is invalid, because the t_c estimate should be the same at each frequency.

The critical thickness, t_c , above which a body no longer behaves as a thin sheet (Lamontagne, 1970) is given by

$$t_c = 291 (\rho/f)^{1/2} \quad 2-12'$$

Numerical modeling indicates that the conductor responsible for the anomaly in Figure 2-30 has a bulk resistivity of 0.1 to 0.3 Ω -m and is about 30 m thick. Thus for $\rho = 0.3 \Omega$ -m, $t_c = 31, 18, 10,$ and 6 m at 26, 77, 232, and 695 Hz, respectively. For $\rho = 0.1 \Omega$ -m, the corresponding t_c values are: 18, 10, 6, and 3 m. The conductor of Figure 2-30 behaves as a "thick" conductor at all frequencies. The problem is general. The resistivities and thicknesses of massive sulfide ore bodies vary widely, but for a representative resistivity of 1 Ω -m and a frequency of 1000 Hz, the thin-sheet model applies only up to 10 m thickness.

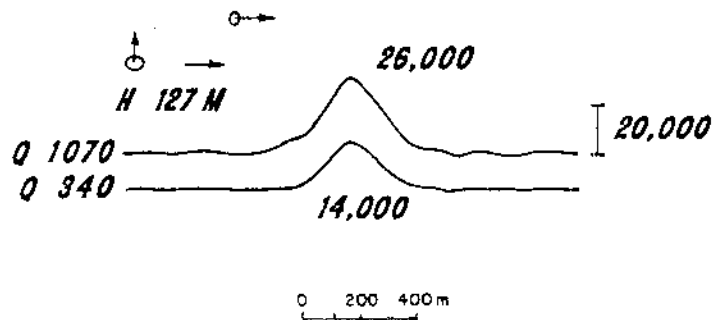
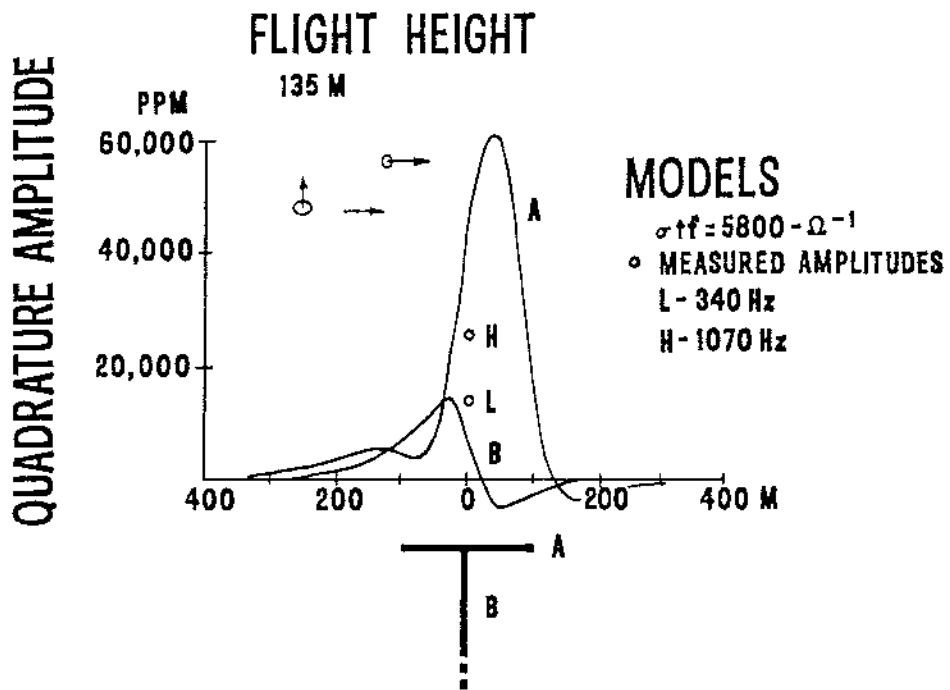
Airborne EM interpretation based on thin-sheet models often is confusing. Anomaly shapes may be different in the field data, and σt estimates for the same conductor with rigid boom and towed bird systems are far different. For example, Ghosh (1972) estimated the conductance of the Whistle orebody near Sudbury, Ontario, Canada, at 2 to 3 mhos based on thin-sheet interpretation of McPhar F-400 two-frequency towed bird quadrature EM data. Fraser (1972), obtained conductances ranging from 60 to 130 mhos on different flight lines over the Whistle orebody with the DIGHEM helicopter electromagnetic (HEM) system operating at 918 Hz. Palacky (1978) used horizontal ribbon models to show that discrepancies such as this are due to using thin-sheet models to interpret anomalies from

thick conductors. Because the important currents concentrate at the top of a thick conductor, the horizontal ribbon is a better interpretational model than the thin sheet. Figure 2-31 shows the difference in F-400 anomaly shape for the two models, along with field data for the Whistle orebody.

Sphere models: The analytic solution for the EM response of a sphere is quite useful for gaining insight and for interpreting anomalies due to roughly equidimensional conductors. The solution can be computed for a conductive sphere in a conductive host rock, but most studies have ignored the conductivity of the surrounding medium. Hence they apply only to resistive terrain, where current channeling is unimportant.

Lodha and West (1976) discuss interpretation procedures for the sphere model and show that the estimated depth to a conductor generally is too small. True depth lies between the depths interpreted for sphere and for vertical thin sheet models. Best and Shamma (1979) compare the responses of a number of AEM systems to a sphere in free space with current channeling neglected. Most importantly, theirs is the first study of AEM lateral attenuation for conductors off the flight line. They show, for example, that the lateral attenuation for the standard DIGHEM system is 50 times larger than that of the EM-30 system.

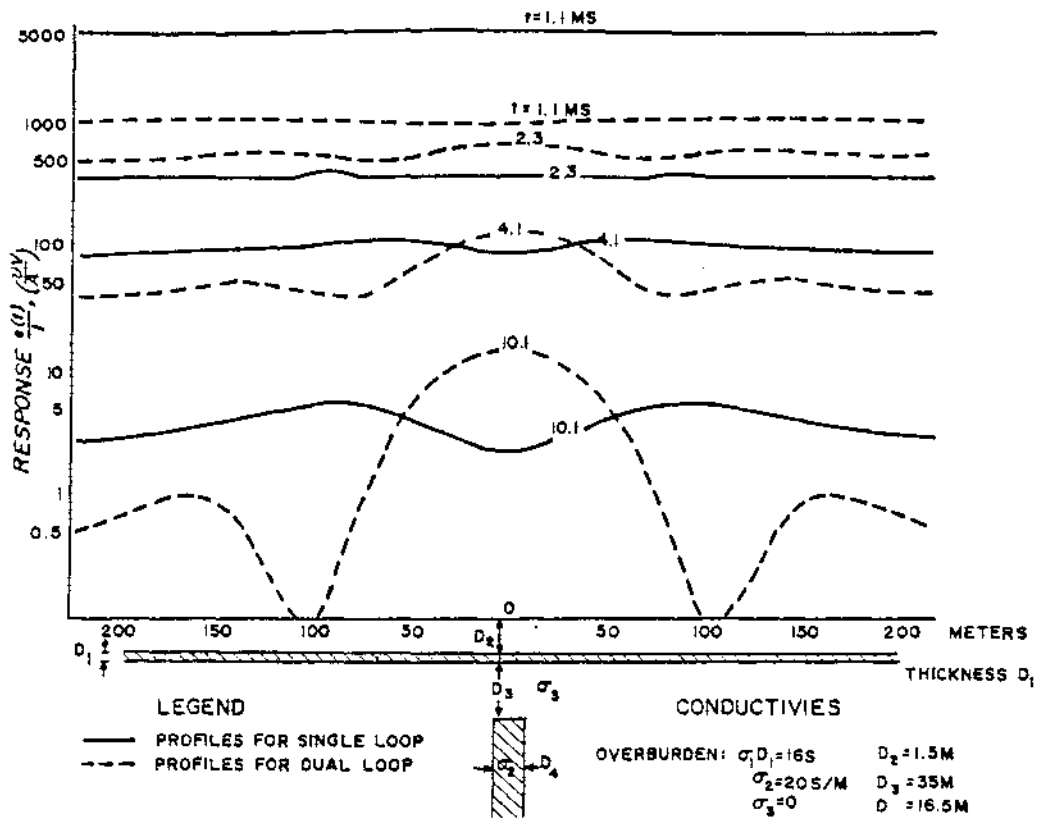
TEM modeling: A number of recent scale model studies have lent new insight to TEM. A particularly important paper (Spies, 1975) compares the single loop and dual loop TEM responses of a vertical conductor beneath homogeneous conductive overburden. A single loop, serving as both transmitter and receiver, couples well with equidimensional or thin horizontal conductors, but produces no response when directly over a



vertical sheet conductor. Two penalties arise if a dual loop survey is performed: a) a single loop system is more efficient than a dual loop system, where separate transmitter and receiver loops both must be moved along a tranverse line, and b) geological noise is higher in a dual loop survey when the overburden is of inhomogeneous conductivity or variable thickness. Of course, single loop operation has been possible only in the time domain, where measurements are made with the primary field off; the Unicoil system described later permits single loop operation in the frequency domain. Typical loop size for single loop time domain systems is 100 m x 100 m.

To compare the two techniques in an environment containing conductive-overburden, Spies set up a model consisting of a 335-mho vertical conductor beneath 16 mho conductive overburden. For example, the overburden might be 16 m of 1 Ω -m material, effectively screening out any response from a deeper body with most EM methods. Profiles for the two configurations are shown in Figure 2-32. For early times up to, say, 2.3 msec after the primary current is cut off, the response is primarily due to the overburden. The response of the dual loop system to the overburden is only one fifth that of the single loop system at 1.1 msec. At later times, the vertical plate response is clearly evident. But at all times the dual loop anomaly of the vertical sheet is larger than the single loop anomaly.

Two and three dimensional modeling: One of the most significant advances in EM interpretation in recent years was made by Lajoie and West (1976), in their study of a thin 3D conductor in a conductive earth. Only numerical solutions with large matrices to invert are possible for such



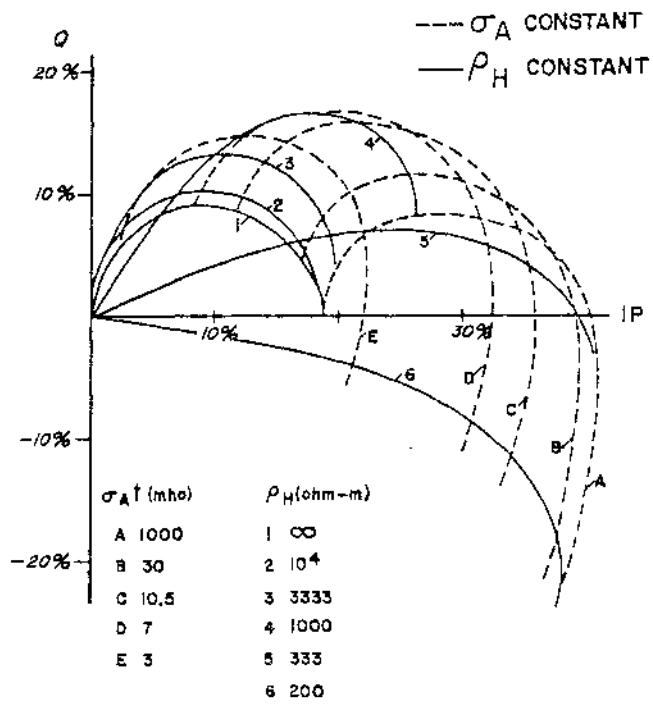
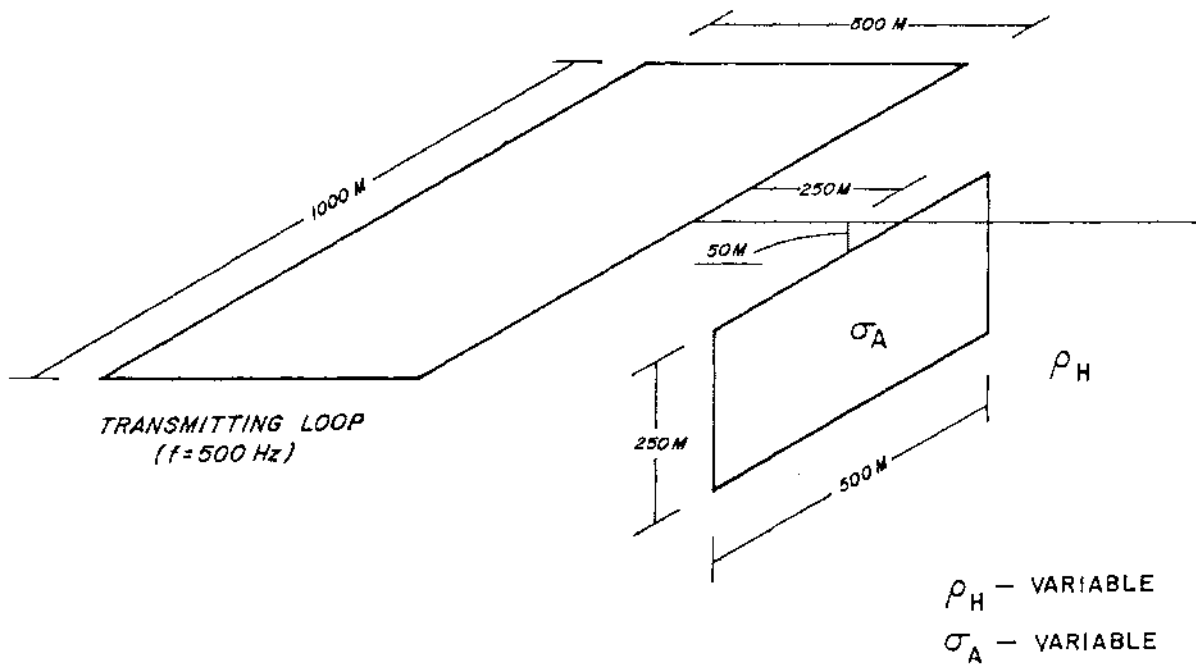
2-32

models. Several good 2D numerical solutions, both differential and integral equation, have appeared in recent years. They are useful for interpreting anomalies due to very long conductors excited by a large loop, current line, or natural fields. However, 2D solutions do not include current channeling and thus are quite limited in application. Only one EM solution (Hohmann, 1975) has been published for the general 3D case in mining applications, and it is limited in conductivity contrast and frequency.

By separating the induction and channeling currents, Lajoie and West were able to obtain accurate results for high contrasts and high frequencies. Theirs is the first thorough analysis of the dramatic effect of current channeling. Although the model is a thin 3D sheet and hence is not a general 3D model, it is sufficient for studying current channeling, and their results greatly increase our understanding of the EM method.

The essential features of conductive host rock effects are shown in Figure 2-33. The transmitter is a large loop through which current is driven at 500 Hz. The conductor is a thin plate buried at 50 m in an earth of variable conductivity. In Figure 2-33b, the in-phase (IP) and quadrature (Q) anomalies are plotted for various plate conductances ($\sigma_A t$) and half-space resistivities (ρ_H). The solid lines show the effect of varying $\sigma_A t$ with ρ_H constant, while the dashed lines show the effect of varying ρ_H with $\sigma_A t$ constant.

Solid curve 1 is the response that would be measured over plates of various conductivity - thickness product in free space. It is the basis for all past conventional interpretation of EM data. The response is mainly quadrature for low $\sigma_A t$ (curve E) and mainly in-phase for high $\sigma_A t$ (curve A) with a gradual transition between. The response is not much



different for a high-resistivity earth ($10^4 \Omega\text{-m}$) as shown by curve 2. However, for $\rho_H = 10^3 \Omega\text{-m}$, as shown by curve 4, the response is quite different from the free-space case, even though this is still a relatively high resistivity. For earth resistivities of 333 and 200 $\Omega\text{-m}$ (curves 5 and 6) the response diagrams hardly resemble that for free space; interpretations based on curve 1 obviously would be erroneous.

For all plate conductances, as the resistivity of the half-space decreases, the quadrature component anomaly increases first, because the currents induced in the weakly conducting earth and channeled into the plate are largely quadrature. As the earth's resistivity is reduced, more current is induced in the earth and channeled into the plate, so that the anomaly increases. The increased anomaly amplitude caused by conductive host rock could result in a serious under-estimate of depth. Unfortunately, anomaly enhancement for those poor conductors which constitute geologic noise is relatively greater than for good conductors. Furthermore, the phase of the anomaly rotates clockwise due to the phase rotations of the channeled currents and of the incident and scattered magnetic fields. Note that for $\rho_H = 200 \Omega\text{-m}$ the quadrature anomaly changes sign. In areas of conductive overburden, a poor conductor may be mistaken for a better conductor, because the overburden rotates the anomaly toward the in-phase component. Finally, current channeling makes a dipping conductor appear to dip more steeply, increasing the chance of drilling it from the wrong side.

Further progress in EM prospecting requires new numerical solutions for general 3D conductors in the earth, coupled with new interpretation techniques for multi frequency and time domain data. Such solutions will

require both sophisticated mathematics and large computers, but they have the exciting potential of greatly improving the effectiveness of EM prospecting techniques.

Field configurations, natural field methods

Introduction: These methods utilize the earth's natural electric and magnetic fields to infer the electrical resistivity of the subsurface. Figure 2-10 is a generalized natural magnetic field amplitude spectrum taken from Matsushita and Campbell (1967). There is, of course, a corresponding electric field spectrum, related through Maxwell's equations.

In general, the fields above 1Hz are due to a) worldwide thunderstorms, the principal centers being in South America, Africa, and the Southwest Pacific, b) radio stations, and c) power distribution systems. Because the ionosphere is a conductive plasma the energy propagates in a wave guide mode in the earth-ionosphere cavity. The small resonant peaks between 5Hz and 50Hz shown in Figure 2-10 are due to constructive interference.

Below 1Hz the fields, called micropulsations, are mainly due to the complex interaction of charged particles from the sun with the earth's magnetic field and ionosphere. As Figure 2-10 shows, the amplitude of the electromagnetic field increases with decreasing frequency below 0.1Hz.

These natural fields represent noise for controlled-source electromagnetic (CSEM) methods, but they are the source fields for natural field electromagnetic (NFEM) methods. Because low frequencies are needed for deep penetration, it is easy to see from Figure 2-10 why NFEM has been used so extensively for crustal studies and deep exploration: the source fields increase at low frequencies for NFEM, while the noise increases at low frequencies for CSEM.

While frequencies below 1Hz can be useful in regional studies, higher

frequencies usually are employed in mineral exploration because of their greater field efficiency and greater resolution.

The magnetotelluric method: In the magnetotelluric (MT) method one measures the ratio between orthogonal electric field (E_x) and magnetic field (H_y) components at the earth's surface over the frequency range 10^{-3} Hz to 10 Hz. This ratio is known as the MT impedance, so one can think of the earth as a linear system with input H_y and output E_x . The MT apparent resistivity is given by

$$\rho = \frac{0.2}{f} \frac{E_x^2}{H_y^2},$$

where f is the frequency, and E_x and H_y are measured in units of mv/km and gammas, respectively.

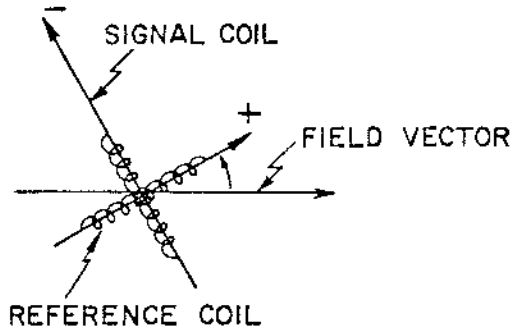
The MT method was invented in the early 1950's. Since then the method has been refined considerably, but it is still beset with problems, primarily due to noise in the measurements and a lack of adequate interpretational aids. Recent advances in data collection (Gamble, et al., 1979), in-field data processing (Wight, et al., 1977) and 3D numerical modeling (Ting and Hohmann, 1980) should alleviate some of these problems.

Audiomagnetotellurics (AMT), the variant of MT most often used in mineral exploration (Strangway, et al., 1973), simply refers to MT in the audio frequency range of 10Hz to 10^4 Hz. The magnetic field is measured with a small coil, while the electric field usually is measured with a 30 m grounded wire. Unfortunately, weak source fields and a lack of sophisticated instruments and interpretation techniques have hindered the application of AMT.

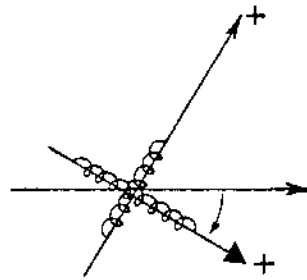
Tensor measurements, i.e. simultaneous measurement of E_x , E_y , H_x , H_y

and H_z , are necessary to compensate for varying source fields, but they must be coupled with 2D and 3D numerical solutions for interpretation. Through recent advances in electronics, portable tensor AMT receivers will soon be available, so that AMT will assume a more prominent role in mineral exploration. It is a simple technique, can be made highly portable, does not require accurate distance measurements, and does not require a transmitter. AMT is particularly useful in searching for flat lying conductors beneath overburden of high resistivity.

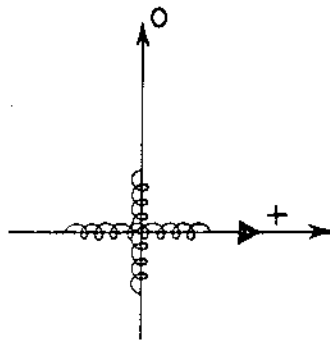
AFMAG: The AFMAG method (Ward et al., 1958; Ward, 1959) utilizes frequencies near the peak of the natural magnetic field spectrum at about 100Hz in Figure 2-10. To make a measurement, a pair of orthogonal coils is rotated about a vertical axis until one of the coils, called the reference coil, lies in a horizontal plane and along the direction of maximum magnetic field strength, while the other, called the signal coil, lies along the direction of minimum magnetic field strength as in Figure 2-34. The direction of maximum field so found is called the *azimuth*. Once this direction is found, the plane of the axes of the two coils is placed in the vertical plane through the azimuth. Again the coils are rotated, this time about a horizontal axis, until the reference coil is aligned along the direction of maximum field strength. The tilt of the reference coil relative to the horizontal is then measured as the *tilt angle*. The tilt angle will vary systematically across subsurface inhomogeneities such that the axes of current flow in the inhomogeneity can be detected and delineated. Because of the distant sources and uniform inducing field, current gathering usually dominates over local induction with the method.



NET NEGATIVE METER READING



NET POSITIVE METER READING



NET ZERO METER READING

However, it can be useful for cheaply and quickly mapping faults and shears and for detecting deep large conductors such as graphitic zones beneath the Athabasca sandstone. An airborne version of AFMAG was flown for several years. The limitations of AFMAG have been described by Ward et al. (1966) and include time variant intensities and directions of inducing fields with concomitant changes in locations and intensities of anomalies.

As with AMT, we can expect a resurgence of AFMAG as microprocessors are utilized to build tensor receivers. Such receivers will compensate for varying source fields by measuring simultaneously the vertical and both horizontal components of magnetic field.

VLF: Because very low frequency (VLF) fields in the range 10 to 30 kHz are generated by distance transmitters for navigation and communication, we classify VLF as a natural field method. At least one station can be monitored anywhere on the earth, so the explorationist requires only a receiver to conduct a survey. However, the frequencies are too high for much penetration, so that the method is useful only for geologic mapping, i.e. locating faults and contacts, and for probing for conductors beneath less than 50 meters of highly resistive surface rocks.

The VLF source is a vertical electric dipole, so that the undisturbed magnetic field lines are horizontal circles concentric about the antenna. The electric field lines are radial. By measuring the surface impedance (E_r/H_ϕ) one can determine an apparent resistivity as in MT. However, a secondary vertical magnetic field is created over a conductor; hence the most common VLF technique measurements are made of the tilt angle and ellipticity of the magnetic field. Receivers consist of orthogonal coils,

weigh less than 5 pounds, and are very reliable and simple to operate. In practice, one determines the polarization ellipse in a vertical plane oriented in the direction of maximum horizontal magnetic field. Strong conductors tend to rotate the horizontal magnetic field to be perpendicular to their strike. If possible, one should choose a transmitter whose azimuth is roughly in the direction of regional strike. Because anomalies are of crossover type it often is useful to process the data so that crossovers become highs (Fraser, 1971).

Several airborne VLF systems are available, and are used primarily for geological mapping.

Field configurations, controlled source, ground methods

Introduction: The number of configurations of transmitter and receiver used in EM prospecting is large (Grant and West, 1965; Ward, 1979). This leads to confusion concerning the selection of a particular configuration for a particular exploration problem. However, some semblance of order can be achieved by assigning each particular configuration to one of the four basic configurations illustrated in Figure 2-35.

Two loop, roving coil pairs, fixed orientation: The transmitting coil (T_x) may be oriented with its axis vertical, called a vertical magnetic dipole or a horizontal loop, or with its axis horizontal, called a horizontal magnetic dipole or a vertical loop. If a horizontal magnetic dipole is used, its axis may be pointed at the receiver (R_x) or be orthogonal to this direction. Three orthogonal transmitting coil orientations are thus possible. Similarly, three orthogonal receiving coil orientations are possible.

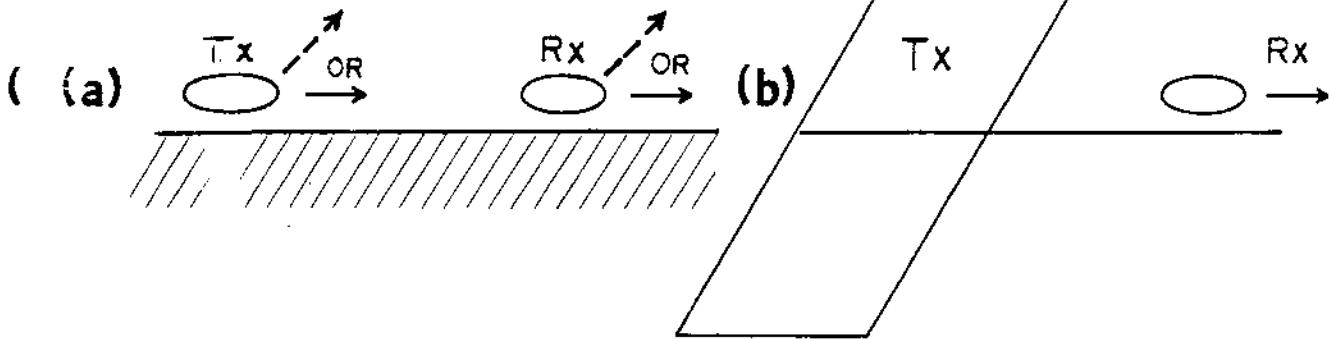
In the so-called *horizontal loop* EM method, both the receiving and transmitting coils have their axes vertical and the coil pair is transported, with constant coil separation, in-line in a direction normal to strike as in Figure 2-36a. This method is one of the oldest and most commonly used (Grant and West, 1965).

In the *vertical coaxial loop* EM method (Fig. 2-36b) both the receiving and transmitting coils have their axes horizontal, in-line, and the pair is transported, with constant coil separation, a) in-line in a direction normal to strike (Grant et al., 1966) or b) broadside in a

GROUND EM METHODS

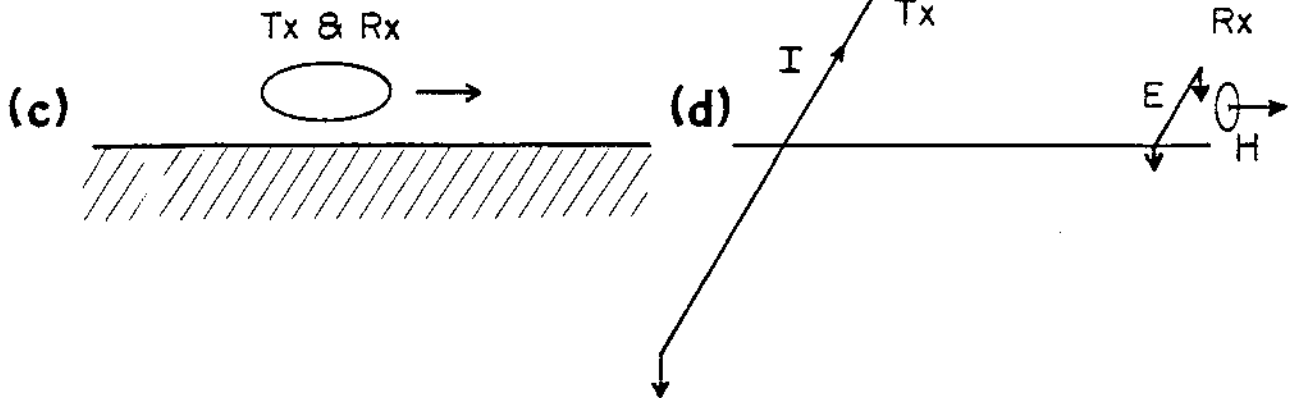
Two-loop

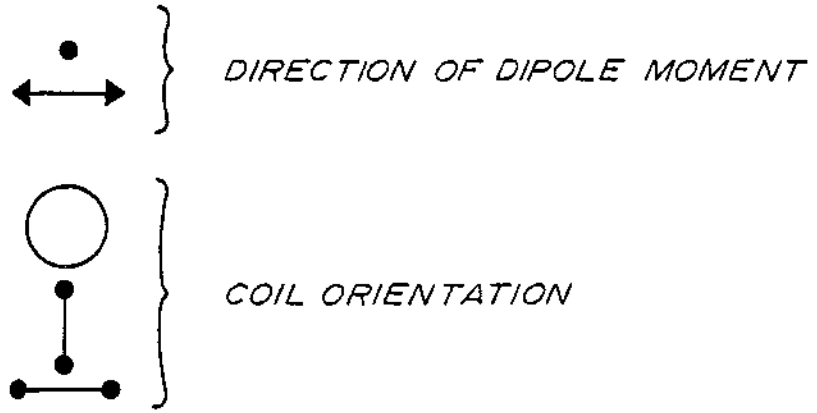
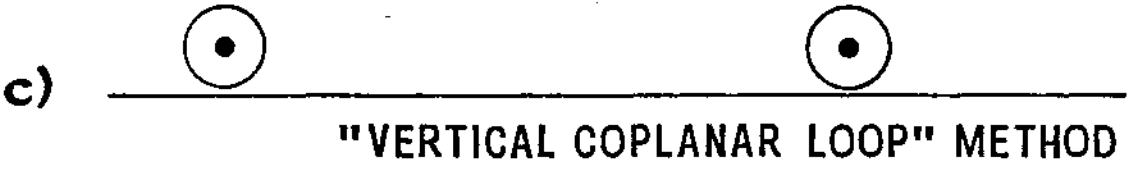
Large source loop



Single-loop

CSAMT





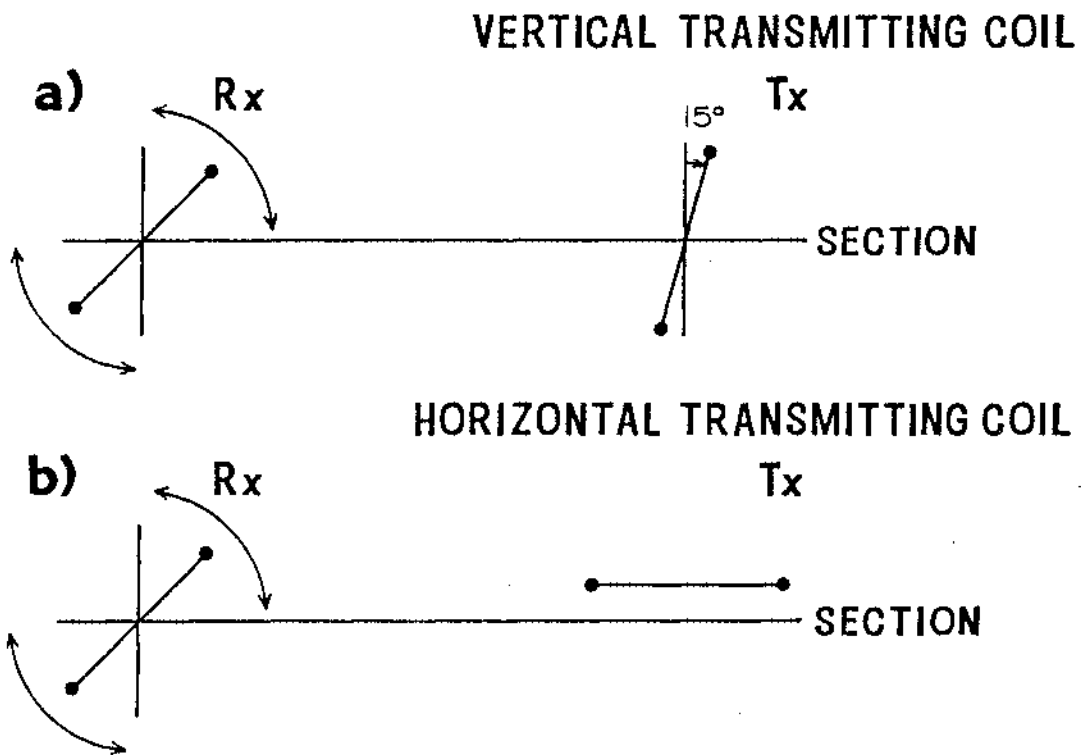
direction normal to strike. This coil configuration is not used routinely.

In the *vertical coplanar loop* EM method, the receiving and transmitting coils have their planes vertical and common and the pair is transported in-line with constant coil separation, in a direction 45 degrees to strike as in Figure 2-35c. This latter configuration is not used commonly. The need to traverse at 45 degrees to strike in order to obtain significant response usually mitigates against use of this configuration.

Two loop, roving coil pairs, rotatable orientation: In the *Crone Shootback* method (Crone, 1966) the receiving and transmitting coils are interchangeable in the sense that each is used both as a receiver and as a transmitter. The remarkable advantage of the method is that the effects of elevation differences between transmitter and receiver are eliminated. Two variations of it, the Crone *horizontal* and *vertical* shootback methods, illustrated in Figure 2-37, are used (Crone, 1966; Crone, 1973). With each, the orientation of the transmitting coil is fixed with its axis at some angle to the horizontal or to the vertical. The receiving coil, however, is rotated about an axis normal to the traverse line until a minimum signal is obtained at which time the tilt of the plane of the receiving coil, from the horizontal or from the vertical, is recorded. Two readings, taken at each observation stop with first one coil as transmitter then the other, are averaged. Elevational effects in the tilt angle reading are thus eliminated. The reader is referred to the literature for specific operational details.

In the *vertical loop broadside* method, the transmitter is transported

CRONE SHOOTBACK METHOD



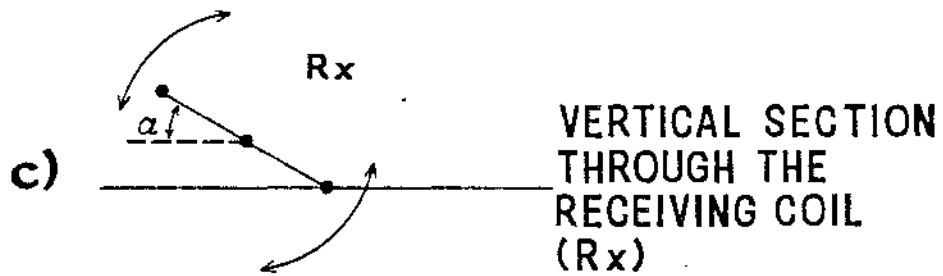
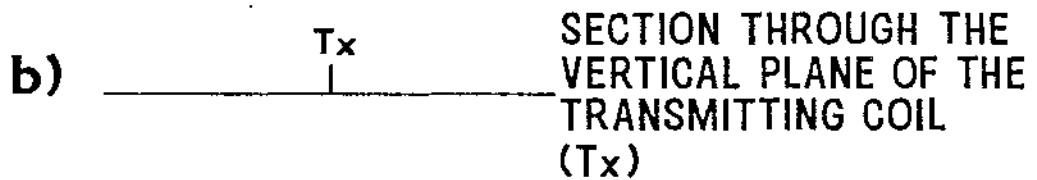
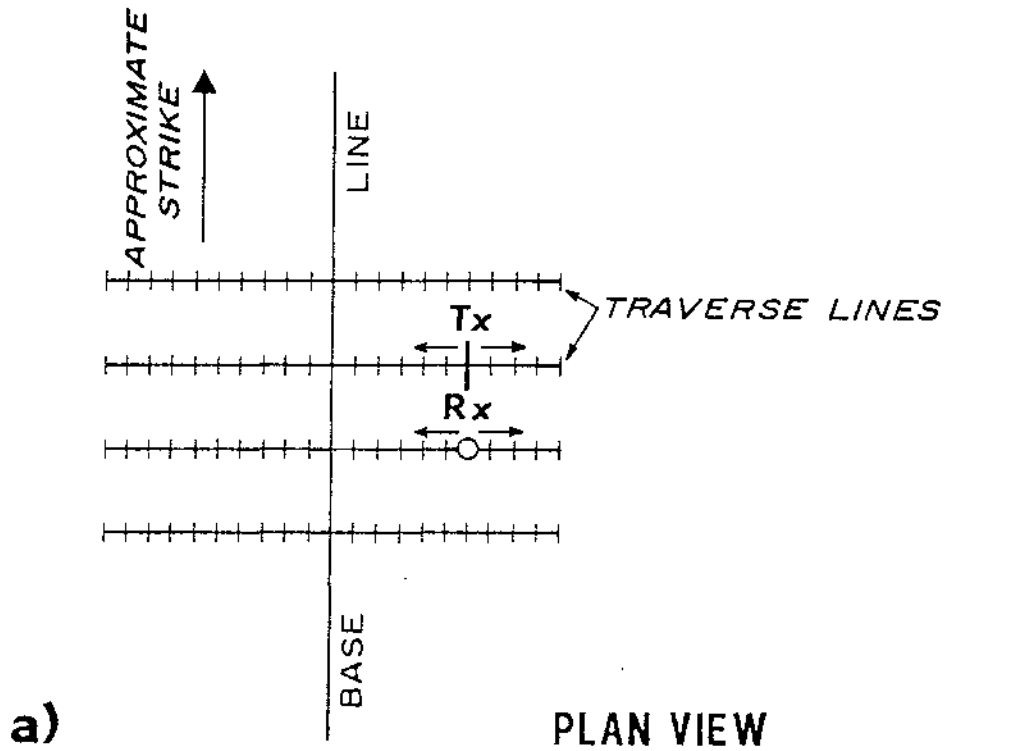
along one traverse line while the receiver is moved in unison along an adjacent traverse line. At each point of observation the transmitting coil is placed in that vertical plane which contains the location of the receiver as in Figure 2-38. The receiving coil is then rotated about an axis normal to the traverse line until a minimum signal is obtained, at which time the tilt of the plane of the receiving coil from the horizontal is recorded, (Grant and West, 1965; Ward, 1967).

Two loop fixed transmitter, roving receiver: With the *rotating vertical loop* method the transmitting coil (T_x) is erected within the survey area (Fig. 2-39a) while the receiving coil (R_x) is carried systematically on traverse lines adjacent to it and oriented normal to strike. The plane of the vertical loop is oriented for each observation so as to contain the point of observation. Tilt angle is measured by the receiver (Grant and West, 1965; Ward, 1967).

For the *fixed vertical loop* method, illustrated in Figure 2-40, the axis of the fixed transmitting coil is oriented normal to strike and the receiving coil is moved incrementally along the axis of the transmitting coil. Then the transmitting coil is moved to an adjacent line and the measuring process repeated. This is not a standard technique but has been used with success where tried (Ward et al., 1974, and Pridmore et al., 1979).

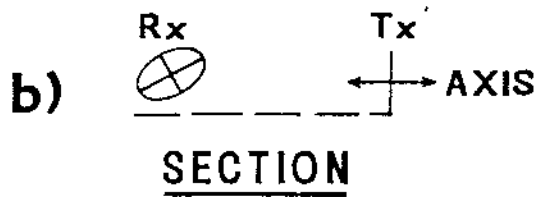
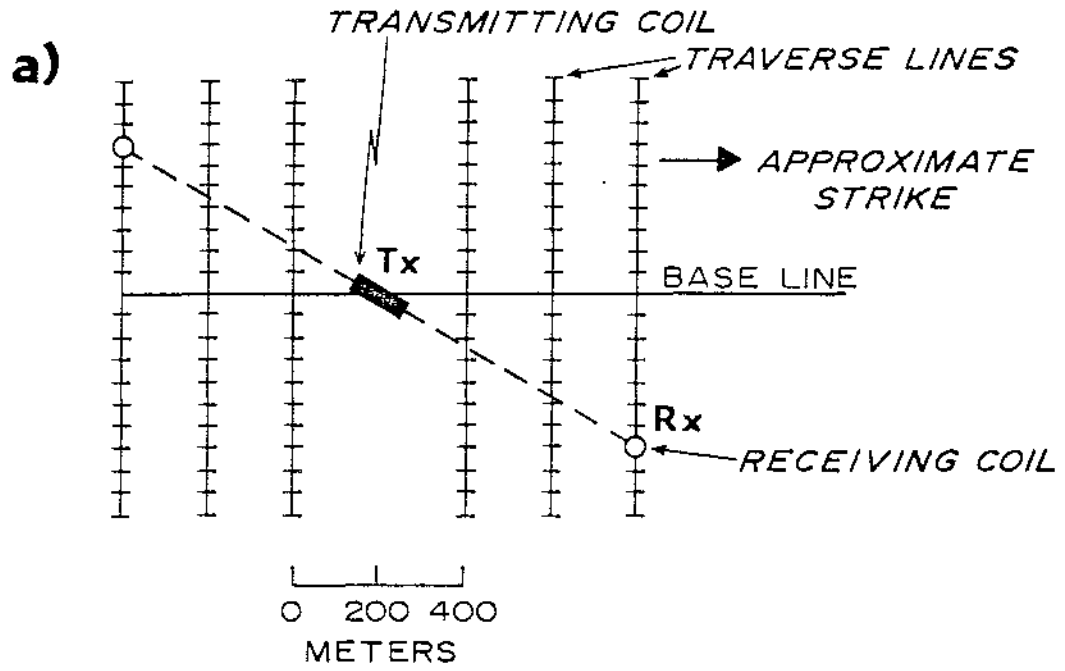
Large loop source: A *fixed horizontal loop* is used where large transmitting coil moments are required. When the loops are tens of meters in diameter or less, the transmitting loop is established at the end of a

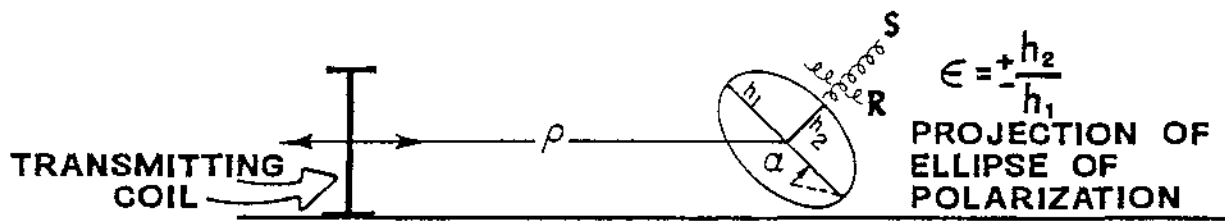
BROADSIDE VERTICAL LOOP METHOD



$\alpha = \text{TILT ANGLE}$

ROTATING VERTICAL LOOP METHOD





traverse line and the receiver traversed in increments along that line (Fig. 2-35b). Then the transmitting coil is moved to an adjacent line and the process repeated.

With the frequency domain *Turam* method (Bosschart, 1964; Grant and West, 1965) a large rectangular transmitting coil, hundreds or even thousands of meters to a side, is laid out on the ground and the field strength ratio and phase difference are recorded between a pair of receiving coils 30 m to 100 m apart, along traverses normal to one of the long sides of the rectangular loop.

The frequency domain GEOPROBE system (Ward, 1979) measures phase and amplitude of horizontal magnetic fields at 16 or more frequencies. The transmitting loop varies in size from tens of meters to thousands of meters and measurements are made along a traverse normal to one of the long sides of the rectangular loop.

UTEM is a wide band, time domain EM prospecting system developed at the University of Toronto by Lamontagne and West (1973). The transmitting loop ranges in size from hundreds of meters to thousands of meters on a side. The time samples of received vertical magnetic field are obtained along a traverse radial to the transmitting loop.

The time domain Crone PEM method (Crone, 1979), uses a 10 m to 1000 m transmitting coil. Usually, when a small transmitting coil is used, transmitter and receiver, separated by 30 m to 1000 m, are moved in unison along a traverse line so that this method could also be listed under the section on roving coil pairs. The transmitter is fixed when larger loops are used.

The time domain Newmont EMP system uses a large fixed rectangular

transmitting loop, hundreds of meters to a side. The received signals are the three orthogonal components of magnetic field recorded at 32 discrete time channels after termination of each transmitted current pulse (Nabighian, 1977).

The frequency domain Kennecott Vector EM system (Hohmann et al, 1978) uses a large fixed rectangular loop of Turam dimensions for reconnaissance exploration. The system can also be used with a rotating vertical loop. The receiver measures amplitude and phase of the vertical component of magnetic field at four frequencies.

Single loop: With the time domain Russian *MPP01* (Velikin and Bulgakov, 1967) and the Australian *Sirotem* (McCracken and Buselli, 1978), a single rectangular loop 50 m to 200 m to a side, is used first as a transmitter, and at appropriate time delays, then as a receiver. *Sirotem* also offers the opportunity for use of separate transmitting and receiving loops separated by 100 m to 200 m.

CSAMT: In a controlled-source audiomagnetotelluric survey, a grounded wire (Fig. 2-35d) is used as a source. Provided measurements are made at distances greater than three skin depths relative to the greatest resistivity in the section, then conventional magnetotelluric interpretations methods may be employed (Goldstein and Strangway, 1975).

Field configurations, controlled source, airborne

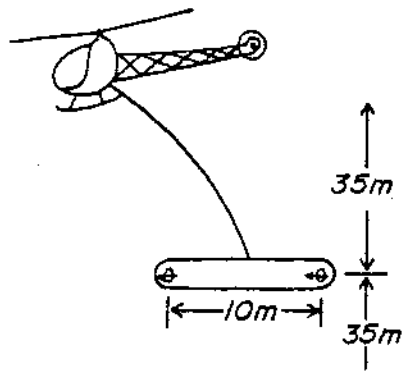
Introduction: Historical and descriptive papers dealing with AEM systems have included those by Pemberton (1962), Ward (1967), Ward (1969), Paterson (1971), Ghosh (1972), and Becker (1979). We shall identify herein

only three basic types of systems and reference the various present systems belonging to these types.

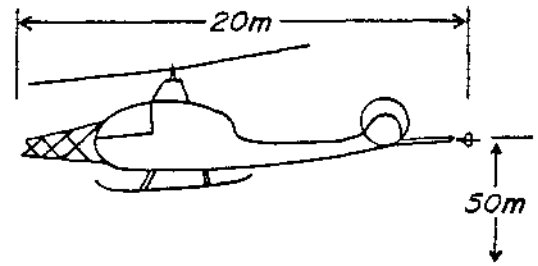
Rigid boom systems: The transmitting and receiving coils are attached to a rigid boom to minimize translation and rotation of one coil relative to the other. In the most common type of rigid boom system, the coils are separated by about 10 m and are attached to a large boom or bird which is towed beneath a helicopter as in Figure 2-41a. The Scintrex HEM-701, Barringer HEM, Geonics HEM, and the DIGHEM systems are of this type. Secondary magnetic fields both in-phase and quadrature with respect to the primary field are recorded at one or more frequencies of order 1000 Hz to 5000 Hz. The helicopter flies at a nominal height of 70 m while the bird flies at a nominal height of about 35 m. Signals less than 1 part per million of the primary field can be recorded.

In another type of rigid boom system, the coils are mounted on structures attached to the airframe of the helicopter or fixed wing aircraft as in Figure 2-41b. The Scintrex TRIDEM (Seigel and Pitcher, 1978), and the Barringer COTRAN systems are of this type. Separation between the coils is 15 m to 30 m while normal flying height is 50 m to 60 m. Secondary magnetic fields both in-phase and quadrature with respect to the 500 Hz, 2000 Hz, and 8000 Hz, primary fields are recorded at a noise level of 20 to 50 ppm for TRIDEM. TRIDEM operates in the frequency domain while COTRAN operates in the time domain. The noise level of the latter has not been stated.

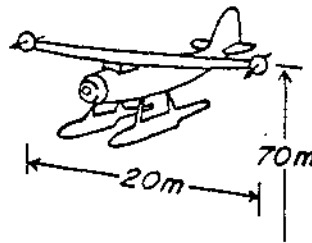
A third type of rigid boom system utilizes two coplanar coils mounted on the wing tips of a fixed wing aircraft. The Geoterrex Otter system is an example of this type (Fig. 2-41c). Separation between the coils is



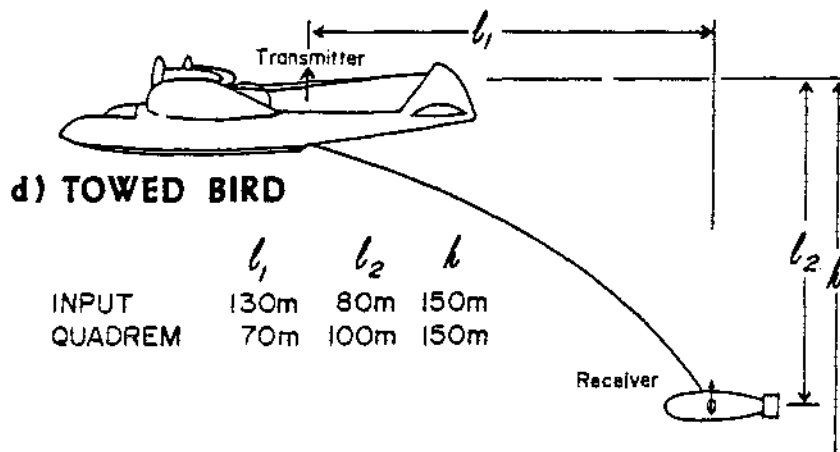
a) HELICOPTER TOWED-BOOM



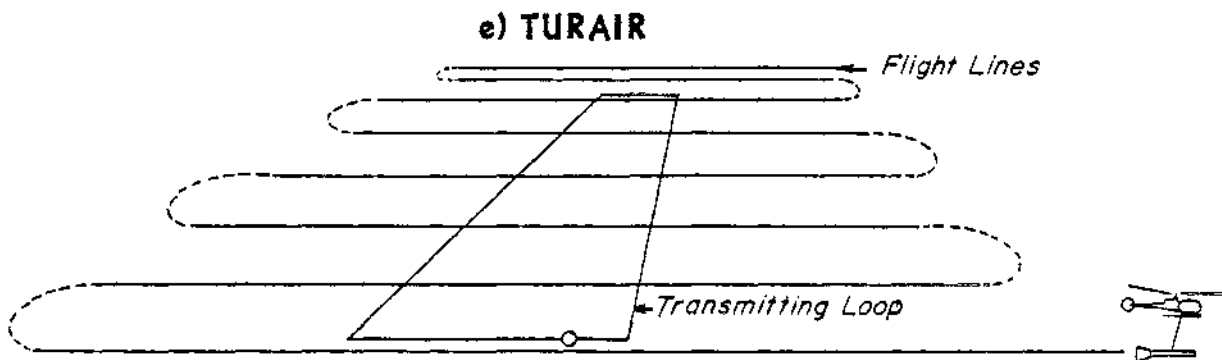
b) HELICOPTER BOOM



c) WING-TIP BOOM



d) TOWED BIRD



e) TURAIR

about 20 m while the normal flying height is 50 m to 70 m. Secondary magnetic fields both in-phase and quadrature with respect to the 320 Hz primary field are recorded at noise levels of about 20 ppm to 50 ppm.

Towed bird system: Figure 2-41d illustrates a small bird, carrying the receiving coil, towed behind and beneath an aircraft. These systems measure quadrature secondary magnetic field, only, when operating in the frequency domain. An example is the McPhar QUADREM system which utilizes several frequencies, simultaneously, in the range 300 Hz to 3000 Hz. INPUT operates in the time domain, providing measurement of six to twelve samples of secondary magnetic field. It can be shown to be equivalent to a frequency domain system which measures the quadrature secondary magnetic field. Separation between coils is nominally 150 m with aircraft heights of 125 m to 150 m.

Semi-airborne systems: TURAIR is akin to the ground TURAM method (Bosschart and Seigel, 1971). Two receiving coils, mounted on opposite ends of a 10 m bird towed beneath a helicopter, allow airborne measurement of field strength ratio and phase difference along traverse lines normal to the long sides of a large rectangular loop. Measurements are made inside and outside the loop at flying heights of order 30 m to 50 m. Typical transmitting loop dimensions are 5 km by 10 km. Figure 2-41e illustrates the field procedure.

Unicoil: At the University of California, Berkeley, a cryogenic unicoil system is under development (Morrison et al., 1976). It promises frequencies as low as 10 Hz with attendant promise of depths of exploration

greater than heretofore. Changes in the resistance of a superconducting coil, introduced by the presence of the earth, are recorded. Noise levels of conventional two coil AEM systems frequently are dependent upon translation and rotation of one coil relative to another; the unicoil avoids this problem.

Sources of noise in electromagnetic surveys

The detectability of an exploration target in a particular environment is determined by the ratio of signal to noise, which in turn depends upon two factors: (1) the characteristics of the target response, and (2) the characteristics of the noise. In order to increase the probability of discovery, we must increase the signal and reduce the noise in a cost effective manner. In geophysical exploration with the EM method, noise arises in the following sources;

disturbance field noise,

instrument noise,

cultural noise,

topographical noise,

and

geological noise.

Disturbance field noise is a general background of ambient electromagnetic fields upon which the transmitted electromagnetic field is superimposed. There are two main sources of this noise type:

- (1) alternating magnetic fields resulting from artificial sources such as transmission lines, telephone lines, radio transmitters, etc., and
- (2) alternating magnetic fields resulting from natural sources such as thunderstorms and other atmospheric discharges.

Analog and/or digital filtering is used to enhance the ratio of signal to noise for this noise source but in culturally developed areas it can prevent acquisition of useful data.

Instrument noise may be electronic, mechanical, or thermal in origin.

An analysis of the various sources of instrument noise as it relates to various ground and airborne systems is given in Table 2-3.

Cultural noise consists of anomalies due to fences, telephone and power distribution ground returns, pipelines, metallic buildings, etc. This noise source cannot be circumvented in general and hence it may limit the application of EM methods in culturally developed areas.

Topographical noise arises in currents induced in the overburden or bedrock by the transmitter. When the earth's surface is flat, the currents in a homogeneous or plane, horizontally-layered, earth are uniformly distributed horizontally and occur at a uniform distance beneath the transmitter-receiver coil pair. As topographic relief increases, these two conditions are increasingly violated. The result is that local anomalies appear that are a direct result of the topography.

Terrain clearance noise, arising in varying terrain clearance in an AEM survey may be considered as topographical noise even though it is conventionally referred to as part of geologic noise, the limiting noise for AEM surveys. While terrain clearance noise can be computed readily above a flat earth (e.g. Ward, 1969), terrain clearance noise and the more general topographical noise have not been analyzed to any significant degree but the effect is known to be a function of transmitter-receiver separation and orientation.

When the earth is highly resistive, topographical noise as described is negligible. However, topographic relief may then enter the picture by its effect on the geometrical part of instrument noise.

Geological noise: By geological noise we mean the EM response of any

TABLE 2-3 ANALYSIS OF INSTRUMENT NOISE

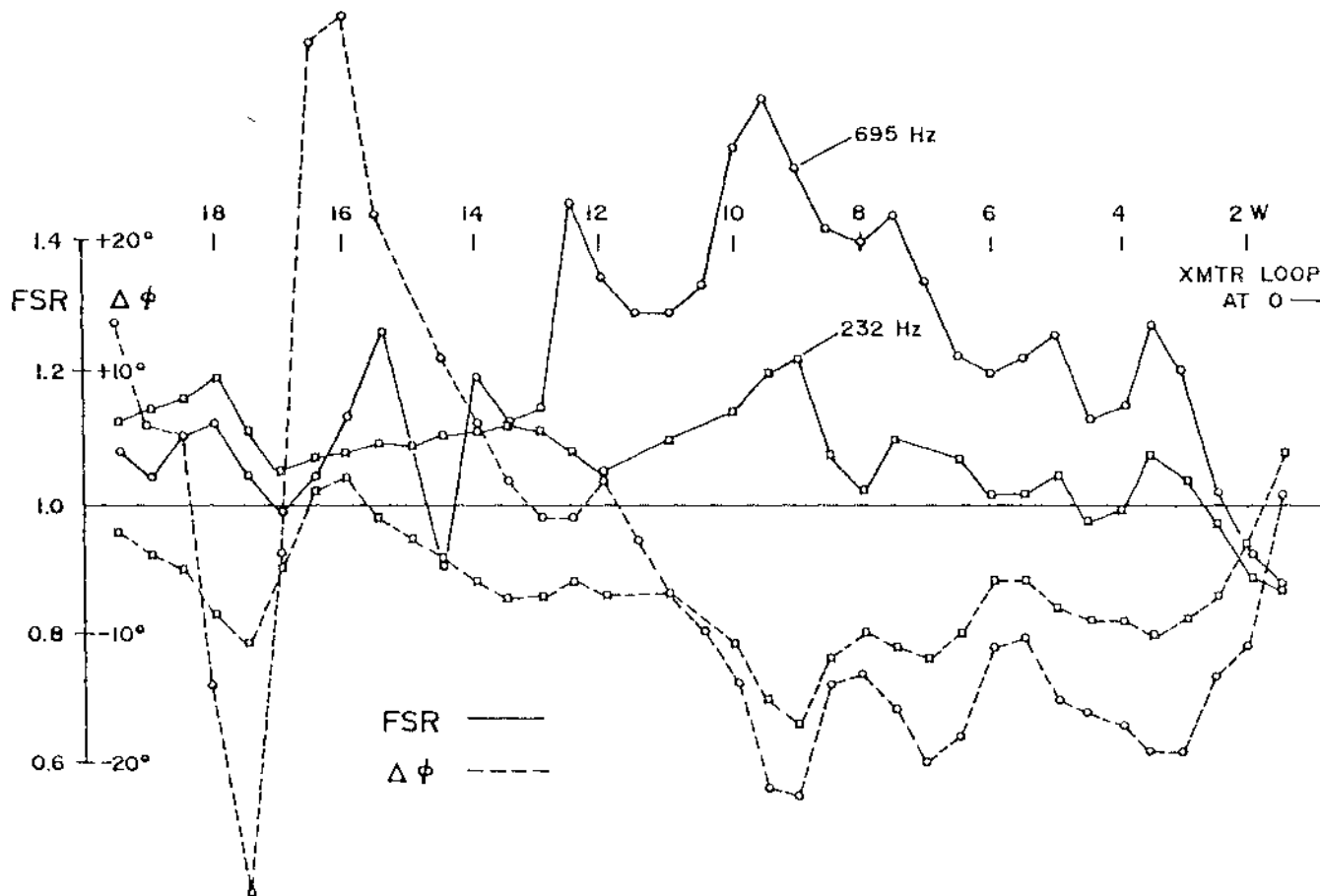
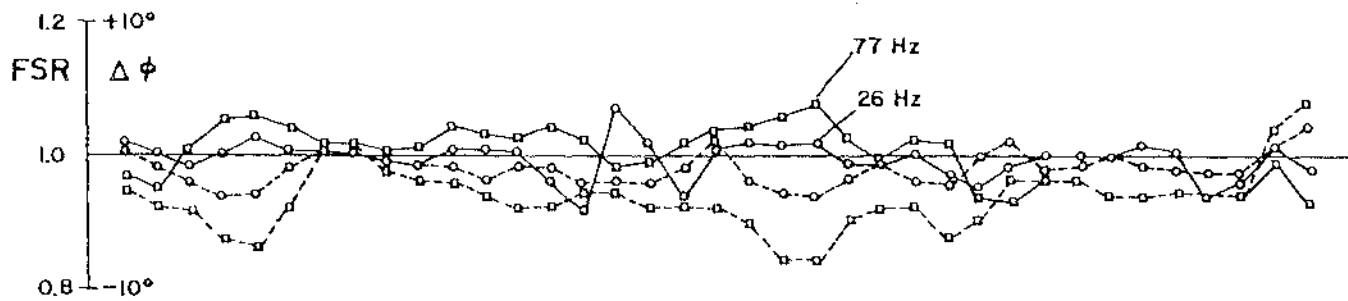
INSTRUMENT NOISE TYPE	MEANS OF REDUCTION AND COMMENTS	SEVERITY-GROUND SYSTEMS										SEVERITY-AIRBORNE SYSTEMS						
		HDRIZ LOOP	VERT COAXIAL LOOP	VERT COPLANAR LOOP	SHOOFBACK	VERT LOOP BACKSIDE	ROTATING VERT LOOP	FIXED VERT LOOP	GEOPHONE	UHAW	PEN	UTEM	EMP	MPPD	CSAMT INPUT	DIGREM	TURAIN	
(11) Noise mechanically induced in the detecting coil, such as magnetostriction in iron-core coils, microphone vibrations, oscillations of the coils in the earth's main magnetic field, and changes in the effective area of the receiving coils caused by wind in ground systems and air turbulence in airborne systems.	Assure that mechanical resonances lie well outside electronic passband. Wipe at the frequencies below 50 Hz or times beyond 20 msec.	4	4	4	4	4	2	2	2	4	2	2	2	3	2	4	4	4
(12) Thermal drift of the parameters of the transmitting or receiving coils or associated electronics.	Use temperature compensating networks or drift correction. Mask difficult airborne system. Substitute calibration.	3	3	3	4	4	4	4	3	3	3	3	3	3	3	2	2	2
(13) Electronic noise in analog circuits or digitizing noise in digital circuits.	Use superior electronic system design.	4	4	4	4	4	4	4	4	4	4	4	4	4	4	4	4	4
(14) Errors or variations in calibration and separation of transmitting and receiving coils.	Pay careful attention to detail in field and use superior mechanical system design. Not important in time domain systems because no primary field present during low saturation. Becomes worse for some systems as topographic relief increases.	1	1	1	3	3	3	3	2	3	4	4	4	4	4	1	1	4
(15) Inaccuracy in measuring or calibrating transmitting coil moment.	Use superior current control in electronics and accurate measurement of current. Ensure accurately measured and insulating area of transmitting loop. Wind and turbulence influence this effect.	4	4	4	4	4	4	4	2	3	3	3	3	3	4	2	4	4
(16) Errors or drift in phase or time reference.	Use superior electronic system design.	3	3	3	4	4	4	4	3	3	3	3	3	3	3	3	3	3
<u>NUMERICAL EVALUATION</u>																		
0 Can be serious																		
1 Can be at major impedance																		
2 Of minor impedance																		
3 Insignificant																		

conductive features in the earth other than the economic target. Graphite and permeable shear zones are important sources of geological noise. In conductive terrain, such as much of Australia, geological noise arising from lateral variations in an overburden of low resistivity often is the most important type of noise.

Overburden of low resistivity tends to attenuate responses from bedrock, but its most deleterious effect is to produce EM anomalies due to lateral porosity changes, thickness variations, and differential weathering. Sources of geological noise in the overburden generally are not as conductive as massive sulfides, but they are shallow and thus may produce anomalies comparable to or greater than anomalies due to good conductors in bedrock.

Some means must be used to discriminate among the numerous EM anomalies that arise in surveys where overburden is thick and conductive. The common means of discrimination are: (1) correlating with other types of information, (2) selecting only good conductors, and (3) selecting conductors having the correct geometry. In the first method, EM anomalies that have associated magnetic, gravity, geochemical, or induced polarization anomalies, for example, are selected for further investigation. Discrimination by conductivity and geometry is an important research and development topic. As we indicated above, conductivity discrimination is by decay rate in the time domain and by amplitude-phase relations with frequency in the frequency domain.

Turam data, at four frequencies, from a deeply weathered nickel prospect in Western Australia (Hohmann et al., 1978) are shown in Figure 2-42. An aeromagnetic survey and trenching defined a prospective



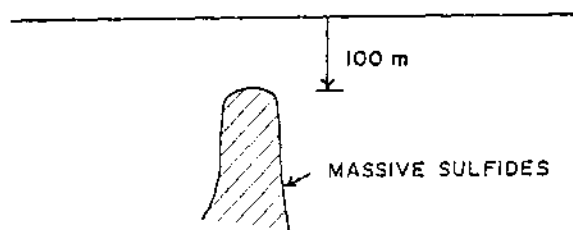
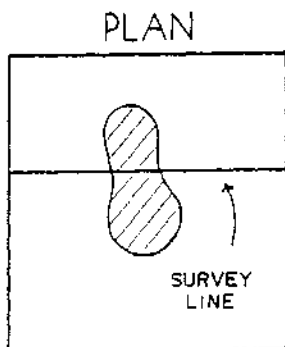
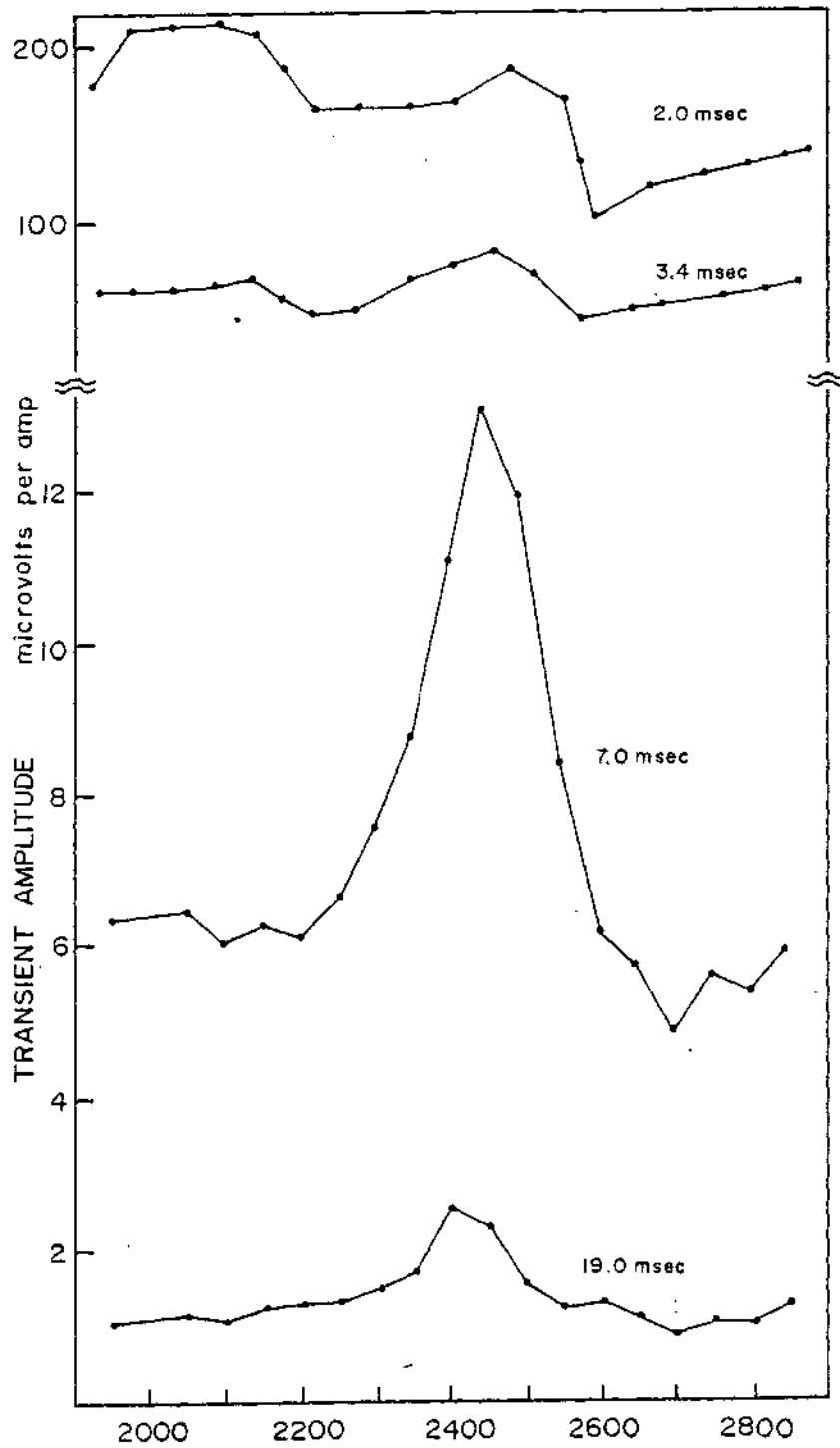
ultramafic body between 2W and 9.5W. Resistivities are as low as 5 Ω -m and highly variable due to differential weathering. The water table is about 15 m deep. The basal contact of the ultramafic was drilled and intersected on this line at 9.5 W and at several other locations along strike without encountering mineralization. Geological noise is very high in the electromagnetic data due to the deep differential weathering. However, geological noise is much less at the lower frequencies, so that it would be possible to detect a conductor with a good response at low frequencies, provided it were not too deep. Figure 2-42 illustrates an unfortunate problem for nickel exploration in Western Australia. Magmatic segregation deposits occur at the basal contact of an ultramafic body but often there is, as at 9.5W in this case, a strong anomaly due to a shallow conductor, probably a permeable shear zone along the entire contact. Detection of a small nickel deposit beneath this shallow conductor would be quite difficult with the EM method.

In contrast, Figure 2-30 (Hohmann et al., 1978) shows four frequency Turam data over the Freddie Well deposit, a shallow massive sulfide body in Western Australia, at a location where overburden conditions are more favorable for application of the EM method. Massive and disseminated mineralization occurs over a 30 m interval centered at 0 on the line. Its electrical conductivity is high due to well-connected pyrite and pyrrhotite lenses. Background resistivity ranges between 30 Ω -m on the west end of the line and 300 Ω -m to the east. The large responses at 26Hz and 77Hz show that the anomaly is due to a very good conductor of the type that could be detected even through the geologic noise of Figure 2-42. Numerical modeling suggests that the bulk resistivity of the body is 0.1 to

0.3 $\Omega\text{-m}$, and its depth is about 30 m.

The geometrical aspects of EM anomalies also can be used to discriminate between geological noise and target response. For example, the 100 m by 100 m loop, with which the data of Figure 2-43 were taken, averages the magnetic field over a large area. Hence the response at short wavelength of a surficial conductor is suppressed with respect to the response at long wavelengths of a deep conductor. Unfortunately, conductive overburden produces anomalies of long wavelength in some instances.

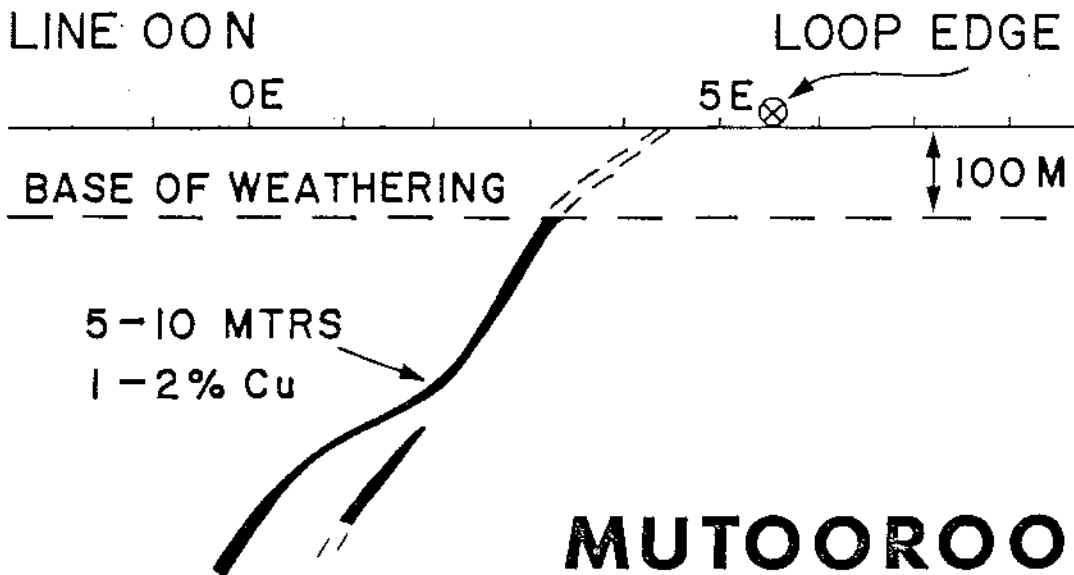
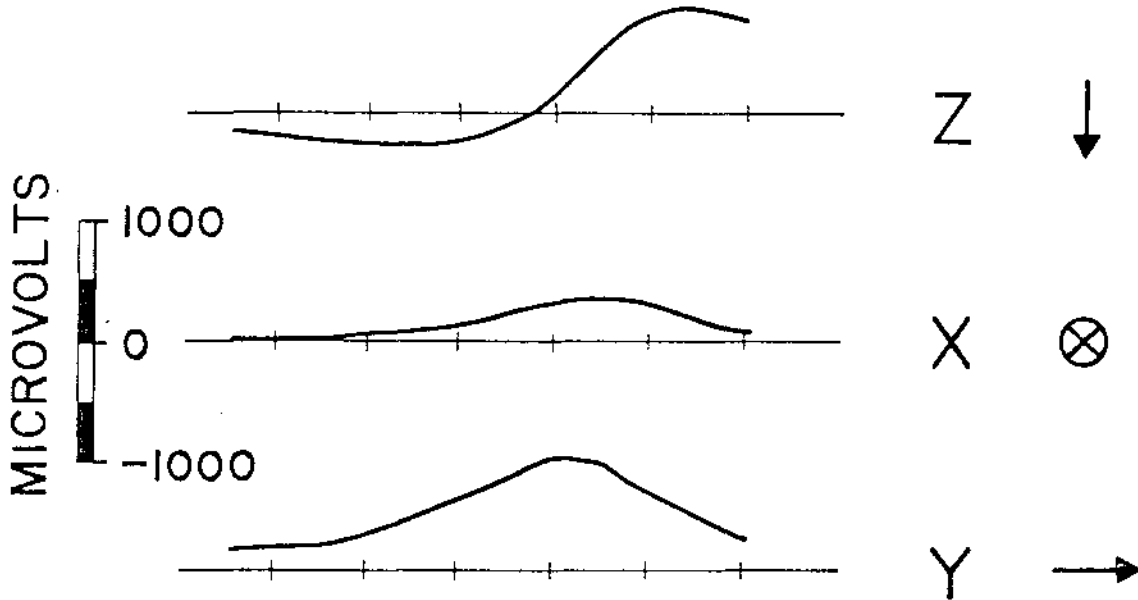
In another approach, the Newmont EMP system (Nabighian, 1977) measures the magnetic fields in three orthogonal directions to obtain geometrical information about conductors. The transmitter is a large Turam-type loop, and measurements are made in the time domain. In an important recent development, Nabighian (1978) finds that at late times a layered earth response can be subtracted from the total response; analysis of the residual anomaly yields the correct parameters for the conductor if current channeling is not significant. Figure 2-44 shows EMP anomalies in the three orthogonal components at 5.63 msec over the Mutooroo deposit near Broken Hill in New South Wales, Australia. The overburden response has disappeared by 5.63 msec. The location of the bedrock conductor lies directly beneath the peak of the Y component and beneath the crossover in the Z component, Figure 2-45 shows that this location lies downdip of the outcrop, as it should since the weathered sulfides are not highly conductive. The strike of the conductor is clearly evident in the EM data as Figure 2-45 shows. Kuo and Cho (1980) discuss the quantitative interpretation of the EM data over this deposit.



ELURA DEPOSIT, N.S.W., AUSTRALIA

2-45

TIME
5.63 MSEC

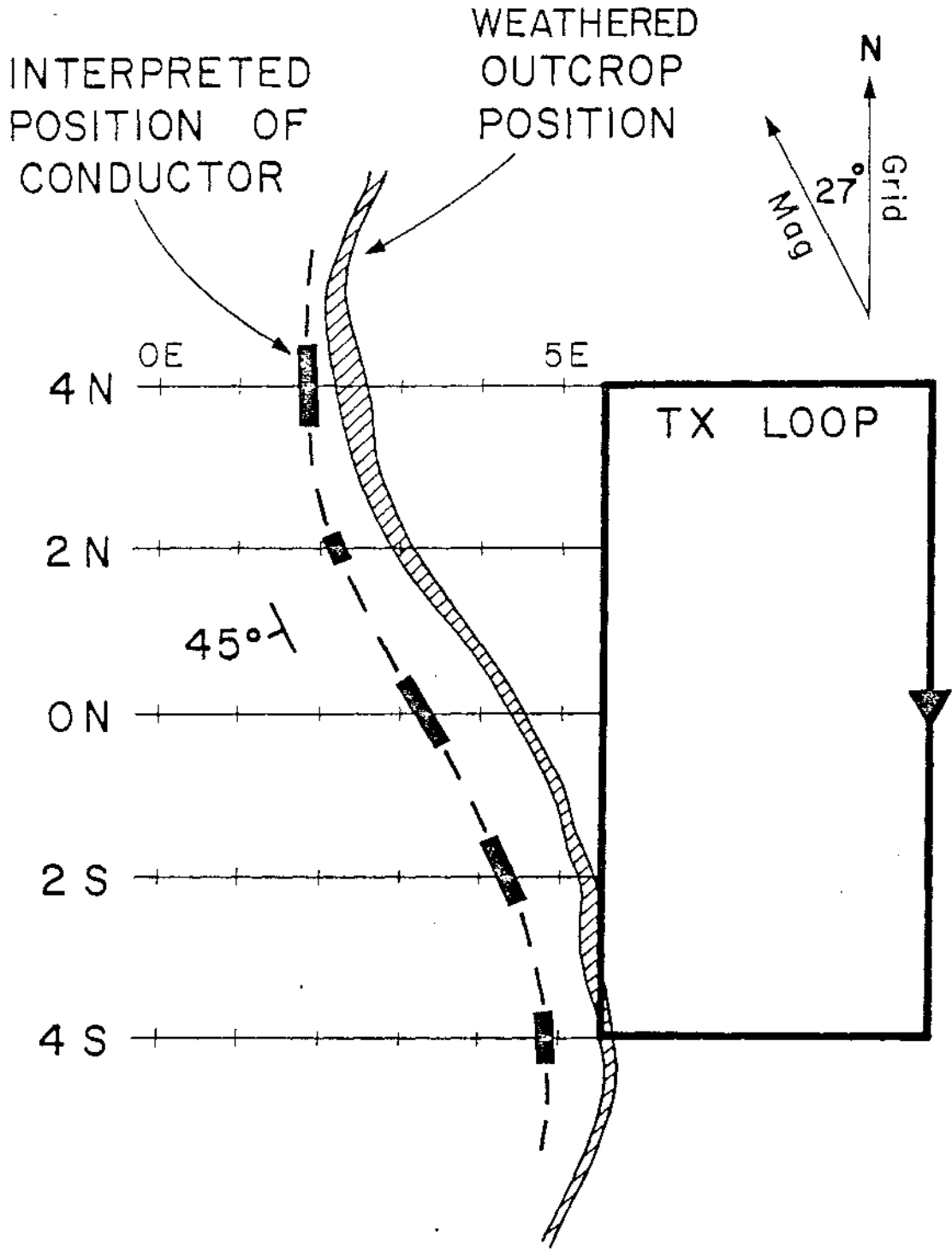


MUTOOROO EMP SURVEY

CHANNEL PLOTS



2-44

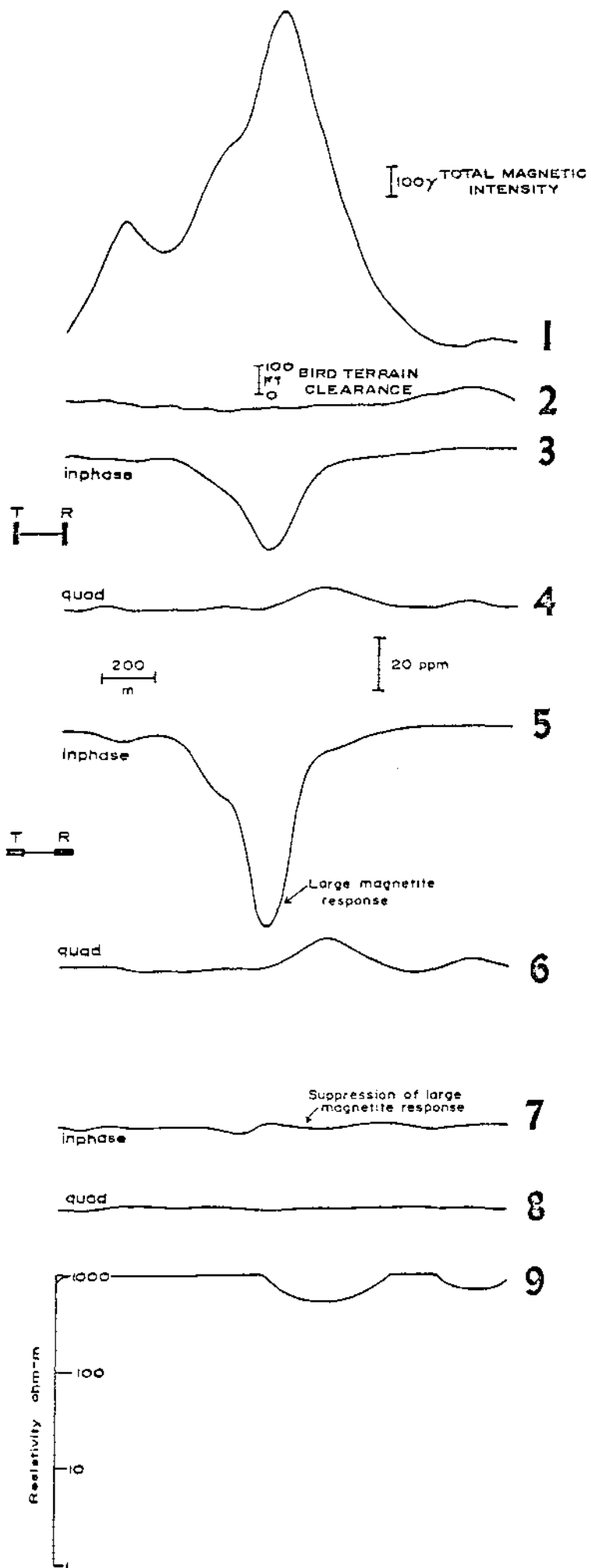


MUTOOROO
EMP SURVEY

2-4

Several other state-of-the-art means of enhancing the ratio of signal to noise are given in the section on applications below.

A geological noise source which becomes of importance in rigid boom AEM systems arises in magnetic bodies. Figure 2-46, from Fraser (1979) shows a large magnetic signature and its suppression by the DIGHEM II system. Figure 2-46 records (1) total magnetic intensity, (2) bird terrain clearance, (3) coaxial coil in-phase, (4) coaxial coil quadrature, (5) horizontal coplanar coil in-phase, (6) horizontal coplanar coil quadrature, (7) the difference between channel (3) and one half of channel (5), (i.e., in-phase difference), (8) the difference between channel (4) and one half of channel (6) (i.e., quadrature difference), and (9) the apparent resistivity of deduced from the horizontal coplanar coil pair. Unless more than one coil configuration is used this noise source cannot be suppressed and can result in obscuring anomalies due to conductive targets as Fraser notes.

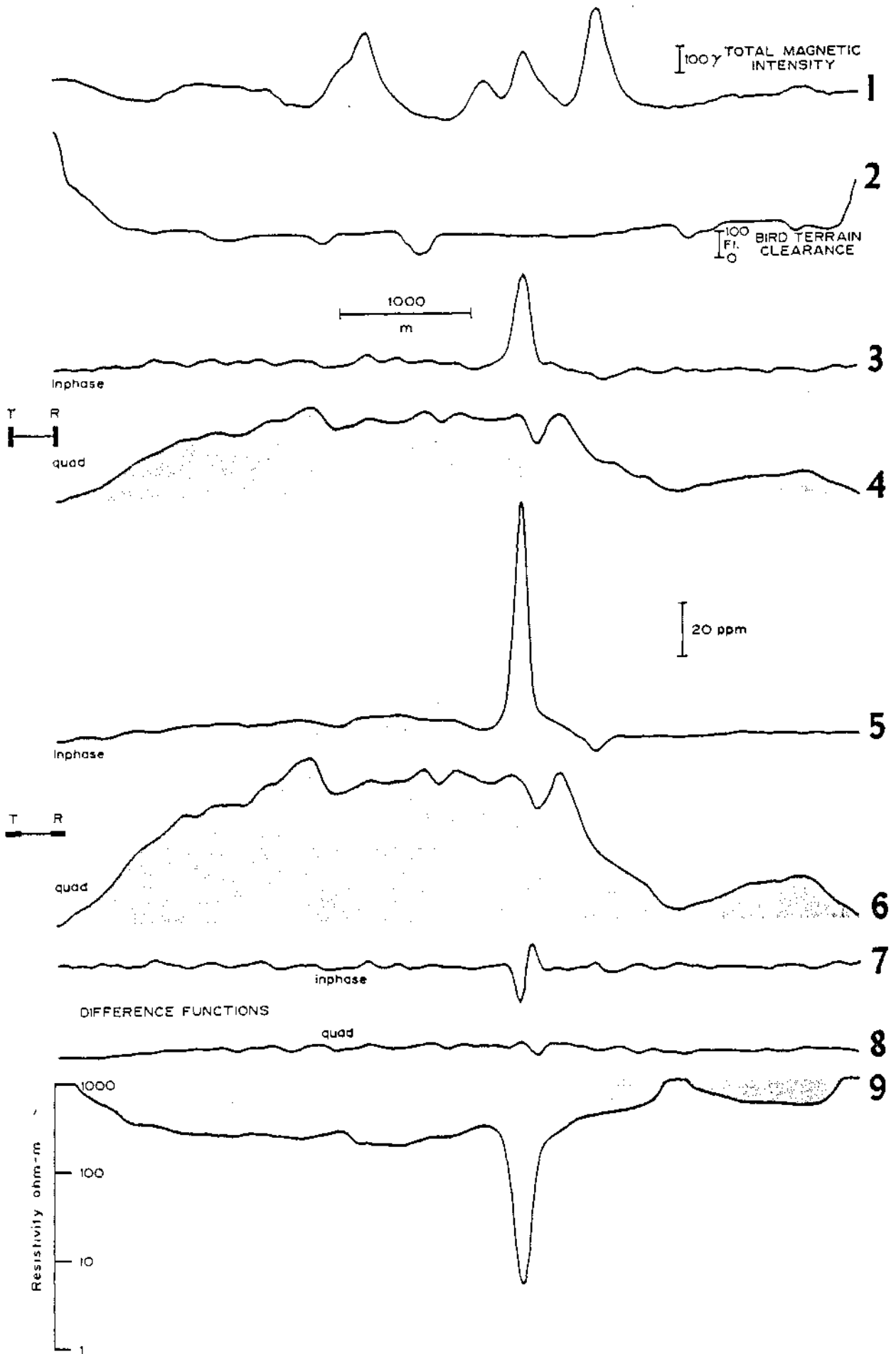


Applications

In this section we present a limited number of examples of solutions, of difficult exploration problems, by use of advanced EM systems.

Airborne electromagnetics in areas of conductive overburden: Early application of the EM method in the Precambrian Shield of Canada and Scandinavia met with remarkable success because the target areas were characteristically devoid of conductive overburden. As Shield exploration targets gradually shifted to areas covered by deep conductive overburden, success at first diminished. Then as experience was acquired with much improved and more versatile equipment, success again became remarkable but at increased cost. Fraser (1979) provides an excellent example of application of the frequency domain DIGHEM II airborne system in an area of conductive overburden. The example is the AEM flight records over the Montcalm deposit in Ontario, Canada (Fig. 2-47). The channel identification is the same as in Figure 2-46. Insofar as both coil pairs respond to a layered earth in the same manner, except that the response of the horizontal coplanar coil pair is twice that of the coaxial coil pair, the difference channels largely eliminate the effect of the overburden which dominates the quadrature channels (4) and (6) and degrades the ratio of signal to noise of the in-phase channels (3) and (5). The resistivity channel is very helpful in mapping overburden type in such areas. Smee and Sinha (1979) discuss the clay overburden problem in light of recent technology.

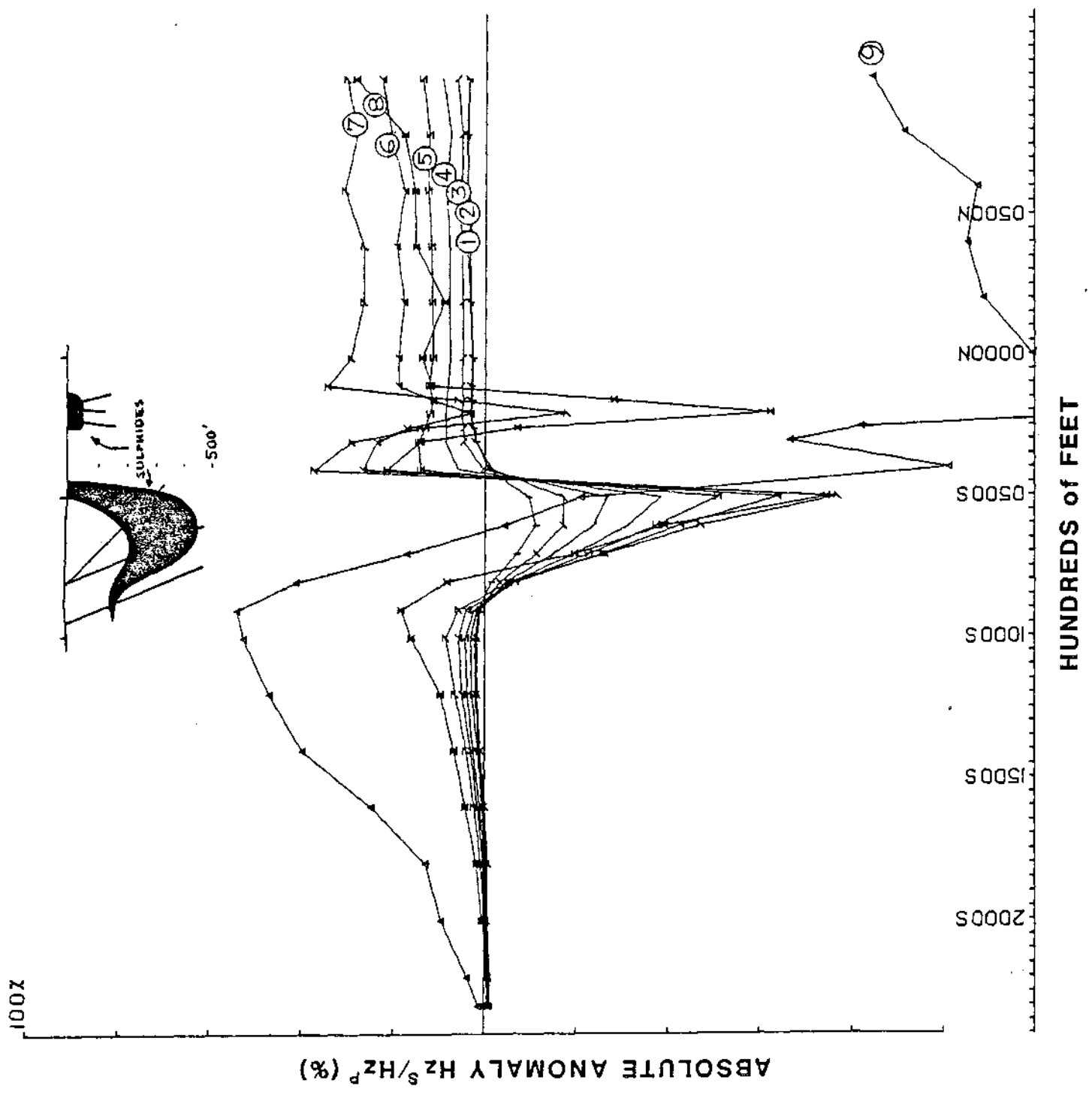
Ground electromagnetics in deeply weathered areas: Figure 2-43 contains data from a SIROTEM survey over the Elura deposit in New South

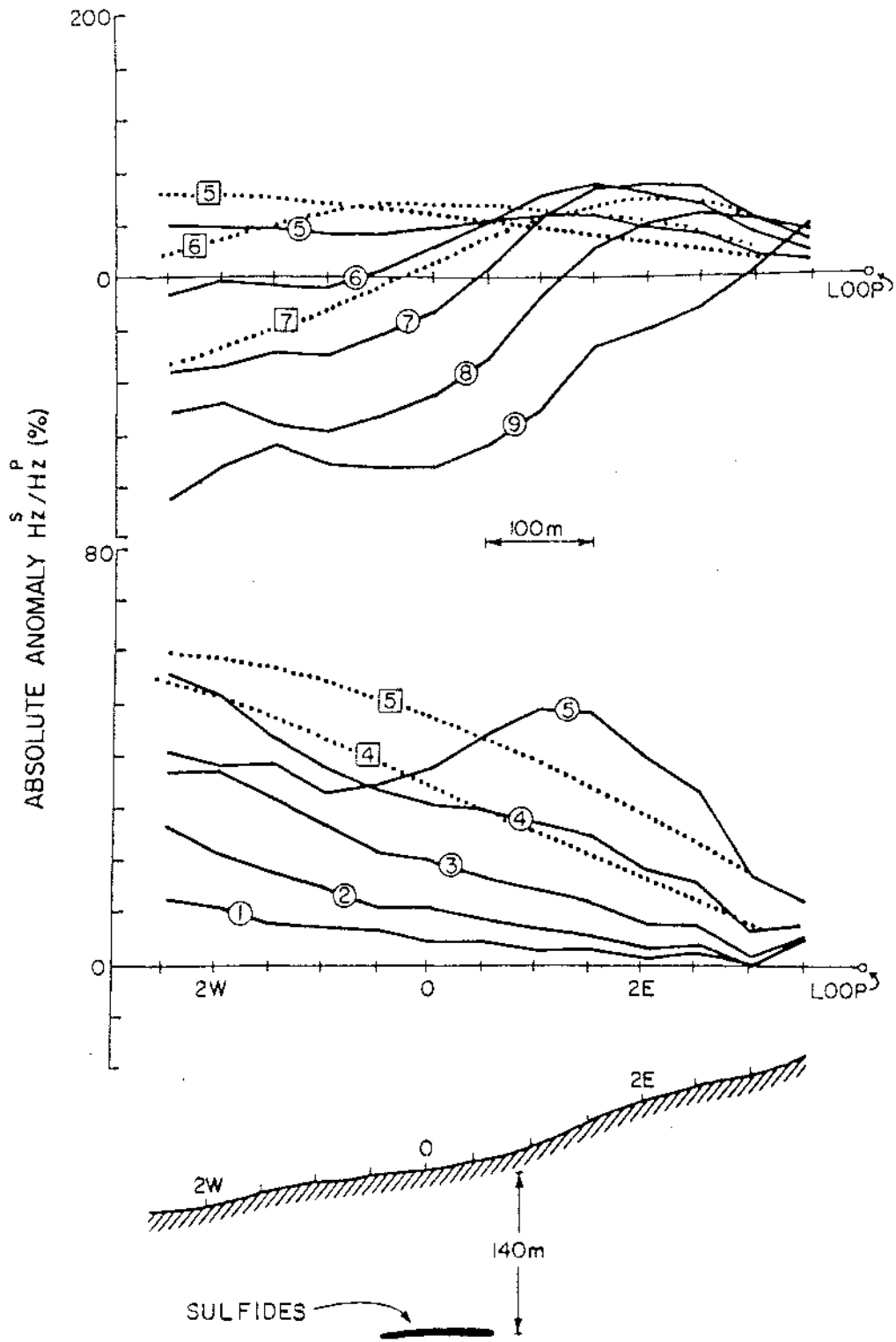


Wales, Australia (McCracken and Buselli, 1978). This massive sulfide deposit is highly conductive ($\sim 0.1 \Omega \text{ m}$) but lies beneath a 100 m weathered layer and hence presents an extremely difficult target. At the 2.0 msec and 3.4 msec sampling time the response is in the hundreds of microvolts of received signal per ampere of transmitted current and is due mostly to the conductive weathered rock; the response of the deposit tends to be obscured. At the 7.0 msec sampling time, the response of the weathered layer is mostly gone while the response of the deposit is decreasing; the ratio of the 7.0 msec response to the 19.0 msec response can provide an estimate of the conductivity of the deposit. Unless a precise broadband instrument had been used, the separation of weathered layer response from sulfide deposit response would not have been possible.

Detecting a sulfide body by current channeling: We first study a more or less routine application of the time domain UTEM system. Figure 2-48 contains one line of a UTEM survey over Texas Gulf Sulfur Company's IZOK massive sulfide deposit in the Northwest Territory, Canada. The transmitting coil is at 2400 s and has dimensions 1000 m by 700 m. The base frequency of the triangular transmitted waveform is 3 Hz. At the earliest delay (chan. 9, 50 μs) the anomalous current is a general unidirectional current flow perpendicular to the profile which gives a large cross-over anomaly on all lines. At all later times, the anomalous currents are vortices induced locally in each conductor as in Figure 2-28a. These currents produce slowly decaying negative anomalies over each body.

Figure 2-49 contains a UTEM profile over a long, ribbon-like sulfide body situated in flat lying unmetamorphosed sediments. The resistivity of





the sediments above the sulfides is about 1000 Ω -m. The rocks below the body are more resistive. The near side of the transmitting loop is at 4 E; the base frequency is 25 Hz. The dotted profiles are estimates of the responses that would have been observed if the sulfides were not present. The residual anomaly is of cross-over type, strongest (80%) at channel 6 (0.5 ms). The anomalous current flow is unidirectional, i.e. of the *current gathering* type. This sulfide body is insufficiently conductive to produce a visible anomaly by local induction of circulating currents. Such an anomaly would be due to a bifilar current flow and would have shown as a weak negative anomaly persisting after the current gathering anomaly died out. This deposit would not have been detected had not current gathering been induced by the intermediate frequency part of the transmitted spectrum. The half-space, or bedrock, response dominates at very short times and the deposit does not respond at very long times. Once again a broad passband and high precision are required to solve a difficult problem.

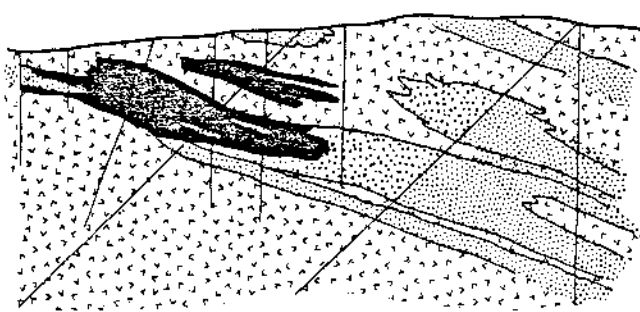
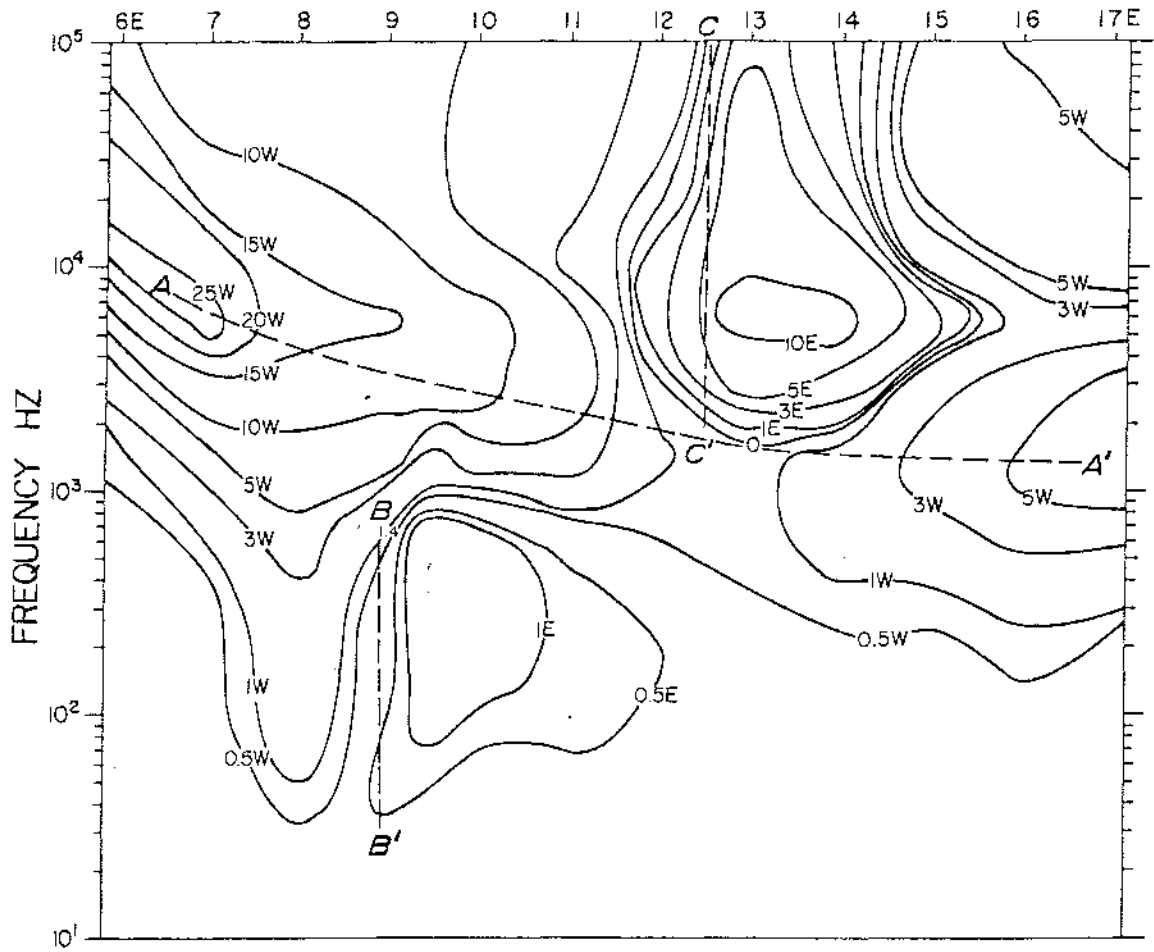
Detecting ore adjacent to disseminated sulfides in conductive terrain: Resolution of adjacent conductors in some exploration problems is essential if one is to minimize drilling of uneconomic sulfides and maximize the probability of intersecting ore. One such problem arose in the Foothills Copper Belt of California (Pridmore, et al., 1979). The deposit in question is a typical volcanogenic massive sulfide pod which grades laterally into a variably disseminated sulfide zone. The problem is to resolve the massive from the disseminated sulfides.

Figure 2-50 contains contours of tilt angle in frequency-distance space for the fixed vertical coil configuration described earlier. The massive sulfide response occurs at BB' over the frequency range 30 Hz to 1000 Hz and is of small amplitude. The disseminated sulfide response occurs at CC' and is ten times larger in amplitude, and occurs at frequencies above 2000 Hz. The overburden and weathered bedrock response occurs at AA' and spans frequencies from 10^3 Hz to 10^5 Hz. By exciting the earth over nearly four decades of frequency and making very precise measurements of tilt angle (precise to 0.1°), it is possible to separate the effects of massive from disseminated sulfides and to recognize the overburden and bedrock response in the data. Turam and induced polarization methods were unsuccessful in this difficult problem of resolution.

Airborne detection of conductors beneath deep resistive cover:

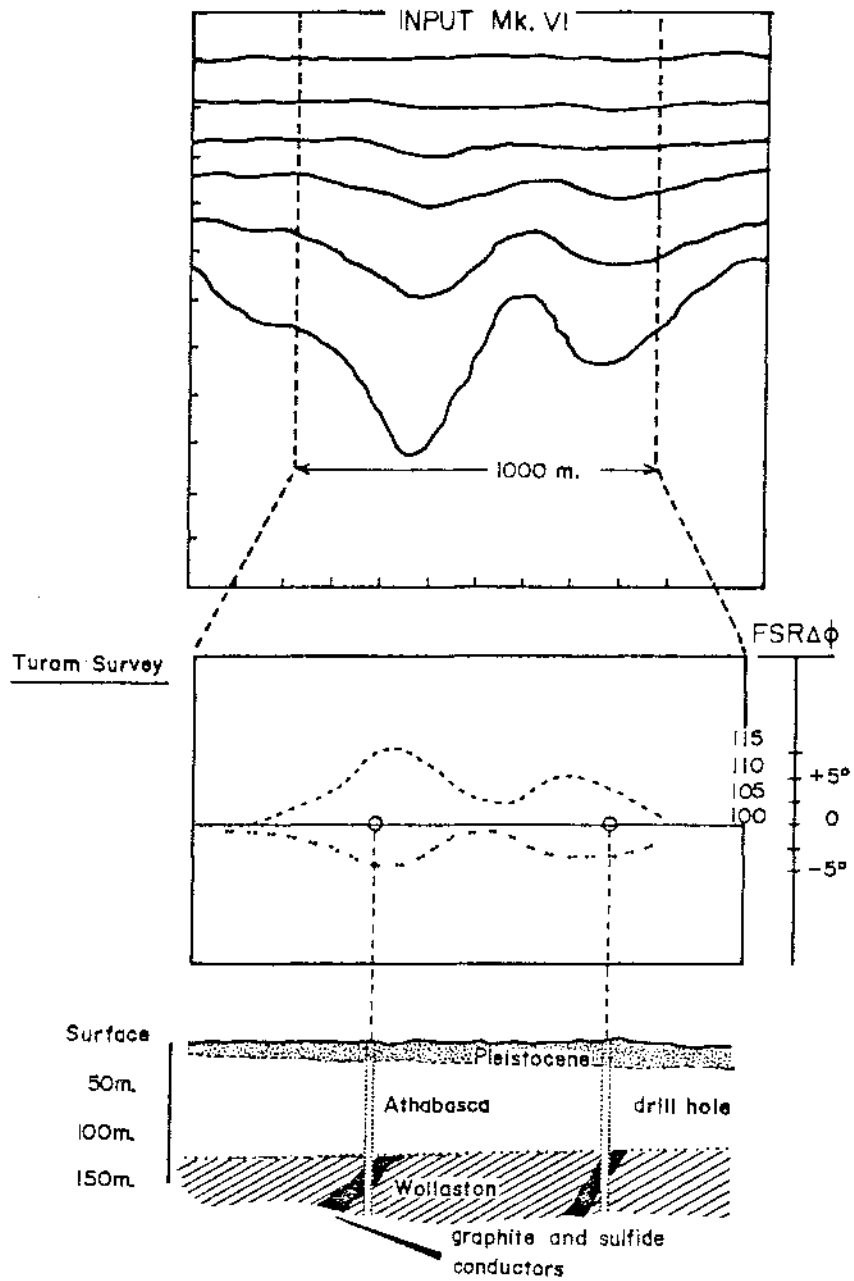
Uranium occurs in association with graphitic pelites in the lower Aphebian beneath the Athabasca sandstones of the Athabasca basin of Saskatchewan, Canada. From outcropping around the basin, the Aphebian metamorphic rocks become increasingly buried until towards the center of the basin these rocks may be covered by more than 1000 m of sandstone. Fortunately the sandstone is resistive ($\sim 3000 \Omega\text{-m}$) so that one can "see through" it with AEM methods rather readily, except in those parts of the basin where the overburden is deep and conductive. INPUT anomalies, due to the graphitic pelites, reportedly have been found beneath 200 m of Athabasca sandstone cover. Figure 2-51 portrays a somewhat less dramatic but still very important example of the ability of INPUT to see through resistive cover of

LINE 20
 VERTICAL AXIAL COIL
 TILT ANGLE-DEGREES
 NORMALIZED TO 10.5 HZ
 Tx 3+00E



-  MASSIVE SULFIDES
-  INTERMEDIATE TO BASIC VOLCANICS
-  FELSIC TUFF (PYRITIC)
-  100 ft.

2-50



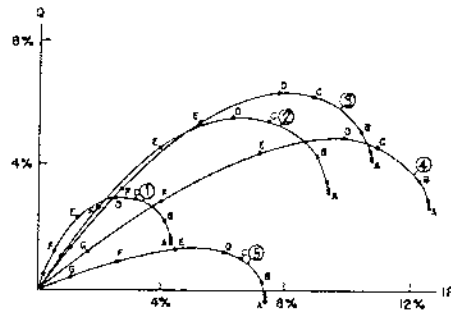
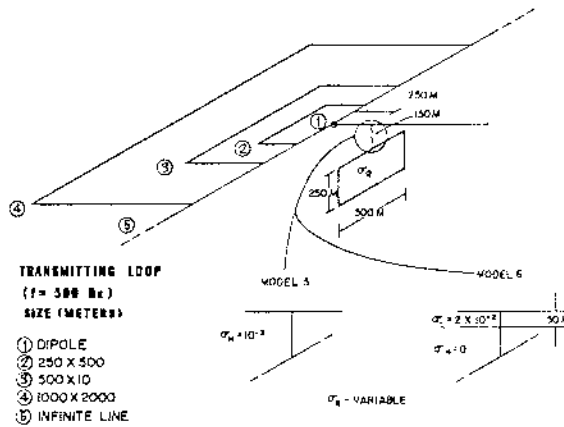
depth about 125 m.

Uses of airborne electromagnetic systems: Initially, AEM systems were used solely to search for anomalies over massive sulfide deposits; this is still their most common use. We refer to this as AEM profiling. In later years, the INPUT, DIGHEM, and TRIDEM systems have been used additionally to produce maps of resistivity from the air. Seigel and Pitcher (1978) report on the use of TRIDEM to map sand, clay, bedrock, and lignite. Fraser (1978, 1979) reports on use of DIGHEM to estimate surficial resistivity and thereby remove surficial conductors from consideration when one is engaged in sulfide search. He also reports on the use of DIGHEM in mapping permafrost, sand, and gravel. Palacky and Kadokaru (1979) report on the use of INPUT in estimating overburden and bedrock resistivities.

Basis for selecting a particular electromagnetic system

Ground systems, transmitting loop size: It can be argued that the larger the loop the larger the potential for exploring to greater depths. The basis for this argument is that in the small dimensional limit the loop is a dipole, whereas in the large dimensional limit the loop becomes four line sources. Fields from a dipole fall off as $1/R^3$ whereas fields from a line source fall off as $1/R$ where R is the distance from the source to the target. Coupled with the attractiveness of using larger loops for greater depth of exploration is an opposing factor which is that a loop couples best with a body of its own dimensions and hence only very large targets would be excited optimally by very large loops. The theoretical computations of Lajoie and West (1976) confirm this analysis in a general way but indicate that the optimum source dimension depends upon the overburden and host rock resistivities as well as upon the dimensions of the inhomogeneity. Figure 2-52 from Lajoie and West (1976) show two models and their respective phasor diagrams. In these figures, the in-phase (IP) and quadrature (Q) amplitudes are normalized with respect to the vertical component of the primary magnetic field intensity on the surface, directly over the thin plate model. Note that the largest percentage anomaly occurs for a 1000 m to 2000 m loop for model 5 while it occurs from a 250 m x 500 m loop for model 6.

Ground systems, domain of acquisition: Electromagnetic data is always collected as a time series describing an electromagnetic field at a point P and a time t . The resulting data may be processed and interpreted in the *frequency domain* (FEM) or in the *time domain* (TEM). In (FEM) the spectrum of the waveform is viewed through some frequency window or passband while in

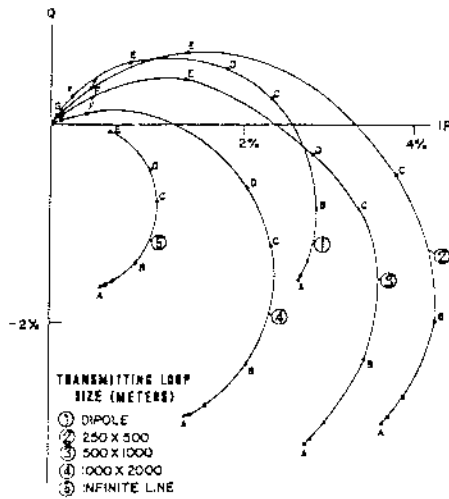


TRANSMITTING LOOP SIZE (METERS)

- ① DIPOLE
- ② 250 X 500
- ③ 500 X 1000
- ④ 1000 X 2000
- ⑤ INFINITE LINE

$I \sigma_g$ (MHD)

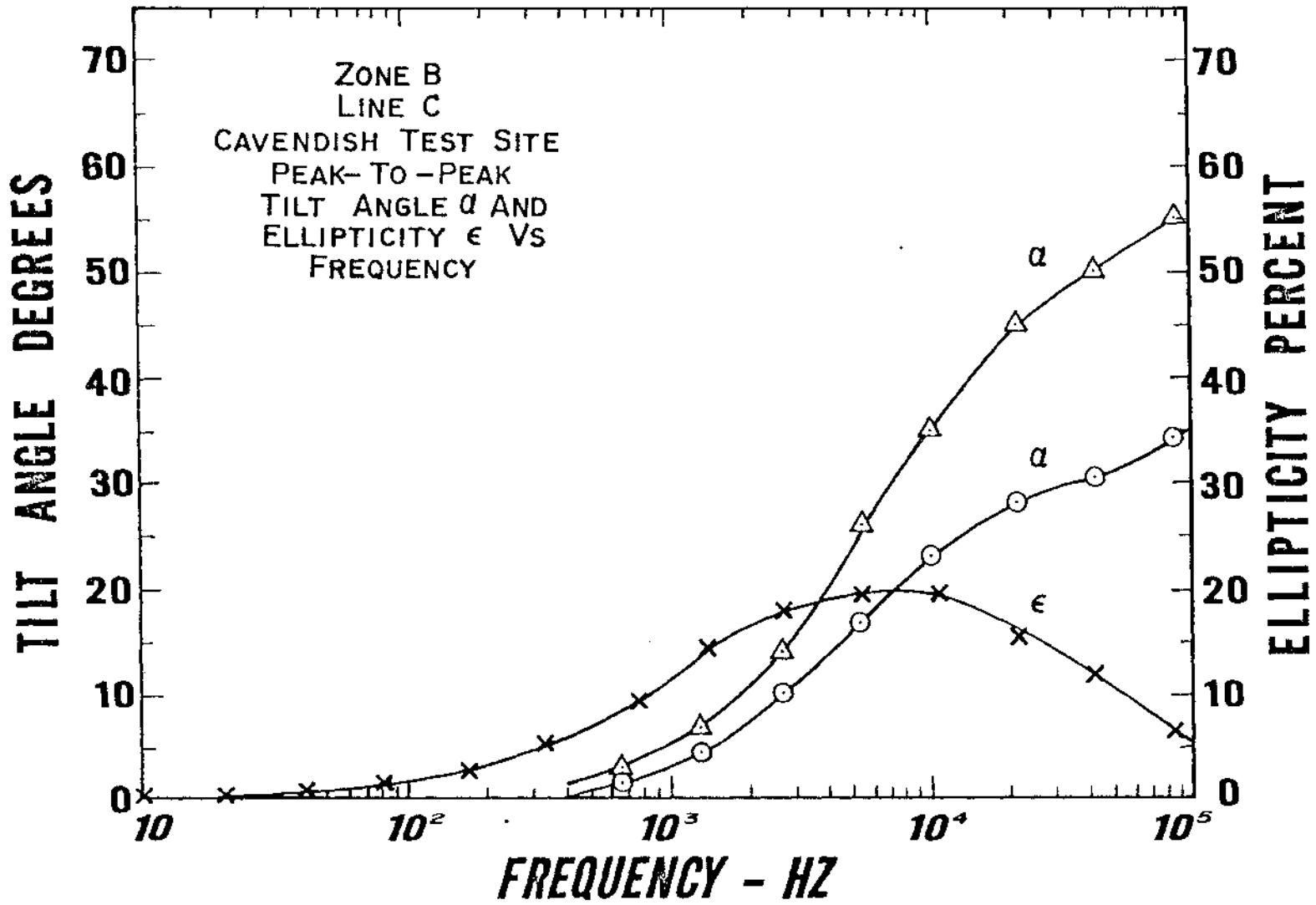
- A 1000
- B 30
- C 10.5
- D 7
- E 5
- F 1
- G 3



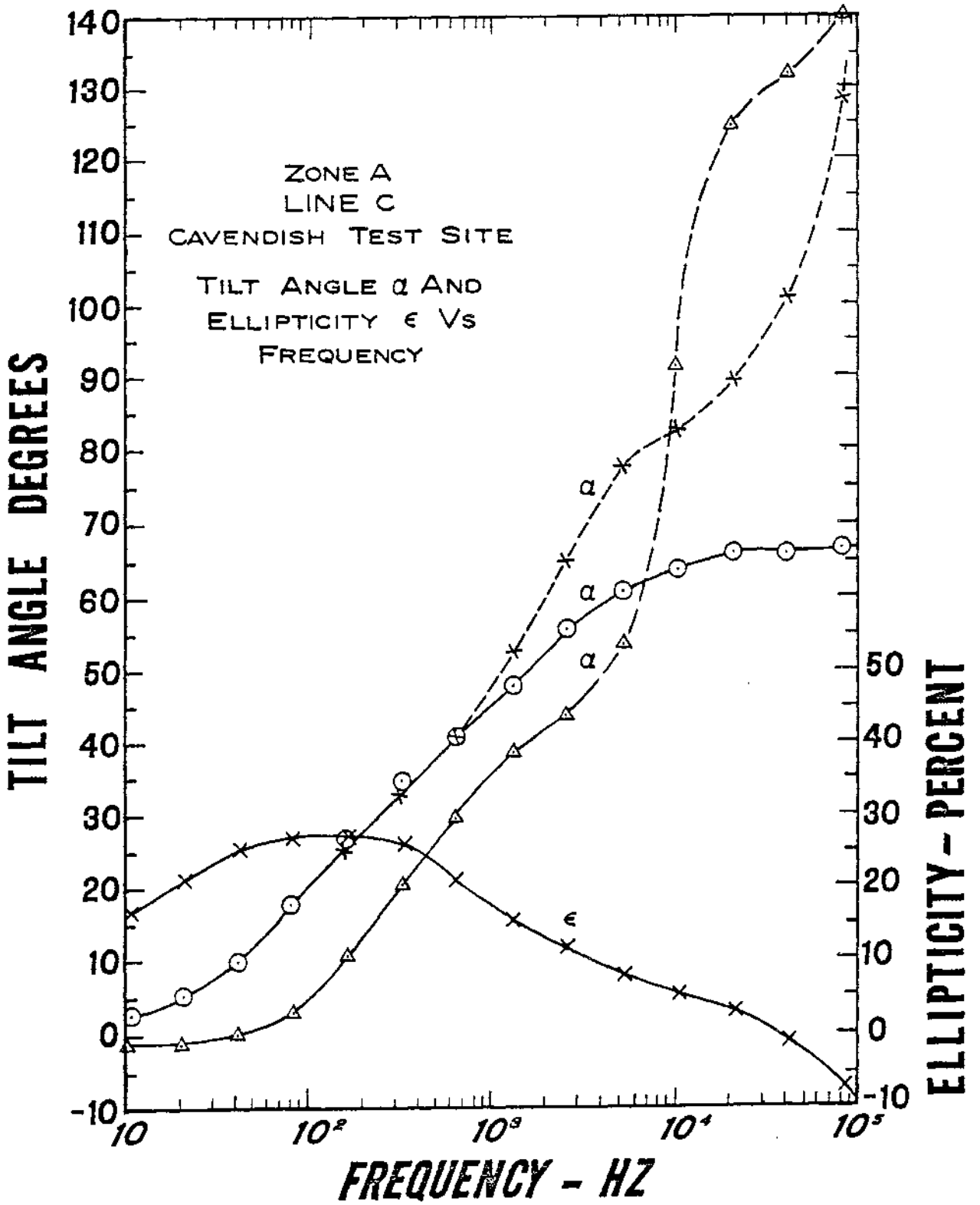
TEM the transient decay of an impulsive waveform is viewed through some time window, also a passband. Observations at discrete frequencies or at discrete times are most commonly made. There is no particular reason why one transmitted waveform cannot be processed and interpreted in the frequency domain, in the time domain, or in both domains simultaneously. Attempts to design optimum waveforms have been made in recent years. Thus, UTEM (Lamontagne and West, 1973) was designed to transmit a triangular waveform and receive its derivative, a square waveform. Pseudo random noise generators (Quincy et al., 1976) and sweep-frequency generators have also been proposed. Enhancement of the ratio of signal to noise is the reason for selecting these latter waveforms. Regardless of the method of data processing and interpretation, the signal sensed at the receiver is a superposition of a primary field, including the effects of a homogeneous earth, and a secondary field reflected from a subsurface inhomogeneity. Oristaglio et al., (1979) have attempted an assessment of the relative merits of time and frequency domain systems. They conclude, among other things, that current technology favors time domain for minimizing the geometrical part of instrument noise and for fast data acquisition with attendant lower costs but at the expense of fewer decades of spectrum and lower ratio of signal to noise.

Ground systems, decades of spectrum : If the earth responded as a single body, the anomaly to which it gave rise with any EM system would, as a function of frequency, trend from a low frequency asymptote to a high frequency asymptote in about three decades of frequency. Zone B at the Cavendish Test Site in southern Ontario, Canada seems to respond this way to both a *fixed vertical coil* and a *fixed horizontal coil* over the

frequency range 10^2 to 10^5 Hz. Figure 2-53 contains plots of a) the tilt α_1 of the major axis of the projection of the ellipse of magnetic field polarization on a vertical plane passing through the axis of a vertical transmitting coil, b) the ratio ϵ_1 of the minor to major axis of this projection of the ellipse of magnetic field polarization on a vertical plane passing through the axis of a vertical transmitting coil, and c) the tilt α_2 of the major axis of the projection of the ellipse of magnetic field polarization on a vertical plane passing through the axes of a horizontal transmitting coil. All curves are both smoothly varying and slowly varying. If the response of a sulfide body were always so simple and predictable, then only two or three frequencies spread over a decade or two, would be needed to learn all there is to know, electrically, about the sulfide body. Indeed, until ten years ago this was the common assumption. However, the earth can behave in a most unusual manner as a function of frequency when not only the sulfide body, but the host rock, the overburden and the other elements of the general earth also contribute in the frequency window used. This is illustrated in Figure 2-54 in which plots of ellipticity and tilt angle over Zone A of the Cavendish Test Site are contained. With vertical axial coil excitation, the tilt angle α_1 trends from asymptote to asymptote over four decades of frequency while the ellipticity ϵ_1 at 10^5 Hz is at the high frequency asymptote, but never does reach a low frequency asymptote four decades below this. With horizontal coil and vertical rotating coil excitations the tilt angles, α_2 and α_3 , respectively, at 10 Hz are at the low frequency asymptote but the high frequency asymptote is never reached. The latter two curves are not at all smoothly varying or even slowly varying. It should be evident from the



8-25



previous illustration that at least four decades and preferably five decades of spectrum (1 Hz to 10^5 Hz) are required to understand the earth. Most commercially available systems use one to two decades and hence are not suited to use over complex earths. On the other hand, advanced systems such as GEOPROBE use four decades of spectrum and hence are to be preferred for complex earths. About four frequency or time samples per decade are necessary to assure delineation of rapid changes of response with frequency or time.

Ground systems, signal-to-noise ratio: As has been described previously, natural field and the geometrical part of instrument noise can be designed to be small in a survey. Assuming that this can be done, one is left with geological noise and cultural noise. The latter two noise sources require very careful attention to detail but can be recognized and/or eliminated using numerical or scaled physical modeling. The cost of assigning a particular part of an EM signature to either geological or cultural noise can be prohibitive and this then identifies a barrier for future study as shall be described below.

Ground systems, lateral resolution: A conventional two loop system is better for resolving two adjacent conductors than any of the other source types. The smaller the size of the transmitting and receiving coils the more this statement is true. However adjacent patches of conductive overburden will be resolved as well as two adjacent thin ore veins; the penalty is higher geological noise. Thus the 50 m to 100 m square loop used as transmitter and receiver with SIROTEM serves to filter out geological noise but at the expense of lack of resolution of deeper subsurface conductors. Further study of this problem is required.

Ground systems, coil configurations : The horizontal loop system is more responsive to overburden and other flat lying conductors than is, say, the rotating vertical loop system. This may be good or bad. Much more numerical or scaled physical modeling is required before all comparative studies of optimum coil configurations for all geologic settings are completed.

Some coil configurations are much less susceptible than others to the geometrical part of instrument noise as Table 2-3 indicates. As noted earlier, one would use any time-domain system, Crone Shootback, or vertical rotating loop if removal of the effect of topography on this noise source was paramount. Topographical noise is dependent upon coil configuration and its recognition and reduction or removal is another barrier for future study.

Airborne systems, transmitting coil size : Except for the semi-airborne Turair system, transmitting coil size cannot be varied to optimize the response of that part of the geoelectric section with which we are concerned. With Turair, the coil dimensions more often than not are selected with the intent of reducing survey costs rather than optimizing the response of a particular element of the geoelectric system.

Airborne systems, domain of acquisition and decades of spectrum : All current AEM systems, whether they operate in the time or frequency domain, can at best achieve one to one-and-one-half decades of frequency or spectrum. This is insufficient to define the geoelectric section completely and hence we should not look to current AEM methods for this achievement.

Airborne systems, signal-to-noise ratio : All current AEM systems are

designed such that geological noise dominates over all noise sources other than cultural under normal conditions of operation. As long as one deals with a modern AEM system in good operating condition, then he must accept geological noise and cultural noise as part of the record he is attempting to secure. The geological noise becomes most severe when terrain clearance varies rapidly over an earth of low apparent resistivity (Ward, 1969). With proper data processing, including removing the effect of variable terrain clearance, this noise can contribute useful information about the shallower parts of the geoelectric section (e.g. Fraser, 1978; Palacky and Kadekaru, 1979). Cultural noise severely limits the application of AEM methods in urban areas.

Airborne systems, lateral resolution, swath width, and depth of exploration: The rigid boom systems exhibit higher lateral resolution than either the towed bird or semi-airborne systems. They do so at the expense of reduction in ability to detect a conductor off to the side of the flight line; costs increase with increase in lateral resolution. Depth of exploration, provided geological noise is sufficiently suppressed, is greater for towed bird and semi-airborne systems than for rigid boom systems.

Airborne systems, coil configurations: Fraser (1979) has clearly established that the more coil configurations one uses in an airborne electromagnetic system, the better is he able to understand the earth. Fraser's work with DIGHEM II is remarkable in this respect. The opportunity to use a spectrum of frequencies is, however, sacrificed in the process.

SELF POTENTIAL METHOD

Principles

The self potential (SP) method is based on the measurement of natural potential differences, essentially direct current (DC), in the ground. These natural potential differences are caused mainly by electrochemical, electrokinetic and thermoelectric sources.

Electrochemical sources are involved with changes in the concentrations of substances in the pore water solution. There are large differences in the oxidation potential (Eh) between the aerated region above the water table and the reducing region at depth (Sato and Mooney, 1960). The classical application of SP in mining exploration involves massive sulfide ore bodies that span these regions. The conducting orebody then acts as a conductor of electrons from the reducing region at depth to the oxidizing region near the surface. The return current is provided by pore water ions in the surrounding medium, and this current flow produces a negative anomaly over the top of the conducting zone. Conductors other than sulfides such as graphite, cased drill holes, pipes, etc. can also generate potential differences by this mechanism. Sato and Mooney (1960) rank the various minerals in their ability to produce anomalies as, graphite (800 mv), pyrite (700 mv), covellite (600 mv), chalcocite (500 mv) and galena (300 mv).

Electrokinetic current and potential differences are caused by the flow of pore water solution when the concentrations and mobilities of cations and anions are different, a condition that can easily be caused by clays and their associated exchange cations. Under these conditions a flow

of fluid drags along an excess of positive ions which constitute a positive current.

Thermoelectric effects have a similar origin except that the driving force is a temperature gradient rather than a pressure gradient. The origin of SP anomalies by all of these mechanisms is discussed in detail by Nourbehecht (1963).

Instrumentation and measurements

One of the advantages of the SP method is the simplicity of the instrumentation and the measurement. All that is needed is wire, a high input impedance voltmeter and a pair of non-polarizable electrodes usually of the porous pot variety. Digital, battery operated voltmeters covering the range from millivolts to volts are readily available off the shelf and rugged, nonpolarizable Cu-CuSO₄ electrodes are common.

The potential measurements are simply made by implanting the electrodes in the soil moisture region, which is usually a few to ten cm deep, and reading the potential difference between the electrodes. The distance between the measurements depends on the size of the source but is usually in the range from 10 m to 100 m. Two techniques are commonly used, the first and easiest makes use of a fixed, short length of wire which is *leap-frogged* along the line, and both electrodes are moved. The successive potential differences between stations are recorded and algebraically summed to get the potential along the line relative to the first electrode. The second technique leaves one electrode fixed, and the other is advanced along the line, and the total potential difference with respect to the fixed electrode is measured directly. Each of the methods has its

advantages and disadvantages which will be discussed later.

Problems

Measurement errors, i.e. noise, arise from the electrodes, small scale variations in the ground potential, and on a larger scale, telluric currents. Electrode generated errors, sometimes called pot noise, can arise from temperature changes, electrolyte concentration changes in the porous pots and in the porous ceramic. These errors usually occur as slow drifts in relative potential over a period of hours. They can be partially compensated by checking the potential differences between the electrodes, at the same location, several times during the course of the survey and using this data to make linear drift corrections. Watering of the electrode stations, to reduce pot resistance should be avoided as it can cause potential transients of 5 to 10 mv, lasting as long as an hour (Corwin and Hoover, 1978).

Small scale (cm to m) potential differences exist in the ground due to changes in the soil and soil moisture and the biological activity of plants. These potential differences are typically in the range from 1 to 10 mv and can be partially compensated by making a number of readings over a small area and averaging the results.

Telluric currents produce potential gradients in the range from 1 to 10 mv/km. On long lines these potentials can be a source of error. Relatively rapid fluctuations (from 1 to 10 sec), when observable on the meter, can be averaged but this is not practical for longer period fluctuations. These could be partially compensated by monitoring the low frequency variations on a fixed dipole but this is not usually done.

Cultural effects due to DC power systems, pipes, cased drill holes, roads (disturbed soil) and cultivated fields (fertilizer) have been observed. Topographic effects, possibly do to the motion of groundwater, are also present.

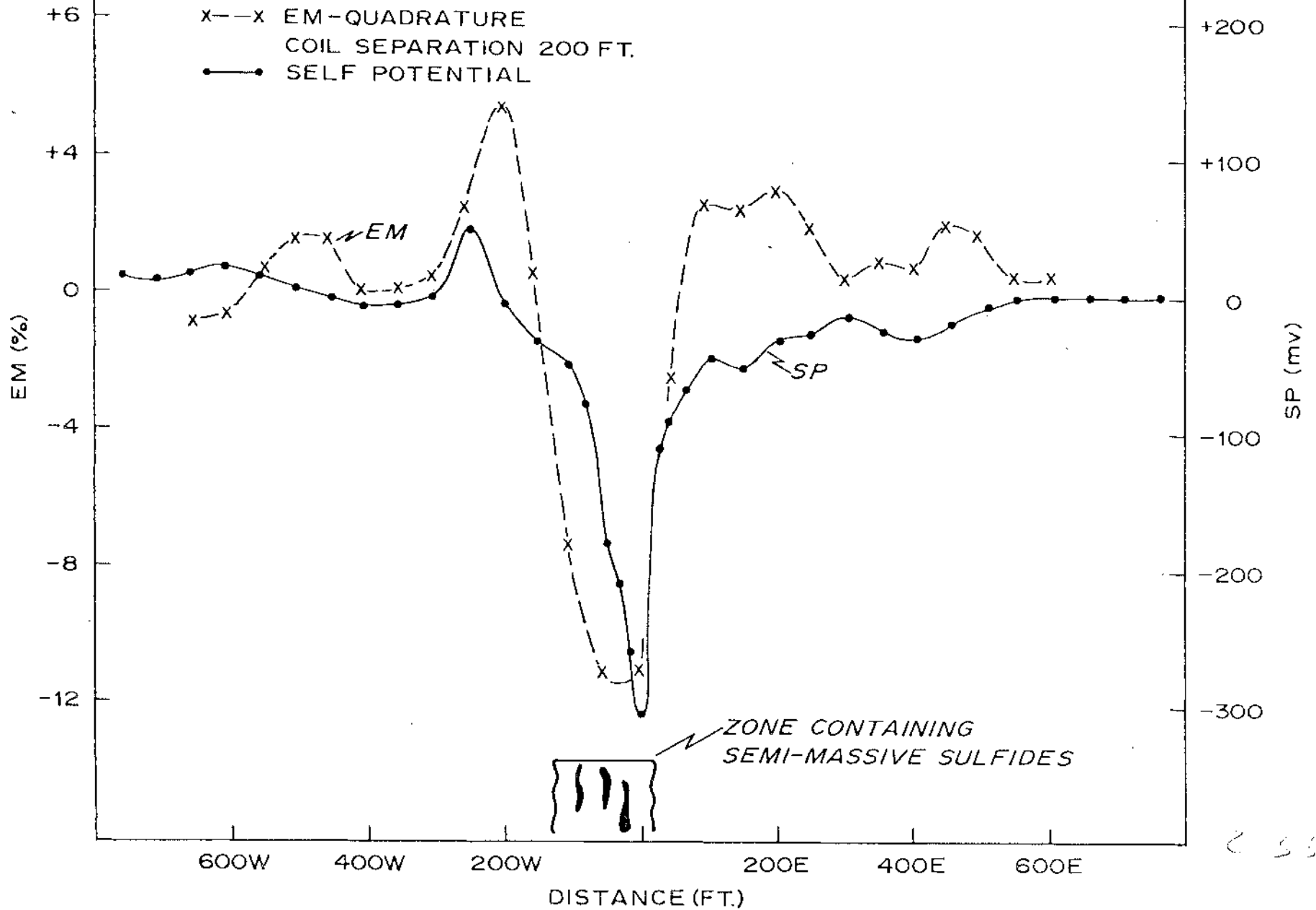
In considering the possible noise sources we see that the leapfrog method has the logistic advantage of using a short line but since both electrodes are moved it is subject to more pot noise. This technique combined with the finite precision of the measurement acts like a high pass spatial filter and attenuates the long wavelength, low amplitude fluctuations. This is effective in reducing the effects of telluric currents, but it will also attenuate the long wave length anomalies due to other sources. The long line method has the advantage of pot noise from only a single electrode but at large distances the telluric current variations can cause problems.

Data quality can be assessed by repeated measurements and by closure errors on closed loop surveys. With reasonable care, repeated surveys show a typical scatter of ± 5 mv to ± 10 mv and closure errors as small as a few tens of millivolts.

Applications

The original application of SP measurements in mining exploration was in the search for massive sulfides. The technique is useful for shallow ore bodies that span the oxidizing-reducing environments. Figure 2-55 shows the SP and horizontal loop EM responses over a zone containing semi-massive sulfides (R. F. Corwin, pers. comm.). Both techniques delineate the ore zone quite nicely. Presently, SP is little used in

SP AND EM RESPONSE OVER MASSIVE SULFIDE



253

mining exploration since shallow massive sulfides are easy targets for many geophysical techniques and most easy targets have been found.

More recent applications of SP are to be found in the search for geothermal resources where the sources of the anomaly are thought to be electrokinetic or streaming potential and possibly thermoelectric and electrochemical (Corwin and Hoover, 1978). Anomalies associated with geothermal areas and hot springs are often dipolar in form; both positive and negative regions exist. The magnitudes of the anomalies are small, usually less than 100 mv, and the wavelengths are large, often of the order of kilometers. These factors make the detection of geothermal anomalies difficult and have led to recent improvements in technique and reliability of the data.

Another area of recent interest is the use of SP in engineering applications. Ogilvy et al. (1969) and Bogoslovsky and Ogilvy (1973) describe the use of SP to outline areas of water leakage around dams and drainage structures. SP methods have also been suggested as a possible tool in the exploration for uranium deposits of the roll front type wherein a redox couple exists. The use of SP in these other applications is still very limited in the U.S.

Interpretation

In general, very little quantitative interpretation is used in conjunction with SP measurements. The form, magnitude and the halfwidth of the anomaly can be used as with other potential methods to put some limits on the depth, size and perhaps the dip of the source. Some modeling with various SP source mechanisms has been done (Nourbehecht, 1963; Corwin and

Hoover, 1978) but generally for simple sources and bodies. The utility of the method in various applications will probably have to be further demonstrated before much additional progress is made in this area.

REFERENCES

- Becker, A., 1980, Airborne electromagnetic methods; *in* Geophysics and Geochemistry in the Search for Metallic Ores; P. J. Hood, ed.; Geol. Surv. Can., Econ. Geol. Rpt. 31, p. 33-43.
- Best, M. E. and Shamma, B. R., 1979, A general solution for a spherical conductor in a magnetic dipole field, *Geophysics*, 44 (4), p. 781-800.
- Bogoslovsky, V. A. and Ogilvy, A. A., 1973, Deformations of natural electric fields near drainage structures, *Geophys. Prosp.*, v. 21, p. 717-723.
- Bosschart, R. A., 1964, Analytical interpretation of fixed source electromagnetic prospecting data, Ph.D. thesis, Delft Uitgeverij Waltman, 103 p.
- Bosschart, R. A. and Seigel, H. O., 1971, Turair; a semi-airborne electromagnetic method for deep mineral exploration, Scintrex brochure.
- Brant, A. A., Dolan, W. M., and Elliot, S. C. L., 1956, Coplanar and coaxial EM tests in Bathurst area, New Brunswick, Canada, *Mining Geophysics* v. 1, Tulsa, Soc. of Explor. Geophys., p. 130-141.
- Coggon, J. H., 1971, Electromagnetic and electrical modeling by the finite element method: *Geophysics*, v. 36 (1), p. 132-155.
- Coggon, J. H., 1973, A comparison of IP electrode arrays: *Geophysics*, v. 38 (4), p. 737-761.
- Corwin, R. F. and D. B. Hoover, 1978, The self-potential method in geothermal exploration, *Geophysics*, v. 44, (1) p. 226-245.
- Crone, J. D., 1966, The development of a new ground EM method for use as a reconnaissance tool; *Mining Geophysics*, v. I, Tulsa, Soc. of Explor. Geophys.
- Crone, J. D., 1973, Model studies with the Shootback method; in *Symposium on electromagnetic exploration methods*, Univ. of Toronto.
- Crone, J. D., 1979, Exploration for massive sulfides in desert areas using the ground pulse electromagnetic method, *in* Geophysics and Geochemistry in the Search for Metallic Ores; P. J. Hood, ed.; Geol. Surv. Can., Econ. Geol. Rpt. 31, p. 745-755.
- Edward, R. N., and Howell, E. C., 1976, A field test of the magnetometric resistivity (MMR) method: *Geophysics*, v. 41, (6A) p. 1170-1183.
- Fountain, D. K., 1972, Geophysical case history of disseminated sulfide deposits in British Columbia; *Geophysics*, v. 32 (1), p. 142-159.

- Fox, R. C., Hohmann, G. W., Killpack, T. J., and Rijo, L., 1980, Topographic effects in resistivity and induced polarization surveys: *Geophysics*, v. 45 (1), p. 75-93.
- Fraser, D. C., 1971, VLF-EM data processing: *CIM Bull.*, v. 64, p. 39-41.
- Fraser, D. C., 1972, A new multicoil aerial electromagnetic prospecting system, *Geophysics*, 37 (3), p. 518-537.
- Fraser, D. C., 1978, Resistivity mapping with an airborne multicoil electro-magnetic system, *Geophysics*, 43 (1), p. 144-172.
- Fraser, D. C., 1979, The multicoil II airborne electromagnetic system, *Geophysics*, 44 (8), p. 1367-1394.
- Gamble, T. D., Goubau, W. M., and Clarke, J., 1979, Magnetotellurics with a remote magnetic reference: *Geophysics*, v. 44 (1), p. 53-68.
- Goldstein, M. A., and Strangway, D. W., 1975, Audio-frequency magnetotellurics with a grounded electric dipole source, *Geophysics* 40 (4), p. 669-683.
- Ghosh, M. K., 1972, Interpretation of airborne EM measurements based on thin sheet models, Ph.D. thesis, Dept. of Physics, University of Toronto, 195 p.
- Grant, F. S., and West, G. F., 1965, Interpretation theory in applied geophysics, New York, McGraw-Hill Book Company, 583 p.
- Hallof, P. G., 1974, The IP phase measurement and inductive coupling: *Geophysics*, v. 39.(5), p. 650-665.
- Halversen, Mark, 1977, IP research and development directions: Univ. of Utah, NSF Report - Workshop on Mining Geophysics.
- Hohmann, G. W., 1975, Three-dimensional induced polarization and electromagnetic modeling, *Geophysics*, 40 (2), p. 309-324.
- Hohmann, G. W., Van Voorhis, G. D., and Nelson, P. H., 1978, A vector EM system and its field applications, *Geophysics* 43 (7), p. 1418-1440.
- Kuo, J. T., and Cho, D. H., 1980, Transient time domain electromagnetics, *Geophysics*, v. 45 (2), p. 271-291.
- Lajoie, J. J., and West, G. F., 1976, The electromagnetic response of a conductive inhomogeneity in a layered earth; *Geophysics*, 41 (6A), p. 1133-1156.
- Lamontagne, Y., 1970, Model studies of the Turam electromagnetic method: M.A.Sc. thesis, University of Toronto.

- Lamontagne, Y., and West, G. F., 1973, A wide-band, time domain, ground EM system; in Proc., Symposium on electromagnetic exploration methods, Univ. of Toronto, p. 2-1 to 2-5.
- Lodha, G. S. and West, G. F., 1976, Practical EM(AEM) interpretation using a sphere model, *Geophysics*, 41 (6A), p. 1157-1169.
- Matsushita and Campbell, eds., 1967, *Geophysics and geomagnetic phenomena*: New York Academic Press, 1398 p.
- McCracken, K. G., and Buselli, G., 1978, Australian exploration geophysics - current performance and future prospects, Second Circum - Pacific Energy and Minerals Resources Conference, July 30-Aug. 4, Honolulu.
- Morrison, H. F., Dolan, W. M., and Dey A., 1976, Earth conductivity determinations employing a single superconducting coil, *Geophysics*, 41 (6A), p. 1184-1206.
- Nabighian, M. N., 1977, The Newmont EMP method; *in* *Geophysics applied to detection and delineation of non-energy, non-renewable resources*, Report on Grant AER76-80802 from the Nat'l Science Foundation; Dept. Geol. and Geophys., Univ. of Utah.
- Nabighian, M. N., 1978, Newmont EMP-Modeling, in Lecture notes from the U.S.-Australia electromagnetics workshop, eds. B. Braham, R. Baren, D. Lappi, H. Lemaire, D. Payne, A. Raiche, B. Spies, and K. Vozoff, *Bull. Aust. Soc. Explor. Geophys.*, 9(1), p. 1-33.
- Nelson, P. H., 1977, Induced polarization effects from grounded structures: *Geophysics*, v. 42 (6), p. 1241-1253.
- Nourbehecht, B., 1963, Irreversible thermodynamic effects in inhomogeneous media and their application in certain geoelectric problems, Ph. D. thesis, Mass. Inst. of Tech. Cambridge, Mass.
- Ogilvy, A. A., Ayed, M. A., and Bogoslovsky, V. A., 1969, Geophysical studies of water leakages from reservoirs, *Geophys. Prosp.*, v. 22, p. 36-62.
- Oristaglio, M., Hohmann, G. W., and McCracken, K. G., 1979, Toward a comparison of time- and frequency domain electromagnetic methods in practical exploration, Abs., Soc. of Explor. Geophys., 49th Annual International Meeting and Exposition, New Orleans, Nov. 4-8, 1979.
- Palacky, G. J., and West, G. F., 1973, Quantitative interpretation of INPUT AEM measurements, *Geophysics*, 38 (6), p. 1145-1158.
- Palacky, G. J., 1975, Interpretation of INPUT AEM measurements in areas of conductive overburden, *Geophysics*, 40 (3), p. 490-502.
- Palacky, G. J., 1978, Selection of a suitable model for quantitative

- interpretation of towed-bird AEM measurements, *Geophysics* 43 (3), p. 576-587.
- Palacky, G. J., and Kadokaru, K., 1979, Effect of tropical weathering on electrical and electromagnetic methods, *Geophysics*, 44 (1), p. 69-88.
- Paterson, N. R., 1971, Airborne electromagnetic methods as applied to the search for sulphide deposits, *Trans, CIMM*, (64), p. 1-10.
- Pelton, W. H., Ward, S. H., Hallof, P. G., Sill, W. R., and Nelson, P. H., 1978, Mineral discrimination and removal of inductive coupling with multifrequency IP: *Geophysics*, v. 43 (3), p. 588-609.
- Pemberton, R. H., 1962, Airborne EM in review, *Geophysics*, 27 (5), p. 691-713.
- Pridmore, D. F., Ward, S. H., and Motter, J.W., 1979, Broadband electromagnetic measurements over a massive sulfide prospect, *Geophysics*, v. 44 (10), p. 1677-1699.
- Quincy, E. H., Davenport, W. H., and Motter, J. W., 1976, Three-dimensional response maps for a new side-band induction system; *IEEE Transactions on Geoscience Electronics*, GE-14 (4), p. 261-269.
- Sato, M., and Mooney, H. M., 1960, The electrochemical mechanism at sulfide self-potentials, *Geophysics*, v. 25, p. 226-249.
- Scott, W. J., and Fraser, D. C., 1973, Drilling of EM anomalies caused by overburden; *Can. Inst. Min. Met. Bull.*, v. 66 (735), p. 72-77.
- Seigel, H. O., and Pitcher, D. H., 1978, Mapping earth conductivities using a multifrequency airborne electromagnetic system, *Geophysics* 43 (3), p. 563-575.
- Smee, B. W., and Sinha, A. K., 1979, Geological, geophysical and geochemical considerations for exploration in clay-covered areas: a review, *C.I.M. Bulletin*, p. 67-82.
- Spies, B. R., 1975, The dual loop configuration of the transient electromagnetic method, *Geophysics*, 40 (6), p. 1051-1057.
- Spies, B. R., 1976, The derivation of absolute units in electromagnetic scale modeling, *Geophysics*, 41 (5), p. 1042-1047.
- Strangway, D. W., Swift, C. M., and Holmer, R. C., 1973, The application of audio-frequency magnetotellurics (AMT) to mineral exploration: *Geophysics*, v. 38 (6), p. 1159-1175.
- Ting, S. C. and Hohmann, G. W., 1980, Integral equation modeling of three-dimensional magnetotelluric response: submitted to *Geophysics*.

- vanVoorhis, G. D., Nelson, P. H., and Drake, R. L., 1973, Complex resistivity spectrum of porphyry copper mineralization: *Geophysics*, v. 38, (1) p. 49-60.
- Velikin, A. B., and Bulgakov, Y. I., 1967, Transient method of electrical prospecting (one loop version): International seminar on geophysical methods of prospecting for ore minerals: Moscow, 1967.
- Ward, S. H., Cartier, W. O., Harvey, H. A., McLaughlin, G. H., and Robinson, W. A., 1958, Prospecting by use of natural alternating fields of audio and sub-audio frequencies; *Bull. CIMM*, v. 51, p. 487-494.
- Ward, S. H., 1959, AFMAG-airborne and ground, *Geophysics*, 24 (4), p. 761-789.
- Ward, S. H., O'Donnell, J., Rivera, R., Ware, G. H., and Fraser, D. C., 1966, AFMAG - Applications and limitations, *Geophysics*, 31 (4), p. 576-605.
- Ward, S. H., 1967, Airborne electromagnetic methods, *Mining and Groundwater Geophysics 1967*, Geol. Survey of Canada, Ec. Geol. Rpt. (26), p. 81-108.
- Ward, S. H., 1969, Low-frequency airborne electromagnetic methods, *Advances in Geophysics*, (13), p. 41-88, New York, Academic Press.
- Ward, S. H., Pridmore, D. F., Rijo, L., and Glenn, W. E., 1974, *in* Multispectral electromagnetic exploration for sulfides, *Geophysics*, v. 39 (5), p. 666-682.
- Ward, S. H., 1979, Ground electromagnetic methods and base metals; *Geophysics and Geochemistry in the Search for Metallic Ores*; P. J. Hood, ed; Geol. Surv. Can., Econ. Geol. Rpt. 31, p. 45-62.
- Wight, D. E., Bostick, F. X., and Smith, H. W., 1977, Real time Fourier transformation of magnetotelluric data: U. of Texas at Austin, ERL Report.
- Wynn, J. C. and Zonge, K. L., 1975, EM coupling, its intrinsic value, its removal and the cultural coupling problem: *Geophysics*, v. 40 (5), p. 831-850.

FIGURE CAPTIONS

- Fig. 2-1. Sine wave decomposed into in-phase and quadrature components. Amplitude is designated by A , phase by ϕ , period by T , and frequency by f .
- Fig. 2-2. Typical time domain waveform.
- Fig. 2-3. Equivalent circuit and response for IP effects in rocks.
- Fig. 2-4. Interpretation models: ρ denotes resistivity and ϕ denotes IP response, 1D - one dimensional, 2D - two dimensional, 3D - three dimensional.
- Fig. 2-5. Common electrode arrays, geometric factors, parameters displayed, and use.
- Fig. 2-6. Typical in-situ IP phase spectra for various types of mineralization.
- Fig. 2-7. Theoretical attenuation of the IP response of a large 2D body or conductive overburden. (Computed by C. M. Swift, Jr.)
- Fig. 2-8. EM coupling due to a 3D conductive (1 Ω -m) prism in a 100 Ω -m earth. Prism width 2000 ft (610 m), depth extent 3000 ft (915 m), length 6000 ft (1830 m), and depth 1000 ft (305 m).
- Fig. 2-9. Extrapolation method of removing EM coupling from IP data.

- Fig. 2-10. Generalized spectrum of natural magnetic fields (after Matsushita and Campbell, 1967).
- Fig. 2-11. Apparent resistivity anomaly due to a 2D valley with 30 degree slopes (after Fox et al., 1980).
- Fig. 2-12. Apparent resistivity anomaly due to a 2D ridge with 30 degree slopes (after Fox et al., 1980).
- Fig. 2-13. Total electric field IP response ($B_2\%$) and quadrature field direction in the earth for a body of units 1 W, 1 DE, and 5 L with no resistivity contrast. Large numbers in pseudosection are IP response for the transmitter dipole considered. Broken arrows show direction of primary field.
- Fig. 2-14. Prism model for IP response study in Figures 15-24.
- Fig. 2-15. Effect of strike length on IP response: $W = 2$, $DE = 4$, $D = 1$, $\rho_2/\rho_1 = 1$.
- Fig. 2-16. Effect of depth on IP response: $W = 2$, $DE = 4$, $L = 5$, $\rho_2/\rho_1 = 1$.
- Fig. 2-17. Effect of width on IP response: $DE = 4$, $L = 5$, $D = 1$, $\rho_2/\rho_1 = 1$.
- Fig. 2-18. Effect of depth extent on IP response: $W = 2$, $L = 5$, $D = 1$, $\rho_2/\rho_1 = 1$.
- Fig. 2-19. Peak dipole-dipole IP response versus resistivity contrast for sphere, 3D prism, and 2D bodies.

- Fig. 2-20. Effect of position of line along strike: $W = 2$, $DE = 4$, $L = 5$,
 $D = 1$, $\rho_2/\rho_1 = 1$.
- Fig. 2-21. Effect of electrode position with respect to body: $W = 2$,
 $DE = 4$, $L = 5$, $D = 0.5$, $\rho_2/\rho_1 = 0.2$.
- Fig. 2-22. IP response of a dipping conductive body: $\rho_2/\rho_1 = 0.2$.
- Fig. 2-23. IP response of a dipping resistive body: $\rho_2/\rho_1 = 5.0$.
- Fig. 2-24. Superposition of IP responses due to two prisms: $W = 1$, $DE =$
 4 , $L = 5$, $D = 1$, $\rho_2/\rho_1 = 0.2$.
- Fig. 2-25. IP response from deep sulfide mineralization beneath resistive
overburden - Kennecott Safford, Arizona, porphyry copper
deposit.
- Fig. 2-26. IP response from sulfide mineralization beneath low-resistivity
cover - Lakeshore, Arizona, porphyry copper deposit.
- Fig. 2-27. The generalized geologic model used for the electromagnetic
method in the search for massive sulfides.
- Fig. 2-28. a) Circulating or vortex currents associated with electro-
magnetic induction in a conductor in a resistive half-space.
The vortex currents add the anomalous ΔE to the normal E
recorded by the receiving coil.
- b) Uniform currents induced in a half-space by a transmitting
coil. The uniform currents add the anomalous ΔE to the
normal E recorded by the receiving coil.

c) A combination of vortex and uniform currents induced in an inhomogeneous half-space. The vortex and the uniform currents, in interaction, both contribute to ΔE . This is also a pictorial representation of current gathering.

Fig. 2-29. Time and frequency domain responses for good and poor conductors (after Oristaglio et al., 1979).

Fig. 2-30. Turam survey over the Freddie Well massive sulfide deposit in Western Australia (after Hohmann et al., 1968).

Fig. 2-31. a) Model curves obtained with the F-400 AEM system over a horizontal ribbon 400 m wide and over a vertical half-plane. Circles indicate peak amplitudes measured over the Whistle orebody, near Sudbury, Ontario, Canada.

b) Quadrature amplitudes (Q) at two frequencies recorded by F-400 system over the Whistle orebody. H is the terrain clearance of the aircraft (after Palacky, 1978).

Fig. 2-32. Profiles of $e(t)/I$ over a thin horizontal conducting overburden overlying a thick vertical plate. The dual loop configuration gives a stronger response from the vertical plate and is less masked by the overburden (after Spies, 1975).

Fig. 2-33. Plot of in-phase and quadrature normalized anomalous field amplitudes, for variable plate and host half-space conductivities (after Lajoie and West, 1976).

Fig. 2-34. Principle of the AFMAG phase detection system.

- Fig. 2-35. The four basic source types used in electromagnetic exploration consist of a) coplanar horizontal, coplanar vertical, or coaxial loop pairs, b) a large rectangular source loop to which a single horizontal or vertical receiving coil is referenced, c) a single loop which is used sequentially as transmitter and as receiver in the time domain or whose impedance is measured in the frequency domain, and d) a grounded wire source to which electric and magnetic field components are referenced.
- Fig. 2-36. The orientation of the planes of the loop and of the magnetic dipole moments for a) the horizontal loop method, b) the vertical coaxial loop method, and c) the vertical coplanar loop method.
- Fig. 2-37. The orientations of the receiving and transmitting coils for the Crone Shootback method in a) vertical transmitting coil mode, and b) horizontal transmitting coil mode.
- Fig. 2-38. The orientations and dispositions of the transmitting and receiving coils for the broadside vertical loop method in a) plan view; b) section through the vertical plane of the transmitting coil, and c) vertical section through the receiving coil.
- Fig. 2-39. The orientations and dispositions of the transmitting and receiving coils for the rotating vertical loop method in a) plan view, and in b) vertical section through the transmitting coil plane.

- Fig. 2-40. Dual coil method of measuring tilt angle α and ellipticity ϵ along the axis of a vertical loop. S is the signal coil, R is the reference coil, while h_1 and h_2 are the major and minor axes, respectively, of the ellipse of magnetic field polarization.
- Fig. 2-41. Basic configurations of airborne electromagnetic systems.
- Fig. 2-42. Turam data obtained in area of high geological noise.
- Fig. 2-43. Profiles at four time delays of single loop SIRTEM survey over the Elura massive sulfide deposit, New South Wales, Australia (after McCracken and Buselli, 1978).
- Fig. 2-44. Profiles of three orthogonal magnetic field components obtained with the Newmont EMP system over the Mutooroo deposit near Broken Hill, S.A., Australia (courtesy Misac Nabighian).
- Fig. 2-45. Plan view of interpreted position of conductor deduced from Newmont EMP results, relative to weathered outcrop positions at the Mutooroo deposit near Broken Hill, S.A., Australia (courtesy Misac Nabighian).
- Fig. 2-46. Profile record from a DIGHEM flight.
- Fig. 2-47. Profile record from a DIGHEM flight perpendicular to Montcalm orebody, Ontario, Canada. The hachures define the contribution from conductive overburden (after Fraser, 1979).

Fig. 2-48. UTEM profiles across the IZOK massive sulfide deposition in the Northwest Territories, Canada (courtesy G. F. West and Y. Lamontagne).

Fig. 2-49. UTEM profiles across a buried flat-lying sulfide body of relatively low conductivity (courtesy G. F. West and Y. Lamontagne).

Fig. 2-50. Contours of tilt angle in frequency-distance space obtained with the University of Utah 14 frequency system across a volcanogenic sulfide deposit in the foothills copper belt of California (after Pridmore et al., 1979).

Fig. 2-51. INPUT profile across graphitic pelite of the Aphebian metamorphic rocks beneath the Cambrian Athabaska sandstone, Saskatchewan, Canada (courtesy Questor Surveys Limited, Asamera Oil Corporation Limited, Saskatchewan Mining Development Corporation, Kelvin Energy, and E. and B. Explorations).

Fig. 2-52. a) Geometry for models 5 and 6, transmitting loop size in meters, $f = 500$ Hz.

b) Plot of in-phase and quadrature normalized anomalous field amplitudes, for variable plate conductivity and transmitting loop size in meters for model 5.

c) Plot of in-phase and quadrature normalized anomalous field amplitudes, for variable plate conductivity and transmitting loop size in meters for model 6 (after Lajoie and West,

1976).

Fig. 2-53. Peak-to-peak tilt angle \odot and ellipticity X for the fixed vertical coil; and peak tilt angle \triangle for the fixed horizontal coil. All are plotted against frequency for Zone B, Cavendish Test site (after Ward et al., 1974).

Fig. 2-54. Peak-to-peak tilt angle \odot and ellipticity X for the fixed vertical coil; peak-to-peak tilt angle X for the vertical rotating coil; and peak tilt angle \triangle for the fixed horizontal coil. All are plotted against frequency for Zone A, Cavendish Test Site (after Ward et al., 1974).

Fig. 2-55. Comparison between SP and EM anomalies over shallow massive sulfide zone (courtesy R. F. Corwin).

LIST OF TABLES

- Table 2-1 Summary of Effects of Extraneous Features in Electro-
magnetic Search for Massive Sulfides.
- Table 2-2 Attenuation and Geometrical Decay.
- Table 2-3 Analysis of Instrument Noise.

SECTION 3 - GRAVITY AND MAGNETIC METHODS

Introduction

Although many differences exist between them, gravity and magnetic methods of prospecting are often discussed together because of similarities in data display and interpretation techniques. In this section we will consider the principles, instrumentation, data collection, data reduction and application separately and then review interpretation methods together. Good general references include Grant and West (1965), Dobrin (1976), Rao and Murthy (1978), and Parasnis (1979). Excellent current reviews are given by Tanner and Gibb (1979) and Hood et al. (1979).

Principles of the Gravity Method

The gravitational force between two bodies of masses M_1 and M_2 is given by Newton's law to be $F = G M_1 M_2 / r^2$, where G is the universal gravitational constant and r is the distance of separation. The force is one of attraction and is directed along the line connecting the bodies. In gravity prospecting we often speak about the acceleration of gravity, which is the acceleration that a freely falling body would experience in the earth's gravitational field. This acceleration is given by $G M_e / r_e^2$, where M_e and r_e are the mass and radius of the earth respectively. It is found by measurement that the earth's gravitational acceleration is about 983 gals (cm/sec^2) at the poles and about 978 gals at the equator. The gal and the milligal are common units, named after Galileo, used in gravity prospecting. Gravity is less at the equator than at the poles because the equatorial radius is greater than the

polar radius and because of the variation with latitude of centrifugal force due to the earth's rotation.

Modern gravity meters routinely measure spatial variations in the earth's gravity field to 0.01 milligals (1 part in 10^8) or better in field application, and the newest generation of instruments is capable of ± 0.002 milligals under ideal field conditions. These spatial variations in gravity are caused by lateral variations in rock density. The average density of the earth is 5.5 gm/cm^3 and the average density of crustal rocks is about 2.67 gm/cm^3 . We conclude that density must increase with depth in the earth. Such vertical density changes are not detected in surface surveys - only lateral density changes are detected. Because near-surface density variations affect the gravimeter more than do deep variations, in accordance with the inverse square nature of Newton's law, most gravity variations of interest in mining exploration result from lateral changes in density within shallow crustal rocks.

Rock density depends upon mineral composition, degree of induration, porosity, and compressibility. Shales display marked variations of density with depth because of their relatively high compressibility. As a general rule, older sedimentary rocks are higher in density than younger sedimentary rocks. Most plutonic and metamorphic rocks display smaller ranges in density than do sedimentary and volcanic rocks. Acid igneous rocks are less dense than basic igneous rocks. Volcanic rocks often display rapid density variations due to porosity changes from place to place. Table 3-1 lists typical values of density for a variety of rock types. Note that density

TABLE 3-1

DENSITIES OF ROCKS AND MINERALS
(Modified from Dobrin, 1976, with additions)

<u>NAME</u>	<u>DENSITY, gm/cm³</u>	
	<u>Range</u>	<u>Average</u>
Alluvium and Soil	1.6-2.2	1.90
Sandstone	1.6-2.6	2.32
Limestone	1.9-2.8	2.54
Dolomite	2.4-2.9	2.70
Shale	1.8-2.5	2.42
Granite	2.5-2.8	2.67
Diorite	2.6-3.0	2.84
Gabbro	2.8-3.1	2.98
Diabase	2.8-3.1	2.97
Dunite	3.2-3.3	3.28
Quartzite	2.6-2.7	2.65
Gneiss	2.6-3.1	2.75
Schist	2.6-3.0	2.82
Slate	2.6-2.8	2.81
Amphibolite	2.7-3.2	2.99
Eclogite	3.3-3.5	3.39
Salt	1.90-2.20	2.15
Pyrite	4.9-5.2	5.00
Pyrrhotite	4.5-4.7	4.60
Sphalerite	3.9-4.1	4.00
Magnetite	5.0-5.2	5.10
Water	---	1.00

variations greater than 25 percent of the average crustal density, 2.67 gm/cm³, are rare in near-surface rocks. This variation is in sharp contrast to electrical and magnetic properties of rocks, which can vary over several orders of magnitude.

Instrumentation

Exploration gravity meters are among the most sensitive mechanical instruments man has made. Modern meters can detect gravity changes of 0.002 milligals, which corresponds to the change in gravity that would be observed by reading the meter and then setting the instrument 0.65 cm higher in elevation and rereading. Gravimeters do not measure the absolute value of the earth's field, but instead detect gravity differences from place to place by measuring the change in the earth's attraction for a small mass of about 1 gm. Changes in the extensions of a delicate system of fused quartz springs that support the small mass are detected. Fused quartz is generally used because of its known and relatively stable thermal and mechanical properties. Even so, temperature compensation and thermostatic control are necessary to decrease drift. Gravity meter construction is an art that few possess and each meter is handcrafted.

For mining purposes, most gravity surveys are conducted on the ground, although shipborne gravity survey techniques are also well developed and are used by the petroleum industry and by geodesists. State of the art in airborne surveys seems to be about 5 to 10 milligal accuracy, which is insufficient for most mining application. Development of an effective airborne gravity gradiometer seems practical, however, and if such a system could be deployed it would have important application to minerals exploration.

Effective borehole gravity meters have been recently developed and are in routine use (Jageler, 1976; Glenn, this paper). Applications include locating bodies that the drill hole has missed and determining bulk rock density, which can often in turn be related to lithology, porosity and fracturing.

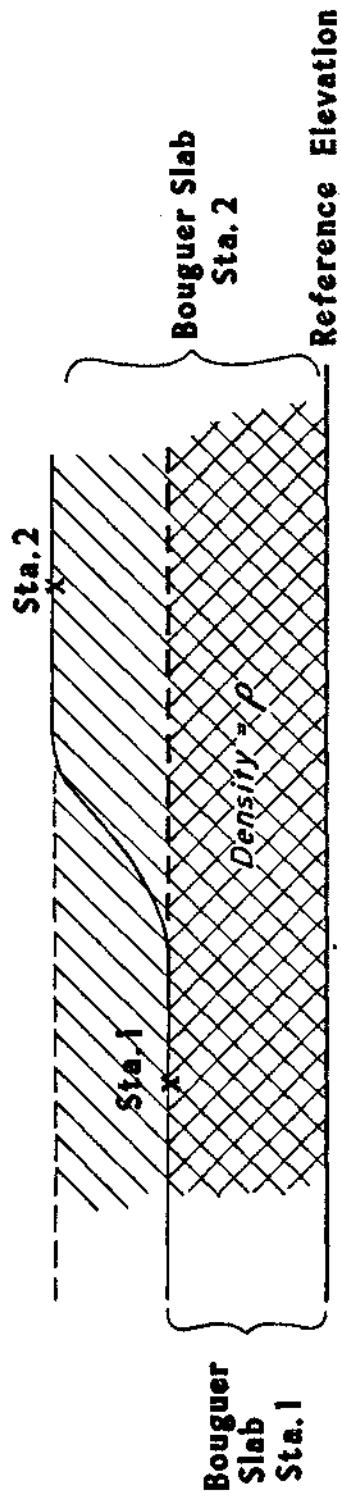
Surveying and data reduction

Field surveys are performed by reading the gravimeter at selected station sites, either on a regular grid or in an irregular pattern as station access and optimum survey design dictate. Repeated readings are commonly made at one- to four-hour intervals, at one or more previously established base stations in order to determine instrument drift and local tidal variations. Variations in base station readings are assumed to be linear or smoothly varying between field station readings, and this information is used to correct field readings.

Information in addition to the gravimeter reading must be known at each site in order to reduce the raw field data. The instrument must be carefully calibrated. Calibration is initially done by the manufacturer, but it should be checked periodically either by repeated readings between two or more stations whose gravity differences are known or by using other methods. Corrections must be made for differences in elevation and latitude among the stations. The latitude correction removes the effects of the northward increase in the earth's field. There are two elevation effects that are usually combined into one correction (Figure 3-1). A reference elevation is selected to which all elevation corrections are made. For simplicity, in the following discussion the reference elevation is assumed to be the elevation of

Free Air Correction = + .3086 mgal/ft

Bouguer Correction = -0.04186 Pmgal/ft



the survey base station although any elevation could be selected. The *free-air* correction accounts for the decrease in the gravity field with increasing distance from the earth's center, but the correction ignores the mass of material that lies between the ground surface and the reference elevation. The Bouguer correction accounts for this mass by assuming it to be an infinite slab of uniform thickness and specified density. Variations from this slab assumption are accounted for by a topographic correction which is commonly applied only in areas of rugged topography. Both the Bouguer and the topographic correction require an assumption for the density of near-surface rocks. This density is often assumed to be 2.67 gm/cm³. An incorrect density assumption will generate false anomalies that correlate with elevation changes (Grant and West, 1965 p. 241). Care must be exercised to choose the correct density, particularly in rugged areas.

By reading the gravity meter in turn at a base station and at a field station, an observed gravity difference between the stations, g_{obs} , is determined as follows:

$$g_{obs} = C(R_{sta} - R_{base} + D) \quad (3-1)$$

Where R_{sta} and R_{base} are the meter readings at the field base stations, D is the drift and tidal variation and C is the instrument calibration in milligals per dial division. In the absence of a gravity anomaly at the field station, the theoretical difference in gravity, g_t , between field and base stations would be:

$$\begin{aligned} g_t &= \text{latitude effect} + \text{free air effect} + \text{Bouguer effect} + \text{terrain effect} \\ &= + 0.8121 \sin 2\phi \text{ mgal/km (north of base station)} - 0.3086 \text{ mgal/m} \end{aligned}$$

(above base station elevation) + 0.04186 ρ mgal/m (above base station elevation) - terrain effect. (3-2)

In this formula ϕ is the geographic latitude and ρ the assumed Bouguer density. Signs are as given for a station north of the base and above the selected reference, i.e. base station, elevation. If the station is south of the base or below the reference elevation, the appropriate signs must be reversed. The terrain effect is always of the same sign. It may be calculated by operation on topographic maps with terrain correction charts or with an appropriate computer program.

The anomalous gravity value, G_{sta} , at the field station relative to the base value, G_{base} , is given by

$$\begin{aligned} G_{sta} &= G_{base} + g_{obs} - g_t \\ &= G_{base} + g_{obs} - 0.8121 \sin 2\phi / \text{mgal/km} \\ &\quad (\text{north}) + 0.3086 \text{ mgal/m (above base)} - 0.04186 \rho \\ &\quad \text{mgal/m (above base)} + \text{terrain correction.} \end{aligned} \quad (3-3)$$

Any convenient value for G_{base} may be taken. If the gravity anomaly relative to the International Ellipsoid is known for the base, then that value is generally used because the field station then becomes tied to other similar stations elsewhere on earth.

From the above formulas we see that north-south station location must be known to about 10 m and elevation must be known to about 0.05 m in order to make the latitude and elevation corrections of the same order as the 0.01 milligal specifications of many surveys. The newer generation of more

sensitive instruments requires correspondingly more accurate location and elevation information. Not all gravity applications require this accuracy, however, and surveys should always be tailored to the problem to be solved.



Applications

The gravity technique can facilitate solution to a wide variety of geological and exploration problems. As with other geophysical techniques successful application depends critically upon trained and experienced geophysicists and technicians who pay attention to detail and who work closely with the geologist during survey design, data reduction, and interpretation.

Because the gravimeter detects lateral variations in rock density, a density contrast must exist between the rock body under investigation and its country rock. If the body under investigation has a smaller density than the country rock, we say that there is a negative density contrast, and we expect the body to show a relative gravity low. Because the range of density in rocks is small, density contrasts of interest in exploration are small compared with the physical property contrasts in magnetic and electrical surveys. Survey variations due to latitude and elevation changes will often be much greater than the anomaly sought. Meticulous care must be taken in survey procedure and data reduction.

In some cases, orebodies have been directly detected by gravity surveys. Copper ore associated with massive pyrite bodies was discovered by underground gravity surveying at Bisbee, Arizona (Rogers, 1952; Sumner and Schnepfe, 1966). Gravity data were acquired along mining levels and were then contoured for interpretation both on levels and on vertical sections. Figure 3-2 shows

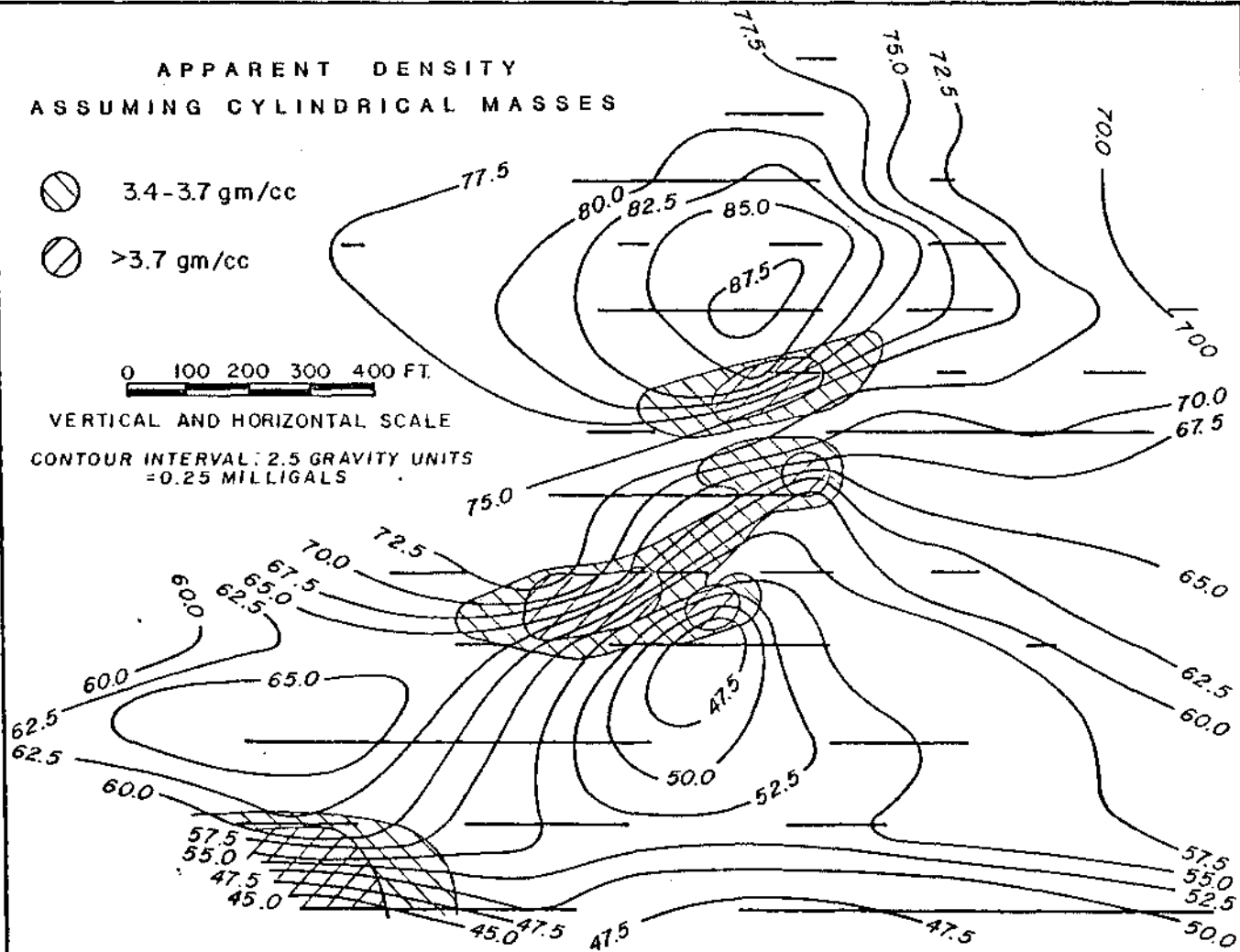
APPARENT DENSITY
ASSUMING CYLINDRICAL MASSES

-  3.4-3.7 gm/cc
-  >3.7 gm/cc

0 100 200 300 400 FT.

VERTICAL AND HORIZONTAL SCALE

CONTOUR INTERVAL: 2.5 GRAVITY UNITS
= 0.25 MILLIGALS



such a vertical section at Bisbee (Sumner and Schnepfe, 1966; Fig. 4). The cross-hatched areas are the interpreted positions of dense sulfide bodies required to explain the observed gravity anomalies. Note the existence of gravity highs above the interpreted bodies and gravity lows below. The authors state that of the recommended drill holes, 80 percent encountered sufficient sulfides to account for the gravity results.

Orebodies are often studied after discovery but prior to mining by gravity surveying to determine orebody dimensions, ore grade, and tonnage. Hinze (1966) gives examples of gravity studies to determine location and grade of iron orebodies in Minnesota, Wisconsin and Ontario, and concludes that gravity techniques can be superior to magnetic techniques in certain cases. Tonnage calculations can be made for some orebodies by calculating the excess mass needed to account for the gravity anomaly (Hammer, 1945; Grant and West, 1965, p. 269). Such calculations usually yield minimum figures for actual tonnage.

Acidic intrusions, that are commonly associated with mineralization, sometimes have an associated gravity low. U.S. Geological Survey open-file data show this effect at the Questa district, New Mexico where the low extends several miles east of known economic mineralization and presumably outlines prospective intrusive rocks at depth. Gravity lows are also observed in many intrusive complexes in the Basin and Range province. Stacy (1976) has documented a correlation between negative gravity anomalies of about 30 milligals and exposed quartz monzonite plutons in British Columbia, and has used this correlation to postulate locations for other plutons beneath

volcanic cover. Ager et al. (1973) used results of a gravity survey to propose a model, for the subsurface configuration of the Guichon Creek batholith in British Columbia. From the model, a relationship between the occurrence of known disseminated mineralization and batholith geometry was postulated and this relationship forms a valuable guide to further prospecting.

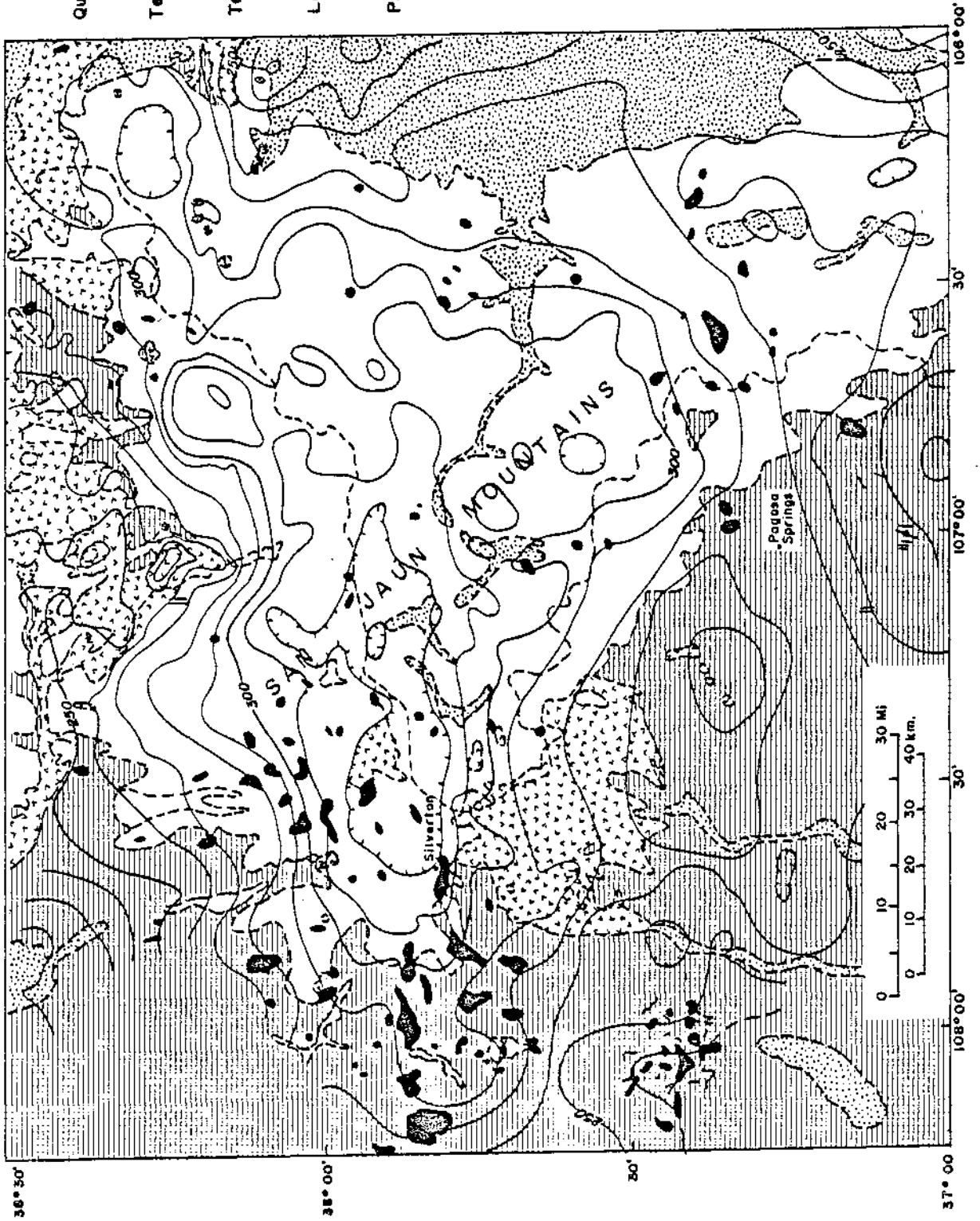
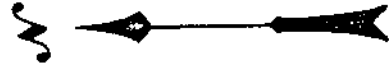
Plouff and Pakiser (1972) show a good example of the use of gravity data to model the geometry of a rather large intrusive complex in southwest Colorado. Figure 3-3 shows the salient features of the area and the gravity data. The large gravity low is postulated to be due to a concealed batholith that underlies a caldera complex in the San Juan Mountains.

Gravity surveys have been done in the Basin and Range Province and in many other areas of similar structure for the purpose of determining the thickness of basin fill. Gravity lows generally correlate with areas of thicker, low density alluvial material. Kane and Pakiser (1961) give a good example of this application in the Owens Valley of California. The method works well except in areas where intercalated volcanic rocks occur or where the alluvium is well consolidated. In both instances the density contrast between bedrock and basin fill becomes small and can approach zero, rendering the method ineffective. Gravity interpretation for alluvial-filled basins usually yields minimum alluvial thickness.

In massive sulfide exploration, the gravity method has been used as detailed follow-up to ground EM surveys to help differentiate sulfide and graphite conductors. Higher priorities for drilling can be given to areas

EXPLANATION

- Quaternary surficial deposits
- Tertiary volcanic rocks
- Tertiary intrusive rocks
- Lower Tertiary,
- Precambrian rocks



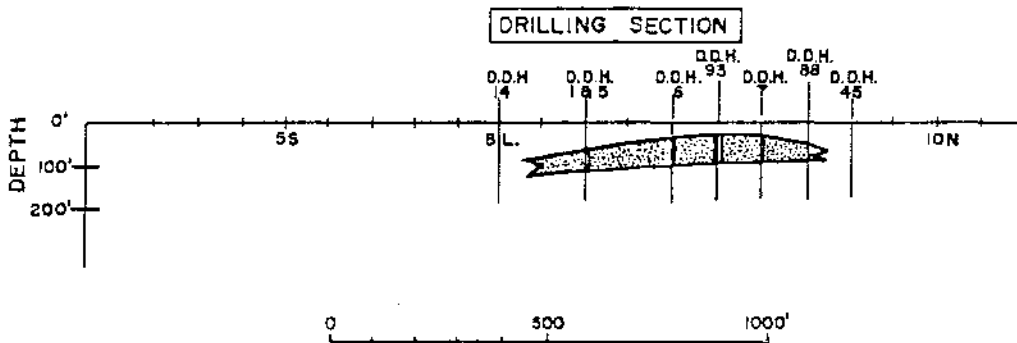
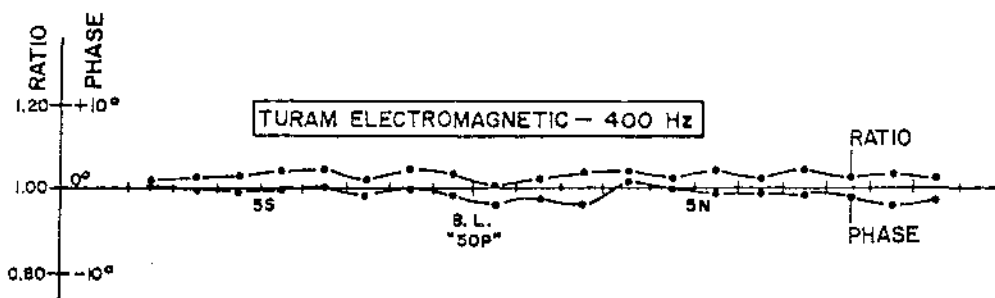
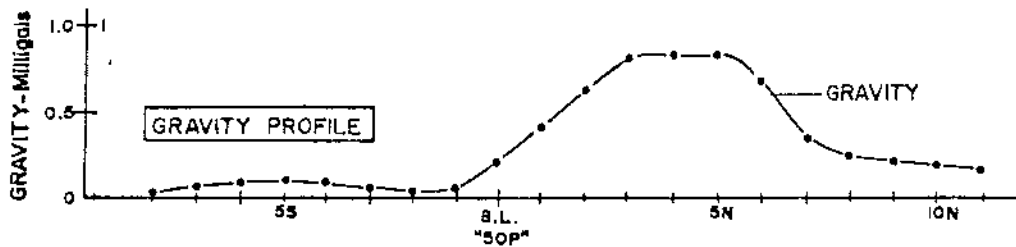
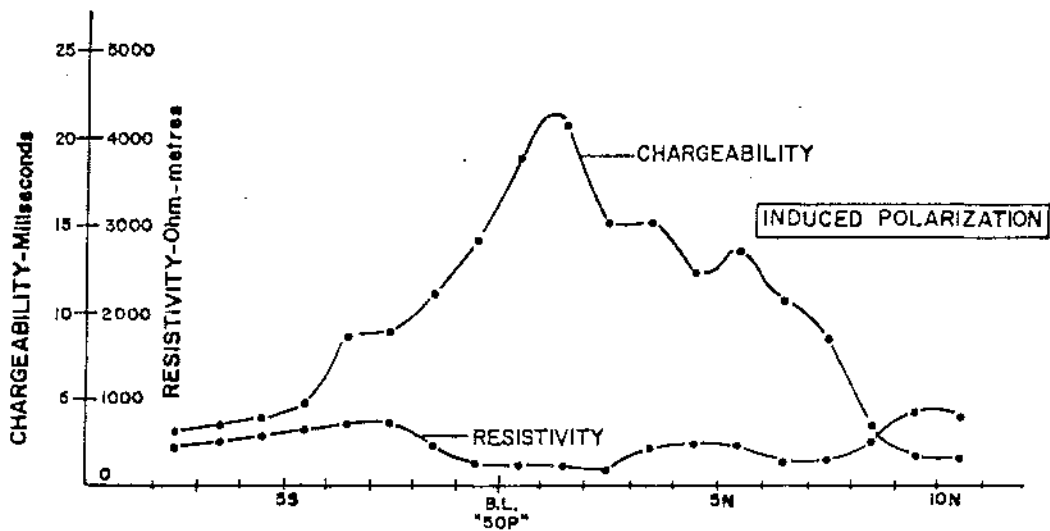
that show coincident positive gravity and EM anomalies, but care must be taken not to drop EM anomalies from consideration simply for lack of a gravity response. If an orebody is narrow or pipelike and is more than a few tens of feet below the surface, the gravity anomaly can be so small as to be lost in geologic noise. For example a vertical tabular orebody, 60 percent sulfide minerals, of 12 million tons that is 10 m wide and buried 30 m to the top will give a maximum gravity anomaly of only 0.5 milligals. Nevertheless, gravity surveys have been found useful in massive sulfide exploration by Seigel et al. (1968) at Pine Point, by Brock (1973) at Faro, Yukon territories, by Schwenk (1974) at Flambeau, Wisconsin, and by many other investigators. A Pine Point example is shown in Figure 3-4.

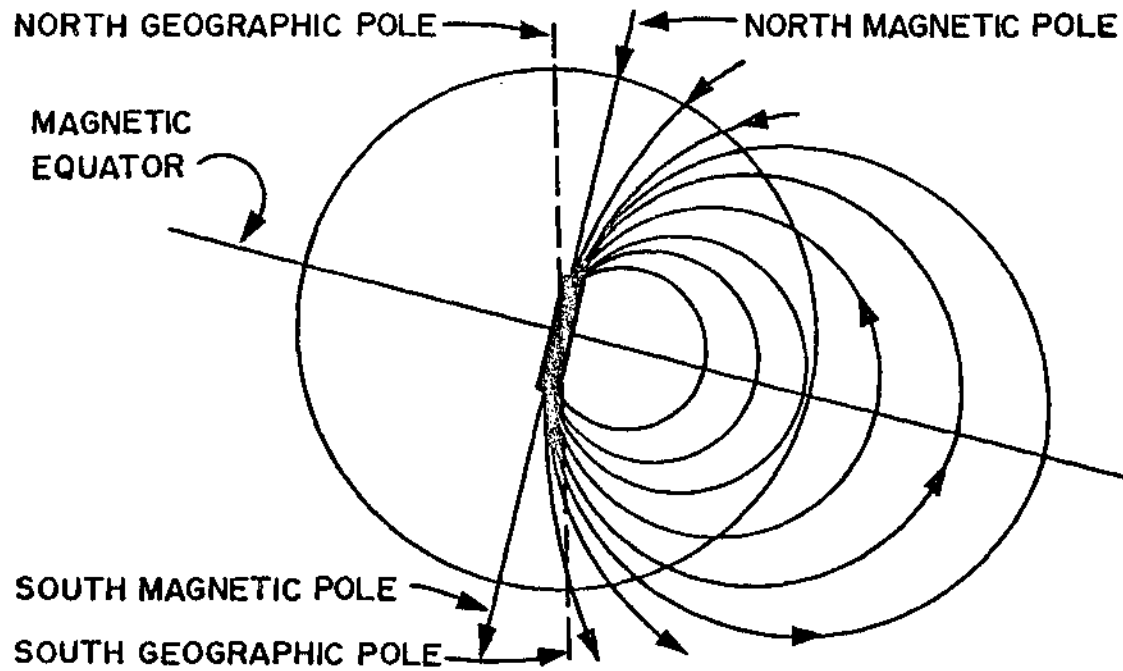
Principles of the Magnetic Method

The earth's magnetic field is believed to originate at great depth, although time-varying perturbations to this field originate outside the earth, principally in the ionosphere. Although many theories have been advanced to explain the earth's magnetism, the favored one is that fluid motions in the electrically conducting iron-nickel core of the earth cause a self-perpetuating dynamo effect that generates and sustains the field. The detailed fluid motions and mechanisms have never been formalized, but the basic concept seems sound.

To a good approximation, the field at the earth's surface is dipolar and thus resembles the field that would occur if a powerful bar magnet were placed at the earth's center. The general shape of the earth's magnetic field is shown in Figure 3-5. The dipolar axis does not correspond with the earth's

LINE 375 W





TOTAL MAGNETIC FIELD AT POLES=0.7 OERSTED

TOTAL MAGNETIC FIELD AT EQUATOR=0.25 OERSTED

1 GAMMA (γ)= .00001 OERSTED, $\frac{.00001}{.7} = \frac{1}{70,000}$

rotational axis but is displaced slightly in direction. Thus the north and south magnetic poles, where the field becomes vertical, do not correspond with the geographic poles. As a result of this and of the existence of very broad-scale, large-amplitude non-dipolar field components that also originate in the earth's core, lines of magnetic longitude and of geographic longitude are not parallel, and the compass needle does not point to geographic north or south.

The earth's field varies in intensity from about 25,000 gammas (1 gamma = 1 nanotesla = 10^{-5} oersted) at the magnetic equator to about 70,000 gammas at the poles (Figure 3-5). In direction the field is horizontal at the equator and vertical at the poles. Over most of the United States the field dips 60 to 70 degrees northward.

Magnetometers, in common use, measure variations in the intensity of the earth's field to about 1 gamma, although instruments that detect changes as small as 0.001 gammas are available. Spatial variations in the earth's magnetic field of interest in exploration are due to lateral variations in the magnetization of rocks near surface. Vertical, that is, layered changes in rock magnetization are not detected in magnetic surveying.

The origin of magnetization in rock materials involves considerations on the atomic and molecular level, and is beyond the scope of this section. Rock magnetism is a complex topic whose details are still being studied. Strangway (1967a and b; 1970) and Doell and Cox (1967) give good summaries of this and related topics. Rock magnetism has been treated in detail by Nagata (1961).

For our purposes there are three main points to note. First, magnetic minerals and rocks have a component of magnetization, often the chief component, due to induction in the earth's field. This induced component is the response of magnetic minerals to the earth's field, is proportional in intensity to the earth's field strength, and is in a direction parallel to the earth's field. The constant of proportionality is termed the *magnetic susceptibility*. Second, another form of magnetization called *remanent* or *permanent* magnetization often exists and is superimposed on induced magnetization. Remanent magnetization can form as a result of cooling of an igneous rock from a molten state, as a result of metamorphism, as a result of chemical changes, or from other causes. The remanent component of magnetization can be either weaker or stronger than the induced component, and it is often not in the same direction as the induced component. Remanent magnetism complicates interpretation. Rocks having small mineral grains commonly have a larger remanent component than those having larger mineral grains because the stability of remanent magnetization is related to grain size. Third, above a temperature known as the Curie temperature, magnetization changes and, for exploration purposes, rocks cease to be magnetic. The Curie temperature of pure magnetite is 580°C, but impurities can alter this value. This temperature is attained in the earth's crust at a nominal depth of 25 km, although the Curie point isotherm is believed to be much shallower in some areas such as areas of high heat flow. Our point is that the majority of the anomalies seen on magnetic maps result from sources in the earth's crust because deeper rocks are above the Curie temperature and therefore do not contribute.

Only a few minerals are sufficiently magnetic to cause measurable changes in the earth's field. These are listed together with their magnetic susceptibility and ranges for the susceptibility of common rocks in Table 3-2. Magnetite is usually the magnetic mineral under consideration in exploration. It is both highly magnetic and widely distributed, principally as an accessory mineral. Empirical relations have been established between magnetite content and magnetic susceptibility of rocks (for example, see Mooney and Bleifuss, 1953). One commonly used rule of thumb is that 1 volume percent magnetite results in a magnetic susceptibility of about 3000×10^{-6} cgs, but this can be highly variable. If remanent magnetization is present and unrecognized, the magnetic susceptibility, and therefore magnetite content, interpreted from the anomaly can be too large or too small.

Most magnetic maps show lateral variations of magnetic susceptibility in rocks of the crust. Magnetic susceptibility depends chiefly on magnetite content. Geologists who understand the meaning of magnetite distribution in particular areas can materially assist the geophysicist in interpretation.

Instrumentation

A number of magnetometer types are in use today. Almost all types are electronic rather than mechanical and most types can be used for airborne, ground, and submarine surveys. Detailed discussion is beyond the scope of this paper, but can be found in Dobrin (1976) or Parasnis (1979). Hood et al. (1979) give a very valuable summary of instruments available today, including manufacturers and specifications. Only a few words will be written here about the most important instrument types.

TABLE 3-2

MAGNETIC SUSCEPTIBILITY FOR COMMON MINERALS AND ROCKS

<u>ROCK OR MINERAL</u>	<u>MAGNETIC SUSCEPTIBILITY X10⁶(cgs)</u>	
	<u>Approx. Range</u>	<u>Typical Value</u>
Sedimentary Rocks	0-2,000	200
Acidic Igneous Rocks	600-6,000	2,500
Basic Igneous Rocks	1,000-20,000	5,000
Magnetite	300,000-800,000	500,000
Pyrrhotite	---	125,000
Ilmenite	---	135,000
Franklinite	---	36,000

The flux-gate magnetometer uses an element whose magnetic saturation value is only slightly larger than the earth's field. Variations in the earth's field are detected by measuring the variation in the additional field that must be applied to the element to cause saturation. This instrument is used to measure the total magnetic field in airborne installations and the vertical field component in ground equipment. Most survey installations are capable of about one gamma resolution.

The proton-precession magnetometer measures the precession frequency of protons in the earth's field. This frequency is proportional to the field strength. The sensor is a wire coil wrapped around a bottle containing a hydrogen-rich source such as kerosene. In both airborne and ground instruments the total field is sensed. Most instruments are capable of about 1 gamma resolution.

Higher sensitivity can be attained by use of optically pumped magnetometers. These instruments measure the difference in energy levels for electron orbits developed in a suitable alkali metal vapor (cesium or rubidium) by the earth's field. These magnetometers have a sensitivity of about 0.005 gammas, which is sufficient to allow two sensors separated by a suitable distance to measure magnetic gradient. Total field and vertical gradient airborne surveys are available to facilitate difficult interpretation problems. Both horizontal and vertical gradient equipment is available for ground use.

Cryogenic magnetometers, using low-temperature physics, are of recent development. The Josephson junction effect is exploited by a device called a

Squid, which stands for *superconducting quantum interference device* , and which is maintained at 4.2°K, the temperature of liquid helium. Squid magnetometers are so sensitive that instruments are under development that will measure magnetic gradients in three orthogonal directions in the same aircraft installation. This installation would, of course, also record total field, and such a comprehensive set of data would facilitate much better interpretation.

Instruments are also available for measuring the magnetic susceptibility and remanent magnetization component in rocks either *in situ* or in the laboratory. Such rock property measurements are of great value to the interpreter because they help him understand the variations of these important properties over the survey area, and because they facilitate correlation of interpreted results with actual rock types.

Surveying and data reduction

Field surveys are performed on the ground, from the air, and by towed sensors under water. On the ground, stations can be occupied either on a regular grid or along available access. Repeated readings are usually made at a base station or, alternatively, a recording base station is operated to facilitate removal of normal diurnal variations and to determine whether or not a magnetic storm is in progress. Surveying should not continue during magnetic storms because reliable exploration data generally cannot be obtained. Data reduction usually consists only of removing the time varying field component by use of the base station readings and then plotting the results. Latitude corrections are not usually necessary except for extensive

surveys because most anomalies of interest will be little affected.

Aeromagnetic surveys provide most of the magnetic data collected for mineral exploration. They have a number of advantages over ground surveys, including generally better coverage, speed, and cost-effectiveness. In mountainous country even helicopter-borne surveys can be cost-effective. Flight path is recovered by comparison of vertical photographs taken at regular intervals during flight with photomosaics. The recovered flight path should be posted to the best available topographic maps before magnetic data are plotted and contoured to avoid distortion of anomalies. Modern aeromagnetic systems often incorporate in-flight digital magnetic recording of data, recording barometric and radar altimeters, and Doppler radar navigation. Fixed-wing aircraft can generally drape survey moderately rugged terrain at 150 to 300 m terrain clearance along lines as dense as 4 per km and are used for higher altitude, constant elevation surveys as well. Helicopters facilitate closer terrain clearance in rugged terrain and closer line spacing. Two or more tie lines, normal to the survey line direction, are usually flown to help remove diurnal effects and to apply line leveling corrections. Good data reduction and plotting is a non-trivial task that requires care and experience. Hood et al. (1979) give a current summary of techniques and pitfalls.

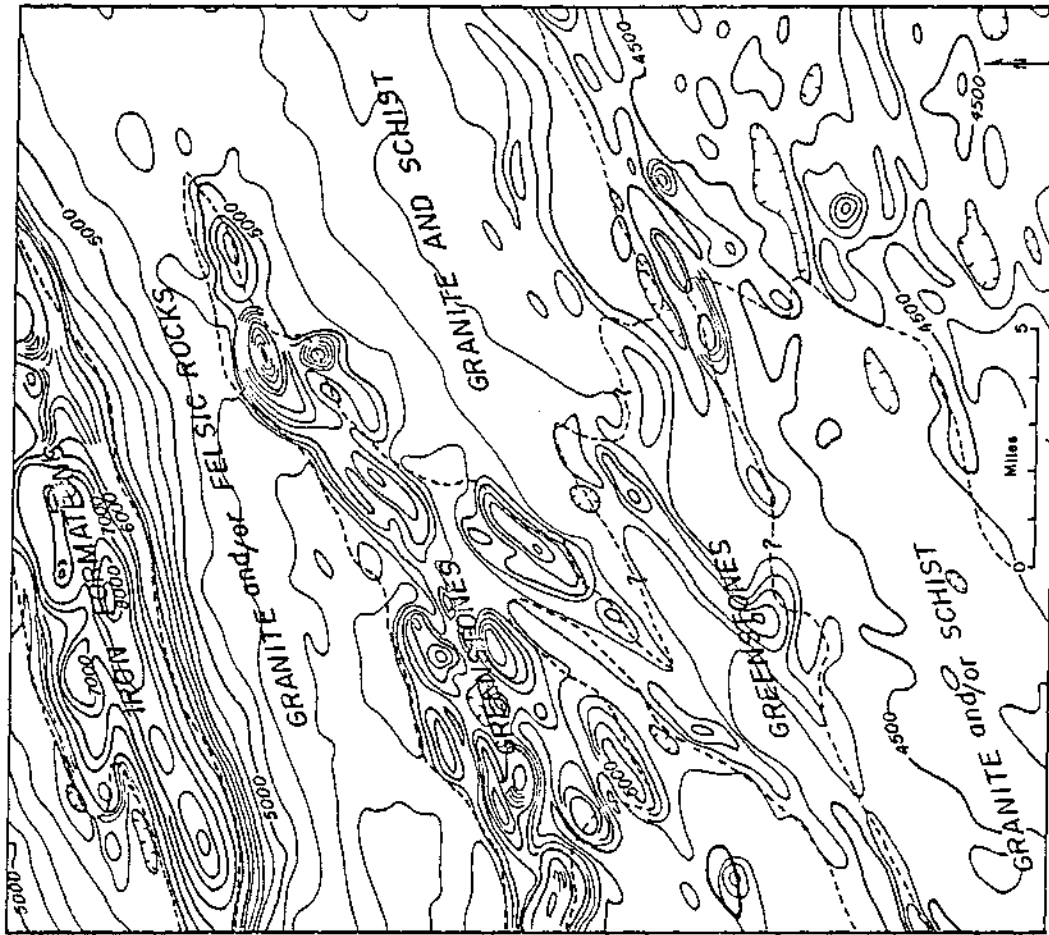
Applications

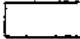

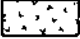
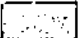
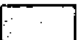
The magnetic method has found very broad application in exploration. Because this method usually maps the distribution of magnetite, it can be used in any application where knowing that distribution might help.

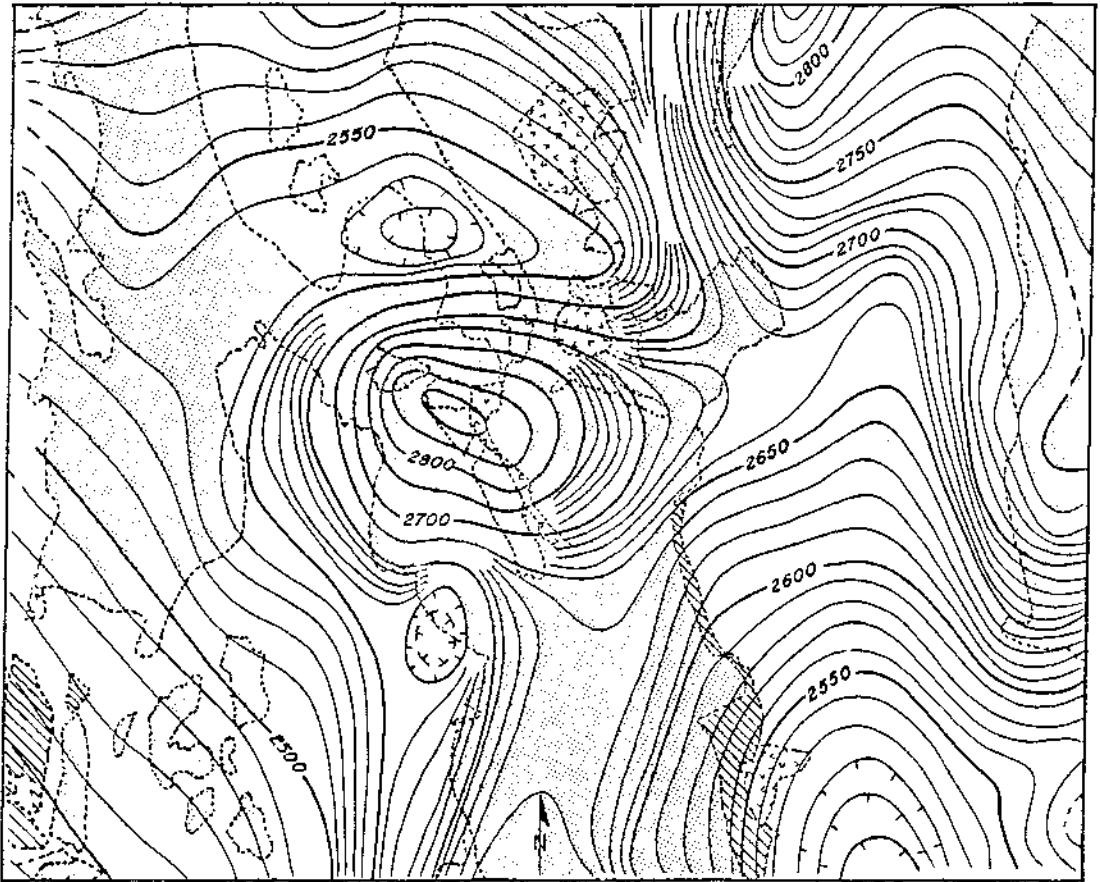
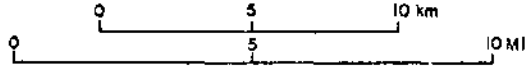
One of the most useful applications of magnetic data is to facilitate geologic mapping. Outcrop geology often can be extended under soil, vegetative, or alluvial cover by observing correlations between magnetic response and observed geology. Structural and magnetic data trends are commonly parallel. Figure 3-6 shows an example of aeromagnetic data and are interpretation in terms of sub-till geology in Wisconsin.

In disseminated copper or molybdenum exploration, the magnetic method is useful in locating and mapping hidden intrusive complexes that can then be surveyed with induced polarization or prospected by other methods to locate sulfide mineralization. Basic portions of these intrusive complexes are commonly more magnetic than acidic bodies. Because acidic rocks commonly have a lower density than basic rocks, gravity and magnetic studies together can help differentiate these.

Magnetic surveying can be very helpful in locating magnetic skarn deposits that are often associated with disseminated and other mineralization in carbonate rocks and are often orebodies themselves. These features are shown by aeromagnetic data from the Ely porphyry copper deposit in eastern Nevada (Figure 3-7). This deposit is underlain by a large quartz-monzonite intrusion whose upper surface dips steeply northward but dips at a gentle angle to the south. The country rocks are sedimentary rocks of Paleozoic and Mesozoic age. Mineralization is both disseminated in igneous and sedimentary rocks and magnetite-copper skarn bodies in carbonate rocks. The magnetic anomaly consists of a large, high amplitude positive anomaly caused by the intrusive rocks with superimposed sharp magnetic anomalies over each skarn



-  - *Quaternary alluvium*
-  - *Tertiary sedimentary rocks*
-  - *Tertiary volcanic rocks*
-  - *Tertiary intrusive rocks*
-  - *Paleozoic and Precambrian sedimentary rocks*



deposit. The calculated susceptibility contrast between the intrusion and the country rock is about $4,500 \times 10^{-6}$ cgs. The magnetic low to the north is simply the normal effect caused by induction in the earth's field and is an integral part of the whole anomaly. Destruction of magnetite by the process of sulfide mineralization can and does cause magnetic lows over some mineralized areas elsewhere, however.

A rather obvious application of the magnetic method is in prospecting for iron ore directly. Successful surveys have been performed in the Mesabe Iron Range and in Nevada, U.S.A. (Riddell, 1966), in Australia (Webb, 1966), and in many other places (Gay, 1966). Hematite ores often contain enough magnetite to be highly magnetic, and taconite ores are often accompanied by magnetite ores. Once an iron orebody has been discovered, magnetic methods can be applied to determine details.

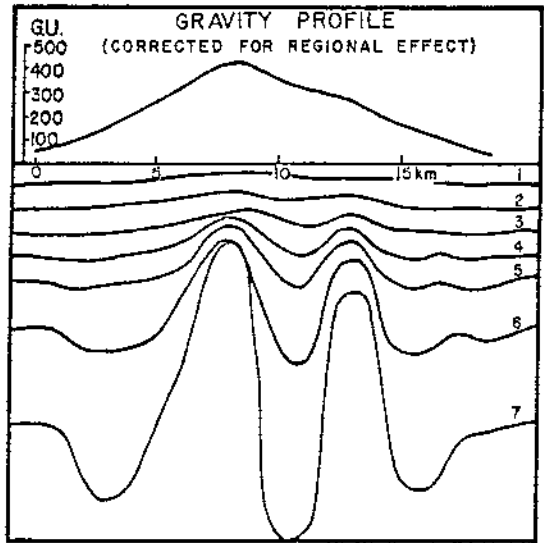
In massive sulfide exploration the magnetic method can be very useful as a follow-up to the EM method in locating copper-nickel deposits, which often contain magnetic pyrrhotite. Many copper-zinc and other massive sulfide deposits are non-magnetic, however, and it is therefore unwise to use magnetic data to eliminate orebody occurrence. Massive sulfide deposits characteristically occur in greenstone belts, typically in Precambrian rocks. Greenstones are usually more magnetic and more magnetically variable from place to place than are the granites that commonly surround them. Thus aeromagnetic reconnaissance can be used to define greenstone belts that are then prospected by airborne and/or ground EM (Figure 3-6).

Gravity and Magnetic Interpretation

Although gravity and magnetic interpretation techniques are in general better developed than are electrical interpretation techniques, much remains to be done. Advances are being made continually. New instrumentation, particularly for precise gradient measurements, will continue to inspire corresponding advances in interpretation methods. The interpreter is obliged to know how to choose and to apply the best techniques.

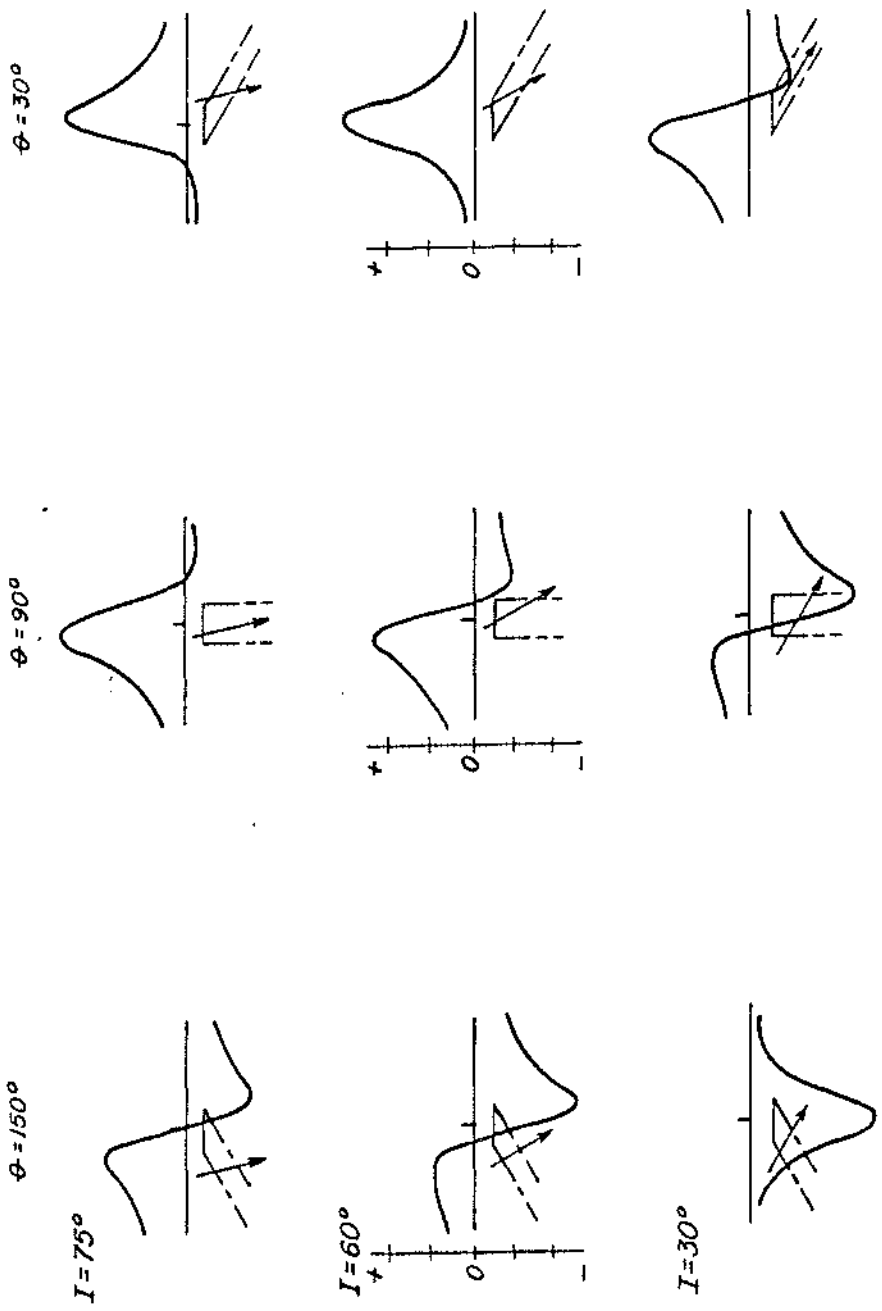
Complete interpretation requires both geophysical and geological considerations. It is the primary goal of the geophysicist to turn the gravity or magnetic map into one or more geologically reasonable subsurface illustrations showing the depths, lateral boundaries, locations, and density or magnetic susceptibility contrasts of the various bodies detected. The geologist then takes this information on physical property distribution and makes the most reasonable geologic interpretation in terms of rock type distribution. These tasks are far from trivial. Success requires appropriate education and experience.

No interpretation of gravity or magnetic data alone is unique. It can be shown that an infinite number of different mass or magnetization distributions can be contrived to explain any given anomaly. Figure 3-8 illustrates this in one particular case for a gravity profile. Each of the alternative basement reliefs explains the observed anomaly equally well. Ambiguity of interpretation can generally be reduced through use of geological or other geophysical data. In fact, the interpreter should strive to use all other data available in order to reduce ambiguity.



Interpretation usually begins with an attempt to isolate individual anomalies from background or regional values. Definition of the regional effects is subjective. Techniques vary from visual hand smoothing of contours or profiles, to manual averaging of values at specific grid points, to complex computer assisted filtering. Once a regional field is determined, it is subtracted from the total field and the residual represents effects due to anomalous bodies of interest. If this process is not properly done, incorrect locations, depths, boundaries, and density or susceptibility contrasts will be inferred.

Interpretation of magnetic data is considerably more complicated than is interpretation of gravity data although both represent applications of potential field theory. One complicating factor in magnetic interpretation is that the inclination of the earth's magnetic field varies from horizontal at the magnetic equator to vertical at the magnetic poles. Therefore, the direction of induced magnetization in rock bodies varies in the same way. By contrast, the gravity field is always vertical. The result is that the gravity anomaly due to a certain body is the same no matter what its latitude or longitude on the earth, but a given magnetic body has an anomaly that is much different at the poles than at the equator. Effects of varying magnetic inclination and body dip are demonstrated in Figure 3-9. Note particularly that in many cases the body does not lie directly beneath the magnetic high. Note also that the accompanying magnetic low is as much a part of the anomaly as is the high--it too needs to be defined in order to interpret the anomaly. This anomaly characteristic is a result of the presence of both positive and negative magnetic poles. Hence, most magnetic bodies have an anomaly that has



both positive and negative components. By contrast, bodies with a positive density contrast yield only positive gravity anomalies.

Yet another complicating factor in magnetic interpretation is the possibility of remanent magnetization, which can be in any direction. The remanent component can be stronger or weaker than the induced component. Reliable location of magnetic bodies and determination of susceptibility are difficult in the presence of remanent magnetization. We can conclude that thorough knowledge must be gained of the effects of varying body shape, depth, and physical property contrasts for gravity interpretation, and to that must be added knowledge of the effects of body dip and strike, and relative magnetic field inclination. In addition, the total field, the vertical and the horizontal magnetic field components can be measured in magnetic surveying. Techniques for interpreting anomalies in each of these cases must be understood by the interpreter. Anyone lacking such knowledge should not attempt interpretation.

Interpretation methods can be divided into four classes: 1) rule-of-thumb, 2) characteristic curve matching, 3) forward modeling, and 4) inverse modeling. Progress in development of techniques in each class has led to better interpretation, especially since the advent of the digital computer. Rules of thumb can be used to get a preliminary overview of location and depth of anomalous bodies before more sophisticated techniques are applied. Peters (1949), Smellie (1967) and Dobrin (1976) give useful summaries of a few of these techniques. Many curve matching techniques are available, generally for interpretation in terms of specific bodies or models (Grant and West, 1965).

These techniques are pursued if no computer modeling capability is available or if only a few profiles or anomalies are to be interpreted.

In more complex situations forward modeling is beneficial. In forward modeling a preliminary estimate (i.e., a model of the subsurface configuration of anomalous masses or magnetic bodies) is formed, perhaps by application of rules of thumb. Then the anomalies to be expected are calculated from the model. The calculated results are compared with the observed anomalies, and the model is modified to start the cycle again. This iterative process is continued until a satisfactory match between computed and observed results is obtained. Any geologic control available can be used to constrain the model so that the results, while not unambiguous, are geologically sound. Computer graphics and user-interactive programs facilitate this approach greatly. At the present time comprehensive 2-D and 3-D computer programs are available from several sources, including Snow (1978) and Nutter and Glenn (1980). Computer modeling has the advantage that more than one body can easily be included in the calculations.

In the inverse approach, sophisticated mathematical techniques are used to calculate a model directly from the data. Inversion does not yield a unique model either, however. The promise that inversion offers is for rapid and inexpensive interpretation of large amounts of data by letting the computer do most of the work. The challenge is to assure appropriate model constraints and to allow input of geologic knowledge so that the final result is geologically sound. Techniques for 2-D inversion have been developed and successfully applied by Hartman et al. (1971) and by O'Brien (1971, 1972). Such modeling is currently at the forefront of development. These techniques

are more reliably applied to rather simple geologic situations such as basement studies for petroleum exploration. Interpretation in the much more complex mining environment still relies heavily on experience in spite of increases in the level of sophistication of interpretational aids.

A wide variety of numerical techniques can be applied to gravity and magnetic data prior to interpretation in terms of subsurface physical property contrasts. Many of these techniques can be classified as filtering techniques in the sense that the data are operated upon, usually by computer, by a numerical operator whose characteristics can be tailored to specific purposes (Fuller, 1966; Battacharyya, 1965, 1978). For example, the data can be numerically filtered so that anomalies of certain spatial wavelengths are retained while others of different wavelengths are rejected. Filtering is accomplished by Fourier transforming the data, in map or profile form, to the frequency domain where frequencies are retained or rejected by simple mathematical operations. The filtered data are then transformed back to the space domain. In this way, magnetic noise due to near-surface volcanic cover can sometimes be partly removed in order to enhance anomalies below the cover.

Operators can be designed to perform other tasks. Gravity and magnetic data can be continued both upward and downward to determine the map or profile as it would be observed at a higher or lower level. Upward continuation is straightforward and reliable, but care must be taken with downward continuation because small errors in the data are amplified. Potential field data can be continued downward only to the top of the uppermost anomaly-producing body. Continuation operations can be of assistance in

matching aeromagnetic surveys at different elevations (Bhattacharyya, et al., 1979).

Sometimes magnetic data are *reduced to the pole*; i.e., an operator is applied to transform the data to appear as they would if the survey had been performed at the magnetic pole where the inducing field direction is vertical (Baranov, 1957).

Advances both in measurement techniques and in interpretation hold promise for continued and even more useful applications for gravity and magnetic data. These methods have contributed much to exploration geophysics, and will do so in the future as well.

REFERENCES

- Ager, C. A., Ulrych, T. J., and McMillan, W. J., 1973, A gravity model for the Guichon Creek batholith, south-central British Columbia: *Can. Jour. Earth Sci.*; v. 10, p. 920-935.
- Baranov, V., 1957, A new method of interpretation of aeromagnetic maps: pseudo-gravimetric anomalies: *Geophysics*, v. 22, p. 359-383
- Bhattacharyya, B. K., 1965, Two-dimensional harmonic analyses as a tool for magnetic interpretation: *Geophysics*, v. 30, pp. 829-857.
- _____, 1978, Computer modeling in gravity and magnetic interpretation: *Geophysics* v. 43, pp. 912-929.
- Bhattacharyya, B. K., Sweeney, R. E., and Godson, R. H., 1979, Integration of data acquired at different times with varying elevations and line spacings: *Geophysics*, v. 44, pp. 742-752.
- Brock, J. S., 1973, Geophysical exploration leading to the discovery of the Faro deposit: *Can. Min. Metall. Bull.*, v.6B, no. 738, p. 97-116.
- Dobrin, M. B., 1976, *Introduction to Geophysical Prospecting*: McGraw-Hill, Inc., 630 p.
- Doell, R., and Cox, A., 1967, Magnetization of rocks: *in Mining Geophysics v. II, Theory*: Society of Exploration Geophysicists, Tulsa, OK., p. 446-453.
- Fuller, B. D., 1966, Two-dimensional frequency analysis and design of grid operators: *in Mining Geophysics, v. II, Theory*; Society of Exploration Geophysicists, Tulsa, OK, p. 658-708.
- Gay, S. P., Jr., 1966, Geophysical case history, Marcona Mining district, Peru: *in Mining Geophysics, v. 1*, Society of Exploration Geophysicists, p. 429-447.
- Grant, F. S., and West, G. F., 1965, *Interpretation Theory in Applied Geophysics*: McGraw Hill, 583 p.
- Hammer, S., 1945, Estimating ore masses in gravity prospecting: *Geophysics*, v. 10., p. 50-62.
- Hartman, R. R., Tesky, D. J., and Frieberg, J. L., 1971, A system for rapid digital aeromagnetic interpretation: *Geophysics*, v. 36, p. 891-918.
- Hinze, W. J., 1966, The gravity method in iron ore exploration: *in Mining Geophysics, v. 1*, Society of Exploration Geophysicists, p. 448-464.

- Hood, P. J., Holroyd, M. T., and McGrath, P. H., 1979, Magnetic methods applied to base metal exploration: in Geophysics and Geochemistry in the Search for Metallic Ores; Peter J. Hood, editor: Geol. Survey of Canada, Econ. Geol. Rept. 31, p. 105-122.
- Jageler, A. H., 1976, Improved hydrocarbon reservoir evaluation through use of borehole-gravimeter data: Jour. Pet. Tech., June, 1976, p. 709-718.
- Kane, M. F., and Pakiser, L. C., 1961, Geophysical study of subsurface structure in Owens Valley California: Geophysics, v. 26, p. 12.
- Mooney, H. M., and Bleifuss, F., 1953, Magnetic susceptibility measurements in Minnesota, Part II, analyses of field results: Geophysics, v. IX, p. 383-393.
- Nagata, T., 1961, Rock Magnetism, 2nd Ed; Maruzan Press, Ltd., Tokyo.
- Nutter, C., and Glenn W. E., 1980, 2 1/2-D Computer programs for gravity and magnetic interpretation: Univ. of Utah Research Inst., Earth Science Laboratory.
- O'Brien, D. P., 1971, An automated method for magnetic anomaly resolution and depth-to-source computations: Proc. Symp. on Treatment and Interpretation of Aeromagnetic Data, Berkeley, CA.
- 1972, Compudepth: a new method for depth-to-basement computation; 42nd Ann. Mtg., Soc. Explor. Geophys., Anaheim, CA.
- Parasnis, D. S., 1979, Principles of applied geophysics: Chapman and Hall, 275 p.
- Peters, L. J., 1949, The direct approach to magnetic interpretation and its practical applications: Geophysics, v. 14, pp. 290-320.
- Plouff, Donald and Pakiser, L. C., 1972, Gravity study of the San Juan mountains, Colorado; U. S. Geol. Survey Prof. Paper 800-B, p. B-183-190.
- Rao, B. S. M., and Murthy, I. V. R., 1978, Gravity and Magnetic Methods of Prospecting: Arnold-Heinenam Publishers, India, 341 p.
- Riddell, P. A., 1966, Magnetic observations at the Dayton iron ore deposit Lyon County, Nevada: in Mining Geophysics, v. 1, Society of Exploration Geophysicist, p. 418-428.
- Rogers, J. R., 1952, Subsurface gravity measurements: Geophysics, v. 17, p. 305-377.
- Schwenk, C. G., 1976, Discovery of the Flambeau deposit, Rush County, Wisconsin; a geophysical case history (abstr.): Econ. Geol., v. 71(3), p. 702.

- Seigel, H. O., Hill, H. L., and Baird, J. G., 1968, Discovery case history of the Pyramid ore bodies, Pine Point, Northwest Territories, Canada: *Geophysics*, v. 33, p. 645-656.
- Smellie, D. W., 1967, Elementary approximations in aeromagnetic interpretation: in *Mining Geophysics*, v. II, Theory; Society of Exploration Geophysicists, Tulsa, OK, p. 474-489.
- Snow, J. H., 1978, Study of structural and tectonic patterns in south-central Utah as interpreted from gravity and aeromagnetic data: M.S. Thesis, Univ. of Utah, Dept. of Geol. and Geophys.
- Stacy, Ra. A., 1976, Deep structure of porphyry ore deposits in the Canadian cordillera; in *Metallogeny and Plate Tectonics* (ed. D. F. Stang), Geol. Assoc. Can Spec. _____, p. 391-412.
- Strangway, D. W., 1967a, Mineral magnetism: in *Mining Geophysics*, v. II, Theory; Society of Exploration Geophysicists, Tulsa, OK, p. 446-453.
- _____, 1967b, Magnetic characteristics of rocks; in *Mining Geophysics*, v. II, Theory; Society of Exploration Geophysicists, Tulsa, OK, p. 446-453.
- _____, 1970, *History of the Earth's Magnetic Field*: McGraw-Hill Book Co., 168 p.
- Sumner, J. S., and Schnepfe, R. N., 1966, Underground gravity surveying at Bisbee, Arizona: in *Mining Geophysics*, v. 1, Society of Exploration Geophysicists, p. 243-251.
- Tanner, J. G., and Gibb, R. A., 1979, Gravity method applied to base metal exploration: in *Geophysics and Geochemistry in the Search for Metallic Ores*; Peter J. Hood, editor: Geol. Survey of Canada, Econ. Geol. Rept. 31, p. 105-122.
- Webb, J. E., 1966, The search for iron ore, Eyre Peninsula, South Australia: in *Mining Geophysics*, v. 1, Society of Exploration Geophysicists, p. 379-390

GRAVITY AND MAGNETIC METHODS
FIGURE CAPTIONS

- 3-1 Elevation corrections to gravity survey data.
- 3-2 Interpretation of underground gravity survey at Bisbee, AZ (after Sumner and Schnepfe, 1966).
- 3-3 Gravity survey of San Juan Mountains, CO. (after Plouff and Pakiser, 1972).
- 3-4 Results of gravity, turam, resistivity and induced polarization surveys at the Pyramid orebody, Pine Point, NWT, Canada (after Seigel, et al., 1968).
- 3-5 Schematic of earth's magnetic field.
- 3-6 Aeromagnetic survey over Precambrian shield area in Wisconsin.
- 3-7 Aeromagnetic map of the Ely area, White Pine County, Nevada (after Carlson and Mabey, 1963).
- 3-8 Ambiguity in gravity interpretation.
- 3-9 Effects of body dip and magnetic field inclination on magnetic interpretation (after Parasnis, 1979).

SECTION 4 - GAMMA-RAY SPECTROMETRY

Introduction

There are two objectives of gamma-ray spectrometry: direct detection of uranium deposits and geologic mapping by detecting and delineating the lateral distribution of uranium, thorium, and potassium in surface rocks and soils. Gamma-ray spectrometry was successful, for example, in recent discovery of the Ranger, Koongarra, and Nabarlek deposits in Northern Territory, Australia, and of the Cluff Lake and Rabbit Lake deposits in Saskatchewan, Canada (Armstrong and Brewster, 1979). However, for direct detection of uranium deposits gamma-ray spectrometry is, today, decreasing in importance because it virtually demands the occurrence of uranium or its radioactive decay products within 0.20 m to 0.45 m of the surface; most such deposits have been found or soon will have been found. Hence geologic mapping ought to be the principal objective of gamma-ray spectrometry in the future. This type of geologic mapping may be useful indirectly in the search for base metal ores of copper, lead, and zinc, as well as detecting and delineating uranium-rich source rocks in which uranium deposits occur or from which uranium deposits may be derived (Hoxham et al., 1965, Pitkin, 1968). Use of a gamma-ray spectrometer will be most effective in mapping those acid igneous rocks, zones of potassium metasomatism, shales, sandstones, carbonates, and evaporites in which uranium, thorium, and/or potassium are enriched. Basic igneous rocks and sediments of low uranium, thorium and/or potassium content are not so easily distinguished from one another. In Table 4-1 appear the mean concentrations of uranium, thorium, and potassium for the rock types referenced above.

Table 4-1 - Mean Concentrations of uranium, thorium, and potassium for several representative classes (after Adams et al., 1959 and Kogan et al., 1971).

Rock Type	Uranium (ppm)		Thorium (ppm)		Potassium (%)	
	<u>Average</u>	<u>Range</u>	<u>Average</u>	<u>Range</u>	<u>Average</u>	<u>Range</u>
Ultrabasic	0.003	-	0.005	-	0.03	-
Basic	1.0	0.2-4.0	4.0	0.5-10.0	0.7	0.2-1.6
Intermediate	1.8	-	7.0	-	2.3	-
Granitic	3.0	1.0-7.0	12.0	1.0-25.0	2.5	1.6-4.8
Shale	3.7	1.5-5.5	12.0	8.0-18.0	2.2	1.3-3.5
Sandstone	0.5	0.2-0.6	1.7	0.7-2.0	1.0	0.6-3.2
Carbonates	2.2	0.1-9.0	1.7	0.1-7.0	0.25	0.0-1.6
Evaporites	0.1	-	0.4	-	0.1	-

The reader is referred, for expanded discussions of the objectives of gamma-ray spectrometry, to the following: Darnley and Fleet (1968), Foote (1969), Darnley (1970), Darnley (1973), Allan and Richardson (1974), Dodd (1974), Darnley (1975), Dodd (1976) and Saunders and Potts (1978).

Concentrations of uranium, thorium and potassium are highly correlated in many geologic materials. However, selective concentration or depletion of each of these elements occurs in certain geologic processes. Thus for many geologic materials, the integrated gamma-radiation arising in the uranium, thorium, and potassium radioactive decay processes is sufficient as an indicator of rock type, while in other geologic materials, gamma-radiation specific to uranium, thorium, and potassium may be useful in identifying rock types. In areas of little outcrop, the surface material must be reasonably representative of the underlying bedrock and be either residual or locally derived before gamma-ray spectrometry can be applied successfully. The usefulness of radioactivity surveys for geological mapping will therefore vary from place to place, depending upon the nature of the overburden.

Standard reference texts on gamma-ray spectrometry to which the reader might wish to refer for expanded discussion of the principles summarized here include Crouthamel (1969), Adams and Gasparini (1970), and Koçan et al. (1971). Useful reference collections of papers on applications of gamma-ray spectrometry appear in proceedings of symposia organized by the International Atomic Energy Agency (1973) and (1976).

Natural Radioactive Decay Processes

Elementary particles

For the purposes of this article, we shall assume the simplistic concept that all matter is composed of the elementary particles, protons, neutrons, and electrons combined in various ways to form atoms. The atom in this model consists of a dense nucleus surrounded by negatively charged electrons. The nucleus is composed of protons and neutrons. An atom of atomic number Z has Z protons in its nucleus. If electrically neutral, Z electrons are distributed about the nucleus in shells. Most elements are composed of a mixture of nuclei having different numbers of neutrons while the number of protons remains the same. These forms of each element are called nuclides or isotopes and have different atomic weights. For instance, hydrogen is a mixture of two isotopes; ${}^1_1\text{H}$ which is a single proton, and ${}^2_1\text{H}$ which is 1 proton and 1 neutron; the latter is familiarly referred to as deuterium. The mass number of an isotope is the mass of the atom in atomic mass units (1 amu = 1.6605×10^{-24} gm.) expressed to the nearest whole number. It is also the sum of the number of protons and the number of neutrons in the nucleus because the weight of each is one atomic mass unit. A helium atom possessing two protons and two neutrons has a mass of 4. The international convention specifies the mass number as a left hand superscript, the atomic number as a left hand subscript, the valence as a right hand superscript, and the number of atoms as a right hand subscript. For our purposes we need only write the left hand superscript and subscript to define the nuclides or isotopes ${}^{40}\text{K}$, ${}^{238}_{92}\text{U}$, ${}^{234}_{92}\text{U}$, and ${}^{232}_{90}\text{Th}$.

A few nuclides are radioactive and decay to produce other nuclides; ^{40}K , ^{238}U , ^{235}U , and ^{232}Th are the most important of these. Most nuclear transformations involve emissions of alpha particles (α), beta particles (β), and gamma-rays (γ). Two other forms of atomic transformations are electron capture and spontaneous nuclear fission. Radioactive decay is an exothermic process in which the excess energies of the unstable nuclei are carried away through the emission of α , β , and γ .

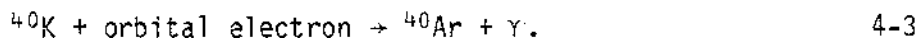
An α -particle, the nucleus of an ^4He atom, is ejected from an unstable nucleus during a *α -decay process*. The daughter nucleus contains two fewer protons and is four nuclear mass units less than the parent nucleus, e.g.



Emission or capture of an *electron* by a parent nucleus occurs in a *β -decay process*. Electrons ejected from the nucleus were originally called β particles. The emission and capture, respectively, are described for ^{40}K by

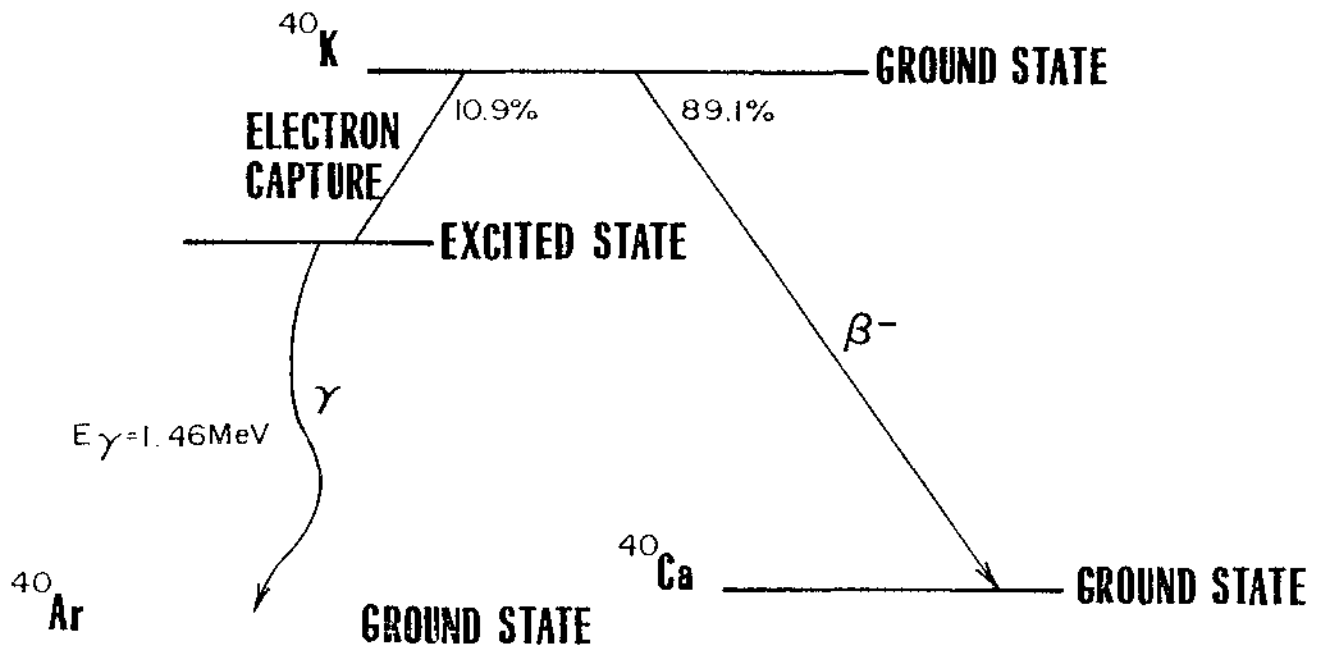


and



These two effects compete as the *branching decay* of Figure 4-1 illustrates.

Gamma emission does not occur as an independent form of radioactivity but is part of the α - or β -decay processes. Gamma-rays are high-energy electromagnetic radiation emitted by an excited nucleus as it drops to a



less excited state. Gamma-rays originate in the nucleus while x-rays originate in the electron shells.

Energies of α , β , and γ

Alpha particles are absorbed by a few centimeters of air, β particles by a meter or so of air, while high energy γ -radiation will travel several hundred meters through air. Their equivalent ranges in rock are practically zero for α and β particles and about 0.20 m to 0.45 m for gamma-rays depending on the energy of the latter. These observations dictate that radioactive decay processes are only realistically monitored in the field by gamma-ray detectors (except for α detection by track etch cups (Pedersen et al., 1979)).

Gamma-rays are emitted in packets or *quanta* of energy called photons. The energy E of each photon depends upon its characteristic wavelength λ or frequency ν and is given by

$$E = h\nu = hc/\lambda \qquad 4-4$$

where h is Planck's constant and c is the velocity of light. Energies are usually expressed in *electron volts* (e.v.). One electron volt is the energy acquired by a charged particle carrying unit electronic charge when it is accelerated through a potential difference of one volt. Gamma-rays exhibit frequencies of 10^{19} to 10^{21} sec⁻¹, wavelengths of 10^{-11} to 10^{-13} m, and energies of 40 KeV to 4 MeV where K stands for 10^3 and M stands for 10^6 .

The decay equation

Radioactive decay is a statistical process in which the number of atoms which disintegrate per unit time is proportional to the number of

atoms present,

$$\frac{dN}{dt} = -\lambda N \quad 4-5$$

where λ is the decay constant characteristic of each element. Integration of this equation leads to

$$N = N_0 e^{-\lambda t} , \quad 4-6$$

where N_0 is the number of atoms present at time $t = t_0$, the start of decay. The half-life is defined as the time at which N equals $1/2 N_0$ and hence is given by

$$\tau_{1/2} = \frac{\ln 2}{\lambda} \quad 4-7$$

The half-lives of the nuclides with which we are concerned vary enormously.

The Gamma-ray Spectrum

The uranium isotope ${}_{92}^{238}\text{U}$ decays to stable ${}_{82}^{206}\text{Pb}$ through 17 intermediate daughter products as shown in Table 4-2. In the process, gamma-rays of 72 discrete energy levels are emitted. The most energetic or the principal gamma lines of this spectrum are listed in Table 4-3. The ratio of the total gamma-ray energy of ${}^{238}\text{U}$ and ${}^{235}\text{U}$, in the natural state, is approximately 50:1 so that the ${}^{235}\text{U}$ lines are of subsidiary interest to the ${}^{238}\text{U}$ lines.

The thorium isotope ${}_{90}^{232}\text{Th}$ decays to stable ${}_{82}^{208}\text{Pb}$ through ten intermediate daughter products as shown in Table 4-4. In the process, gamma-rays of 46 discrete energy levels are emitted. The principal lines of this spectrum are listed in Table 4-5.

Table 4-2 ^{238}U Decay Series
(after Crouthamel, 1969)

<u>Isotope</u>		<u>Half-life</u>	<u>Radiation</u>
Uranium	238	4.51×10^9 yr	α , γ
Thorium	234	24.1 day	α , γ
Protactinium	234	6.7 hr	β , γ
Uranium	234	2.48×10^5 yr	α , γ
Thorium	230	8×10^4 yr	α , γ
Radium	226	1622 yr	α , γ
Radon	222	3.82 day	α , γ
Polonium	218	3.05 min	α , β
Astatine	218	1.35 sec	α
Radon	218	0.03 sec	α
Bismuth	214	19.7 min	β , α , γ
Polonium	214	1.64×10^{-4} sec	α
Lead	214	26.8 min	β , γ
Lead	210	21 yr	β , γ
Bismuth	210	5 day	β
Polonium	210	138.4 day	α , γ
Thallium	210	1.3 min	β , γ
Thallium	206	4.2 min	β
Lead	206	stable	—

Table 4-3 - Principal Lines of the $^{238}_{92}\text{U}$ Gamma-ray Spectrum
 (after Crouthamel, 1969)

Isotope	Half-life	Energy of Each Quantum (MeV)	Number of Quanta per Decay Event
$^{214}_{83}\text{Bi}$	19.7 min	2.204	0.052
		1.764	0.163
		1.120	0.166
$^{214}_{82}\text{Pb}$	26.8 min	0.609	0.417
		0.352	0.377

Table 4-4 - ^{232}Th Decay Series
(after Crouthamel, 1969)

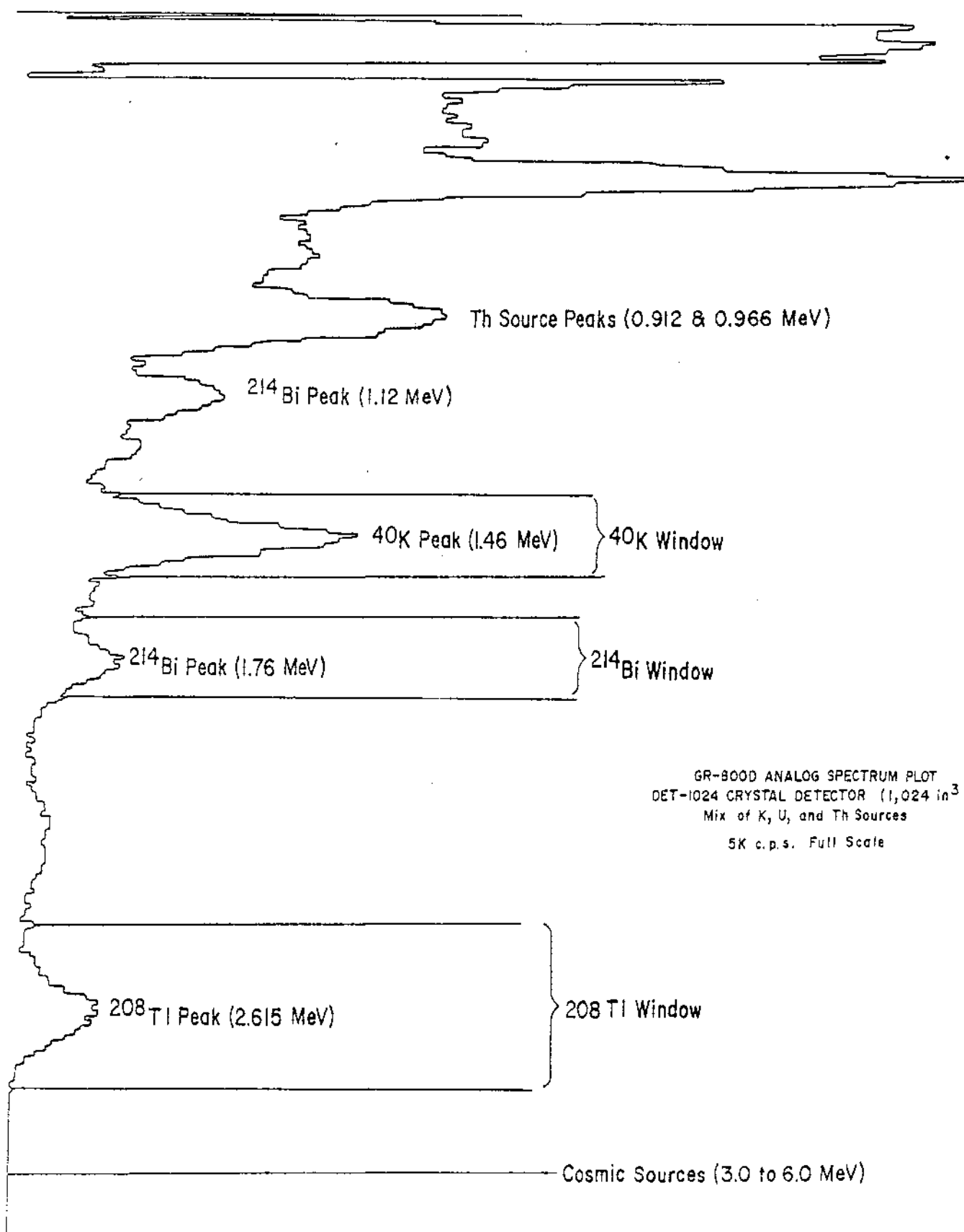
<u>Isotope</u>		<u>Half-life</u>	<u>Radiation</u>
Thorium	232	1.4×10^{10} yr	α , γ
Radium	228	5.7 yr	β , γ
Actinium	228	6.1 hr	β , γ
Thorium	228	1.91 yr	α , γ
Radium	224	3.64 day	α , γ
Radon	220	51 sec	α , γ
Polonium	216	0.16 sec	α
Lead	212	10.6 hr	β , γ
Bismuth	212	60.6 min	β , α , γ
Polonium	212	0.3×10^{-6} sec	α
Thallium	208	3.1 min	β , γ
Lead	208	stable	-

Table 4-5 - Principal Lines of the $^{232}_{90}\text{Th}$ Gamma-ray Spectrum
 (after Crouthamel, 1969)

Isotope	Half-life	Energy of Each Quantum (MeV)	Number of Quanta per Decay Event
$^{228}_{89}\text{Ac}$	6.1 hr	0.960	0.100
$^{212}_{82}\text{Pb}$	10.6 hr	0.239	0.470
$^{208}_{81}\text{Tl}$	3.1 min	2.620	0.337
		0.583	0.293

The potassium isotope ^{40}K emits gamma-rays of 1.46 MeV through electron capture; 0.012 percent of potassium is ^{40}K .

When a mix of uranium, thorium, and potassium is present, the composite spectrum might look like that displayed in Figure 4-2 in which the individual lines have been broadened into peaks by the thallium-activated sodium iodide crystal. Line broadening will be discussed later.



GR-800D ANALOG SPECTRUM PLOT
DET-1024 CRYSTAL DETECTOR (1,024 in³)
Mix of K, U, and Th Sources
5K c.p.s. Full Scale

Equilibrium and Disequilibrium

At equilibrium the number of atoms of each daughter disintegrating per second is the same as the number being created by disintegrations of the parent. This result is easily obtained from the decay equation. For the parent, this equation is

$$N_1 = N_0 e^{-\lambda_1 t}. \quad 4-8$$

The rate of decay of the parent then is

$$\frac{dN_1}{dt} = -\lambda_1 N_0 e^{-\lambda_1 t} = -\lambda_1 N_1, \quad 4-9$$

but this must be identical to the rate of production of the first daughter. Simultaneously the atoms of the first daughter are disintegrating at the rate

$$\left. \frac{dN_2}{dt} \right|_{\text{disint.}} = \lambda_2 N_2 \quad 4-10$$

Hence the rate of accumulation of the atoms of the first daughter is the difference between production and decay

$$\left. \frac{dN_2}{dt} \right|_{\text{total}} = \lambda_1 N_1 - \lambda_2 N_2 \quad 4-11$$

For the parent and the first daughter to be in equilibrium, we must have

$$\lambda_1 N_1 = \lambda_2 N_2$$

and by logical extension

$$\lambda_1 N_1 = \lambda_2 N_2 = \lambda_3 N_3 = \dots = \lambda_n N_n \quad 4-12$$

We can solve equation 4-10 by assuming that

$$N_2 = Ae^{-\lambda_1 t} + Be^{-\lambda_2 t}, \text{ with the} \quad 4-13$$

condition that when $t=0$ then $N=0$. The result is

$$N_2 = \frac{\lambda_1 N_0}{\lambda_2 - \lambda_1} (e^{-\lambda_1 t} - e^{-\lambda_2 t}). \quad 4-14$$

From equations 4-8 and 4-14 we can obtain the ratio of the number of atoms of parent to daughter at any time

$$\frac{N_2}{N_1} = \frac{\lambda_1}{\lambda_2 - \lambda_1} \left\{ 1 - e^{-(\lambda_1 - \lambda_2)t} \right\} \quad 4-15$$

When equilibrium has been reached, $N_1 \lambda_1$ is equal to $N_2 \lambda_2$, so that 4-15 yields

$$\frac{\lambda_1}{\lambda_2} = \frac{\lambda_1}{\lambda_2 - \lambda_1} \left\{ 1 - e^{-(\lambda_1 - \lambda_2)t_e} \right\}, \text{ or}$$

$$e^{-(\lambda_1 - \lambda_2)t_e} = \lambda_1 / \lambda_2.$$

Hence, we have

$$t_e = \frac{1}{(\lambda_1 - \lambda_2)} \ln \frac{\lambda_1}{\lambda_2} \quad 4-16$$

In the case of a series with n products, the time to reach equilibrium can be found, by this type of analysis, to be less than 100 years for the thorium decay process and about 10^6 years for the two uranium decay processes.

Measurement of gamma-radiation associated with daughters in a decay process in which equilibrium has been established permits determining the amount of a parent by measuring the amount of a daughter. Thus it has

become recent practice to measure four quantities in gamma-ray spectrometry. These four quantities are:

TC = Total count integrated under the spectrum between 0.4 MeV and 2.82 MeV.

^{40}K = Radioactive potassium content via integrated count between 1.36 MeV and 1.56 MeV (the so-called 1.46 MeV ^{40}K peak of Figure 4-2).

^{238}U = Uranium via integrated count between 1.66 MeV and 1.86 MeV (the so-called 1.76 MeV ^{214}Bi peak of Figure 4-2).

^{232}Th = Thorium via integrated count between 2.42 MeV and 2.82 MeV (the so-called 2.62 MeV ^{208}Th peak of Figure 4-2).

Much more capability for identifying peaks with specific daughters of each of the decay series now exist. For example, it has become common practice to record 256, or even 1024, channels of information over the gamma-ray spectrum extending from 0.4 MeV to 6 MeV. Thus, many spectral peaks may be utilized in determining the ratios of uranium, thorium, and potassium, and indeed of determining whether or not equilibrium exists in the ^{238}U and ^{232}Th decay processes. Processing such a massive amount of data has not become routine. However, attempts are being made to use the ratios of the peaks to determine whether or not the ^{238}U and the ^{232}U decay processes are in equilibrium.

One should note from Table 4-2 that ^{214}Bi is many steps removed from ^{238}U and that the intermediate daughters include radium and radon. The solubility of radium is different from that of uranium so that radium can separate from uranium in common geological processes. Radon is a light gas

which emanates from the earth's surface and so also readily separates from uranium. Therefore, in an open environment, ^{214}Bi may be spatially separated from its parent ^{238}U through migration of earlier daughters in the decay process. For this reason, an estimation of the abundance of uranium based on a measurement of ^{214}Bi is correct only if the radioactive decay process is in equilibrium. Thus, Darnley (1970) advocates use of the term eU to indicate uranium equivalent when deducing uranium concentrations from gamma-ray spectrometry. In an identical sense one should use eTh for equivalent thorium. Insofar as potassium does not decay via a chain decay process, the concentration of it, as estimated from gamma-ray spectrometry, is simply given as K.

Generally, equilibrium conditions can be assumed for the thorium decay series because of the comparatively short half-lives of all of its daughters as seen from Table 4-4. Given that there are no disequilibrium problems with potassium, then the geologic processes most likely to produce significant disequilibria are associated with the ^{238}U decay series and are listed in Table 4-6.

Scattering and Absorption of Gamma-rays

Scattering

When gamma photons pass through matter, they interact with the electrons and with the atomic nuclei of the matter via various mechanisms. These mechanisms can be divided into a) elastic interactions in which the photon does not transfer its energy to other particles, known as Thomson scattering, and b) inelastic interactions in which the photon loses either part of its energy and is deflected from its initial direction or gives up

Table 4-6

Possible Significant Disequilibria in the ^{238}U Decay Series
(from Saunders and Potts, 1978)

Isotope and half-life	
^{238}U 4.5×10^9 yrs	May be leached from Th and Ra daughters as uranyl ion by oxidizing groundwaters to form very young minerals with anomalously low ^{214}Bi gamma radiation.
↓ ^{226}Ra 1602 yrs	May be leached from parents in reducing H_2S -bearing groundwaters and reprecipitated in hot spring deposits to cause high ^{214}Bi anomalies with essentially no uranium present.
↓ ^{222}Rn 3.8 days	May diffuse away from parents in soil gases or the atmosphere and form near-surface accumulations, resulting in false uranium anomalies.
↓ ^{214}Bi 19.7 min	May be washed out of the atmosphere with other ^{222}Rn daughters by rainfall to cause relatively large but short-lived "spikes" in the surface ^{214}Bi gamma activity.

all of its energy to an atomic electron or nucleus and ceases to exist. For photons with energies from a few KeV to a few MeV, the important inelastic interactions are nuclear photoelectric effect, formation of electron-positron pairs, photoelectric effect, and Compton scattering.

Thomson scattering occurs only for low energy photons and is not important relative to the inelastic interactions, so far as gamma-ray spectrometry is concerned.

For photons emitted by natural radioactive elements, the *nuclear photoelectric effect* is known only for ${}_{81}^{208}\text{Tl}$ ($E_\gamma = 2.52 \text{ MeV}$) in the photodisintegration of deuterium ($E_\gamma + {}_1^2\text{H} \rightarrow n + p$) and the reaction of gamma photons of ${}_{83}^{214}\text{Bi}$ ($E_\gamma = 1.76 \text{ MeV}$) with beryllium ($E_\gamma + {}_4^9\text{Be} \rightarrow {}_4^8\text{Be} + n$). Natural concentrations of ${}_1^2\text{H}$ and ${}_4^9\text{Be}$ are negligibly small so that this inelastic interaction is unimportant.

The *formation of electron-positron pairs* occurs when $E_\gamma > 2 M_0 c^2$ in which M_0 is the rest mass of the electron or proton. The presence of other particles is required to absorb part of the energy of the incident photon. If the mass of the other particle is large, it will only absorb a small part of the energy E_γ of the incident photon. The surplus energy of the incident gamma photon is divided roughly equally between the electron and the positron. The probability of pair formation in nature is quite large for high energy gamma photons. The process of electron-positron pair formation is particularly effective in nuclei of high atomic number Z .

The *photoelectric effect* occurs when the incident gamma photon transfers all its energy to bound electrons and ceases, thereby, to exist. If E_i is the binding energy of the i^{th} atomic shell, the photoelectric

effect is possible for $E_\gamma > E_i$. The energy of the electron ejected from the atom is $E_e = E_\gamma - E_i$. The atom becomes excited and when the i^{th} energy level is filled, light energy equal to E_i is emitted. The photoelectric effect is the principal mechanism of absorption of low-energy gamma photons in nuclei of high atomic number Z .

Compton scattering of gamma photons is the principal interaction mechanism for $E_\gamma = 0.4$ to 3.0 MeV and for an intermediate value of the atomic number of the medium. The incident photon changes direction in Compton scattering and hence is readily available for repeated scattering events. Hence, the larger the volume of the scatterer, the higher the probability of total dissipation of the incident photon.

Absorption

When a beam of collimated mono-energetic photons passes through an absorber, the number of photons per cm per sec (N) is given by

$$N = N_0 e^{-\mu x} \qquad 4-17$$

where N_0 is the incident intensity at $x = 0$, and μ is the total absorption coefficient reflecting the sum of the attenuations due to the photo-electric effect, Compton scattering, and pair production. The thickness of the material which reduces the intensity N to half of N_0 is referred to as the half-thickness. For $\frac{N}{N_0} = 1/2$, we find $x = \frac{\ln 2}{\mu}$ from the previous equation. Table 4-7 shows the half-thickness at various energies for water, air at 20°C and 76 cm Hg, and for rock of density 2.35 gm/cm³. As expected, photons of higher energy penetrate farthest.

At aircraft altitudes of 100 m or more, the intensity of gamma rays of energies below 0.10 MeV, emitted by rocks and soils, will be considerably

reduced; indeed the dominant energy below 0.10 MeV will arise in low energy gamma-rays generated by Compton scattering in the air.

Ninety percent of the gamma-rays observed at the surface of rock outcrop of density 2.7 gm/cm^3 is emitted from the top 15-25 cm while 90% of the gamma-rays observed at the surface of dry overburden of 1.5 gm/cm^3 is received from the top 30 to 45 cm. Moisture in the soil increases the attenuation significantly.

Table 4-7.

Half-Thicknesses for Air, Water, and Rock

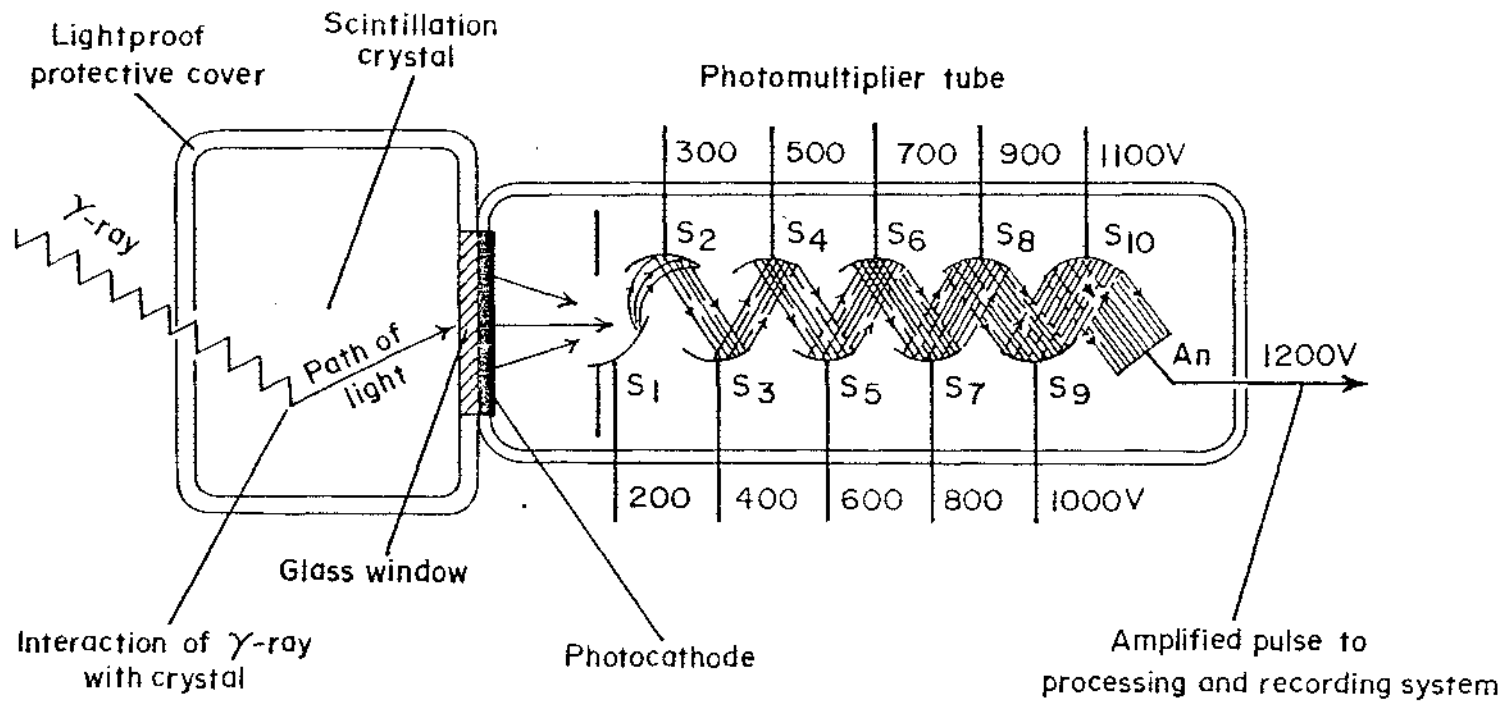
Energy (MeV)	Air (m)	Water (cm)	Rock (cm)
0.01	1.2	0.1	0.01
0.10	38.1	4.1	1.7
1.0	90.6	9.8	4.6
2.0	129.3	14.1	6.6
3.0	161.1	17.5	8.1

Gamma-ray Detector Systems

Introduction

Crystals of certain compounds, when will scintillate, i.e. emit visible light pulses when irradiated with gamma-rays. These light pulses are converted to electrical voltage pulses by means of a *photomultiplier tube* attached to the crystal (Grasty, 1974) as in Figure 4-3. These electrical voltage pulses are sorted into the various voltages associated with specific incident gamma photons via voltage-dependent multichannel analysers (MCA). The schematic circuitry is illustrated in Figure 4-3. The thallium activated sodium iodide NaI(Tl) crystal is the most commonly used scintillator. An alternate scintillator is *lithium-drifted* germanium Ge(Li) .

Within the energy range of natural gamma photons of interest to us (0.4 to 3 MeV), linear absorption of them is the sum of the pair production, photoelectric, and Compton scattering effects; Compton scattering dominates this part of the spectrum. Unfortunately, the Compton effect produces a continuum of scattered gamma-rays and, with no clear spectral peaks related to the energy of the incident gamma photon. Hence this effect is of no value in gamma-ray spectrometry and indeed degrades resolution of the diagnostic lines which we hope to use for mineral identification. A material of high atomic number Z will, according to earlier arguments, favor the photoelectric effect and pair production over Compton scattering. The Compton effect is decreased, also, by increasing the volume of a detector since multiple Compton interactions make more probable the total dissipation of an incident gamma photon. Increasing



detector volume size also leads to interaction with more of the incident gamma-rays.

Principles of scintillation

Gamma-rays transfer all or part of their energy to electrons in the detector for the photoelectric effect, pair production, and Compton scattering in a *detector* or *phosphor*. The excited electrons dissipate their energy in turn by ionization or excitation of the molecules; the de-excitation results in fluorescent radiation. In short, the detector, i.e. a scintillator or phosphor, converts a fraction of the energy of the incident gamma photon to light photons. Since the directions of the incident gamma photons are random, it is desirable to surround the phosphor by a reflector to ensure maximization of the number of light photons striking the photosensitive cathode of the *photomultiplier tube* (PMT) of Figure 4-3. The photoelectrons are accelerated by the applied electric field of the PMT stages via a cascade process. Typical multiplication factors of a PMT are 10^5 to 10^8 . The output pulse of the PMT, for each incident gamma photon, is further amplified by conventional electronic circuitry. When the resulting *output pulse height* is proportional to the energy of the incident gamma photon, then the system can be used as a gamma-ray spectrometer.

Selection and design of NaI (Tl) crystals and PMT detectors

The following four factors are important in the selection and design of a gamma-ray detector system:

- 1) The *resolving power* which determines the ability of the system to resolve individual lines appearing as a spectral peak of finite width

within a spectrum. Resolving power, or resolution is usually defined as the full-width at half-maximum (FWHM) of the Cs-137 peak expressed as a fraction of the peak energy

$$\frac{\Delta E(\text{FWHM})(\text{Cs-137})}{E(\text{Cs-137})}$$

Cs-137 is used as a convenient standard in resolution calibration.

2) The *detection efficiency* which dictates the source strength necessary for measurement of a spectrum. Usually the detection efficiency increases with volume of an NaI(Tl) crystal.

3) The efficiency of the coupling of the NaI(Tl) crystal to the following PMT.

4) Secondary factors such as the linearity of response of the system, the stability of the system, and the ratio of the photoelectric interactions to Compton interactions. Accuracy and stability of timing of the arrival of each gamma photon are of fundamental importance also.

NaI(Tl) crystals emit at a light wavelength of 4200Å and thus the PMT is designed to be efficient at this wavelength. Further, the crystals are highly transparent to their own radiation and thus are efficient in this respect. Unfortunately, the crystals always contain some K impurity of the order of a few ppm with the result that some 1.46 MeV energy is always emitted as natural background or noise without external excitation.

Field portable gamma-ray spectrometers are limited by size and weight to crystals of about 10 cm equidimensions; such crystals are readily *grown* in cylindrical form to produce a standard volume of 347 cc.

For airborne gamma-ray spectrometers, the optimum basic unit is a 10 cm x 10 cm x 40 cm *extruded* crystal attached closely to a PMT. Collections

of such units lead to crystal volumes ranging from 256 cu. in. (4.2×10^3 cc) for one unit to 5420 cu. in. (8.4×10^4 cc) for twenty units. Typically, helicopter-borne gamma ray spectrometer units employ 1024 cu. in. (16.8×10^3 cc) crystals while fixed-wing aircraft systems employ 3072 cu. in. (5.0×10^4 cc) or more in order to ensure adequate count statistics as will be discussed later.

NaI(Tl) crystals and their coupled PMT's drift due to temperature variations; additionally PMT's drift due to supply voltage variations. An apparent spread in incident gamma photons results which is exhibited as a skewing of the gamma-ray spectrum toward higher or lower overall apparent energies. Counts per second or per minute in any narrow energy window centered on one of the gamma-ray peaks of Figure 4-2 can thereby vary enormously. Unless these drift problems are obviated, reliable gamma-ray spectrometry becomes impossible. Accordingly, tight control of supply voltage and crystal ambient temperature becomes essential. Short term variations in supply voltage and/or crystal temperature result in *peak broadening* with an attendant loss in ability to resolve one peak from another. Peak resolution is the very essence of gamma-ray spectrometry.

Ge(Li) detectors, because of a different physical principle involved in producing electrons in a PMT from incident gamma photons, exhibit nearly 100 times the resolution of NaI(Tl) detectors at the expense of lower efficiency, i.e. longer required count times, and of the need for liquid nitrogen cooling. Until now, the disadvantages have outweighed the advantages of Ge(Li) detectors versus NaI(Tl) detectors for field use; they are, however, routinely used in the laboratory. Their use in field systems may be expected in the future. For details on the luminescent

properties of activated alkali halides, the reader might wish to refer to Dekker (1957).

During the processing of an incident gamma photon into a photoelectron and then into a voltage pulse of height h , a finite time elapses. Since a crystal detector system is unable to resolve simultaneous reactions, once a reaction is first indicated at the *photocathode* of the PMT, an electronic circuit is designed into the system to assure, automatically, that no other reactions will enter into the time window of any given incident gamma photon. The *dead time* of the system, resulting from this automation, only becomes important at high count rates. The dead time per pulse is typically of the order of 1 to 10 microseconds, which ensures an ability to count to 100,000 incident gamma photons per second.

Stability of NaI(Tl) crystals and PMT detectors

Several methods exist for stabilizing NaI(Tl) crystals and their coupled PMT detectors, or correcting for their drifts. These techniques are:

- 1) Use reference isotope specimens in proximity to the crystal, such as americium 241, cesium 137, barium 133, or cobalt 57, or even all of them as representatives of specific energy levels which, if sufficiently strong, can readily be identified in the PMT voltage output. Needless to say, this approach interferes with the natural spectrum and is not usually acceptable for continuous monitoring of the performance of systems used for airborne gamma-ray spectrometry. On the other hand, cesium 137 *buttons* are used routinely to permit adjustment of the voltage *windows* of hand-held ground spectrometers so that these windows of measurement truly span the spectral

peaks to which they have been assigned. Voltage or temperature drift correction with the aid of cesium 137 buttons is carried out about every half hour or so, depending upon the particular instrument.

2) Use the natural peak of ^{40}K in airborne systems for automatic voltage adjustment. A digital or analog system is usually designed to search automatically for symmetry about the 1.46 MeV ^{40}K peak

$$\frac{\Delta \text{ Counts}}{\Delta \text{ Energy}} \left| \begin{array}{l} \text{below the} \\ \text{apparent} \\ \text{peak} \end{array} \right. = \frac{\Delta \text{ Counts}}{\Delta \text{ Energy}} \left| \begin{array}{l} \text{above the} \\ \text{apparent} \\ \text{peak} \end{array} \right.$$

If this equality is not satisfied, the PMT voltage is automatically adjusted to make it so. The Δ Energy windows above and below the peak are made identical. Temperature and voltage drifts in the PMT and temperature drifts in the crystal detector are eliminated by this technique.

3) Use a thermally-controlled housing around the crystal detector. This procedure is in standard use in airborne systems and eliminates temperature drift leaving only PMT voltage drift to control.

4) Use an internally-mounted stabilized light source of constant output to check the voltage and temperature drift of the PMT.

5) Use temperature-compensated circuits to eliminate temperature drift of the PMT.

6) Use a multi-channel spectrometer to measure and reconstitute the full gamma-ray spectrum from 0.4 to 3.0 MeV. This approach requires 256 to 1024 windows. If the total spectrum apparently contracts or expands with temperature or voltage variations, it really does not matter since one can automatically search the full spectrum for any desired peak or peaks. A digital data acquisition system is required for this procedure, which ought to be the common technique of the future. While it demands recording of

the full spectrum, it does not demand printing it out; rather selected peaks and peak ratios are printed out.

Volume of crystal

Experience has shown that to secure adequate certainty in count statistics, in airborne surveys, the ratio of the crystal volume (V) in cc to the ground velocity (v) of the aircraft in km/hr shall be $V/v \geq 186$. For example, an aircraft flying at 200 km/hr (v) would require a minimum crystal volume (V) of 186×200 or 3.72×10^4 cc. On the other hand, a helicopter flying at 100 km/hr would require a minimum crystal volume of 1.86×10^4 cc.

For precise ground spectrometer surveys, a crystal volume of 347 cc with a two minute integration time will produce excellent data.

Operational Considerations

Background

The discrete spectral lines which provide us information on the radionuclide abundances are degraded by the Compton continuum, the Bremsstrahlung, and *background radiation*. The latter arises from a) ^{40}K contamination in the crystal, b) ^{238}U , ^{232}Th , and ^{40}K contamination in the materials used in construction of the photomultiplier tube and the crystal/PMT housing, c) radioactive accumulations on or in the aircraft structure (for airborne systems), d) radium luminized instruments (e.g., navigation instruments in airborne surveys and watches in ground surveys), e) cosmic ray interactions with nuclei present in the air, an aircraft, or the detector, f) atmospheric radioactivity arising from daughter products of radon gas of the uranium decay series.

Every effort must be expended in ground and airborne surveys to minimize background radiation and to remove it prior to attempting to utilize spectrometer data for estimates of nuclide concentrations.

Careful quality control of materials selected for detectors, and PMT's and housing can usually keep contamination in these items to an acceptable level. However, background from the detectors may contribute as much as 50 counts per second within the ^{214}Bi window for a 3072 cu. in (5.0×10^4 cc) crystal array. At the same level, approximately, is the ^{214}Bi channel count from 5 ppm uranium from a half-space 125 m beneath the aircraft.

Radioactive nuclides can precipitate and adhere to the skin of an aircraft, be contaminants in aircraft materials, be used to illuminate instruments, or occur in luminescent strips or signs on the aircraft. The

aircraft should be checked for these sources with a hand-held spectrometer and the offending nuclides removed where possible. Crystal detectors should be placed sufficiently far from the instrument panel, after reduction of panel luminescence to low level, that the remaining luminescence contributes insignificantly within the energy windows studied. Periodic checks of the aircraft with a hand-held spectrometer are customary.

Cosmic-rays are fast moving charged particles of extraterrestrial origin. One type of cosmic-ray is dominated by time-variant fluxes of particles of high energy and it is always present at the earth's surface. These particles are believed to originate in our galaxy and to be distributed throughout it; they are referred to as *galactic cosmic-rays* with energies to 10^7 e.v. The composition of this radiation is 85% hydrogen nuclei (or protons), 14% helium nuclei (or α particles,) and 1% heavier nuclei which are mostly carbon, nitrogen, and oxygen. The second type of cosmic-rays originate in the sun in connection with solar flares; they exhibit energies up to 3×10^{10} e.v., but they are usually of lesser energy.

The galactic cosmic-rays interact with the earth's atmosphere via nuclear and electromagnetic processes with a resultant loss in cosmic-ray intensity. Secondary particles produced in the interactions, readily detected at the earth's surface, increase in intensity from the equator to the auroral zones. Gamma photons covering the complete spectrum of our interest (i.e. 0.4 to 3.0 MeV) arise as a result of the secondary particles. Indeed, the secondary radiation extends to about 6.0 MeV, a fact which permits us to extrapolate the 6.0 MeV to 3.0 MeV flux to the 3.0

MeV to 0.40 MeV range to permit subtraction of cosmic radiation from the 0.4 MeV to 3.0 MeV spectrum. The intensity of cosmic radiation increases with barometric altitude as would be expected for any external flux whose energy is dissipated with depth into the earth's atmosphere.

Past nuclear explosions have resulted in a residue of nuclides in the atmosphere which, depending upon their half-lives, will decay with time.

Background radiation emanating from the daughters in the uranium decay series is a subject which requires substantial elaboration because it can be intense and is intensely time-variant; it will be the subject of a special discussion under *meteorological effects*.

Meteorological effects

Atmospheric Bismuth 214: Radon, with a half-life of 3.8 days, can diffuse from the ground with a rate dependent upon air pressure, soil moisture, ground cover, wind, and temperature. Radon decays to ^{214}Bi , the uranium indicator in gamma-ray spectrometry. A temperature inversion in the atmosphere finds temperature increasing with altitude. Under this condition the ^{214}Bi will accumulate near the earth's surface (Foote, 1969). Anomalous uranium indications will occur, on this account, which will have no relation to the uranium content of rocks and soils beneath the detector. Darnley and Crasty (1971) report that on the average 70 percent of the counts in the uranium window arise in this source. Removal of such background becomes mandatory.

The above effect should be particularly worrisome in hilly terrain where, in still air, the inversion will be pronounced in the valleys. One can presume that this effect will be minimized when breezes homogenize the

air about mid-morning of a still day, but there is no means to predict the magnitude of the atmospheric inversion problem. The inversion layer may be entirely absent during several months of the year depending upon local climatology. Further, it may readily be a very local and seasonal phenomenon, occurring in some valleys and not in others.

Thunderstorms bring increased air conductivity which can lead to removal of charged particles with which some atmospheric radiation is associated.

Attempts to minimize the atmospheric effect by subtracting the gamma counts, for each energy window, of the background measured by an upward-looking detector, shielded by 0.10 m of lead from ground radiation, are used in some airborne surveys. However, because the atmosphere above and below the aircraft will, in general, have different radon concentrations, this correction is imperfect and can be misleading. It removes, however, the cosmic flux. Flying over a large body of water before and after each flight aids materially in recognizing and eliminating atmospheric background since water contains negligible concentrations of radioactive nuclides. Since atmospheric background is time variant, every opportunity should be taken to fly over an extended body of water *during* as well as at the beginning and end of each flight. For ground surveys with hand-held spectrometers, this latter technique should be used. Finally, for airborne surveys, the aircraft should be taken to terrain clearances of 1000 m and more where the ground radiation is reduced to negligible proportions through absorption in the air.

Rainfall: The following effects of rainfall have been observed:

- 1) moisture increases the attenuation in an energy-dependent manner and hence leads to skewing of the observed spectrum towards the high energy gamma-rays;
- 2) radioactive elements and their daughter products can be removed selectively over local areas by rapid runoff of rain,
- 3) some nuclides may not reach the top 0.20 m to 0.45 m, the zone of radiation, because of downward percolation due to rain,
- 4) extra moisture in the soil may prevent radon from escaping to the atmosphere so that the ground contribution to the ^{214}Bi window is reduced and
- 5) rain may wash ^{214}Bi from the atmosphere and hence reduce background in the channel selected to detect ^{235}U .

These effects are interrelated and are not completely understood. Experience to date indicates that recovery to pre-rainfall conditions may take place in several hours, but the recovery time is peculiar to every climatic and physiographic sub area on earth. Drainage of soils, atmospheric inversions, barometric pressure, and amount and lateral extent of rainfall are all to be considered in evaluating this problem. The data of Figure 4-4 were obtained from long-term monitoring of the gamma-ray flux at Dallax, Texas, but while peculiar to a specific area, can serve as a guide to recovery to pre-rainfall conditions.

Calibration of Gamma-ray Spectrometers

Introduction

Key articles which describe calibration facilities for and calibration of ground and airborne gamma-ray spectrometers include Darnley et al. (1968), Grasty and Darnley (1971), Grasty and Charbonneau (1974), Grasty (1976), Løvborg et al. (1977), Ward (1978), Ward and Stromswold (1978), and Kirton and Lyus (1979).

The purpose of calibration is to convert the recorded count rates into equivalent ground concentrations of potassium, uranium, and thorium. To do this, it is necessary to know the Compton stripping ratios and their variation with altitude, the height attenuation coefficients, and the sensitivities of the spectrometer for airborne systems. For ground systems the altitude variability of the Compton stripping ratios and the height attenuation coefficients are unimportant. If the calibration is performed correctly, then *assaying* by gamma-ray spectrometry can predict concentrations of the principle radionuclides to accuracies of better than 1 ppm uranium, 1 ppm thorium, and 0.1% potassium for either an airborne or a ground system.

Ground level calibration of airborne and ground systems

Compton stripping: Some counts will be recorded in the lower energy uranium and potassium windows due to Compton scattering in the ground, in the air, or in the detector, from a pure thorium source. Similarly, counts will be recorded in the lower energy potassium window from a pure uranium source. Table 4-8 illustrates these features.

The ratio of the counts in a lower energy window to those in a higher

Table 4-8: Compton Scattering (•→)

Nuclide	^{208}Tl	^{214}Bi	^{40}K
Indicator	Th	U	K
Energy	2.62 MeV	1.76 MeV	1.46 MeV

energy window from a pure uranium or thorium source is termed a stripping ratio or spectral stripping coefficient. These coefficients are peculiar to each detector system. Due to the presence of ^{214}Bi photons at 2.43 MeV in the ^{238}U decay series, some counts will be recorded in the thorium window from a pure uranium source.

The equations relating the corrected potassium, uranium, and thorium count rates K_C , U_C , and T_C to the uncorrected values K_U , U_U , and T_U are (Grasty, 1976)

$$T_U = T_C + b U_C, \quad 4-18$$

$$U_U = \alpha T_C + U_C, \quad 4-19$$

and

$$K_U = \beta T_C + \gamma U_C + K_C, \quad 4-20$$

in which α , β , and γ are the three spectral stripping ratios and b is the fraction of the counts in the uranium window that appear in the thorium window from a pure uranium source. Since b is found experimentally to be small (~ 0.05), we may obtain the corrected counts from these equations as follows:

$$T_C = T_U, \quad 4-21$$

$$U_C = U_U - \alpha T_U, \quad 4-22$$

and

$$K_C = K_U - (\beta U_U - \alpha \gamma T_U) - \beta T_U. \quad 4-23$$

The U.S. Department of Energy through its contractor, Bendix Field Engineering Corporation, has established test pads for ground and airborne system calibration at Grand Junction, Colorado (Ward, 1978; Ward and Stromswold, 1978). The Geological Survey of Canada earlier did likewise at

Ottawa (Grasty and Darnley, 1971; Grasty and Charbonneau, 1974). These pads contain known concentrations of uranium, thorium, and potassium, which vary from pad to pad. The pads are about 0.46 m thick, to appear infinite in depth considering attenuation arguments given earlier. The equations relating the thorium, uranium, and potassium *uncorrected* count rates to the concentrations of each element are derived simply. If we subtract the thorium background (T_B) from the first Compton scattering relation, we obtain

$$T_C - T_B = T_U - T_B, \quad 4-24$$

but this should be proportional to the thorium concentration (T_{ppm}), or

$$T_U - T_B = k_1 T_{ppm}, \quad 4-25$$

in which k_1 is the *sensitivity* to thorium concentration.

Similarly we may write

$$U_C - U_B = U_U - \alpha T_U - U_B \quad 4-26$$

However, a background thorium photon will Compton scatter into the uranium window also so that this latter relation should be written

$$U_C - U_B = U_U - U_B - \alpha(T_U - T_B). \quad 4-27$$

The concentration of uranium is then found from

$$U_U - U_B - \alpha(T_U - T_B) = k_2 U_{ppm} \quad 4-28$$

in which k_2 is the *sensitivity* to uranium concentration.

In a like manner a third relation is established,

$$K_U - K_B - \beta(T_U - T_B) - [\gamma(U_U - U_B) - \alpha(T_U - T_B)] = k_3 K_{pct} \quad 4-29$$

in which K_{pct} is the *sensitivity* to potassium concentration given in percent.

The data obtained by observing T_U , U_U , and K_U for each of five pads, plus the T_{ppm} , U_{ppm} , and T_{pct} for each pad, can be fitted sequentially to the last three equations via least squares techniques to determine the nine unknowns α , β , γ , k_1 , k_2 , k_3 , T_B , U_B , and K_B . Grasty (1976) describes the procedure. The backgrounds so calculated are peculiar to the test sites at a specific time and are determined solely to permit computation of the stripping ratios and the sensitivities. Once so calibrated, a gamma-ray spectrometer may be used as an assay instrument for a year or more before requiring recalibration due to aging of the detector or the PMT. In-field checks on calibration should be used frequently, however, to detect any aging which might set in. Hand samples of known concentrations may be used for this purpose.

Airborne level calibration of airborne systems

Introduction: When an attenuator of thickness H is placed between a detector and a *point source* of mono-energetic γ rays, the number of γ rays received per second by the detector is

$$N = N_0 e^{-\mu H} \quad 4-30$$

in which N_0 is the number of γ rays which would be received per second without the attenuator present and μ is the linear attenuation coefficient of the attenuator. If the detector is in an aircraft and the attenuator is air, the μ is the attenuation coefficient of air, and H is the aircraft height. However, the attenuation is influenced by both the attenuation of the air and the geometrical response of the detector to the extended source below. Darnley et al. (1968) give the count rate N obtained from a half-space of diameter $2R$ at a distance H by

$$N = 2\pi\epsilon C \int_{\mu H}^{\mu\sqrt{H^2 + R^2}} \frac{e^{-x'}}{x'} dx' \quad 4-31$$

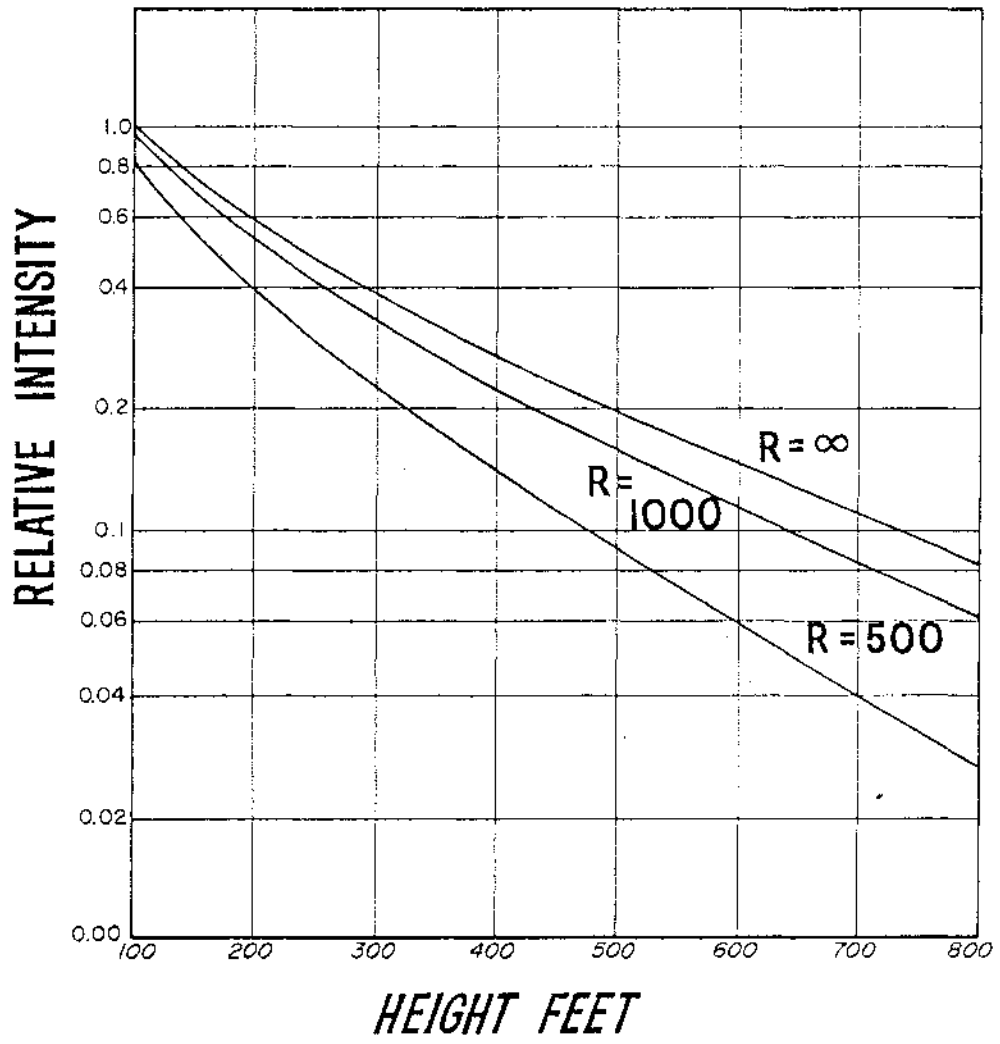
$$= 2\pi\epsilon C \left[E_1(\mu H) - E_1(\mu\sqrt{H^2 + R^2}) \right] \quad 4-32$$

in which

$$E(x) = \int_x^{\infty} \frac{e^{-x'}}{x'} dx' \quad 4-33$$

is a tabulated function, C is the source strength per unit area, and ϵ is the detector efficiency.

Figure 4-5 shows plots of the relative intensity as a function of height H for source diameters of 500 ft (152 m), 1000 ft (305 m), and infinite. On this semi-logarithmic plot, the response functions are almost



4-5

linear over the range 250 ft. (76 m) to 800 feet (244 m). Hence for such source dimensions, the height dependence can once again be expressed by an exponential variation given by

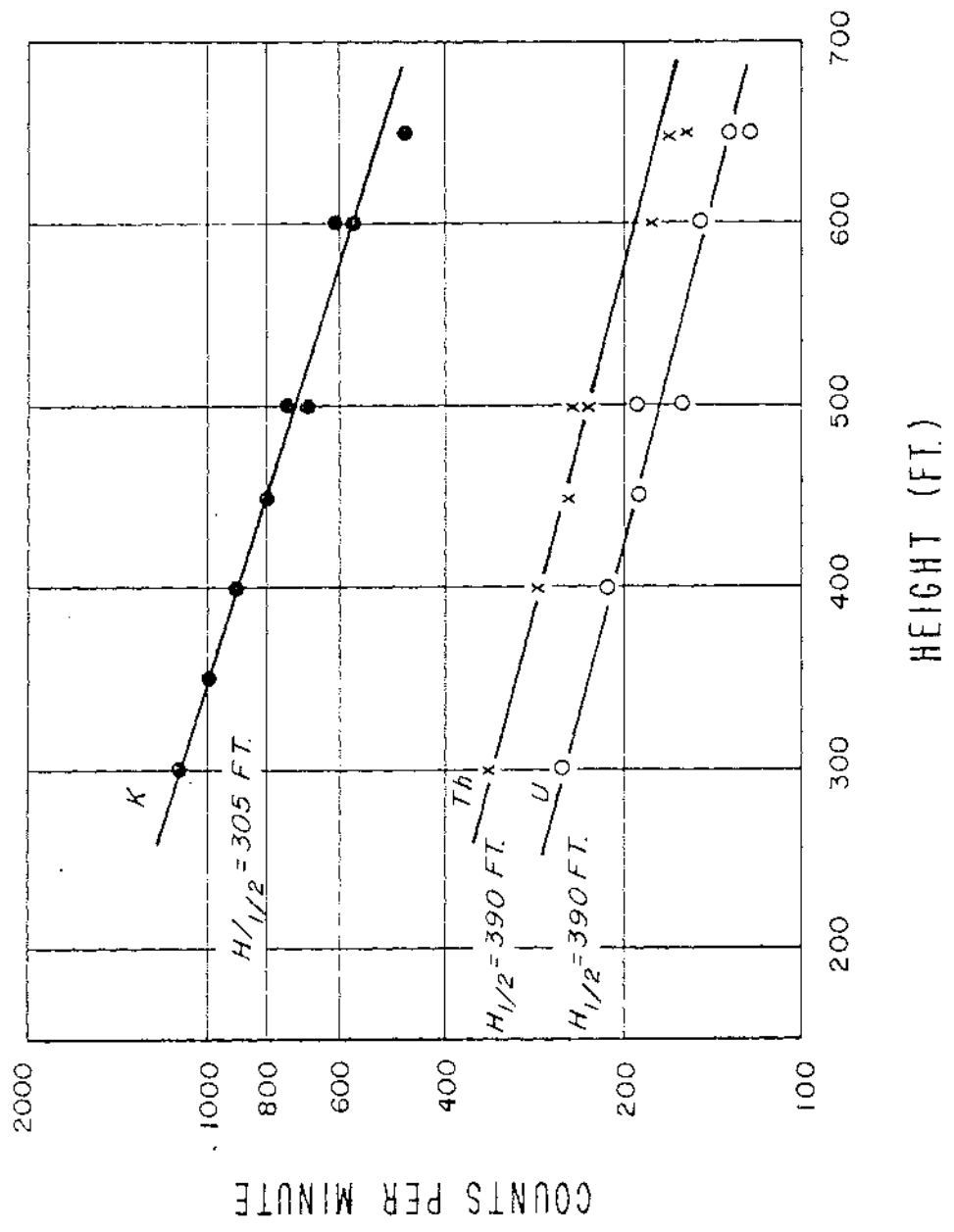
$$N = N_0 e^{-\bar{\mu}H} \quad 4-34$$

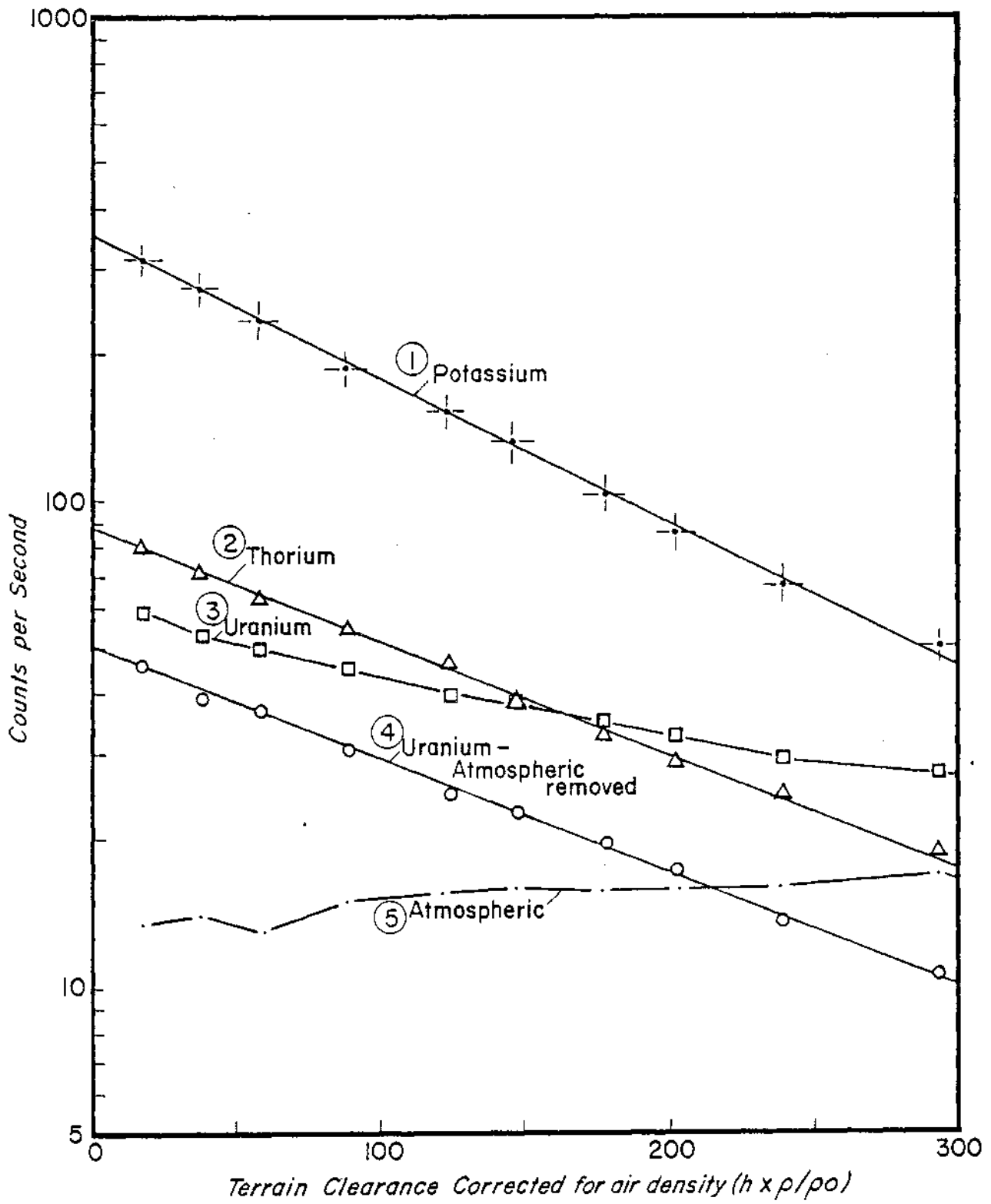
where $\bar{\mu}$ is the mean attenuation coefficient derived by flying at different altitudes over sources of different diameters. Experimental data collected for this purpose is given in Figure 4-6; clearly an exponential variation will fit each data set, at least over the height range 300 ft. (41 m) to 650 ft. (198 m). Because of this fact, it has become common practice to normalize airborne measurements to the nominal terrain clearance of the aircraft, even though it is accepted that the sources range in size from point to infinitely extended. However, this observation does demand that a *test strip* be established *within the survey area* to permit determination of it experimentally.

In addition, calibration of $\bar{\mu}$ for every detector installation should be made at standard test strips such as operated by the Geological Survey of Canada near Breckenridge, Ontario and by Bendix Field Engineering Company at Lake Mead, Arizona.

Unless background is removed from the uranium channel, the apparent $\bar{\mu}$ will not be linear as curve (3) of Figure 4-7 illustrates. When uranium background was removed, using an upwards looking detector as in curve 4 of Figure 4-7, the true attenuation coefficient was obtained.

Effects of air temperature and pressure: The exponential height correction factors $\bar{\mu}$ are proportional to air density. Thus, the effective flying height H of the aircraft at 0°C and 76 mm of mercury is given by





$$H = H_T \times \frac{273 \times P}{T \times 76} \quad 4-35$$

In practice no atmospheric pressure correction is made so that this equation reduces to

$$H = H_T \times \frac{273}{T}, \quad 4-36$$

requiring the observed counts to be corrected to the observed T.

Correction of spectral stripping coefficients for aircraft altitude:

Grasty (1975) has demonstrated that the stripping coefficients vary with aircraft altitude. If one can tolerate a maximum of 50 percent error in uranium counts, then this correction can be ignored.

Sequence of corrections, airborne surveys

There is debate over which correction should be applied first. The Geological Survey of Canada (Grasty, 1976) has adopted the following sequence and hence it is recommended:

- 1) experimentally determine the three spectral stripping coefficients at ground level using calibration pads,
- 2) calculate the theoretical increase with aircraft altitude of the spectral stripping coefficient that is to be applied in the uranium window,
- 3) effect the background and Compton stripping,
- 4) convert the corrected count rates in the three windows to the nominal aircraft altitude at 0°C using experimentally measured-exponential variation of count rate with aircraft over a standard test strip,

- 5) convert these corrected count rates to ground concentrations using results from laboratory analyses on soil samples from the test strip.

Both altitude corrections and the conversion of airborne count rates to ground concentrations are far from ideal for sources whose diameters are much less than 500 m. In order to convert count rates to ground concentrations for all possible source dimensions, a more sophisticated procedure, such as computer modeling (Kosanke and Koch, 1979), is required.

Statistical Errors in Count Rates

The error in a gamma-ray count is usually estimated by computing one standard deviation (1σ) as (Darnley et al., 1968)

$$1\sigma = \pm\sqrt{N} \qquad 4-37$$

where N is the Compton-corrected count for any given time interval, and 1σ represents the 68% confidence level assuming a normal distribution. Referring to the real data set of Table 4-9a, obtained in a 30 sec interval with a McPhar Instrument Co. Spectra 44 spectrometer (347 c.c. volume), we observe 6 percent uncertainty in the uranium count. On the other hand, if a two minute integration time had been used, and if by chance the counts were four times those of Table 4-9a, then the results of Table 4-9b would have been obtained. The uncertainty in the uranium count is reduced to 3 percent.

The above estimates of percent standard deviation are only satisfactory if any one of K, U, or Th occurs alone and without background or Compton scattering. When the latter two effects are both present and

Table 4-9
Count Statistics

	CHANNEL	TC	K	U	Th	TIME	COMMENT
a)	COUNTS	13100	634	285	304	30 SEC	REAL DATA
	1 σ	115	25	17	18		
	1 σ (%)	0.9%	3.9%	6.0%	5.9%		
b)	COUNTS	52400	2536	1140	1216	2 MIN	DATA OF TABLE
	1 σ	229	50	34	35		9a MULTIPLIED BY
	1 σ (%)	0.4%	2.0%	3.0%	2.9%		FOUR

corrections for both have been made, there is greater uncertainty in any one count rate, and hence we should use (Darnley et al., 1968)

$$\sigma_{Th} = \pm [N_{Th}^o + N_{Th}^b]^{1/2}, \quad 4-38$$

$$\sigma_U = \pm [N_U^o + N_U^b + \alpha^2 \sigma_{Th}^2]^{1/2}, \quad 4-39$$

and

$$\sigma_K = \pm [N_K^o + N_K^b + \beta^2 \sigma_{Th}^2 + \gamma^2 \sigma_U^2]^{1/2}, \quad 4-40$$

in which the superscripts o and b refer to observed and background respectively, and in which α , β , and γ are the Compton scattering coefficients, and N_{Th} , N_U , and N_K are the counts per unit time in the thorium, uranium, and potassium windows, respectively.

To estimate how important it is to take into account the uncertainties introduced through background removal, the data of Table 4-10 is included. For this particular combination of signal and background, obtained with a 1024 cu. in. (16×10^3 cc) airborne detector, the effect of background on count statistics is very small.

Fields of View of Airborne Gamma-ray Detectors

Introduction

An airborne gamma-ray detector receives ground radiation from horizon to horizon, a total angle of 180 degrees. However, by studying the attenuation of gamma-rays, via equation 4-32, from a half-space to a detector at an altitude H above the surface, it can be established that 56 percent of the counts come from an area of diameter approximately equal to

Table 4-10
Count Statistics

CHANNEL	TC	K	U	Th	TIME
COUNTS	7000	400	180	200	2.5 SEC.
1 σ	83.7	20.0	13.4	14.1	
1 σ (%)	12.0	5.0	7.4	7.1	
BACKGROUND	-	35	20	15	2.5 SEC.
NEW 1 σ	-	20.9	14.1	14.7	
NEW 1 σ (%)	-	5.2	7.9	7.3	

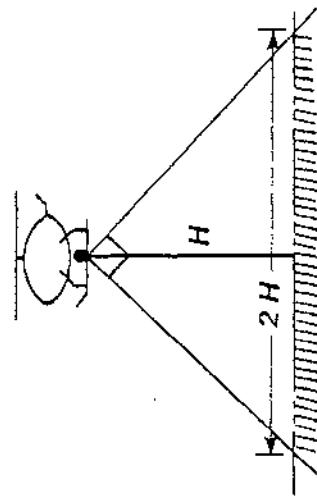
twice the terrain clearance as illustrated in Figure 4-8a. Grasty et al. (1979) show that the width of the strip that produces a fixed percentage radiation detected by a moving airborne system is *significantly less* than the diameter of the circle contributing the same percentage of the radiation detected by a stationary system. This result occurs "because in integrating the detector response of circular sources along the flight line, the same point on the ground is in effect sampled many times, and points closer to the flight line repeatedly generate a greater contribution to the detected count rate than do those far away." (Grasty et al., 1979). The article by Grasty et al. (1979) establishes that *significantly less* in this instance ranges between 1/3 and 2/3 of the diameter similarly influenced by the stationary detector. Later, under *deposit detection*, we shall assume a mean value of 1/2.

The effect of topography

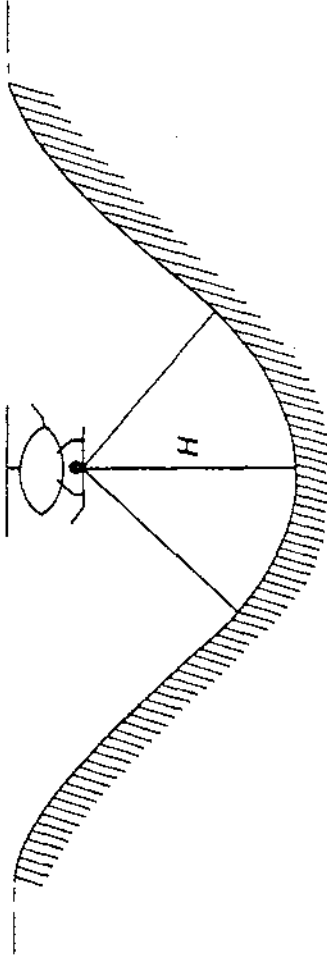
Figures 4-8b through 4-8d show the effect of topography on count rates observed, with an airborne detector, over ridges and valleys. The valley or the ridge can produce either a low or a high count rate depending upon adherence to or deviation from nominal terrain clearance.

Deposit detection

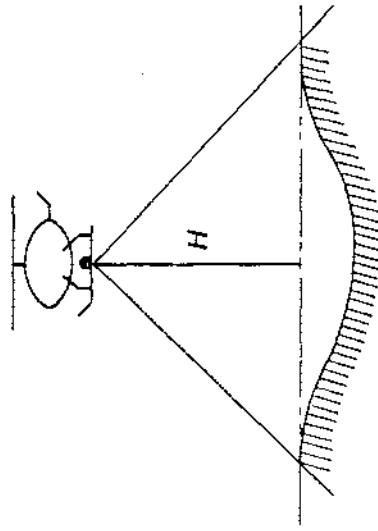
The probability of detecting a uranium deposit with an airborne gamma-ray detector is not large. Figure 4-9 illustrates the geometry of the problem; a thin strip of highly radioactive material oriented normal to the flight line, ideally, occurs within a circular *field of view* of the detector. The anomaly observed by a stationary detector is then



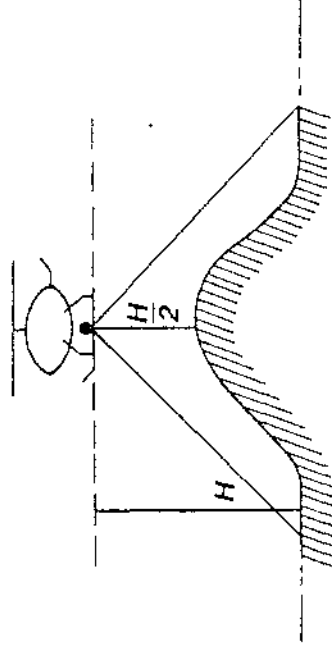
a) NORMAL COUNT RATE



b) HIGH COUNT RATE

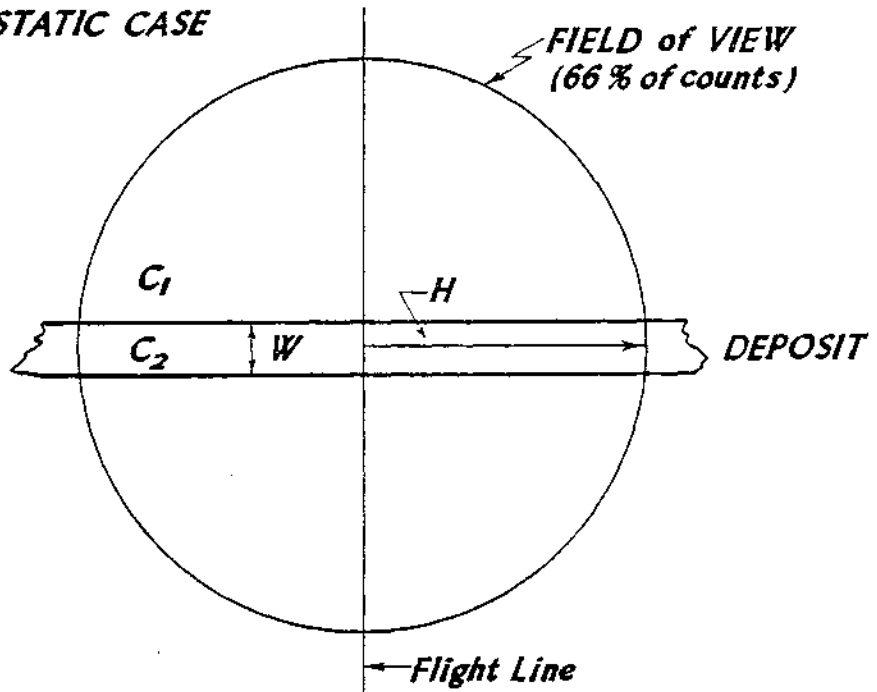


c) LOW COUNT RATE

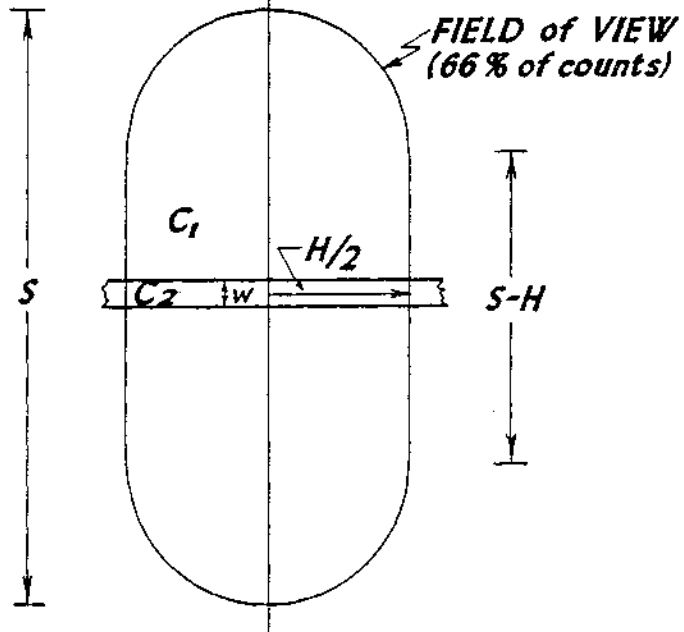


d) HIGH COUNT RATE

A) STATIC CASE



B) DYNAMIC CASE



$$\begin{aligned} \text{STATIC ANOMALY} &= \frac{(\pi H^2 - HW)C_1 + HWC_2}{\pi H^2 C_1} \\ &= \frac{(H - W) + WC_2/C_1}{\pi H}, \end{aligned} \quad 4-41$$

whereas the anomaly observed by a moving detector is

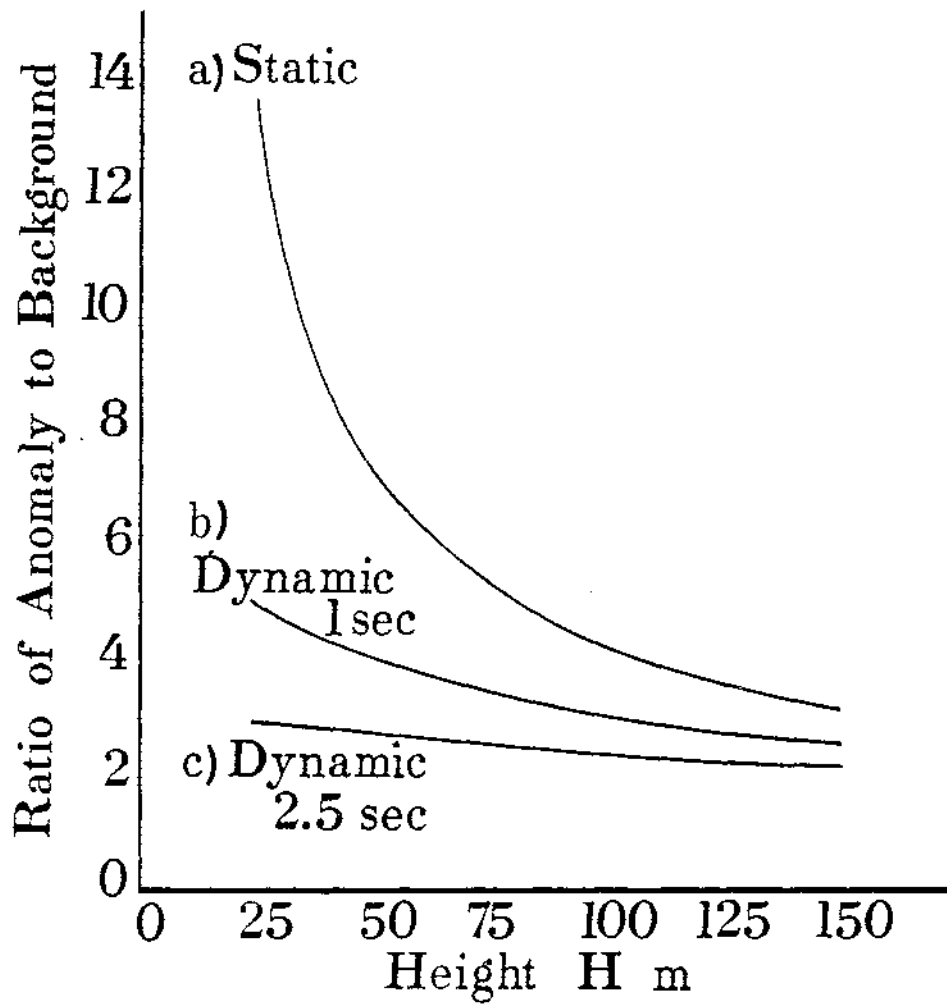
$$\begin{aligned} \text{DYNAMIC ANOMALY} &= \frac{[\pi(\frac{H}{2})S - (\frac{H}{2})W]C_1 + (\frac{H}{2})WC_2}{(\frac{H}{2})SC_1} \\ &= \frac{(\pi S - W) + WC_2/C_1}{\pi S} \end{aligned} \quad 4-42$$

wherein the detection with $H/2$ is given as half its static value H , according to previous arguments.

If we postulate a deposit 10 m wide by 150 m length, striking normal to the flight line, and containing U_3O_8 in concentration 100 times background, then, the *static anomaly* is given by curve a of Figure 4-10. The ratio of anomaly to background ranges from 13.6 for 25 m flight altitude to 3.1 for 150 m flight altitude; statistical and other uncertainties could readily obscure anomalies at altitudes of 100 m and greater. The *dynamic anomaly* over the same deposit appears as curves b) and c) for 1.0 sec and 2.5 sec integration times, respectively, for an aircraft travelling at 200 km/hr. Clearly, aircraft speed and integration time affect the ability of an airborne system to detect a surface deposit.

Hand specimens

If a hand specimen is held at a distance of 0.25 m to 0.50 m from a spectrometer of, say 347 cc, it will subtend a solid angle at the detector of much less than 90 degrees. Hence, if the half-space response formula for U, Th, or K concentration versus counts is to be used to estimate



concentration, then the hand specimen must be held right on the flat end face of the spectrometer and should be larger than the end face.

The Effect of Overburden

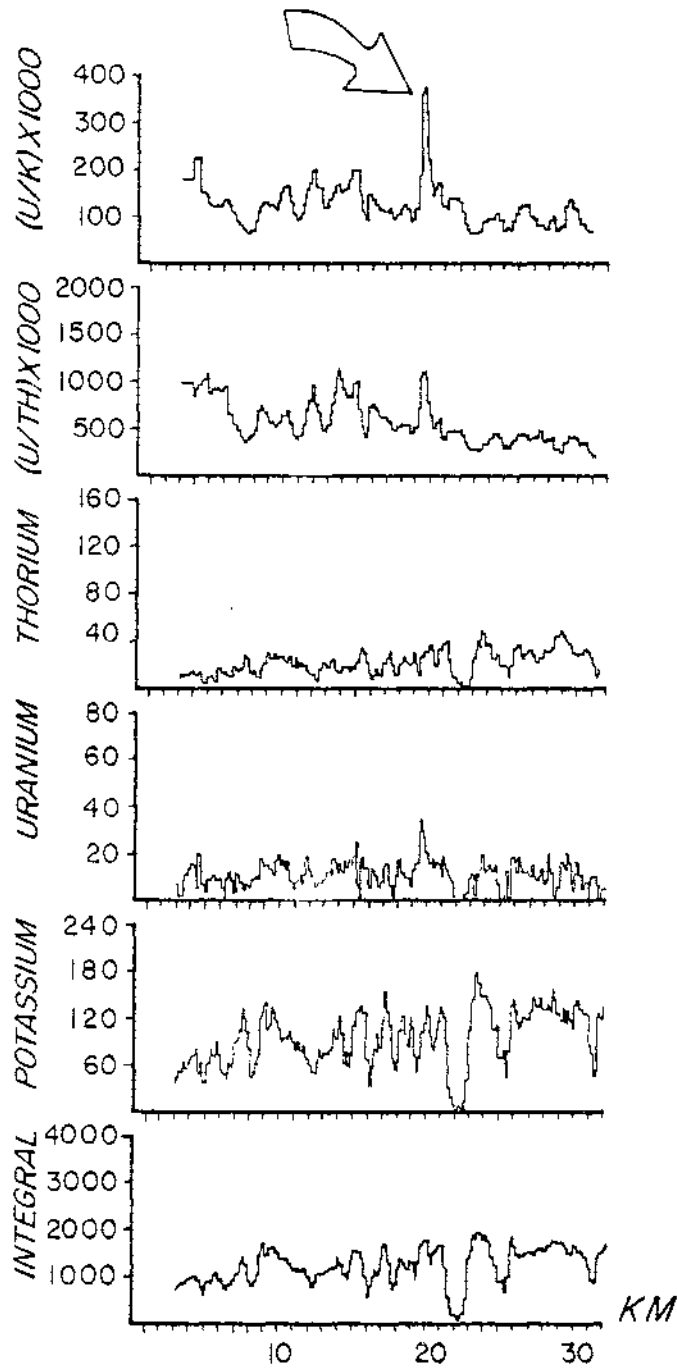
As noted earlier, an overburden of a few tens of centimeters will markedly attenuate the gamma radiation from the bedrock. If the overburden is residual, radiation from it in many cases will be representative of the bedrock, depending upon the weathering processes. Transported overburden may produce radiation entirely misrepresentative of the bedrock.

Further, the area of the exposed rock lying within the field of view of the detector markedly influences the counts recorded in each channel. The ratios U/Th, U/K, and Th/K are not affected to the same extent. Further, if a deposit is in the field of view, its response relative to background may be much more favorably represented in either the U/Th or U/K ratios than Figure 11 depicts because the deposit would be enriched relative to the host rock in U_3O_8 . Figure 4-11 shows the K, U, and Th counts plus the U/Th and U/K ratios over a small uranium deposit in the Bancroft area of Ontario (Darnley and Grasty, 1970). Only by ratioing of spectrometer data could this deposit be detected.

Dickson et al. (1980) have shown that counts, in either of the two energy windows 0.56 to 0.64 MeV or 0.66 to 1.01 MeV may be used to correct for the decrease in total count rate as a result of the presence of barren overburden.

BANCROFT SURVEY 1969

LINE 118



Applications

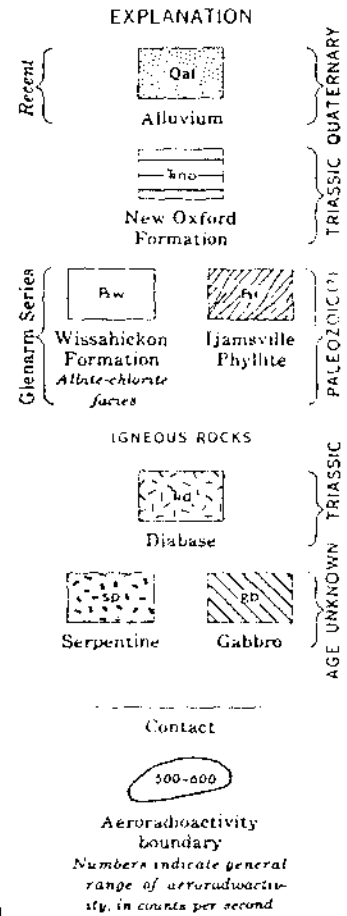
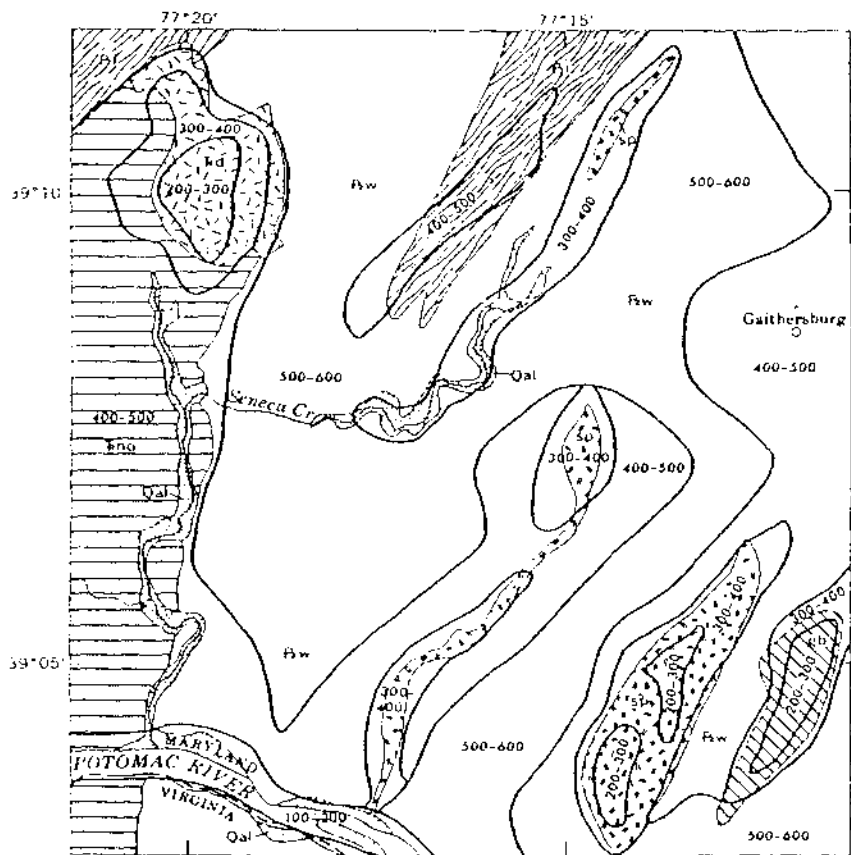
Geological mapping

Figure 4-12, from Pitkin (1968) shows total integrated radioactivity in relation to geologic units. Several mafic and ultramafic bodies are outlined by the airborne total count survey. "Serpentines and a gabbro are lows of 200 to 400 counts per second in a higher matrix of 500 counts per second of the Wissahickon Formation. Also delineated is a sill of Triassic diabase --- an obvious low of 200 to 400 counts per second," (Pitkin, 1968).

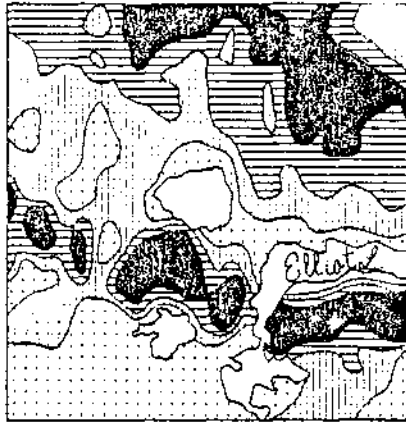
Figure 4-13, from Charbonneau et al. (1973), provides an unusual example wherein the ratio of thorium to potassium could be as useful as total radioactivity in geologic mapping. In other instances, the ratios are better for geologic mapping than are the absolute values of U, Th, or K.

Deposit detection

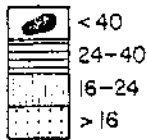
Figure 4-11 illustrates the capability of gamma-ray spectrometers in detecting deposits. Unfortunately this application is decreasing in importance as the deposits with surface radioactivity signatures decrease.



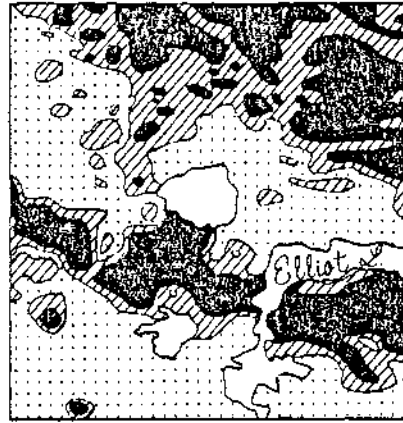
THORIUM



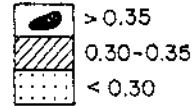
THORIUM
COUNTS/SEC



THORIUM/POTASSIUM RATIO



THORIUM/POTASSIUM
COUNT RATIO



GEOLOGY



Kilometers
0 2

HURONIAN SEDIMENTARY
SEQUENCE

- COBALT GROUP
Graywacke, argillite, quartzite, conglomerate
- QUIRKE LAKE GROUP
Carbonate, siltstone, quartzite, conglomerate
- HOUGH LAKE GROUP
Argillite, quartzite, conglomerate
- ELLIOT LAKE GROUP
Siltstone, argillite, quartzite, arkose, conglomerate
- ARCHEAN BASEMENT

--- LINEAMENT OR FAULT

List of Tables

- Table 4-1 Mean Concentrations of uranium, thorium, and potassium for several representative classes (after Adams et al., 1959 and Kogan et al., 1971).
- Table 4-2 ^{238}U decay series (after Crouthamel, 1969).
- Table 4-3 Principal lines of the $^{238}_{92}\text{U}$ gamma-ray spectrum (after Crouthamel, 1969).
- Table 4-4 ^{232}U decay series (after Crouthamel, 1969).
- Table 4-5 Principal lines of the $^{232}_{90}\text{Th}$ gamma-ray spectrum (after Crouthamel, 1969).
- Table 4-6 Possible significant disequilibria in the ^{238}U decay series (from Saunders and Potts, 1978).
- Table 4-7 Half-Thicknesses for Air, Water, and Rock.
- Table 4-8 Compton Scattering.
- Table 4-9 Count Statistics.
- Table 4-10 Count Statistics.

Figure Captions

- Fig. 4-1 Branching decay by which ^{40}K disintegrates to ^{40}Ca and ^{40}Ar with the emission of γ rays and β particles.
- Fig. 4-2 Gamma-ray spectrum observed with a 1024 cu (16.8 X 10 m) in crystal detector over a mix of K, Th, and U sources (courtesy GeoMetrics).
- Fig. 4-3 Schematic diagram of a scintillation detector.
- Fig. 4-4 ^{214}Bi counting rate recovery times back to pre-rainfall conditions versus rainfall, Dallax, TX (after Saunders and Potts, 1978).
- Fig. 4-5 Plots of the relative intensity as a function of detector height H for source diameters of 500 ft (152 m), 1000 ft (305 m), and infinite (after Darnley et al., 1968).
- Fig. 4-6 Height dependence of count-rate in 1.46 MeV (K), 1.76 MeV (U), and 2.62 MeV (Th) channels (after Darnley et al., 1968).
- Fig. 4-7 Counts per second versus altitude. 1 Potassium, 2 Thorium, 3 Uranium with no atmospheric correction, 4 uranium with atmospheric correction, and 5 atmospheric counts obtained with upward looking detector. (after Richardson and McSharry, 1979).
- Fig. 4-8 The effect of source geometry upon count rate (after Grasty, 1976).
- Fig. 4-9 Fields of view of a) static airborne detector, and b) dynamic (or moving) detector.
- Fig. 4-10 Ratio of anomaly to background for a) static case, b) dynamic case with 1 sec. integration time, and c) dynamic case with 2.5 sec integration time.
- Fig. 4-11 Gamma-ray spectrometer profiles over small deposit, Bancroft, Ontario (after Darnley and Grasty, 1970).
- Fig. 4-12 Total count radioactivity and geology of an area in Montgomery County, MD (after Pitkin, 1968).
- Fig. 4-13 Geology, throrium and thorium/potassium ratio map, Elliot Lake, Ontario, Canada (after Charbonneau et al., 1973).

REFERENCES

- Adams, J. A. S., Osmond, J. K., and Rogers, J. J. W., 1959, *Physics and Chemistry of the Earth* (ed. L. H. Ahrens), v. 3, New York, Pergamon Press, 464 p.
- Adams, J. A. S., and Gasparini, P., 1970, *Gamma-ray spectrometry of rocks*, Elsevier Publishing Company, New York, 295 p.
- Allan, R. J., and Richardson, K. A., 1974, Uranium and potassium distribution by lake-sediment geochemistry and airborne gamma-ray spectrometry: a comparison of reconnaissance techniques, *CIM Bulletin*, p. 109-120.
- Armstrong, C. W., and Brewster, N. E., 1979, A comparison of exploration techniques for uranium deposits occurring in Saskatchewan and the Northern Territory, *Extended Abstracts, Internat. Uranium Sympos. on the Pine Creek geosyncline, Australia*, p. 4-7.
- Charbonneau, B. W., Richardson, K. A., and Grasty, R. L., Airborne gamma-ray spectrometry as an aid to geological mapping township 155 Elliot Lake Area, Ontario, *Geol. Surv. Can. Pap. 73-1, pt. B.*, p. 39-47.
- Crouthamel, C. E., 1969, *Applied gamma-ray spectrometry*, New York, Pergamon Press.
- Darnley, A. G., 1970, Airborne Gamma-ray spectrometry, *Trans., CIM, LXX (III)*, p. 20-29.
- Darnley, A. G., 1973, Airborne gamma-ray techniques: present and future, *Uranium exploration methods, Proc. Series, Int. Atomic Energy Agency, Vienna*, p. 67-108.
- Darnley, A. G., 1975, Geophysics in uranium exploration, *Paper 75-26, Geol. Survey of Canada, Ottawa*, p. 21-31.
- Darnley, A. G., Bristow, Q., and Donhoffer, D. K., 1968, Airborne gamma-ray spectrometer experiments over the Canadian Shield, in *Nuclear Technology and Mineral Resources, IAWA*, p. 163-186.
- Darnley, A. G., and Fleet, M., 1968, Evaluation of airborne gamma-ray spectrometry in the Bancroft and Elliott Lake areas of Ontario, *Canada: Proc. 5th Symposium on remote sensing of environment, University of Michigan, Ann Arbor*, p. 833.
- Darnley, A. G., and Grastly, R. L., 1970, Airborne radiometric survey of the Bancroft Area, *Geol. Surv. Can., Open File Release No. 45*.
- Darnley, A. G., and Grasty, R. L., 1971, Mapping from the air by gamma-

ray spectrometer experiments over the Canadian Shield, in Nuclear Technology and Mineral Resources, IAWA, p. 163-186.

- Dekker, A. J., 1957, Solid State Physics, Englewood Cliffs, N.J., Prentice-Hall, Inc., 540 p.
- Dickson, B. L., Clark, G. J., and McGregor, B. J., 1980, Technique for correcting for overburden effects in ground level radiometric surveys of uranium orebodies, Geophysics, v. 45, p. .
- Dodd, P. H., 1974, Geophysical exploration for uranium, a review of methods and economics, paper presented at 103rd Annual meeting, AIME, Dallas, Texas.
- Dodd, P. H., 1976, Airborne radiometric reconnaissance: the why's and wherefore's, uranium geophysical technical symposium, U.S. Energy, Research and Development Administration, Bendix Field Engineering Corporation, Grand Junction, Co., Sept. 14-16, p. 13-20.
- Foote, R. S., 1969, Improvement in airborne gamma-radiation analyses for anomalous radiation by removal of environmental and pedologic radiation changes, Proc. Symp. on use of nuclear techniques in the prospecting and development of mineral resources, I.A.E.A., Vienna.
- Grasty, R. L., 1974, Applications of gamma radiation in remote sensing, in Methods of Remote Sensing, Berlin, Springer-Verlag.
- Grasty, R. L., 1975, Uranium measurement by airborne gamma-ray spectrometry, Geophysics, v. 40, no. 3, p. 503-519.
- Grasty, R. L., 1976, A calibration procedure for an airborne gamma-ray spectrometer, Geol. Surv. Can. prof paper 76-16.
- Grasty, R. L., and Charbonneau, B. W., 1974, Gamma-ray spectrometer calibration facilities, in Report of Activities, Part B., Geol. Surv. Can., Paper 74-1, Pt. B, p. 69-71.
- Grasty, R. L., and Darnley, A. G., 1971, The calibration of gamma-ray spectrometers for ground and airborne use, Geol. Surv. Can., Paper 71-17.
- Grasty, R. L., Kosanke, K. L., and Foote, R. S., 1979, Fields of view of airborne gamma-ray detectors, Geophysics, v. 44 (8), p. 1447-1457.
- International Atomic Energy Agency, 1973, Uranium Exploration Methods, UNIPUB, Murray Hill Station, New York, New York.
- International Atomic Energy Agency, 1976, Exploration for Uranium Ore Deposits, 807p., UNIPUB, Murray Hill Station, New York, New York.
- Kirton, M., and Lyus, D., 1979, Calibration of an airborne gamma-ray

spectrometer over Mary Kathleen Uranium Mine, Bull., Aust. Soc. of Expl. Geophys., v. 10 (4), p. 69-74.

- Kogan, R. M., Nazarov, I. M., and Fridman, Sh. D., 1971, Gamma spectrometry of natural environments and formations, Moscow, Atomizdat, translated from the Russian by the Israel Program for Scientific Translations, Jerusalem.
- Kosanke, K. L., and Koch, C. D., 1974, An aerial radiometric data modeling program, paper presented to IEEE meeting, San Francisco.
- Løvborg, L., Grasty, R. L., and Kirkegaard, P., 1977, A guide to the calibration constants for aerial gamma-ray surveys in geoexploration, paper presented at American Nuclear Society Symposium: Aerial Techniques for Environmental Monitoring, Las Vegas, Nevada.
- Moxham, R. M., Foote, R. S., and Bunker, C. M., 1965, Gamma-ray spectrometer studies on hydrothermally altered rocks, Economic Geology, v. 60, n. 4, p. .
- Pedersen, G. P., Dunbier, J., and Gingrich, J. E., 1979, Experience with track etch method for uranium exploration in northern Australia, Extended Abstracts, Internat. Uranium Sympos. on the Pine Creek geosyncline, Australia, p. 159-162.
- Pitkin, J. A., 1968, Airborne measurements of terrestrial radioactivity as an aid to geologic mapping, USGS Prof. Paper 516-F, 29 p.
- Richardson, R., and McSharry, P. J., 1979, Application of high sensitivity airborne spectrometer methods to uranium exploration in the Pine Creek Geosyncline, extended abstract in International Uranium Symposium on the Pine Creek Geosyncline, Australia, p. 166-168.
- Saunders, D. F., and Potts, M. J., 1978, Manual for the application of NURE 1974-1977 aerial gamma-ray spectrometer data, Dept. of Energy rpt. GJ BX-13(78).
- Ward, D. L., 1978, Construction of calibration pads facility, Walker Field, Grand Junction, Colorado, Report GJBX-37(78) by Bendix Field Engineering Corporation, Grand Junction, Colorado.
- Ward, D. L., and Stromswold, D. C., 1978, Procedures and regulations for airport calibration pads, Walker Field, Grand Junction, Colorado, Report GJBX-38 (78) by Bendix Field Engineering Corporation, Grand Junction, Colorado.

SECTION FIVE - WELL LOGGING AND BOREHOLE GEOPHYSICS

Introduction

Well logging is the measurement of physical or chemical properties in boreholes of either the borehole environment or the geologic formations surrounding the borehole. It is a significant component of oil and gas exploration and development programs (Johnson, 1962; Pickett, 1970) and most of the available technology has been pioneered by the petroleum industry (Evans, 1970). It is also important to uranium, coal, geothermal and non-metallic mineral exploration and development but on a much smaller scale than used in the petroleum industry. Very limited application has been made of well logging in the base metal industry (Dyck et al., 1975, Glenn and Nelson, 1977).

Well logging in the base metal industry has been limited largely to use of some very specialized tools such as magnetic susceptibility and induced polarization. Moore (1957), Zablocki and Keller (1957), Zablocki (1966), Baltosser and Lawrence (1970), Czubek (1971), Scott et al. (1977), and Glenn and Nelson (1977) have published on the use of well logging in the minerals industry. However, the base metals industries has developed and used tools designed to make measurements between boreholes and between boreholes and the surface. These techniques are commonly called borehole geophysics.

The requirements for research in well logging and borehole geophysics for minerals exploration and development have been identified by representatives of the mining industry (Ward et al., 1977) as 1) determination of physical properties, 2) development of direct assay

logging, and 3) expanding the radius of investigation from the borehole. Much research has been done in recent years in direct assay logging methods, particularly radiation techniques (IRT Corporation, 1976; Czubek, 1977; Wilson and Cosby, 1980), but most of the technology is only now at the point where some techniques can be applied routinely. The objectives of a good logging technology are to reduce exploration and development costs and to provide information unobtainable in any other way. Logging becomes important as new mining technologies arise, such as in-situ, or solution mining, and as ore targets become deeper and more expensive to evaluate.

Various logging tools, their measurements and applications are listed in Table 5-1. We will illustrate each of these tools and techniques with examples. Table 5-1 includes an evaluation of each method on the basis of its ability to measure directly or indirectly the physical or chemical property of interest. The data may be either quantitative or qualitative. The basis for this evaluation will become obvious when each tool and technique is discussed.

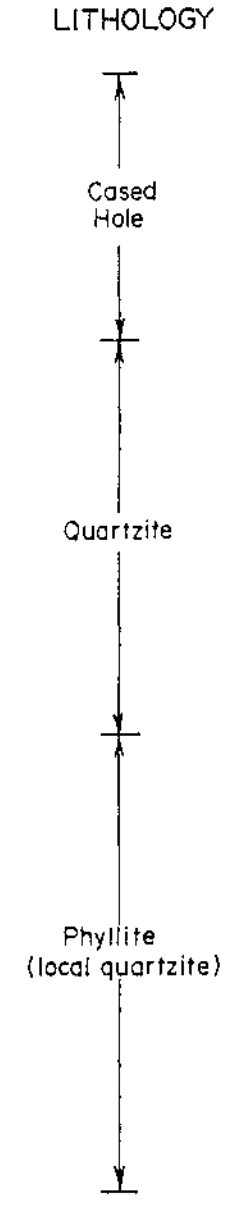
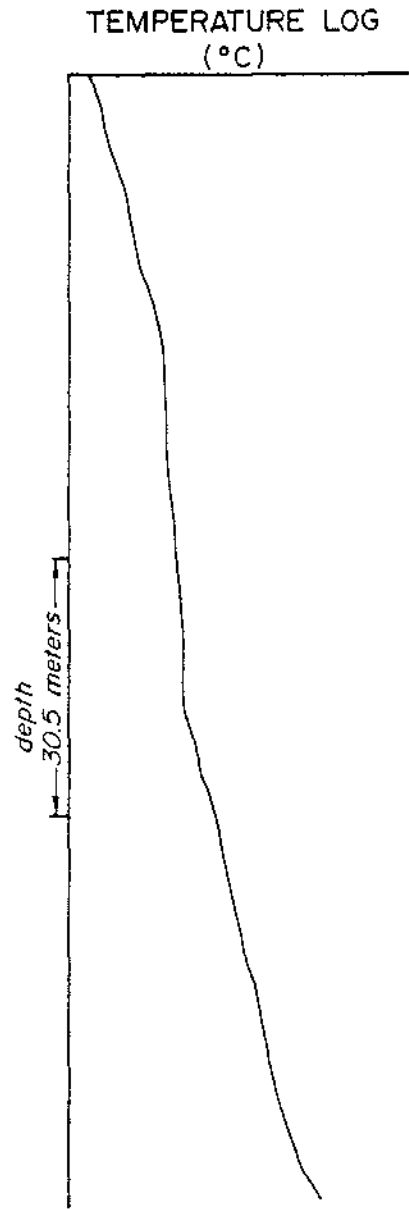
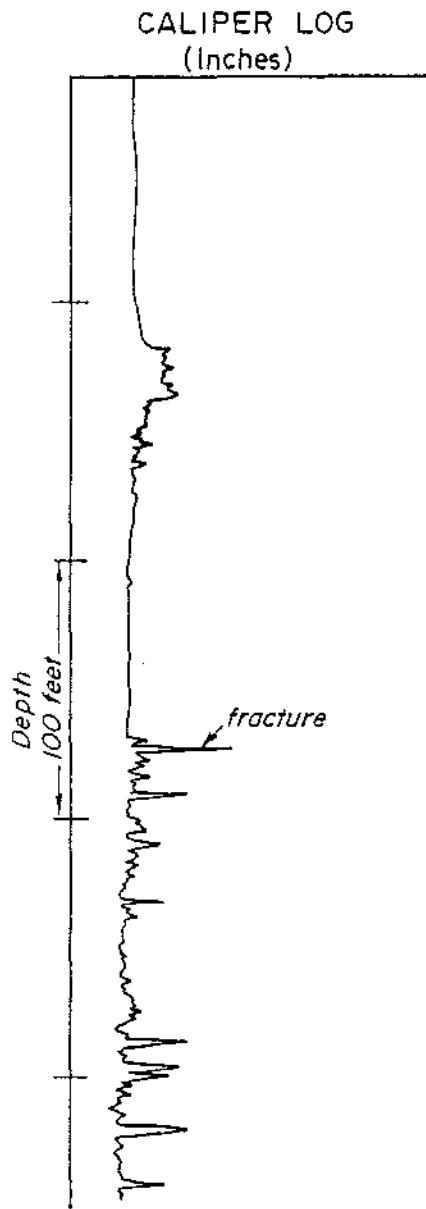
Caliper and Temperature Logging

The *caliper log* is a measurement of borehole diameter and can be obtained separately or in combination with other tools. Various caliper tools are available but most common tools are one, two or three arm calipers. Hole size information is valuable for several reasons. Many borehole measurements are sensitive to borehole size and can be corrected if these data are available. Some tools which require caliper corrections include a caliper, and corrections are made automatically during the

Table 5-1: Logging tools, property measured and application in mining

<u>Logging Tool</u>	<u>Property Measured</u>	<u>Application</u>
Caliper	Hole Size	Hole completion ¹ , fractures ³ , lithology ³ , corrections of other measurements ¹ .
Temperature	Temperature	Fracturing ³ , fluid flow ^{1,3} , oxidation ³ , lithology ^{1,3} , corrections of other measurements ¹ .
Magnetic susceptibility	Magnetic susceptibility	Lithology identification ¹ , correlation ³ , magnetite content ¹ .
Spontaneous Polarization	Natural voltage in the earth	Lithology ³ , mineralization ³ , oxidation-reduction ^{2,3} .
Resistivity/IP	Complex resistivity	Lithology identification ^{2,3} , sulfide and clay content ^{2,3} , correlation ³ .
Natural gamma	Natural gamma radiation, (total count or spectral)	Lithology ^{1,3} , correlation ¹ , U ₃ O ₈ ¹ , K ₂ O ¹ (borehole assaying) ¹ .
Gamma-Gamma	Scattered gamma-rays	Bulk density ¹ , porosity ² , lithology ² , borehole assaying ² .
Neutron	Capture gamma-rays; thermal, epithermal, or fission neutrons	Borehole assay ² , porosity ² , chemically bound water ² , lithology ² .
3-component magnetometer	Magnetic field components	Type and location of ore zone ² .
Gravity meter	Gravity field, gradient	Excess mass and location of ore zone ² .

1. Direct quantitative
2. Indirect quantitative
3. Direct qualitative
4. Indirect qualitative

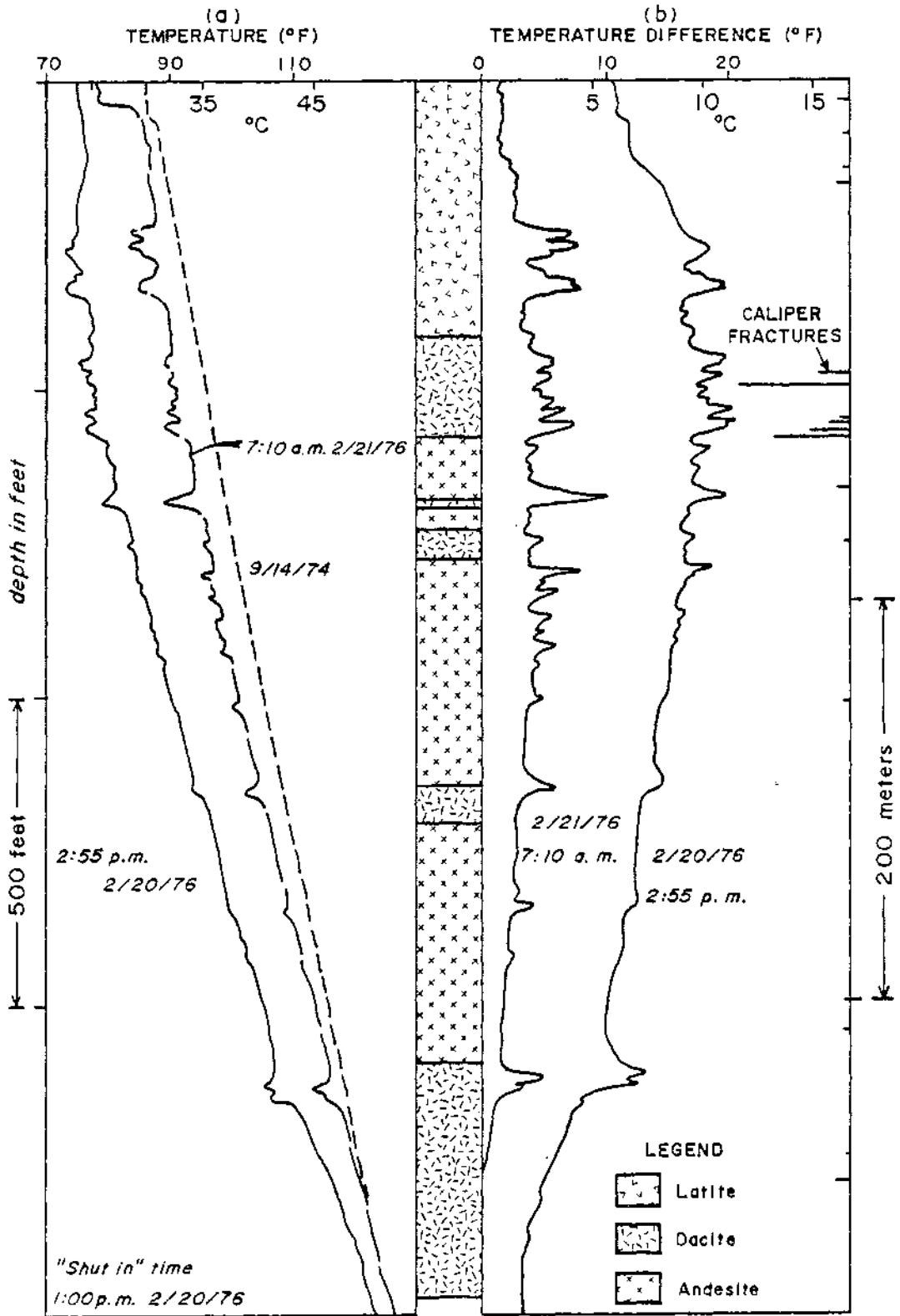


logging process. A caliper log is shown in Figure 5-1.

Fractured zones or poorly consolidated formations commonly sluff material into the borehole leaving cavities. Hence the caliper can be used to locate fractures, to identify certain lithologies and to ascertain hole completion problems. Also, the caliper log, if run as one of the first tools into the borehole, can alert the logging operator of poor hole conditions and potential risks of using other tools in the borehole.

Temperature logging is not extensively used by the minerals industry but can be useful in certain situations. Temperature logs can be used to locate fluid flow zones in a borehole (Smith and Steffensen, 1970; Keys and MacCary, 1971). In most drill holes the geothermal gradient has been modified by circulating drill fluids during drilling. The gradient can be purposely modified by pumping fluid from or injecting fluid into a borehole. In either case a temperature log could reveal permeable zones in the borehole. Figure 5-2 shows an example of a temperature injection profile. Logs were obtained at various times after fluid was injected into the hole. The cooler surface water injected into the drill hole cooled the permeable zones where it flowed into the rock. These zones recover slowest and are evident in the temperature log. The flow zones in this example correlate with fractures or rock contacts.

The borehole temperature, once drilling has ceased and if the fluid column remains undisturbed, will recover to the geothermal gradient. This recovery time will depend on a number of things including the temperature contrast between mud and formation, the length of drilling time and fluid flow in the borehole (Goguel, 1976, p. 50). Once in thermal equilibrium the temperature log may yield lithologic information. The temperature



gradient, in the absence of convection and groundwater flow, will reflect the relative thermal conductivities (Conaway and Beck, 1977) or heat generation in (Guyod, 1946a, b; Howell et al., 1978) the formations intersected by the borehole. An example of lithology and temperature gradient correlation is shown in Figure 5-1. Guyod (1946b) reports that temperature increases of more than 10°F have been noted near pyrite deposits. The heat is generated by oxidation-reduction reactions.

In the absence of temperature logs, bottom hole temperatures are recorded while logging with other tools. This information is needed to perform temperature corrections or interpretations of other logs, particularly resistivity logs.

Electrical Logging

Introduction

Electrical logging methods employed by the minerals industry fall into two groups: (1) the single hole methods or conventional well logging, and (2) hole-to-surface and hole-to-hole borehole geophysics. Either of these methods may employ electrodes, loops, or measurement techniques commonly used in surface geophysics. Resistivity, IP, EM, and SP logging are all popular techniques. Dyck (1975) has made a review of these various methods.

Spontaneous Polarization

Spontaneous Polarization (SP) is usually taken as the measured, natural voltage of a downhole electrode relative to a surface electrode. Measurement of SP in boreholes is routine in conventional well logging. It is often a part of combination tools such as resistivity, nuclear and

acoustic tools.

The origin of SP in the earth has been discussed extensively in the logging literature (Doll, 1948; Goudouin et al., 1957; Wyllie et al., 1958; Hill and Anderson, 1959; Dakhnov, 1962) and in an earlier section of this paper. Natural voltage variations in a borehole may arise from (1) the diffusion of ions from the drilling fluid into the formation or the reverse and (2) oxidation-reduction reactions of minerals in the vicinity of the borehole. The first source of SP is the one commonly measured in oil and gas logging (Schlumberger, 1972) and will not be discussed here. The second source of SP is the one commonly measured in minerals logging.

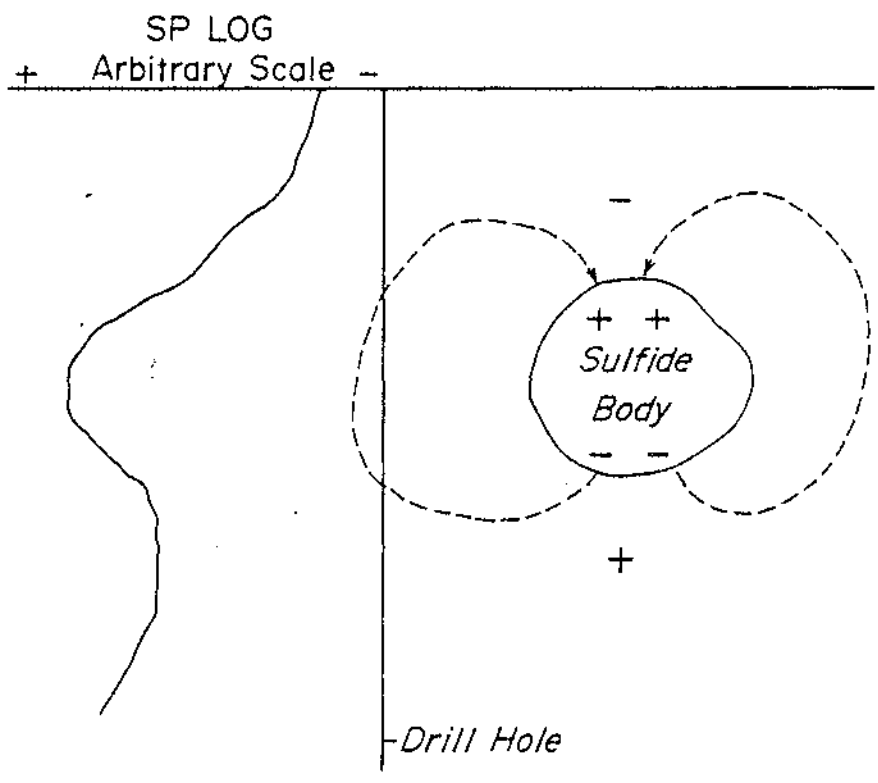
While SP variations are normally less than 75mv in oil and gas logging, sulfide SP anomalies may be as large as 700-800mv (Telford et al., 1976). The SP source is the potential developed by the chemical reactions of oxidation and reduction of the metallic minerals in the subsurface. Figure 5-3 schematically illustrates an idealized SP cell and SP log.

SP can be measured at the surface but in cases where it is masked by a poorly conducting surface layer or if the upper portion of the orebody is imbedded in clay (Becker and Telford, 1965; Parasnis, 1974), borehole measurements are recommended. Field examples can be found in Bower (1968), Becker and Telford (1965), Logn and Bolviken (1974) and Parasnis (1974).

SP logs are commonly obtained in uranium exploration drill holes in sedimentary environments. The log can be used to identify lithology, and the log may also reflect the redox potential (Eh) in the vicinity of the ore zone (Pirson and Wong, 1972; Veneziani et al., 1972).

Resistivity/IP logging

The measurement of resistivity and/or induced polarization in



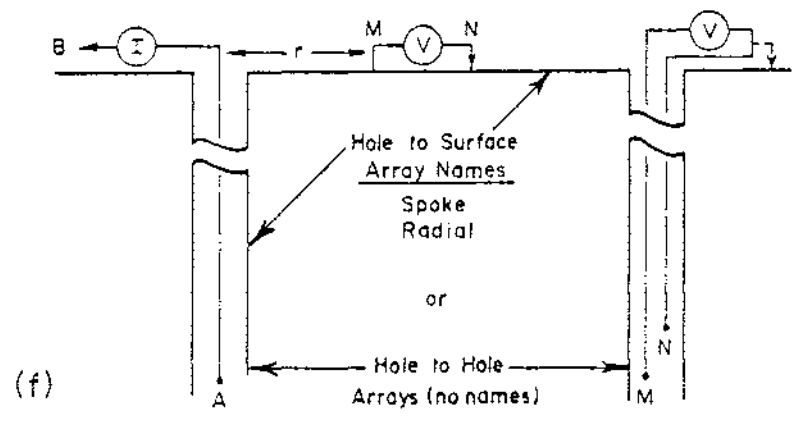
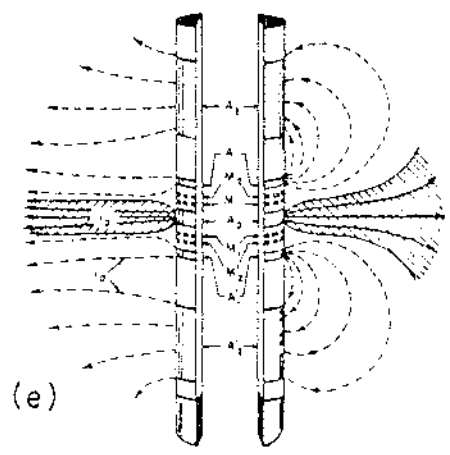
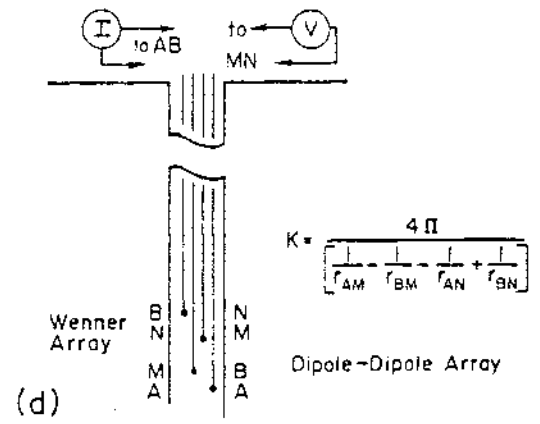
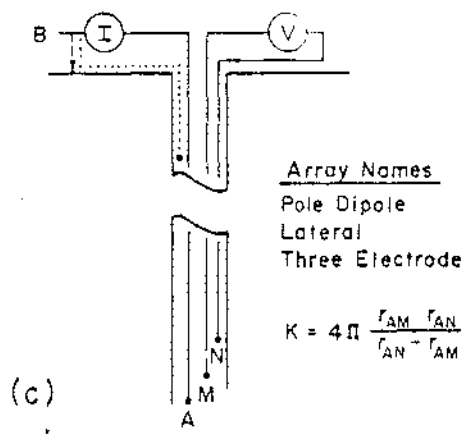
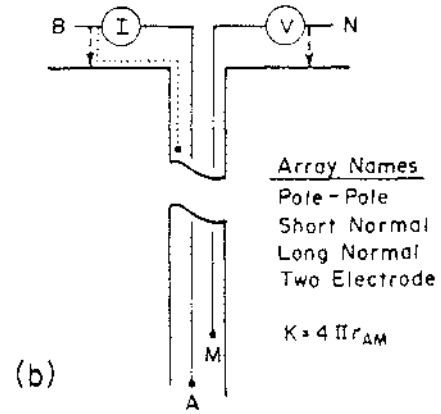
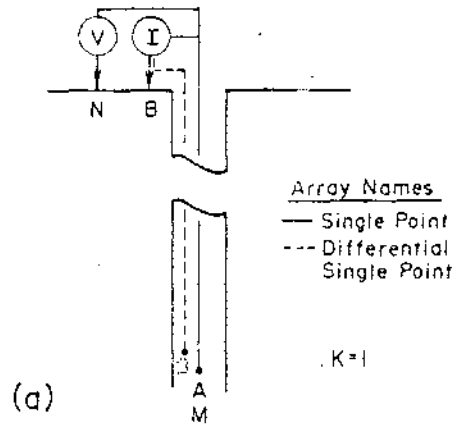
boreholes is the most popular well logging technique employed by the minerals industry. The measurements may be made in a single hole, between holes and between a hole and the surface. The instrumentation and techniques used are numerous. Only the most commonly applied methods will be discussed.

Figure 5-4a through 5-4e schematically illustrate the various single hole electrode configurations, and their most common name, employed in electric logging. The popular hole-to-hole and hole-to-surface electrode systems are sketched in Figure 5-4f.

In nearly all resistivity systems a constant current source is used such that the measured potential is directly proportional to the formation and borehole fluid resistivity; i.e., $\rho_a = K V/I$ where ρ_a is apparent resistivity, K is a geometric factor for a particular electrode configuration, V is the measured voltage, and I is the transmitted current. The geometric factor for various tools are noted in Figure 5-4.

The single point resistance tool, Figure 5-4a, is routinely included in many mineral logging programs, particularly uranium exploration. Basically, the measurement is the variation of downhole electrode impedance. The single point resistance measurement can be obtained in combination with other measurements and requires a minimum number of cable conductors. Also, SP can be measured simultaneously from the same electrode. The resistance measured can be used for correlation or lithology identification. The method seldom provides quantitative information. A good discussion of the conventional single point tool and the differential single point tool can be found in Keys and MacCary (1971).

The long and short normal and lateral logs (Figure 5-4b and 5-4c) were



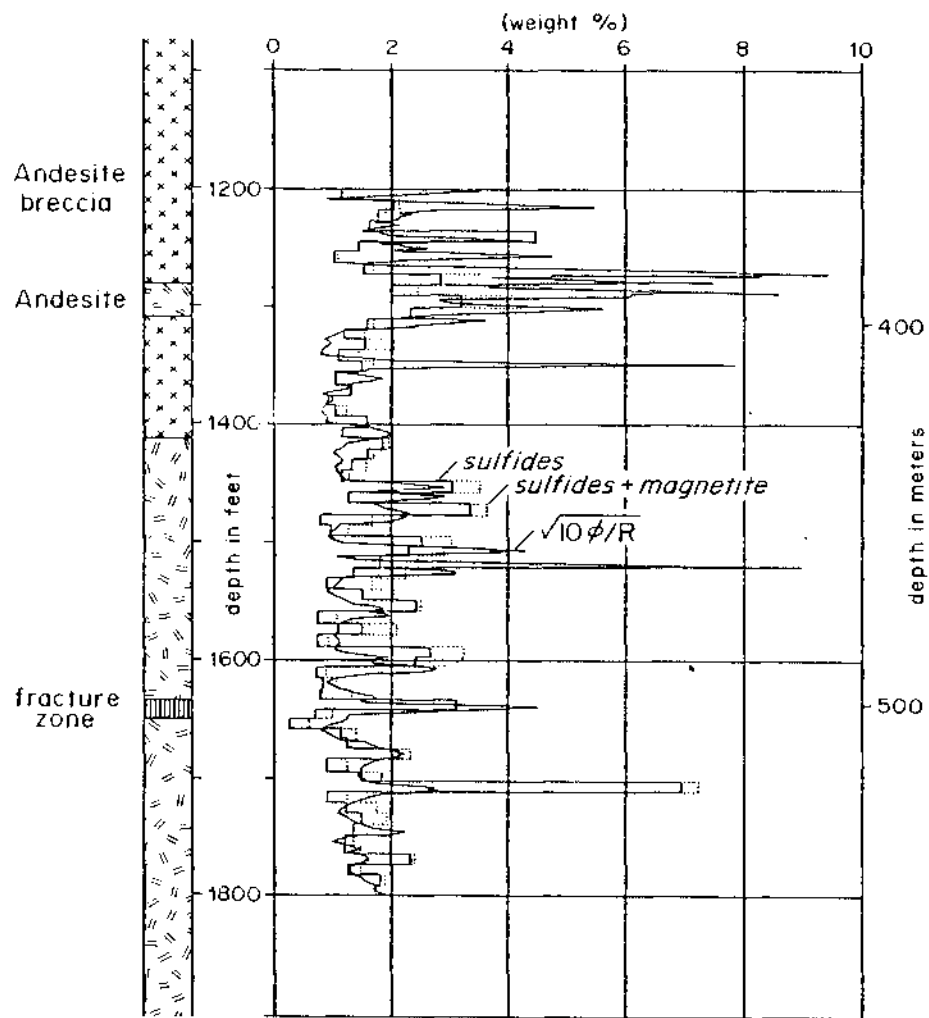
Example of a focused electrode array - dual laterolog (Courtesy of Schlumberger)

among the first electrode systems used in oil and gas logging. This industry seldom employs the long normal and short normal log. The measurements are very sensitive to borehole diameter and bed thickness. The minerals industry still finds these electrode systems valuable since boreholes are usually of very small diameter, and the concept of a layered resistivity is seldom appropriate. However, the minerals industry commonly measures IP and resistivity rather than only resistivity with these systems. Both time and frequency domain systems are used. The electronics may be totally on the surface, partially on the surface and partially downhole or totally downhole. Placing the electronics entirely downhole or using the time domain method minimizes capacitive and inductive coupling between the transmitter and receiver cable lines. Good shielding of the cable lines has also been used with some success (Brant et al., 1966). Snyder et al. (1977) published an excellent review of the measurement of IP in boreholes.

Figure 5-5 shows data from two different drill holes (Glenn and Nelson, 1977) in an Arizona porphyry copper deposit. The measurements were made by Kennecott Copper Corporation using a 1 m normal electrode array. Both amplitude and phase were measured at 14 Hz. The data from drill hole A show a strong correlation between total sulfides and $\sqrt{10\phi R}$, where ϕ is phase and R is apparent resistivity, Figure 5b. In drill hole B the correlation is between phase and total sulfides, Figure 5c. Glenn and Nelson suggest that the different correlations can be attributed, possibly, to the difference in character of the sulfide mineralization of the two holes. The mineralization in hole A is predominately pyrite and chalcopyrite in veins with minor amounts disseminated in the rock. Clearly

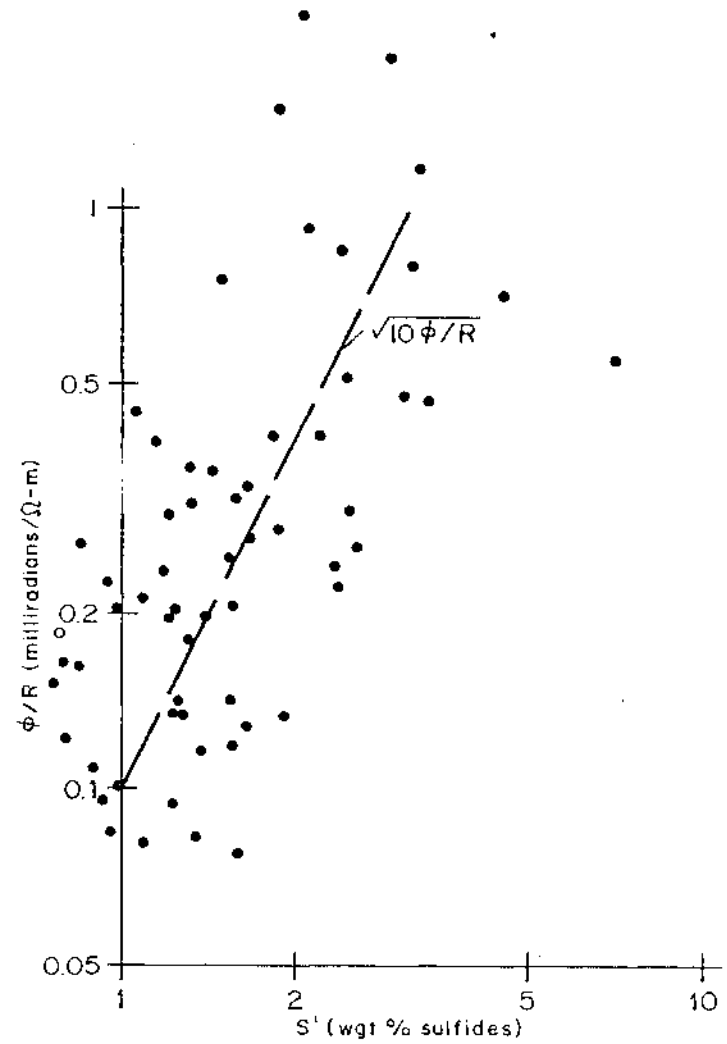
GEOLOGY

TOTAL SULFIDE - $\sqrt{10 \phi/R}$



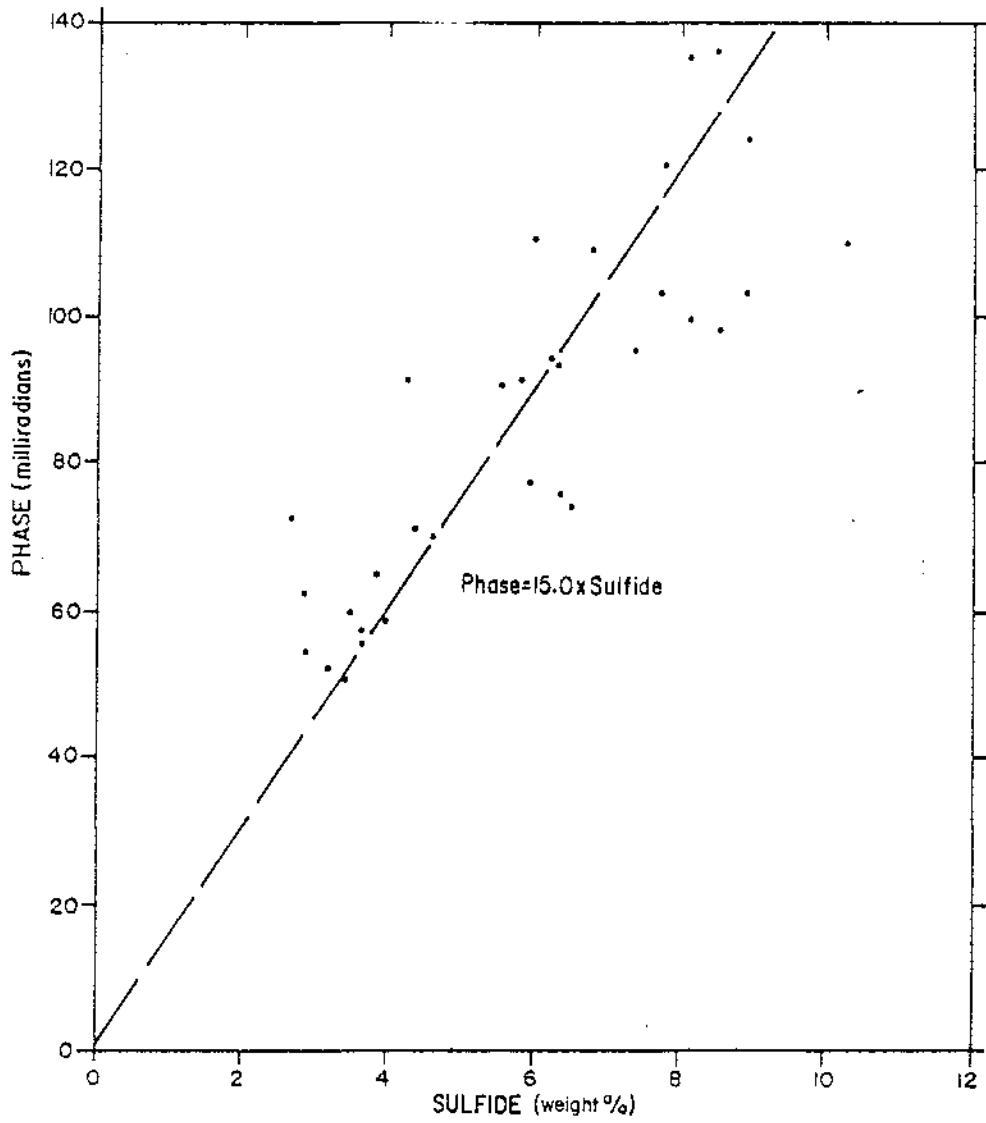
5a)

Drill Hole A



5b)

Drill Hole A



Phase values averaged over 10 foot interval vs. sulfide content.

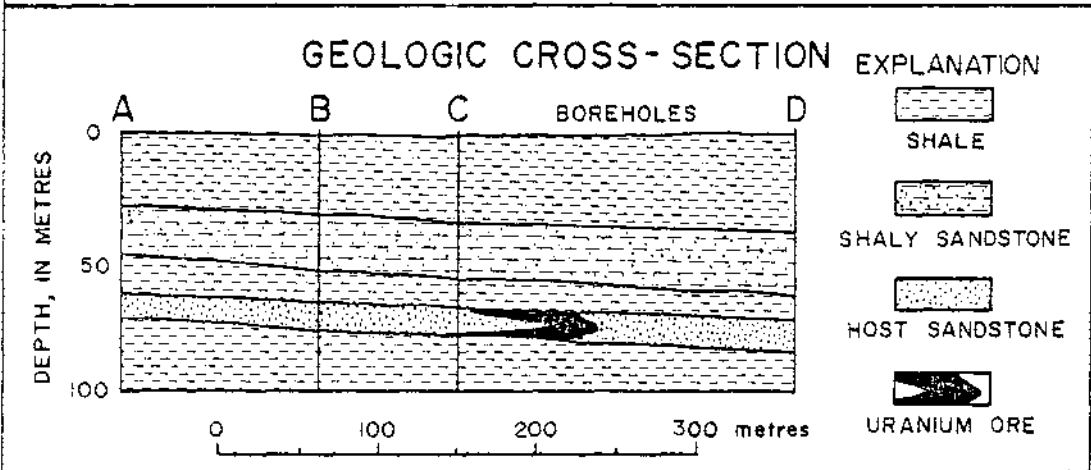
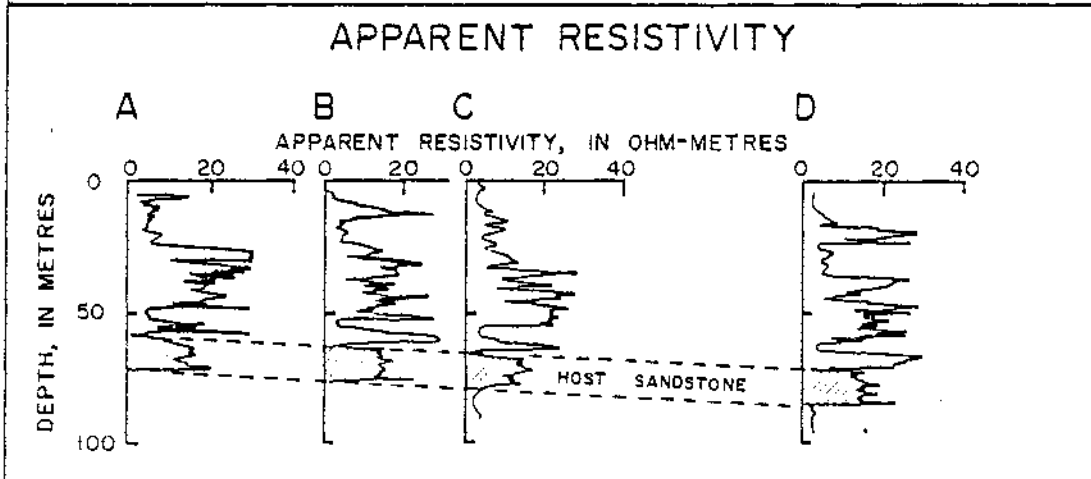
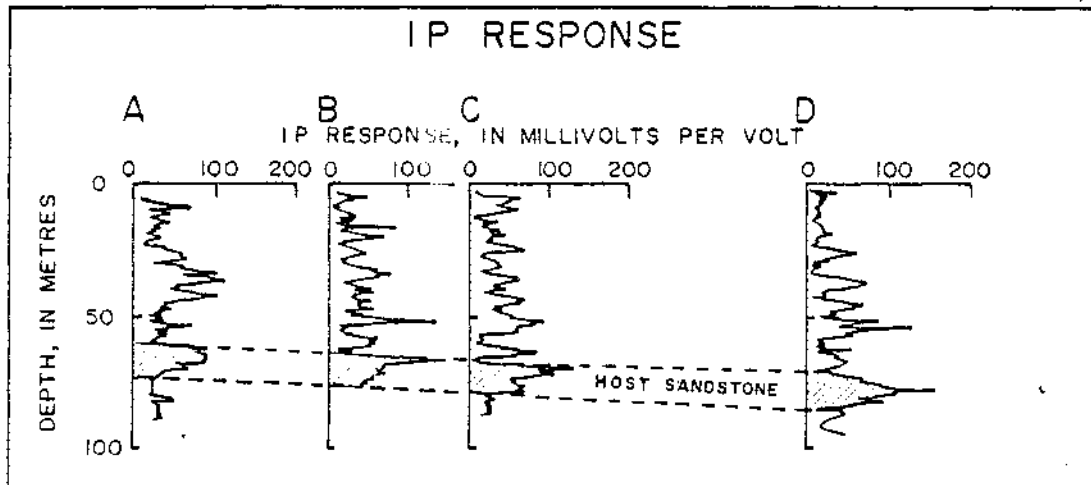
5c)

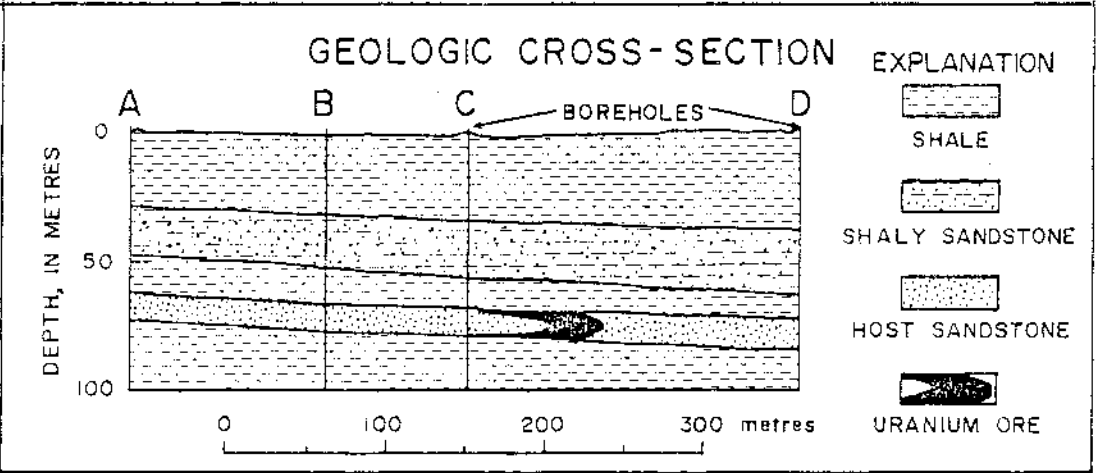
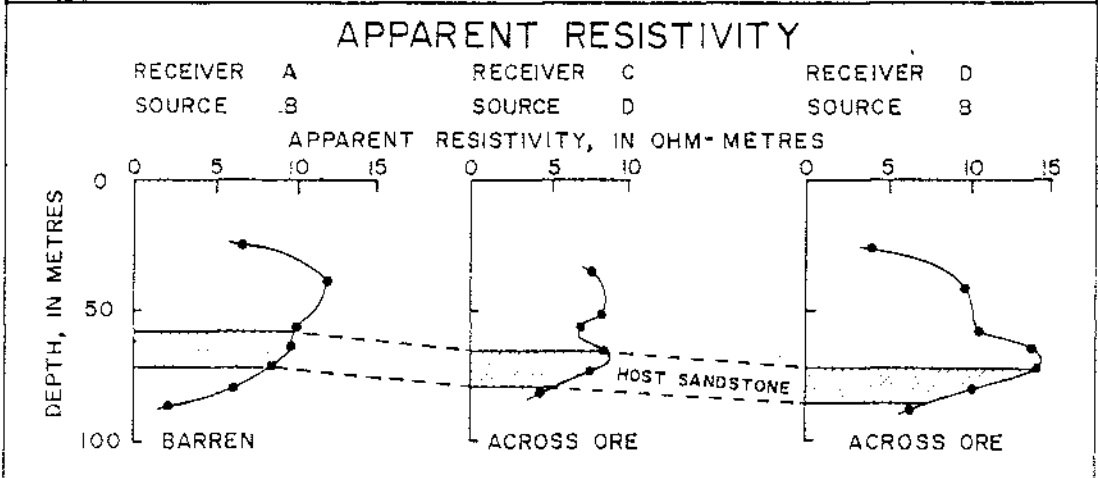
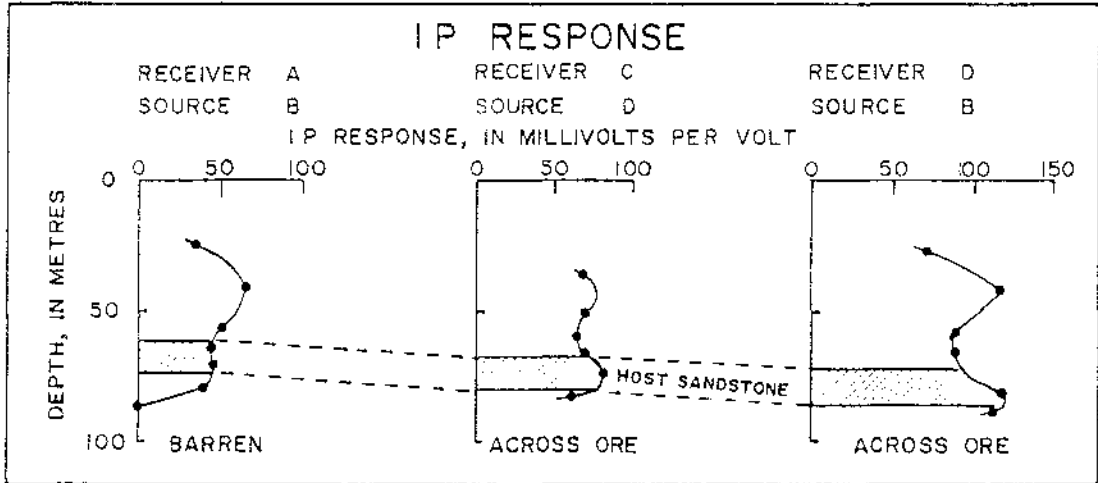
Drill Hole B

the vein mineralization should affect the measured resistivity of the rock. In contrast, the sulfide mineralization in drill hole B is predominantly disseminated in the rock. Intuitively, the phase is most and resistivity is least affected by disseminated minerals. However, Glenn and Nelson note that other correlations had been observed, and these results could not be generalized. The results are unquestionably dependent on lithology, texture, mineralization and porosity of the rocks. Insufficient studies have been made to assess the importance of these factors.

Scott et al. (1975) made resistivity/IP measurements in a south Texas uranium roll-front ore deposit. Both single hole and between-hole measurements were made. Figure 5-6 shows the conventional single hole well logging data obtained in four holes. A time domain system was used. Daniels et al. (1977) made a comparison of core analyses with the IP data and demonstrated a clear correlation between both clay and pyrite content and IP response. Daniels et al. conclude that logging in uranium exploration can delineate ore zones and help minimize drilling costs.

Scott et al. (1975) illustrate the use of hole-to-hole measurements in a uranium roll front deposit in south Texas. The example is taken from the same publication as the single hole example given above. The measurement is made with a time domain system where the transmitter included one surface and one downhole electrode, and the receiver was a pair of downhole electrodes. The electrode configuration is shown in Figure 5-4f and the results in Figure 5-7. Scott et al. correlate an increase in IP across the roll-front ore zone (hole pairs C and D, and D and B) in contrast to IP measurements off the roll front (hole pair A and B). This result is consistent with the single hole data shown in Figure 5-6. The hole-to-hole



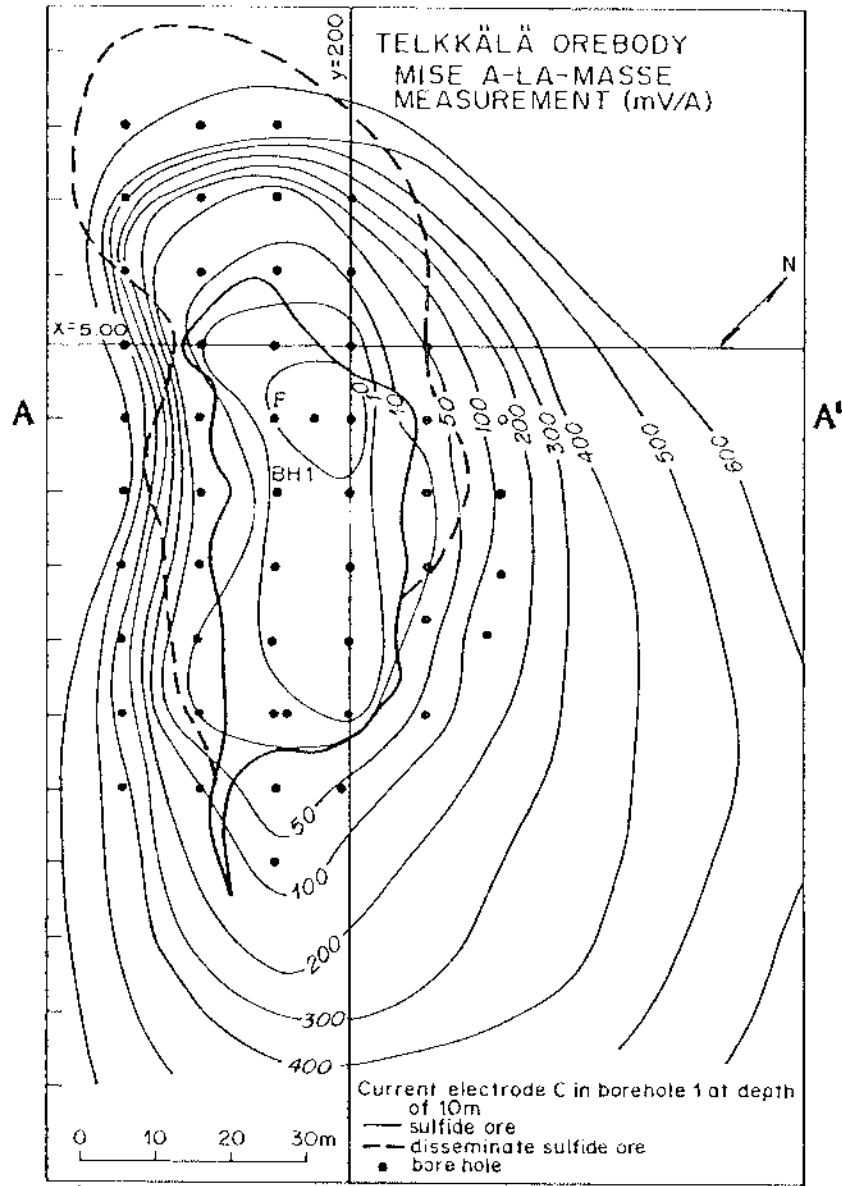


data not only identified the ore zone but revealed a changing resistivity structure between the holes.

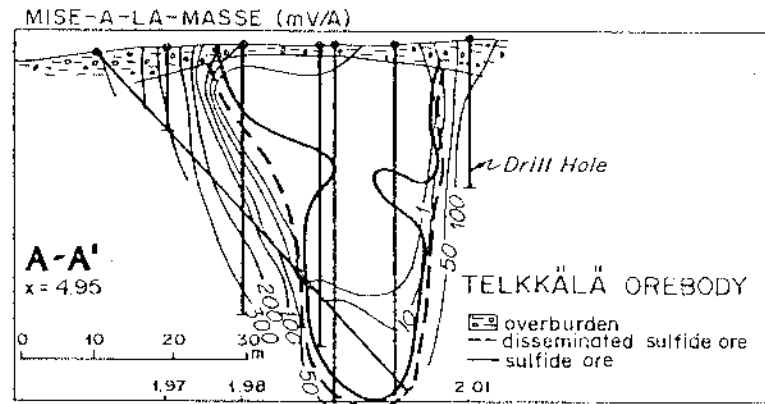
When a current electrode is placed in a borehole in a conducting body, and potential measurements are made with an electrode pair either on the surface or in other boreholes, it is a special case of both a three array hole-to-hole or hole-to-surface technique and of the mise-a-la-masse method (Telford et al., 1976, p. 658). Numerous examples of this technique have appeared in the literature (e.g., McMurray and Hoagland, 1956; Parasnis, 1967 and Ketola, 1972).

Ketola (1972) examines several electrode systems and presents a number of case histories. Figure 5-4f depicts the measurement system employed by Ketola. Figure 5-8 shows examples of data obtained with this system at a small nickel ore deposit at Teikkala, Finland. The data in Figure 5-8a were obtained with current electrode C 10 m deep in bore hole BH1, current electrode D situated .5 km to the west of the deposit, and the fixed potential electrode F situated as shown in the figure. Measurements were made by moving the second potential electrode E. Ketola noted that the 10 mv/A contour delineates the limit of sulfide ore fairly accurately. Figures 5-8b and 5-8c show a vertical section through $x = 4.95$ (refer to Figure 5-8a for location of section) and data obtained in five drill holes. The contours of the mise-a-la-masse potential pattern, Figure 5-8b, reflect the shape of the deposit, and the potential increases rapidly outside the limits of the deposit. The resistivity data in Figure 5-8c suggest the ore body is in three separate lenses.

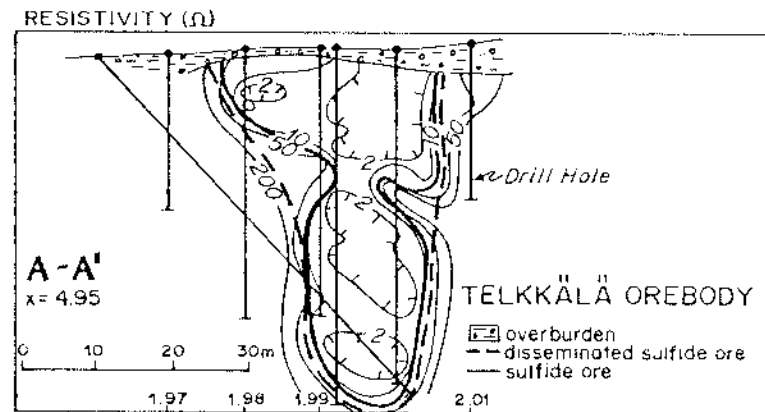
Further examples of the application of borehole resistivity measurements can be found in the literature. Schillinger (1964) and Bacon



a)



b)

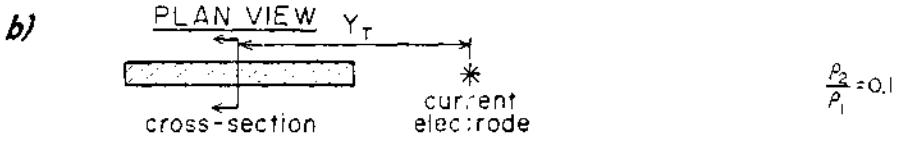
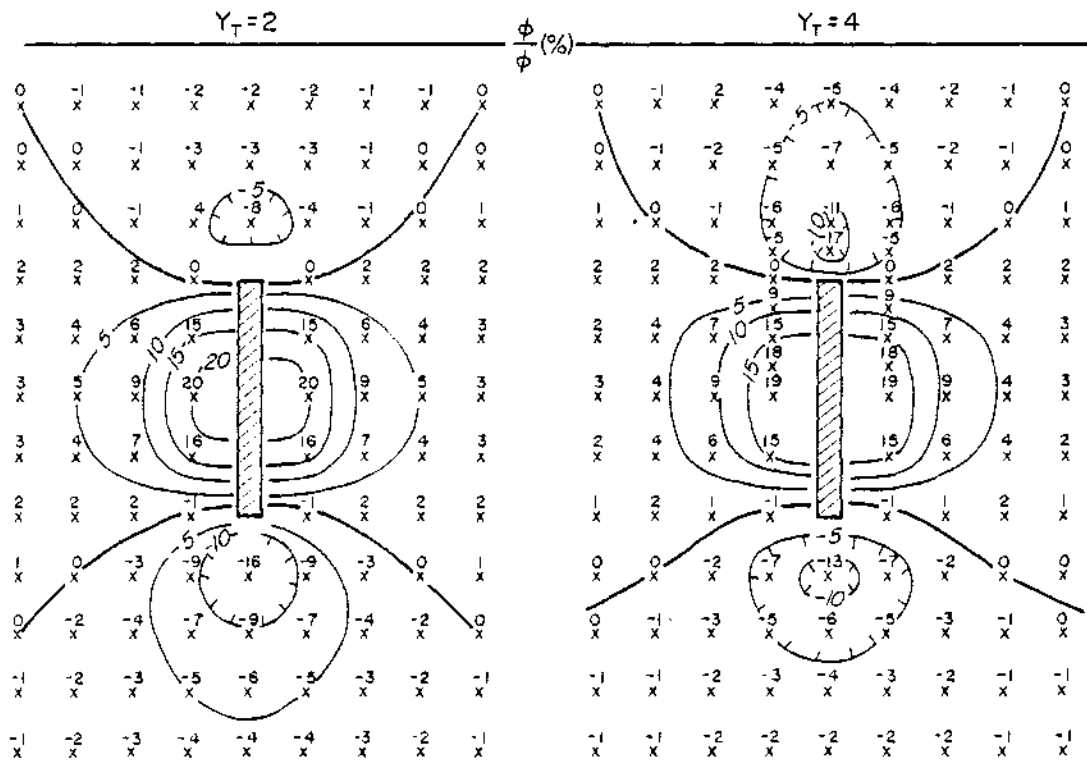
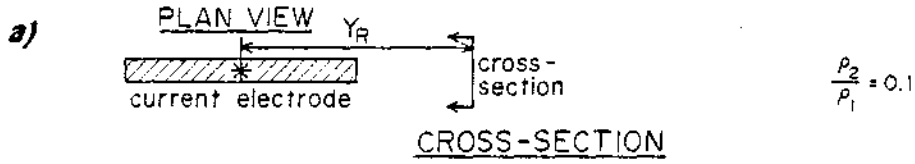
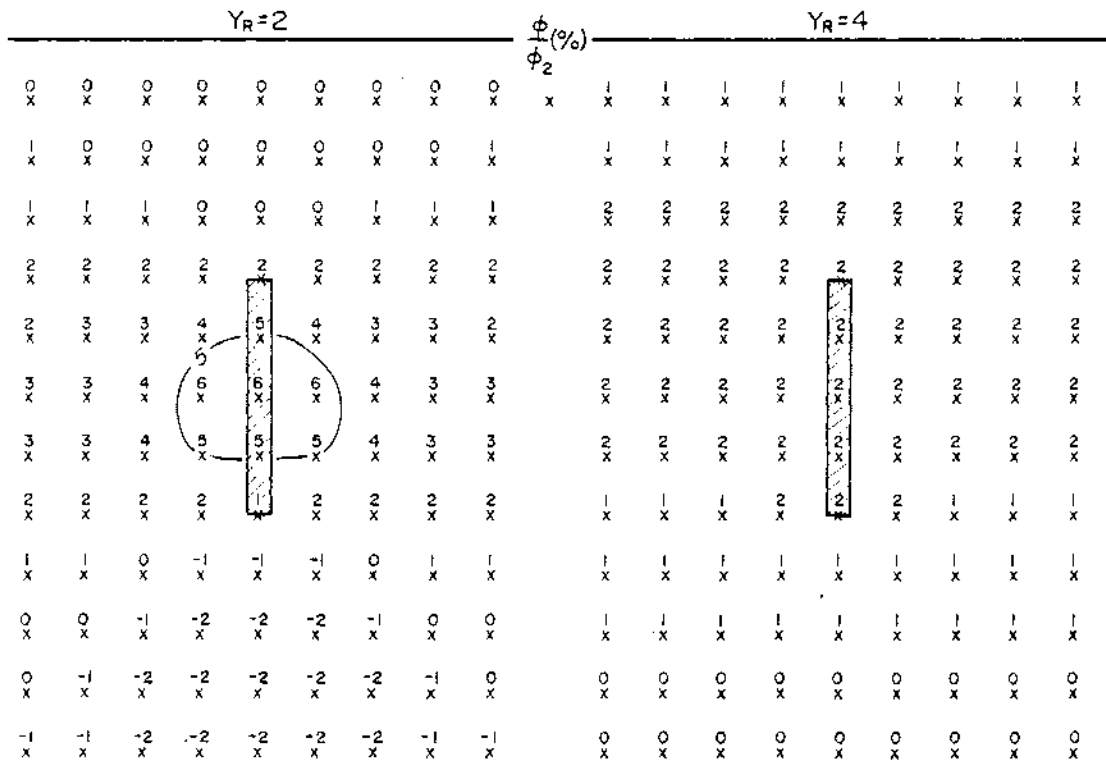


c)

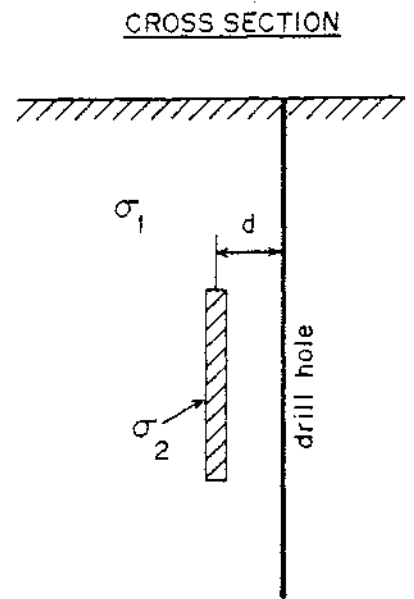
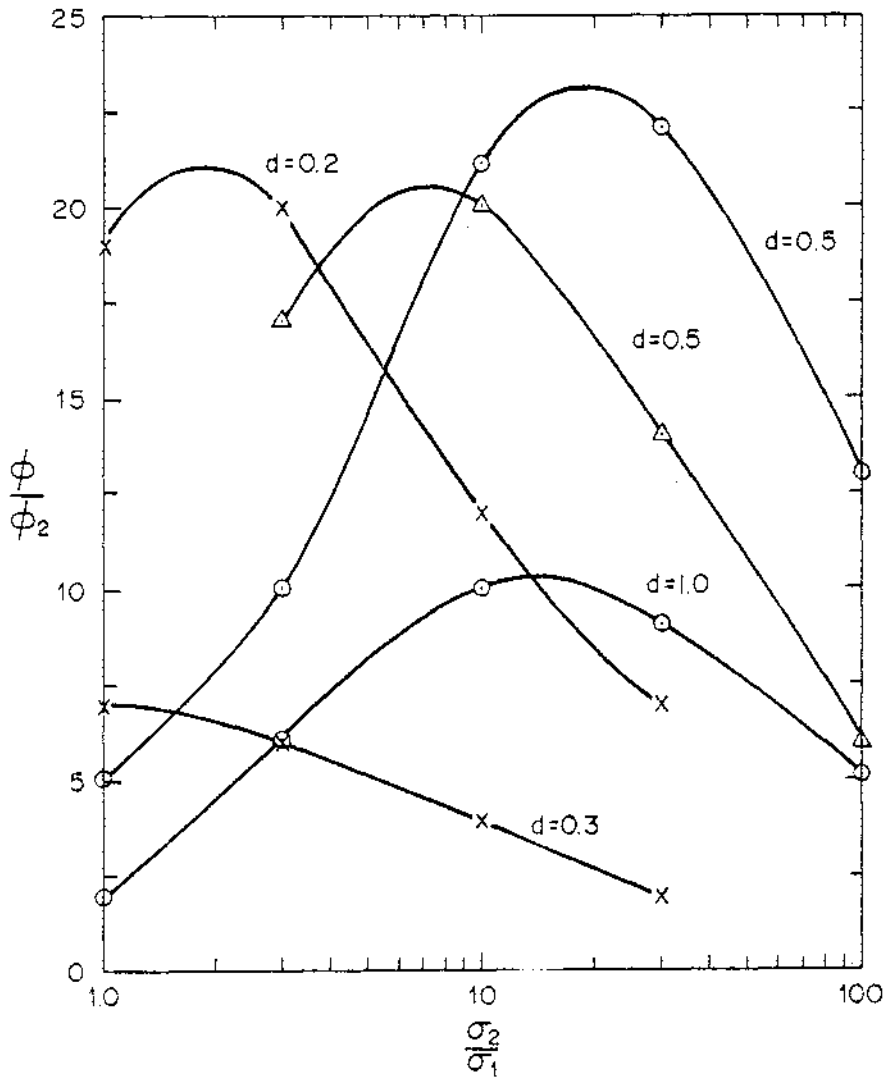
(1965) employed the method in native copper exploration in Michigan. Mithisrud and Sumner (1967) describe borehole resistivity/IP results from the Black Hills mining district of South Dakota. Measurements were made in the frequency domain (0.3 and 2.5 Hz). The current electrodes were placed at opposite ends of a drift while the potential electrodes were placed in drill holes various distances from the transmitter. Wagg and Seigel (1963) describe the measurement of IP in hole-to-surface applications.

As noted in an earlier section, in recent years more sophisticated algorithms have evolved for interpreting surface electrical survey data over complex geologic structures. The integral equation solution described by Hohmann (1975) has been used to model borehole resistivity/IP systems. The results for a pole transmitter on the surface, with the second current electrode at a large distance, and a downhole two electrode receiver are shown in Figure 5-9. The receiver is assumed sufficiently small and is approximated by a dipole. Data are the phase of the electric field, given as a percent of the intrinsic response of the anomalous body. Figure 5-9a shows a cross-section of data points situated one dipole length apart down each of nine drill holes. The drill holes also are spaced one dipole apart so that the data points are equi-spaced in the cross-section which is located four dipole lengths from the center of the body. The near current electrode is situated at the surface directly over the center of the body. The configuration does not detect the body. By contrast, Figure 5-9b shows a large downhole anomaly when the near current electrode is at the surface four dipole units along strike from the center of the body and the section is through the center of the body. Figure 5-10 summarizes the responses of the three most important arrays as a function of resistivity contrast. The

CROSS-SECTION



- △ downhole transmitter - surface receiver
- surface transmitter - downhole receiver
- x downhole three array



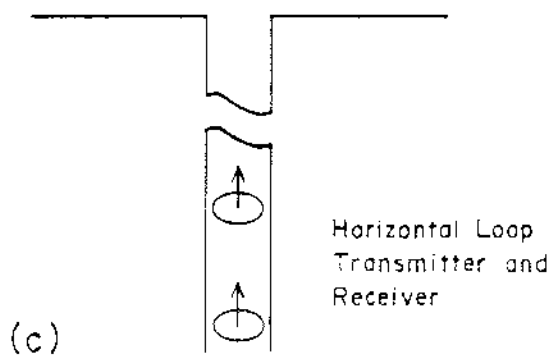
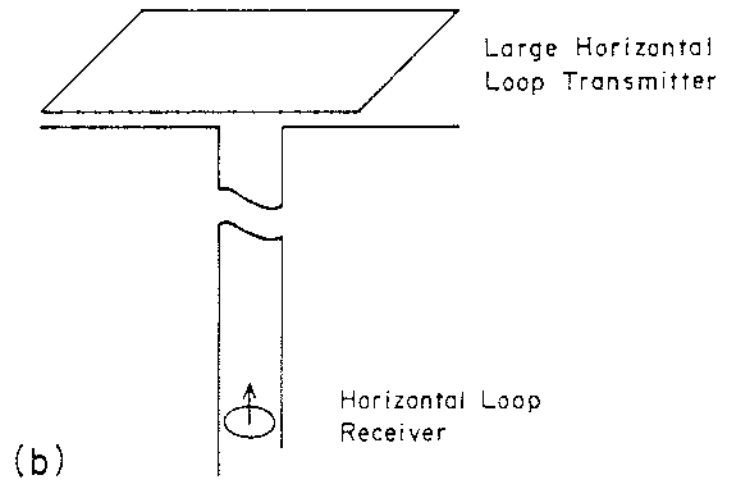
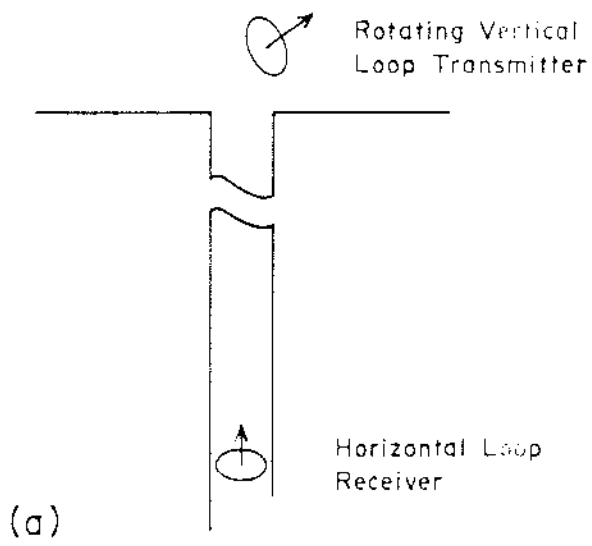
results indicate that the surface transmitter-downhole receiver is the best configuration in terms of peak IP anomalies, provided the resistivity contrast between ore and host rock is at least 10. Snyder and Merkel (1973) and Merkel and Alexander (1971) present results for buried electrodes and a spherical conductor buried in a whole space. Daniels (1978) gives a solution and shows results for buried electrodes in a layered earth.

Oristaglio (1978) has studied inversion of layered and two-dimensional structures using surface and borehole data and has determined that borehole measurements are very important to resolution of the parameters of the conducting body.

Recent work has indicated a potential use of non-linear electrical impedance variations for mineral identifications in boreholes (Klein and Shuey, 1978).

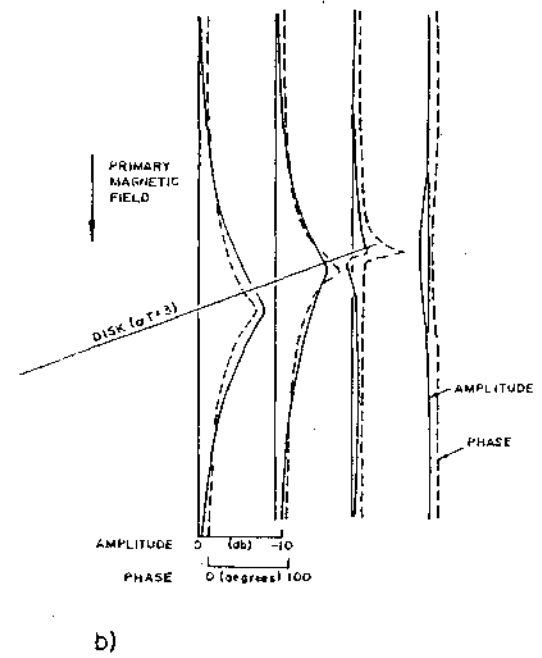
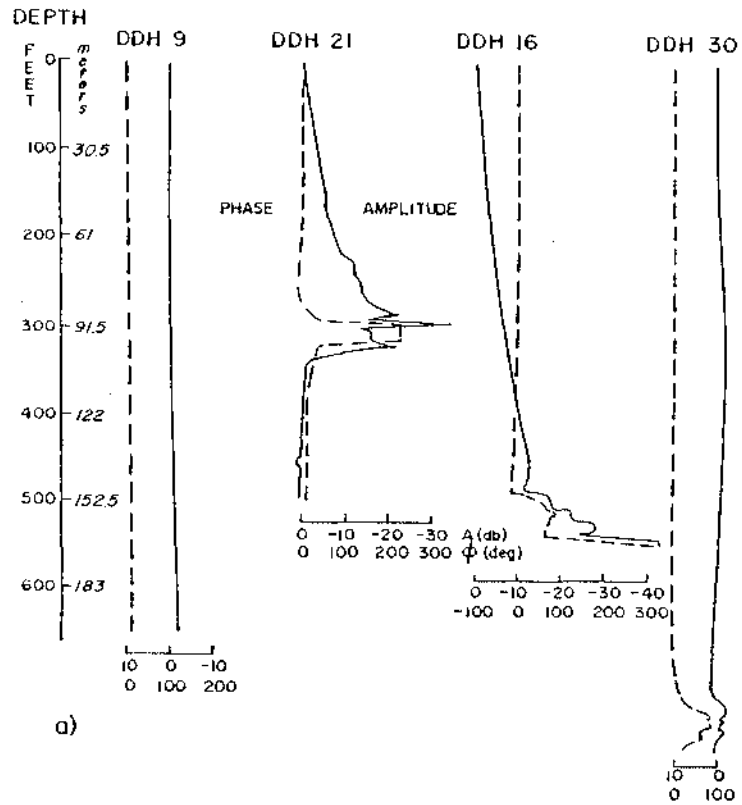
Electromagnetic logging

A second type of borehole electrical measurements is one which utilizes current loops, induction logging. Again the measurements may be made with frequency or time domain systems. Often the systems are only slightly modified versions of surface instrumentation. The applications are typically in single hole, hole-to-hole and hole-to-surface studies as depicted in Figure 5-11. Typically only coils are placed downhole with little or no electronics package. Highly sophisticated induction logging, Figure 5-11c, is popular in the oil and gas industry, but this technology is seldom used by the mining industry. However, model curves have been developed for various dipping conductors adjacent to a borehole (Drinkow



and Duffin, 1978). This area of logging is one pioneered and advanced almost entirely by the minerals industry, and field studies have been reported as early as 1954 (Ward and Harvey, 1954). In recent years advances have been made in applications of radar frequencies in boreholes (Lytle et al., 1979). The technique has not been used in a mineral deposit environment for location of minerals because of the low resistivity. Borehole EM systems typically are operated over the frequency range of 10 to 5000 Hz, although measurements are commonly made at only a few frequencies. Time domain instruments are designed to operate over an equivalent spectrum. The higher the frequency, the greater the signal attenuation and the smaller the range of investigation, particularly in conductive environments. Two examples of borehole EM systems will be discussed.

The first example is from Hohmann et al. (1978). The system used was a Kennecott Copper Corporation vector electromagnetic system (VEM) that measures magnetic field amplitude and phase at four frequencies: 26, 77, 232 and 695 Hz. The system is used in either surface or borehole applications. A borehole example is shown in Figure 5-12. The VEM data were obtained in four boreholes at Kennecott's Arctic massive sulfide deposit in Alaska. A four mile square transmitter loop was placed on the ground around the deposit, and a receiver coil was placed in the boreholes (refer to Figure 5-11b). Measurements were made at 695 Hz. The results of Figure 5-12a are compared to theoretical data for a conducting disk in a uniform field in Figure 5-12b. The comparison is quite good despite the heterogeneity of the deposit and the differences in the excitation fields. Note that drill hole 9, which did not intersect the sulfide body, does not

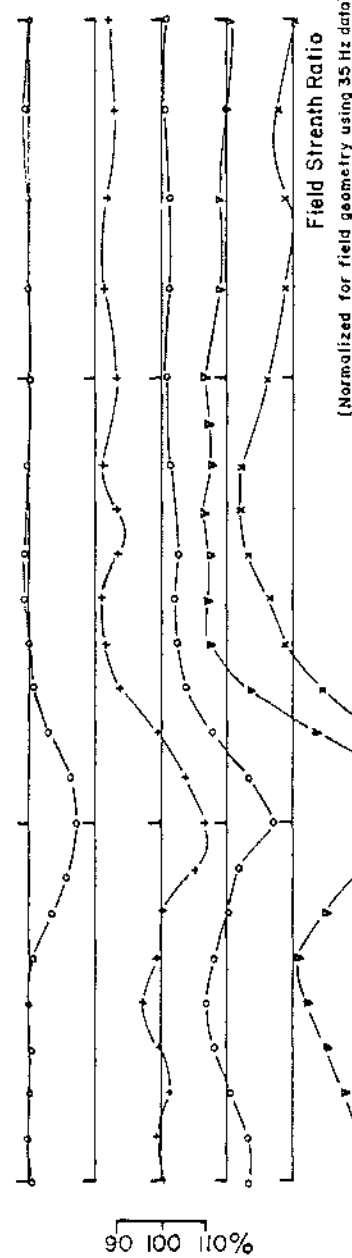
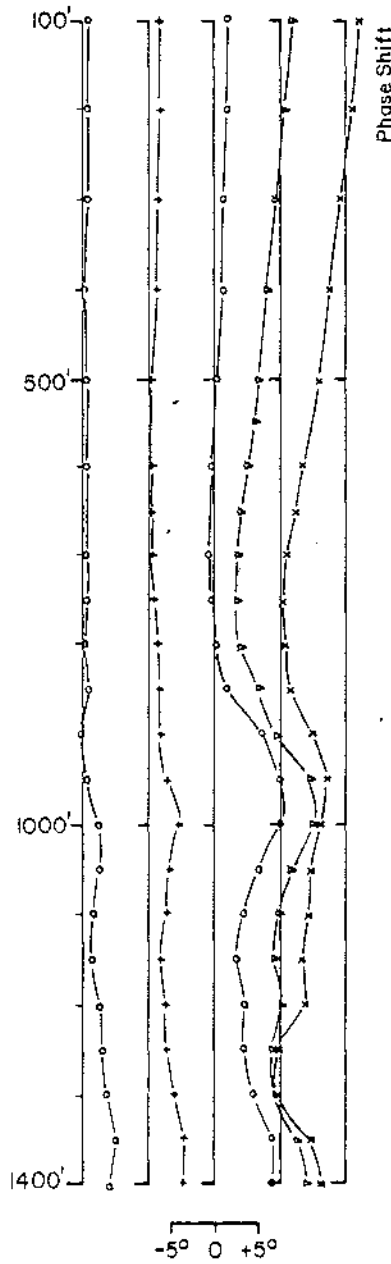


PHASE SHIFT

FIELD STRENGTH RATIO

35 Hz 105 Hz 315 Hz 945 Hz 2835 Hz

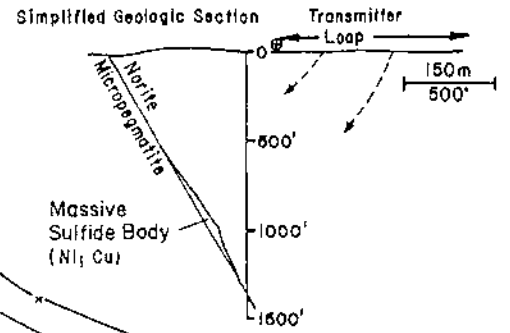
35 Hz 105 Hz 315 Hz 945 Hz 2835 Hz



(Normalized for field geometry using 35 Hz data)

Multi-Frequency
Electromagnetic
Drill Hole Log
SE-77/DHEM-5

30m
100'



show any response. The drill hole survey was done to determine whether the surface electrical anomaly was produced by sulfides and/or graphite which were both known to be present. The borehole results clearly correlated with sulfide mineralization.

A second example of a hole-to-surface frequency domain system is shown in Figure 5-13 (Scintrex, 1978). This system can use a number of frequencies and measures phase between the transmitted and received fields and the ratio of the amplitude of the received field to the amplitude of a reference field coil placed near the transmitter. The system may be used to 1500 meters depth, depending on the host rock conductivity, and over a frequency range of 35 to 5000 Hz. The example in Figure 5-13 illustrates that a conductor missed by the drill hole is detected by both the phase and the amplitude EM measurements.

In Figure 5-14, eight samples of the transient EM secondary field are measured after the primary pulse is turned off such that an equivalent frequency range of 2000 to 16 Hz is covered. Model curves for this Crone PEM system have been developed by Woods (1975). The borehole anomaly is greater than would be expected from the two minor sulfide intercepts in the drill hole. One would suspect a wider zone of sulfides near the borehole. The dual negative peaks in the data, shifted above the sulfide intercepts, are interpreted to mean the borehole lies below the main sulfide body. On the basis of this borehole and two others Crone calculated a product of conductivity times thickness for the sulfide body of 10 to 18 mhos, well within the expected range for massive sulfides.

Radioactivity Logging

Introduction

Radioactivity logging techniques have been used for many years by the oil and gas, coal, uranium, groundwater and non-metallic minerals industries. Only in recent years have these methods been employed by the base minerals industry (Czubek, 1977; Glenn and Nelson, 1977). A summary of the various methods is given in Table 2.

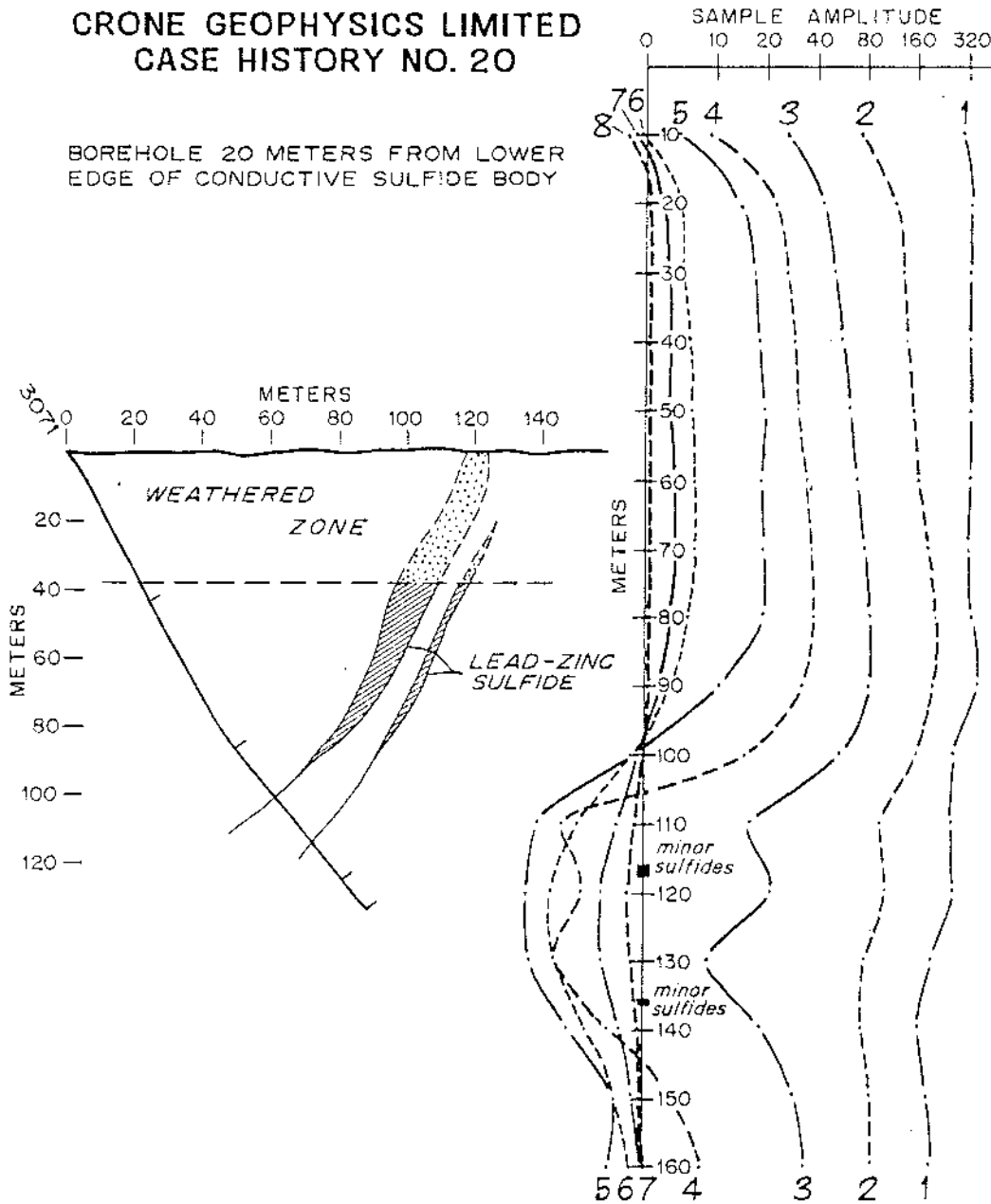
There are two basic types of radioactive well logs: active and passive. In passive methods one measures the natural radioactivity of the rocks. Natural radioactivity and a typical spectrum (Figure 4-2) have been discussed earlier. Tools may measure total count above some threshold gamma ray energy, counts in several selected energy windows and counts in one thousand to 4000 or more channels. In active methods, a source of radiation, natural or induced, is placed in the logging tool, and various kinds of scattered radiation may be observed. Many tools may be used for qualitative or quantitative examination of rock formations behind casing. Czubek (1971, 1977) discusses the many nuclear borehole techniques both by theoretical developments and by examples.

Passive radioactive methods

The only, passive radioactivity logging method is gamma-ray logging, where the gamma-rays from the radioactive decay of elements in rocks are measured. As noted earlier, the major causes of natural radioactivity in rocks are the radioactive isotope of potassium (^{40}K) and the various daughters in the decay chain of isotopes of uranium and thorium. The most common gamma-ray logging tools measure total counts, and the data are for

**CRONE GEOPHYSICS LIMITED
CASE HISTORY NO. 20**

BOREHOLE 20 METERS FROM LOWER
EDGE OF CONDUCTIVE SULFIDE BODY



CRONE BOREHOLE P.E.M. SURVEY
 FLYING DOCTOR PROSPECT, NORTH BROKEN HILL AREA
 AUSTRALIA
 SECTION 2525W, BOREHOLE 3071

Table 5-2: Radioactivity logging methods in base minerals exploration.

Radiation or Particle Source	Logging Technique			
	Radiation of Particle Detected	General Name	Applications	Limitations
Radioactive decay of radioactive isotopes in nature.	Gamma-ray (commonly detected with NaI(Tl) scintillometers)	<ol style="list-style-type: none"> 1. Natural Gamma 2. Spectral Gamma 	<ol style="list-style-type: none"> 1. Lithologic identification 2. Correlation 3. Facies changes 4. Thickness formation 5. U, Th, & K assay 	<ol style="list-style-type: none"> 1. Calibration 2. Corrections for casing, cement, borehole fluid, dead time, hole size 3. For assay work logging speeds may be slow 4. Statistical
Gamma-ray emitter (commonly Cs-137 which emits a .662 MeV gamma-ray)	Scattered gamma-rays (detected with NaI(Tl) scintillometers)	<ol style="list-style-type: none"> 1. Gamma-gamma density 2. Gamma-gamma selective 	<ol style="list-style-type: none"> 1. Bulk density of rock 2. Porosity of rock 3. Heavy mineral content of rock 4. Lithologic identification 5. Assay 	<ol style="list-style-type: none"> 1. Very sensitive to borehole size variation, mud cake 2. Very limited use through casing 3. Low depth of identification 4. Statistical 5. Calibration
Neutron emitter 1. Several isotopic sources - (e.g. of AmBe)	<ol style="list-style-type: none"> 1. *Scattered neutrons <ol style="list-style-type: none"> a) Thermal b) Epithermal 2. *Capture gammas <p>*Both measurements can be total count or spectral</p>	<ol style="list-style-type: none"> 1. Neutron or neutron porosity 2. Neutron activation 	<ol style="list-style-type: none"> 1. Total hydrogen information, porosity, boundwater 2. Lithologic identification 3. Alteration mineralogy 1. Borehole Assay 	<ol style="list-style-type: none"> 1. Epithermal measurement less sensitive to large capture cross section minerals than thermal neutron or gamma tools so may be better for porosity in some cases but poorer for lithology in some cases. 2. Calibration 3. Borehole effects 4. For assay work method is slow, source is always "turned on," calibration and interpretation difficult
2. Pulsed neutron generator Deuteron nuclei hitting Tritium target produces 14 MeV neutrons	<ol style="list-style-type: none"> 1. Time decay of scattered neutrons 2. Spectral gamma or neutron 	<ol style="list-style-type: none"> 1. Neutron lifetime, thermal decay time 2. Neutron activation 	<ol style="list-style-type: none"> 1. Mineralogy 2. Lithologic identification 1. Borehole Assay 	Same limitations as above

lithologic identification and qualitative assay of uranium.

Undoubtedly, the greatest application of the gamma-ray log by the mining industry is in uranium exploration. Obviously, in addition to uranium daughters the total counts will reflect the presence of ^{40}K and thorium daughters, and the uranium series may be in disequilibrium. Hence the total counts measurement is commonly recorded either in equivalent uranium concentration or counts/sec, but it is only a qualitative indicator of possible uranium occurrence. Interpretation of total count logs has been developed by Scott et al. (1961), Scott (1963), Conaway and Killeen (1976), Fink (1978), and others. Four-channel spectral logging, comprising measurements in gamma-ray energy windows for each of thorium, uranium and potassium and of total counts, has been developed in recent years (Killeen et al., 1978; Evans et al., 1979; Stromwold and Kosanke, 1979). This technique would minimize the effect of thorium and potassium contributions in the gamma-ray counts attributed to uranium.

Many logging companies today compute real-time eU_3O_8 directly. This calculation may include corrections for dead time, borehole size and fluid, formation moisture content, and casing (Scott et al., 1961; Dodd and Eschliman, 1970; Wilson et al., 1979; Conaway and Killeen, 1980).

According to Scott et al. (1961) and Fink (1978) the area, A , under the total count curve (Figure 5-15) is directly related to ore grade G and bed thickness, T ,

$$GT = KA$$

5-1

where K is an empirically determined constant for the tool obtained in zones of known uranium concentration. Bed thickness is typically interpreted from the half amplitude points, although this is not

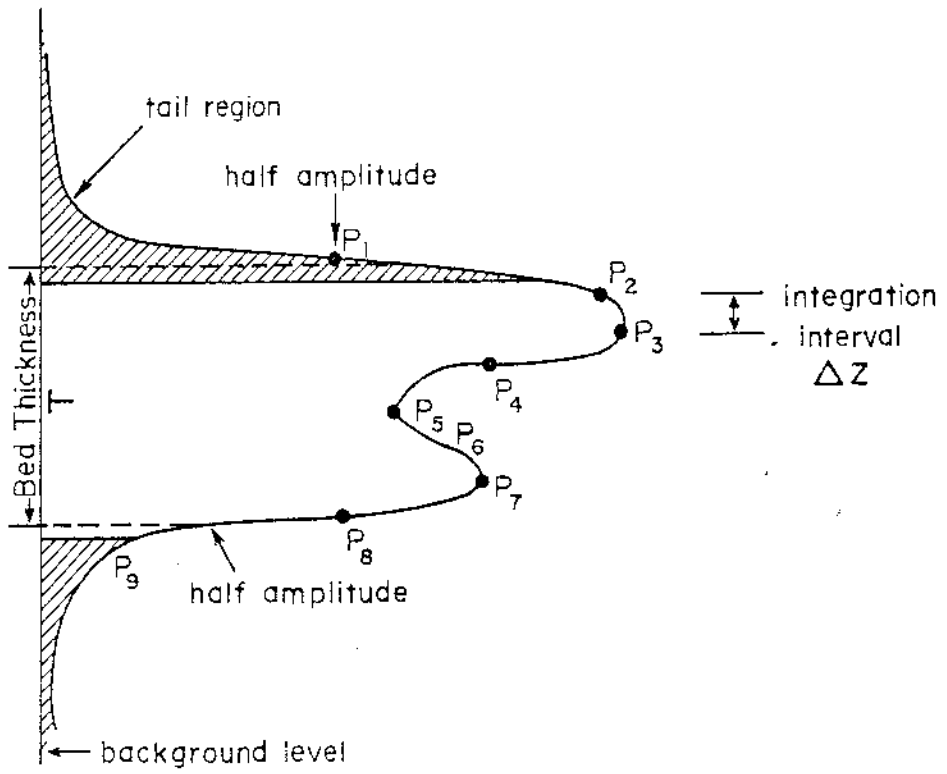
particularly accurate in thin beds (Conaway and Killeen, 1980). As noted by Fink (1978) 5-1 is commonly solved as

$$GT = wKa \quad 5-2$$

where K is determined for a particular thickness, say one-half foot, and A is in counts rather than counts-thickness (counts-feet). The K -factor in either case is quite different, and in the latter case w is needed because K was defined for a particular thickness. Calculating the area in counts-thickness would eliminate any need for w and any chance of error due to use of a w different from the one used to compute K . The area may be computed as depicted in Figure 5-15 where integration of area under the curve is completed only between points P_2 and P_3 and end corrections made to compensate for the tail regions shown hatched in Figure 5-15.

Alternatively the entire area could be computed. Computer programs are available to compute 5-1 whereby a curve such as shown in Figure 5-15 is assumed to be composed of a number curves due to several small beds (Scott, 1963; Conaway and Killeen, 1980).

One may note from Table 4-2 that protactinium-234 is a short half-life daughter of ^{238}U early in the decay chain. A measure of its characteristic spectral peak of gamma-ray emission should provide a more accurate estimate of uranium concentration in disequilibrium situations than would the customary measurement of ^{214}Bi . A tool which employs this technique has been described by Goldman and Marr (1979). The probe contains an intrinsic germanium detector, cooled to liquid nitrogen temperatures using frozen propane in a canister, and a 4000-channel analyzer. The logging speed, measurements and data processing are all automated and computer controlled. The logging speed is controlled to optimize counting statistics and grade



accuracy.

Active radioactive methods

Two basic types of active radioactive logging techniques are used; one uses a source of gamma-rays, commonly Cobalt-60 (1.17 and 1.33 MeV γ -rays) or Cesium 137 (.662 MeV γ -ray) (Czubek, 1977); the other uses neutrons either from radioactive emitters or neutron generators.

Gamma-ray density logging: The principles of gamma-ray attenuation in material have been discussed previously. The attenuation and absorption of gamma-rays by low atomic number elements is not too different between .1 and .10 MeV which is dominated by Compton scattering. Below this range photoelectric attenuation becomes important and above this range, pair production becomes more important with increasing energy. For elements with Z greater than about 20 the dominant Compton region shrinks; for example, for lead this region lies between 1 and 3 MeV (Price, 1964, Figures 1-13, 1-14, and 1-15, p. 24-25). Gamma-ray *density* tools are designed to operate in the Compton region where γ -ray scattering is least sensitive to element variations in the rock. Tittman and Wahl (1965) discuss the basic principles of density logging. Detectors, almost always NaI(Tl) crystals, may be coated with material having a high attenuation coefficient for low gamma-ray energies or a pulse height threshold between .1 and .4 MeV may be established in the counting device. Either way the objective is to eliminate gamma-rays detected in the region where photoelectric absorption becomes important. Pair production is unimportant for ^{137}Cs since its gamma-ray energy is .622 MeV.

Sherman and Locke (1975) showed that for a 35% porosity sand, 90% of the scattered gamma-rays came from $\rho_{gr}=42 \text{ gm/cm}^2$. For a bulk density, ρ_b ,

of 2.60 gm/cm³, the depth of investigation (90% of scattered gamma-rays), r , is 16 cm (6.4 inches). The density tool is very sensitive to borehole size and to minimize this problem the gamma ray source is placed to one side of the tool with all but this side enclosed by a lead shield. The unshielded side of the tool is held firmly against the side of the hole by one or two arms on the other side of the tool. However, mudcake and hole rugosity can still be serious with this design. A two detector system (Wahl et al., 1964) has been developed and routinely used since its introduction. The dual detector system is expected to eliminate mudcake effects and minimize borehole rugosity effects. Small scale, heavy mineral variations may generate inappropriate correction with these systems. A simultaneously recorded caliper can be used to correct the log further. A caliper log should be recorded in any logging suite, particularly if a density log is recorded.

The gamma-ray intensity I at the detector can be expressed in terms of source intensity I_0 , the formation mass attenuation coefficient μ_m and distance r and bulk density ρ_b

$$I = I_0 e^{-\mu_m \rho_b r} \quad 5-3$$

or

$$\log I - \log I_0 = -\mu_m \rho_b r \quad 5-4$$

For constant I_0 and $\mu_m r$ the log of detector counts should show a linear relationship to bulk density. This relationship is quite good for most rocks.

The bulk density can be expressed in terms of the fractions of the densities of the components in the rock:

$$\rho_b = V_1\rho_{m1} + V_2\rho_{m2} + \dots + V_m\rho_{mn} \quad 5-5$$

where V_i and ρ_{mi} are the volume fractions and densities of the mineral fraction i . In cases where the various minerals have fairly similar densities, and relative amounts vary slightly one may write

$$\rho_b = \rho_f + (1-\phi)\rho_{ma} \quad 5-6$$

where ϕ is porosity, ρ_{ma} is average matrix mineral density and ρ_f is the fluid density. If the matrix mineral density can be divided into a base metal density (e.g., for pyrite and chalcopyrite ρ is about 4 gm/cm³) and non-metallic mineral density (e.g., 2.62 gm/cm³ for an acidic igneous rock) the bulk density expression may be written

$$\rho_b = \phi\rho_f + (1-\phi-x)\rho_{ma} + x\rho_s \quad 5-7$$

where x is volume fraction of base metal minerals with density ρ_s . In many igneous and metamorphic rocks the porosity ϕ is very low and fairly constant. Hence, ρ_b variations can reflect base metal mineral concentrations (Glenn and Nelson, 1977).

Gamma ray assaying: Gamma-ray scattering properties of rock formations can be used for mineral assaying. Most techniques are in the experimental stage (IRT Corporation, 1976), and much of the literature is in Russian (Czubek, 1965, 1971, and 1977).

One technique that has been tried successfully is the selective gamma technique (Czubek, 1965). A measure of scattered gamma-rays in the density region (Compton scattering region) and in the lower energy region is made. A ratio of the two counts can be qualitatively or quantitatively related to

Z or Z- equivalent of the rock. A recent publication by Charbucinski et al. (1977) describes a logging tool and technique and the successful application to assay of iron in blast holes. Charbucinski et al. were able to assay iron to .8% at the 95% confidence level. They concluded that their system could assay 10 blast holes per shift, and costs compared favorably with those of analytical laboratories. However, their applications were to highly mineralized rocks. Application of this method to lower grade ore bodies such as porphyry copper deposits may be less successful.

Most other gamma ray or related techniques such as XRF are still primarily in the research stage, and space does not permit discussion of these methods. Table 5-2 lists the various gamma ray or related techniques. Brief descriptions of each one can be found in IRT Corporation (1976), and many of the applications, with a comprehensive reference list, can be found in Scott and Tibbetts (1974) and Czubek (1977).

Principles of neutron logging

Description of various neutron logging tools and techniques can be found in Little (1961), Youmans et al. (1964), Wahl et al. (1964), Tittman et al. (1966), Senftle et al. (1971), Allen et al. (1972, Hoyer and Locke (1972), Nargolwalla (1973), Allen et al. (1974), Eisler et al. (1977), Kosanke (1978) Randall et al. (1978), and Wilson and Cosby (1980), among others. Various neutron logging systems and their applications are outlined in Table 5-2. Often, the many papers on neutron logging techniques emphasize a particular process of interaction of neutrons with matter, which is the one being monitored for the particular application, and little mention is made of other processes which are taking place. These other processes, in individual circumstances, can seriously change the measurement being made.

Neutrons interact with the nuclei of elements and those not so interacting will decay to a proton and an electron with a half-life of 15 minutes. These interactions involve a number of competing processes which depend on the neutron energy and on the neutron capture and scattering characteristics of the nuclei present. The probability of a certain type of process, or reaction, occurring is expressed as a microscopic cross section σ measured in barns (10^{-24}cm^2) or as a macroscopic cross section defined in the logging literature by

$$\Sigma = \frac{0.602}{A} \sigma \rho \text{ cm}^{-1} \quad 5-8$$

where σ is the microscopic cross section, ρ is the density, and A is the atomic weight of the element. Note that the unit for Σ is cm^{-1} and Σ is considered to be the total cross section in one cm^3 of material. Also, Σ

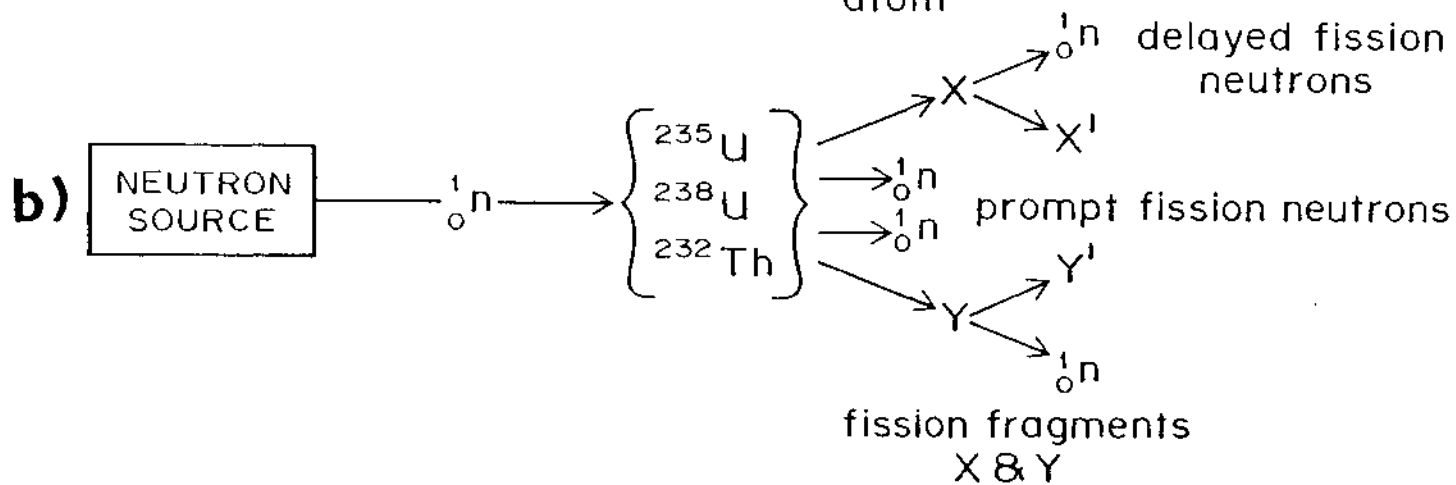
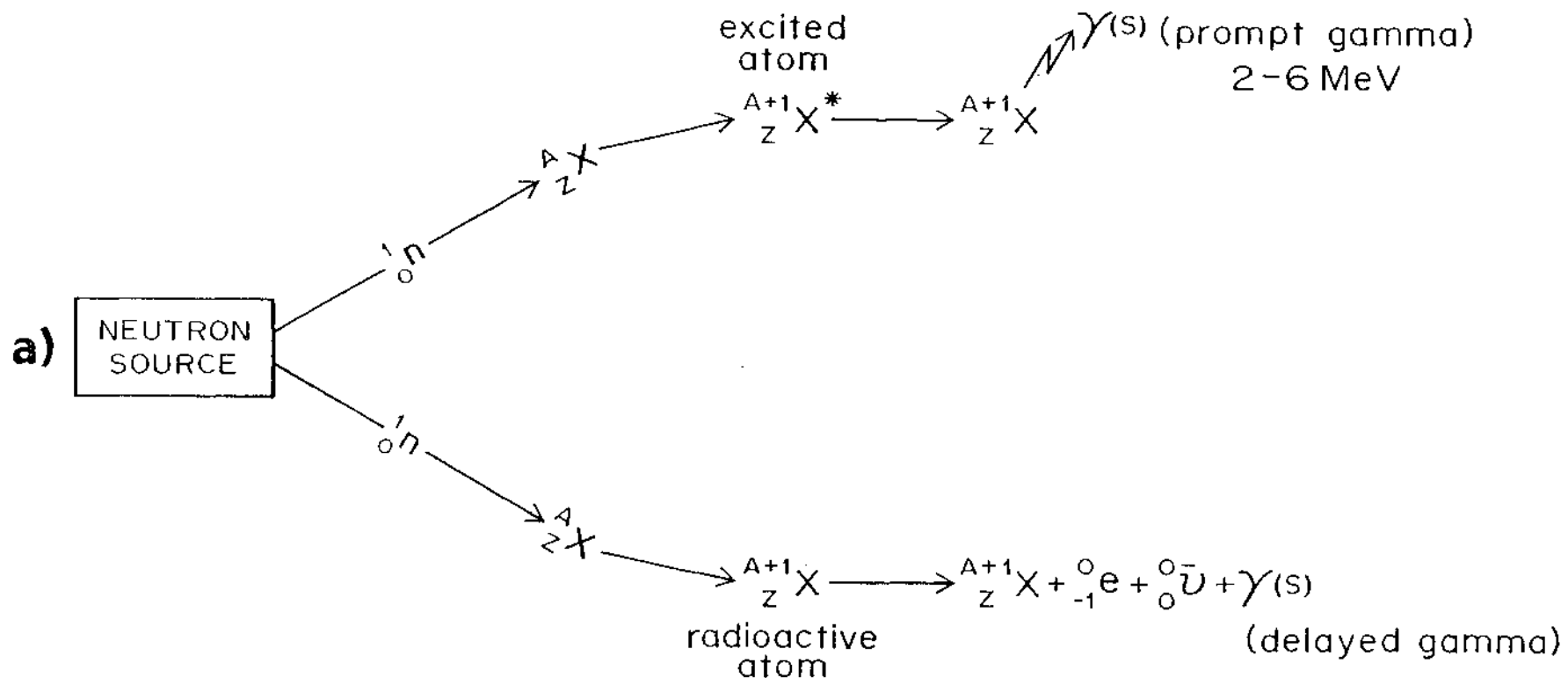
can be interpreted as the probability of absorption per unit path length and its reciprocal as the average distance a neutron will travel before the process occurs. If n is the number of neutrons per cubic centimeter with mean velocity v , then the rate of reaction, R , per cubic centimeter is:

$$R = nv\Sigma = \phi\Sigma \quad 5-9$$

where ϕ is the neutron flux. Since rocks are composed of many minerals which, in turn, are composed of many elements, the Σ for rocks will represent a sum of Σ 's for the many elements present in the rock. Tables of Σ for various minerals can be found in Gearhart - Owen (1978) and Edmundson and Ramier (1979).

De Sote et al. (1972) note that the total scattering cross section is composed of three parts, elastic, inelastic, and all other reactions. Elastic scattering occurs when the potential energy of the system remains unaltered during the collision. The scattering is inelastic if one of the particles is left in an excited state after the collision. The following inelastic processes are possible:

1. The nucleus is excited to a higher energy level from which it returns to ground state by emission of a gamma ray (e.g., Au hit by a 1MeV neutron is excited to a higher energy level and then emits a 260 keV gamma ray).
2. The neutron is captured, and a compound nucleus is formed which is either stable or radioactive. Most neutron capture events are accompanied by emission of a characteristic gamma ray (Figure 5-16a).
3. The neutron is captured, and some other particle is emitted such as a proton, one or more neutrons, and an alpha particle (Figure



5-16a); and

4. The neutron causes spallation, fragmentation, or fission of the target nucleus (Figure 5-16b).

The neutron either loses energy or is captured in any of the above inelastic reactions. Only neutron energy is lost in elastic reactions.

Neutron porosity logging: The neutron tool was developed initially to measure porosity. In porosity applications of neutron logging, one supposes that most of the interactions involve elastic collisions between the neutrons and hydrogen nuclei. This process is most likely elastic since the neutron and hydrogen nucleus have near equal mass. Once the neutrons have been slowed, or moderated, to thermal energies (approximately 0.025ev, electron volts), they are easily captured by any number of elements in the formation. Neutron tools have been designed to measure either the thermal neutron population or the capture gamma-rays. The assumptions made are that the processes are dominated by hydrogen nuclei in the formation, that the hydrogen is entirely in water and that the water is entirely in the pore space. However, in many rocks hydrous minerals are quite abundant and the water of hydration can appear as porosity on a neutron log. Examples of neutron logs in a porphyry copper deposit which Nelson and Glenn (1975) give illustrate this problem.

In many igneous and metamorphic rocks, porosity is commonly very low, and the neutron log responds primarily to the water in hydrous minerals. This result can be used to identify particular lithologies. A second problem is the different moderating or capture properties of the matrix material in the rock (Segesman and Lui, 1971). If the neutron tool is calibrated in a particular lithology, and this lithology is encountered

during logging, then the porosity measurement should be quite good. However, if the lithology is different and has different neutron moderating or capture properties, the log must be corrected to determine the true porosity. This process is routinely used in the oil industry where logs are calibrated in limestone, sandstone and dolomite units. Again, this property is used to identify lithology. Unfortunately, good calibration of commercially available neutron logging tools does not exist for rocks commonly associated with base metal ore deposits. Also, trace elements such as gadolinium have extremely high thermal neutron capture cross sections, and their presence can seriously affect the log response. Other common elements such as chlorine have a significantly greater neutron capture cross section than the majority of rock forming minerals and if present in sufficient quantity will significantly affect the log response.

Tools have been designed to measure neutrons in the epithermal energy range 0.4 to 1.0ev, just above the thermal energy. The belief is that the epithermal neutrons reflect the moderating influence of hydrogen in the formation and are less sensitive to neutron capture properties of the formation.

The neutron log may need to be corrected further for borehole size, borehole fluid salinity, temperature and mud cake. In every case, the empirical relationship between neutron counts, ND, and porosity, ϕ , is

$$ND = C + D \log \phi \qquad 5-10$$

where C and D are constants.

Neutron assaying: Probably the most important application of neutron

logging to minerals exploration is borehole assaying. Although recognition of this use of neutron logging appeared in the literature some years ago, it has been only recently that a number of commercial systems, in each case designed for only a few select elements, have been available in North America (Seigel and Nargolwalla, 1975; Wilson and Cosby, 1980). The United States Bureau of Mines is currently field testing a multi-element borehole assaying tool (Schneider, 1979).

Before discussing the various neutron assaying tools it is necessary to outline briefly the different neutron sources and detectors used. Sources of neutrons are of two types: (1) isotopic and (2) generator. Isotopic sources commonly used in neutron logging are listed in Table 5-3. The ^{252}Cf source is used in borehole assaying while the other sources listed are used in porosity logging. Also, 14MeV neutron generators are used in neutron tools that have been developed for direct assay of uranium in boreholes (Wilson and Cosby, 1980). These tools and techniques are listed in Table 5-4. Wilson and Cosby describe each tool in detail, the measurement techniques used and calibration problems. The tools measure either the prompt or delayed fission neutrons as shown in Figure 5-16b. The Century Geophysics 14 MeV/DFN and IRT Corp. ^{252}Cf /DHAA tools measure these neutrons once they are thermalized, while Sandia's 14MeV/DFN measures the epithermal neutrons. Kerr McGee Corporation has reported on successful development of a ^{252}Cf delayed fission neutron tool (California - 252 Progress, 1972). In nearly all neutron logging tools, a ^3He gas-filled proportional counter is used to detect the neutrons. A coating of Cadmium or Boron on the outside of these detectors effectively absorbs thermal neutrons such that the detector becomes an epithermal neutron detector.

Table 5-3

List of commonly used neutron sources in well logging.
Alpha particles and, in most cases, numerous gamma-rays accompany
the emission of neutrons.

Neutron Source	Symbol	Half Life	Neutrons per Curie (per sec)	Neutron (Avg)	Energy MeV (Max)
Polonium-beryllium	$^{210}\text{Po-Be}$	138 days	2.5×10^6	4.2	10.87
Californium	^{252}Cf	2.65 years	4.4×10^9	2.3	6
Americium-beryllium	$^{241}\text{Am-Be}$	458.1 years	2.2×10^6	4.0	11
Radium-beryllium	$^{226}\text{R-Be}$	1,620 years	1.5×10^7	3.9	13.08
Plutonium-beryllium	$^{239}\text{Pu-Be}$	24,000 years	2.2×10^6	4.5	10.74
or	$^{238}\text{Pu-Be}$	86.4 years	2.5×10^6	NA	NA

Table 5-4

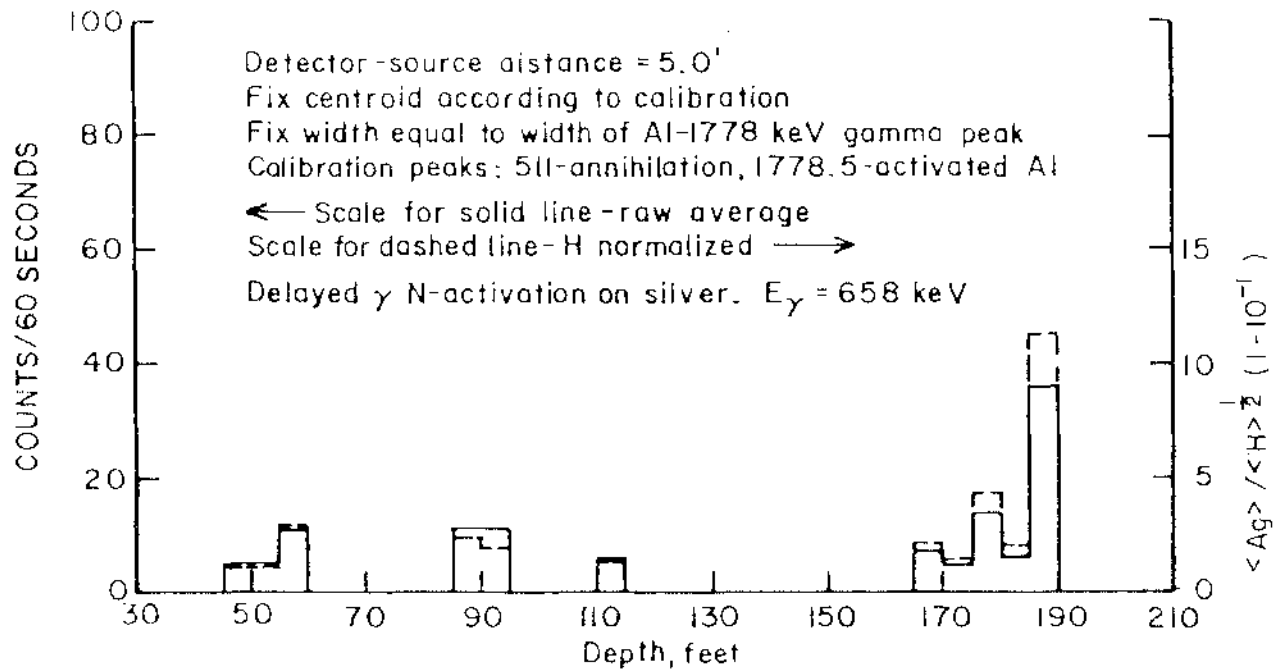
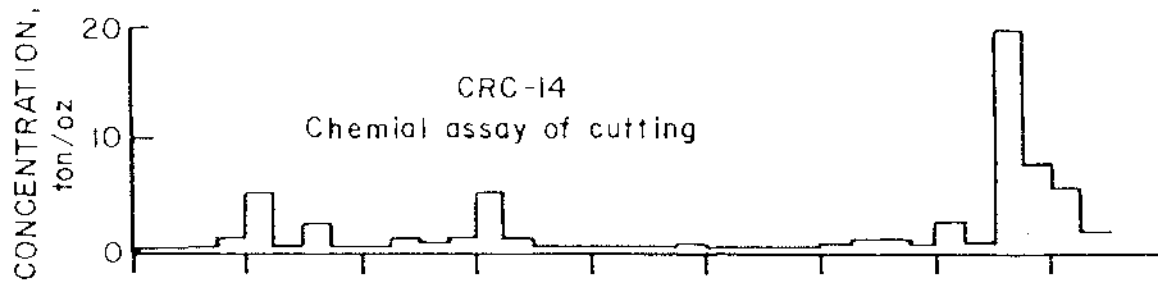
Commercially available tools and techniques used in neutron analysis of uranium deposits

<u>Source</u>	<u>Detector</u>	<u>Method</u>
1. 14 Mev	Cd - ^3He	Epithermal neutron detector - prompt fission neutrons, from ^{235}U by time gating (Sandia).
2. 14 Mev	^3He	Delayed fission neutron (DFN Mobil Oil Corporation licensed to Century Geophysical Corporation).
3. ^{252}Cf	2- ^3He detectors	Source jerk method (IRT DNAA, delayed fission neutrons).

The tool developed by Princeton Gamma Tech for the United States Bureau of Mines is currently being field tested in copper, iron, gold and silver deposits, and this tool also uses a ^{252}Cf source. The detector is a 4000 channel gamma-ray spectrometer. Figure 5-17 shows some data obtained using the Bureau of Mines system in an area mineralized with silver and located near Creed, Colorado (Schneider, 1979). The accuracy, calibration, sensitivity and logging techniques have yet to be fully resolved (Wilson and Cosby, 1980) but are being investigated. These problems should be resolved in the near future. The basis for the method is neutron activation (Figure 5-16a) and is described in the literature by Senftle et al., 1971a, b; Eisler et al., 1971a, b; Hoyer and Locke, 1972; Nargolwalla, 1973; Senftle et al., 1977 and Eisler et al., 1977.

The tool and techniques described by Nargolwalla (1973) and by Seigel and Nargolwalla (1975) are dedicated to Cu and Ni assay. Cu can be determined at .5% level \pm .075%, and Ni can be determined at 1.0% level \pm .05%. The detector used in this tool is a NaI (Tl) crystal. Hence, this tool, like the Bureau of Mines tool, is designed to measure the capture gamma-rays, and as used, the prompt gamma-rays are measured. High resolution spectral analysis is essential for accurate assays using either tool.

The task of neutron assaying is not easy, and some techniques used are described by Caldwell et al. (1963), Jain et al. (1978), Zikovsky and Schweikert (1978), Kruse (1978), Heydorn (1978), Nullens and Van Espen (1978), Gunnick (1978), Myklebust and Fiori (1978) and Parr et al. (1978), among others.



Acoustic Logging

The logging of acoustic velocity in boreholes is routine in several fields but is seldom applied to base minerals exploration (Glenn and Nelson, 1977). The measurement of formation velocity is accomplished by measurement of time difference in arrival at two or more receivers, separated one to two m apart, of a signal from one or two transmitters several m distant mounted in a single tool (Summers and Broding, 1952; Tixier et al., 1958; Kokesh et al., 1965). The recorded measurement is interval transit time, Δt . Compressional wave velocity is simply the reciprocal of Δt .

Wyllie et al. (1956, 1958) determined an empirical relationship between porosity and travel time

$$\phi = \frac{\Delta t - \Delta t_m}{\Delta t - \Delta t_f} \quad 5-11$$

where ϕ is porosity, Δt is the measured travel time, Δt_m is the rock matrix travel time and Δt_f is the fluid travel time. Pickett (1960) has demonstrated that this expression can be generalized to $\Delta t = \Delta t_m + B\phi$, where B is a constant. The sonic log can be used, in conjunction with the density log, to generate synthetic seismograms which are used to interpret surface seismic reflection data (Durschner, 1958; Dennison, 1960; and Lindseth, 1979).

The sonic log correlation to RQD has been demonstrated by Myung and Helander (1973) and Nelson and Glenn (1977). If the full wave form of the received velocity signal is recorded (Myung and Helander, 1972), the log

can be used to locate fractures. The best acoustic tool for fracture identification is the seisviewer, or televiwer, which is described by Zameneck et al. (1970) and Myung and Baltosser (1972). The tool can be used to locate fractures and to determine both strike and dip of the fractures. An example of its use in a porphyry copper deposit has been given by Glenn and Nelson (1977) and in a variety of igneous and metamorphic rocks by Keys (1979).

Gravity Logging

Borehole gravity measurements have been suggested and investigated for thirty years (Smith, 1950; Hammer, 1950; McCulloh, 1965; Howell et al., 1966; Rasmussen, 1975; among others). Only in the last decade has sufficient progress been made in the design of sensitive, small diameter and rugged gravity meters to allow routine, useful borehole measurements to be made (Jageler, 1976). These tools have been designed by and for the petroleum industry although their potential use by the minerals industry has been suggested (Dyck et al., 1975; Telford et al., 1976). Current instruments have sensitivities approaching 0.002 mgal and operating specifications of 250°F (121°C) and 10,000 psi (689 bars) pressure, more than adequate for minerals applications. The only serious limitation for minerals use is the tool size, 4 3/8 inches (11 cm) in diameter.

In petroleum applications, borehole measurements are commonly expressed in terms of density, ρ , where

$$\rho = 3.687 - 128.56 \Delta G / \Delta Z$$

5-12

and ΔG is gravity difference in mgals and the station separation ΔZ is in

meters.

Snyder (1976) suggests that an alternative approach is to utilize the borehole Bouguer Gravity anomaly, G_B . The borehole Bouguer anomaly can be computed as (Snyder, 1976):

$$G_B = G_{OB} - G_T - (Z_0 - Z)FA + B \quad 5-13$$

where

G_B = Bouguer anomaly

G_{OB} = Observed borehole gravity

G_T = Theoretical gravity at mean sea level (Heiskanen and Meinesz, 1958)

FA = Free air gradient

Z = Depth of gravity measurement in borehole

B = Bouguer contribution (41.90ρ $\mu\text{gal}/\text{m}$)

ρ = bulk density

$$\text{and } \Delta\rho = -.12856\Delta G_B/\Delta Z \quad 5-14$$

where $\Delta\rho$ is the anomalous density.

Snyder notes that in the absence of any anomalous density difference near the borehole, the Bouguer and Free Air corrections, previously discussed in the gravity section, can explain the change in gravity with depth. Here we assume instrument drift, terrain and tide corrections either are made or can be neglected. The borehole anomalies can be interpreted by the same methods used in surface gravity interpretations. Snyder has published type curves or solutions for a sphere, a cylinder, a horizontal slab of anomalous density near the borehole and for dipping beds. Successful application of the method to location of gas deposits missed by the borehole have been reported by Jones (1972), Bradley (1975),

Rasmussen (1975) and Jageler (1976).

The many successful applications of the borehole gravity tool were for situations that had very small, e.g., $.1 \text{ gm/cm}^3$, density contrasts. In minerals applications, one would expect very good results since density contrasts should be much greater.

Magnetic Logging

Two types of borehole magnetic logging are utilized by the minerals industry: (1) the measurement of three components of the magnetic field (Levanto, 1959; Lantto, 1973) and (2) the measurement of magnetic susceptibility (Broding et al., 1952; Zablocki, 1966; Anderson, 1968; Hood, 1970; Snyder, 1973; Glenn and Nelson, 1977). The various instruments and techniques that are used have been reviewed by Hood and Dyck (1975). The logical and principal application of borehole magnetic methods is to investigation of iron ore deposits (Stadukkin, 1963; Zablocki, 1966, 1974)

The three component borehole magnetic field measurement has great promise as indicated by theoretical studies made by Silva and Hohmann (1979) and by earlier work of Levanto (1959) and Lantto (1973). However, very little reported application of the method has appeared in the literature. This absence of use can be attributed to the tool's greater electronic sophistication than those usually employed by the minerals industry. Minerals industry holes are typically small diameter, three inches or less, and are difficult to keep open. Loss of expensive tools becomes a serious consideration. Packaging high technology in small diameter tools is quite difficult.

A second, popular application is the measurement of magnetic

susceptibility for lithologic identification (Glenn and Nelson, 1977). Glenn and Nelson document the use of borehole magnetic susceptibility measurements for the differentiation of acidic and basic igneous rock units in a porphyry copper deposit. The lithologic identification, often in rotary drilled holes, aided structural interpretations. Hafen et al. (1976) describe the application of magnetic susceptibility measurements to the identification of uranium ore zones in the Grant's district of New Mexico. Magnetite conversion to hematite in ore zones resulted in reduced magnetic susceptibility in the ore zones.

Borehole magnetic data interpretation is accomplished using the same techniques of surface surveys which have been discussed earlier. Therefore, there is no need to repeat them here.

Cross Plots

The successful application and interpretation of well logs by the petroleum industry has resulted from a judicious use of a combination of logs. As indicated in previous sections, many logging tools respond to more than one formation property. Since each tool may respond to a different set of properties or the same set but in a different manner, a plot of one type of data versus another type can often reveal which properties are dominant and the various properties may be determined (Savre, 1963; Burke et al., 1969; Poupon et al., 1970; and Pickett, 1973). Cross plots of well log data from igneous and metamorphic rock environments can be found in Snyder (1973), Ritch (1975), Glenn and Hulen (1979), Keys (1979), Sanyal et al. (1979), and Keller et al. (1979). Ritch (1975) and Glenn and Hulen (1979) demonstrate the use of cross plots to separate

matrix and porosity effects in either igneous or metamorphic rocks.

The Outlook for Borehole Assaying

In previous sections, where each logging method was discussed, the application of each method to borehole assaying was outlined. Since application of logging to borehole assaying is important to exploration by the minerals industry, a summary of the various methods is presented here in Table 5-5. Figure 5-18 (Schneider, 1979) lists the various elements in the Periodic Table Format and the various radioactivity logging methods and their sensitivity for assaying of the various elements are also indicated in the figure. As noted in earlier sections, only a few of the techniques have been developed to a stage where commercial tools are available. However, research in these areas is substantial, and further progress can be expected.

Application of magnetic, gravity and resistivity methods in the borehole for quantitative or qualitative estimate of mineralization has been demonstrated and should experience greater use in the future.

Borehole assaying has many advantages. Drilling rocks could be substantially lowered since core drilling would not be required. Logging tools sample a greater volume of rock and would minimize assay errors in ore bodies having highly variable mineralization. The data would be available quite soon after drilling is completed, often with the drill rig still over the hole. Repeat runs are easily made to improve measurement statistics. Assays on core are commonly done on two to three composite samples, whereas borehole assays would be a continuous measurement limited only by source receiver separations, typically less

Table 5-5: Techniques for borehole assaying.

A.	Nuclear	
	I. Active	
	*1.	Neutron Activation Analysis NAAA
	2.	Gamma Activation Analysis AA
	*3.	Gamma-gamma Selective -selective
	4.	Photoneutron H
	5.	Mossbauer Effect Spectroscopy ME
	6.	X-ray Fluorescence XRF
	7.	X-ray Diffraction XRD
	8.	Photoluminescence PL
	9.	Raman Scattering RAMAN
	10.	Infrared Spectroscopy IR
	11.	Nuclear Magnetic Resonance NMR
	12.	Nuclear Quadrupole Resonance NQR
	13.	Electron Spin Resonance ESR
	*14.	Gamma-gamma Density D

Principal materials of interest today: Metallic minerals - Uranium, Copper, Nickel, Gold, Iron, Aluminum, Tungsten, Chromium, Non-metallic minerals - sulfur, potash, flourspar, fuels - coal, oil shale, oil and gas.

	II. Passive	
	1.	Gamma NG

B.	Electrical	
	I. Active	
	1.	Induced Polarization IP

	II. Passive	
	None	

C.	Gravity	
	I. Density, excess mass, ore tonnage	

D.	Magnetics	
	I. Magnetite/magnetic susceptibility.	

IN SITU ASSAY METHODS

															He				
α Li _{λ}	γ Be _{ι}													α γ B _{λ}		κ γ N _{ι}	δ ϵ O _{ι}	κ ϵ F _{ι}	β Ne _{ι}
κ γ Na _{β}	β Mg _{κ}													γ β Al _{λ}	γ Si _{ι}		γ S _{η}	α γ Cl _{ι}	β Ar _{ι}
γ β ζ K _{κ}	δ γ Ca _{ι}	β Sc	κ γ Ti _{ι}	λ β V _{β}	κ γ Cr _{η}	α γ β Mn _{θ}	δ γ Fe _{ι}	α β Co	γ Ni _{η}	δ γ β κ Cu _{θ}	κ γ Zn _{ι}	β Ga	β Ge _{η}	β As _{γ}	γ β Se _{κ}	β Br _{κ}	β Kr		
β Rb	β Sr _{η}	β Y _{η}	κ β Zr _{ι}	κ Nb _{η}	κ β Mo _{η}	Tc	β Ru _{η}	β Rh	β Pd	α κ β Ag _{η}	γ β Cd _{η}	κ β In	δ β Sn _{η}	λ β Sb _{θ}	β Te _{η}	β I	β Xe		
β Cs	γ β Ba _{θ}	α β La	β Hf _{β}	κ Ta _{η}	β κ W _{θ}	α β Re	β Os	β Ir	β Pt _{η}	γ β κ Au _{η}	γ α β θ Hg _{κ}	β Tl _{η}	κ γ θ Pb _{λ}	β Bi _{η}	Po	At	ζ Rn		
Fr	β ζ Ra	ζ Ac																	

Ce	Pr	Nd	Pm	Sm	Eu	Gd	Tb	Dy	Ho	Er	Tm	Yb	Lu
β ζ Th _{η}	β ζ Pa	α β ζ U _{θ}	Np	Pu	Am	Cm	Bk	Cf	Es	Fm	Md	No	Lw

ESTIMATED MINIMUM SENSITIVITY

- < 1%
- > 1%
- > 100ppm
- > 1 ppm

METHODS

- α Neutron-fission neutron
- β Thermal neutron activation, decay gamma ray spectroscopy
- γ Thermal neutron activation, prompt capture gamma ray spectrometry
- δ Fast neutron, inelastic scattering
- ϵ Fast neutron activation
- ζ Natural radioactive decay
- η X-ray fluorescence
- θ Selective gamma ray spectrometry
- ι Photon-activation
- κ High energy gamma and charged particle activation
- λ Electro Magnetic Resonance

than one meter. Borehole assaying can be done in holes where core recovery is bad and in holes in old prospects where core has been lost or is unavailable. Now that the technology for borehole assaying and the application of other logging tools are routinely available and highly useful, the mineral industry should begin to use borehole logging more effectively. As the use of logging increases, the methods of interpreting log data in minerals exploration will be improved.

Figure Captions

- 5-1 Examples of caliper and temperature logs that illustrate both the nature of the logs and their correlation to geologic features, lithology and fractures.
- 5-2 Temperature injection profiles in mineralized igneous rocks.
- 5-3 Schematic illustration of an SP cell and an SP log.
- 5-4 Schematic of various popular single hole, hole-to-hole and hole-to-surface electrode configurations used in resistivity/IP logging. As noted, several names may be given to a particular electrode configuration. The electrode array in e is an example of a focused system.
- 5-5 Examples of IP resistivity and phase measured in two holes in a porphyry copper deposit in the southwestern United States. The measurements were made with 1 meter normal array (Figure 4b) and at a frequency of 14 Hz (after Glenn and Nelson, 1977).
- 5-6 IP measurements in a Roll-Front uranium deposit in southeast Texas. Measurements were made with a time domain system (after Scott et al., 1975).
- 5-7 Hole-to-hole IP and resistivity measurements across a known roll-front uranium deposit in south Texas. The source electrodes were located at the surface and downhole at 45 m depth. The receiver dipole was 15.24 m in length. The configuration is outlined in Figure 4f (after Scott et al., 1975).
- 5-8 Mise-a-la-masse measurements about the Telkkala nickel ore body in Finland: (a) measurements on the surface, (b) measurements made in several boreholes with mise-a-la-masse, and (c) measurements made in several boreholes with resistivity (after Ketola, 1972).
- 5-9 Computed phase of the electric field as a percent of the intrinsic response of the anomalous body for two different electrode positions (Figure 4f), and for the cases of the current electrode over the body and off the end of the body. Drill holes are along a line perpendicular to the strike of the anomalous body.
- 5-10 A comparison of the effect of conductivity contrast for three electrode configurations and several drill hole offsets from the anomalous body.
- 5-11 Hole-to-surface and single hole electromagnetic logging systems.
- 5-12 Example (a) of a hole-to-surface frequency domain survey in a

massive sulfide deposit, Arctic, Alaska and (b) of a comparison to a theoretical response of a thin conductor in a uniform field (after Hohmann et al., 1978).

- 5-13 Example of a multi-frequency drill hole survey, Scintrex Limited SE 77/DHEM-5.
- 5-14 Example of a time domain hole-to-surface measurement in the Flying Doctor Prospect, North Broken Hill Area, Australia, (Crone Case Study 20, Crone Geophysics, Ltd., 1978).
- 5-15 Illustration of graphical uranium ore grade determination from a total count natural gamma log (after Scott et al., 1961).
- 5-16 Illustrations of several neutron interactions with matter: (a) neutron capture and emission of a prompt and a delayed characteristic gamma-ray and (b) neutron capture and subsequent fission of uranium and thorium.
- 5-17 Data obtained with United States Bureau of Mines borehole neutron activation tool in a silver mineralized area near Creed, Colorado (Schneider, 1979).
- 5-18 Periodic Table of the elements and an indication of the various methods that could possibly be used in borehole assay methods and the sensitivity of the method (Schneider, 1979).

List of Tables

- 5-1 Logging tools, property measured and application in mining.
- 5-2 Radioactivity logging methods in base metal minerals exploration.
- 5-3 List of commonly used neutron sources in well logging. Alpha particles and, in most cases, numerous gamma rays accompany the emission of neutrons.
- 5-4 Commercially available tools and techniques used in neutron analysis of uranium deposits.
- 5-5 Techniques for borehole assaying.

References

- Allen, L. S., and Mills, Jr., W. R., 1974, Measurement of the thermal neutron absorption cross section of rock samples by a pulsed source method; SPWLA Fifteenth Annual Logging Symposium, June 2-5, McAllen, Texas, Paper B.
- Allen, L. S., Mills, W. R., Desai, K. P., and Caldwell, R. L., 1972, Some features of dual-spaced neutron porosity logging; SPWLA Thirteenth Annual Logging Symposium, May 7-10, Tulsa, Oklahoma, Paper G.
- Anderson, W. L., 1968, Theory of borehole magnetic susceptibility measurements with coil pairs; *Geophysics*, Vol. 33, (6), p. 962-971.
- Bacon, L. O., 1965, Induced polarization logging in the search for native copper; *Geophysics*, Vol. 30, (2), p. 246-256.
- Baltosser, R. W., and Lawrence, H. W., 1970, Application of well logging techniques in metallic mineral mining; *Geophysics*, Vol. 35, (1), p.143-152.
- Becker, A., and Telford, W. M., 1965, Spontaneous polarization studies; *Geophys. Prosp.* Vol. 13, (2), p. 173-178.
- Bower, E. J., 1968, Resistivity and self-potential logging studies in sulfide zones; unpubl. M. Eng. Thesis, McGill University, Montreal, Canada.
- Bradley, J. W., 1975, The application of the borehole gravimeter to the evaluation and exploration of oil and gas reservoirs; paper presented at SEG 45th Annual Meeting, Denver, Colo.
- Brant, A. A., and the Newmont Exploration Staff, 1966, Examples of induced polarization field results in the time domain; *Min. Geophysics Vol. 1, Soc. Exp. Geophys.*, Tulsa, Oklahoma, p. 289-505.
- Broding, R. A., Zimmerman, C. W., Somers, E. V., Wilhelm, E. S., and Stripling, A. A., 1952, Magnetic Well logging; *Geophysics*, Vol. 17, (1), pp. 1-26.
- Burke, J. A., Schmidt, A. W., and Campbell, Jr., R. L., 1969, The litho-porosity crossplot; *The Log Analyst*, Nov.-Dec.; also in SPWLA Reprint Volume Gamma Ray, Neutron and Density Logging, March, 1978.
- Caldwell, R. L., Baldwin, W. F., Bargainer, J. D., Berry, J. E., Salita, G. N., and Sloan, R. W., 1963, Gamma-ray spectroscopy in well logging; *Geophysics*, Vol. 28, (6), p. 617-632.
- Californium-252 Progress Report, 1972, Kerr-McGee Corporation, (12), July, pp. 31-39.

- Charbucinski, J., Eisler, P. L., Mathew, P. J., and Hylie, A. W., 1977, Use of backscattered gamma radiation for determining grade of iron ores in blast holes and development drill holes; Proc. Austr. Inst. of Min. and Met., (262), p. 29-37.
- Conaway, J. G., and Beck, A. E., 1977, Fine-scale correlation between temperature gradient logs and lithology; Geophysics, Vol. 42, (7), p. 1401-1410.
- Conaway, J. G., and Killeen, P. G., 1978, Quantitative uranium determinations from gamma-ray logs by application of digital time series analyses; Geophysics, Vol. 43, (6), p. 1201-1204.
- Conaway, J. G., and Killeen, P. G., 1980, Gamma-ray spectral logging for uranium; CIM Bull., Vol. 72, (813), p. 115-122.
- Crone, Geophysics Limited, 1978, Crone Geophysics Limited Case History Δ20; Tech. Pub. of Crone Geophysics, Mississauga, Ontario, Canada.
- Czubek, J. A., 1965, Physical possibilities of gamma-gamma logging; in Radioisotopes Inst. in Industry and Geophys. IAEA, Vol. 2, Vienna, p. 249-275.
- _____, 1971, Recent Russian and European developments in nuclear geophysics applied to mineral exploration and mining; The Log Analyst, Vol. 12, (6), p. 20-34.
- _____, 1977, Modern trends in mining geophysics and nuclear well logging methods for mineral exploration -- a review paper; Paper No. 11 at the Mt. Symp. on Geophys. and Geochem. Appl. to the Search for Met. Ores, EXPLORATION 77, Ottawa, Canada, publ. Econ. Geol. Rept. 31, Geol. Surv., Canada, 1979.
- Dakhnov, V. N., 1962, Geophysical Well Logging; Quart. of the Colorado School of Mines, Vol. 57, (2), trans. from Russian by G. V. Keller, p. 445.
- Daniels, J. J., 1978, Interpretation of buried electrode resistivity data using a layered earth model; Geophysics, Vol. 43, (5), p. 988-1001.
- Daniels, J. J., Scott, J. H., Blackman, R. D., and Starkey, H. S., 1977, Borehole geophysical investigations in the South Texas uranium district; Jour. Res. U.S.G.S., Vol. 5, (3), p. 343-357.
- Dennison, A. T., 1960, An introduction to synthetic seismograms; Geophys. Prosp. Vol. 8, (2), p. 231-241.
- De Sote, D., Gijbels, R., and Hoste, J., 1972, Neutron Activation Analysis, Wiley-Interscience, N. Y., p. 836.
- Dodd, P. H., and Eschliman, D. H., 1971, Borehole logging techniques for

- uranium exploration and evaluation; NATO Advanced Study Institute on Methods of Prospecting for Uranium Minerals, London, England.
- Doll, H. G., 1948, The S. P. Log: Theoretical analysis and principles of interpretation; in SPE reprint No. 1, Soc. Petr. Eng. of AIME, p. 45-64.
- Drinkow, R. L., and Duffin, R. H., 1978, Scale models results for inductive logging in the region of single and multiple conductive bodies; Geophysics, Vol. 43, (4), p. 804-818.
- Durschner, H., 1958, Synthetic seismograms from continuous-velocity logs; Geophys. Prosp. Vol. 6, (3), p. 272- .
- Dyck, A. V., 1975, Electrical borehole methods applied to mineral prospecting; in Borehole Geophysics Applied to Metallic Mineral Prospecting: A review, ed. A. V. Dyck, Geol. Surv. Canada, Paper 75-31, p. 13-30.
- Dyck, A. V., Hood, P. J., Hunter, J. A., Killeen, P. G., Overton, A., Jessop, A. M., and Judge, A. S., 1975, Borehole Geophysics Applied to Metallic Mineral Prospecting: A review; Geol. Surv. Canada Paper 75-31, p. 67.
- Edmundson, H. N. and Ramier, L. L., 1979, Radioactive Logging Parameters for common minerals; The Log Analyst, Vol. 20, (5), p. 38-47.
- Eisler, P. L., Huppert, P., and Wylie, A. W., 1971, Logging of copper in simulated boreholes by gamma spectroscopy, I. Activation of copper with fast neutrons; Geoexploration, Vol. 9, (4), p. 181-194.
- Eisler, P. L., Huppert, P., Mathew, P. J., Wylie, A. W., and Yaul, S. F., 1977, Use of neutron capture radiation for determining grade of iron ore in blast holes and exploration holes; in Nuclear Techniques and Mineral Resources, IAEA, Vienna, p. 215-228.
- Evans, H. B., 1970, Status and trends in logging; Geophysics, Vol. 35, (1), p. 93-112.
- Evans, H. B. et al., 1979, A borehole gamma ray spectrometer for uranium exploration; SPWLA twentieth logging symposium, June 3-6, Tulsa, Oklahoma, Paper X.
- Fink, J. B., 1978, On K-factors and gamma log calculations; Geophysics, Vol. 43, (7), p. 1546-1550.
- Gearhart-Owen, 1978, Formation Evaluation Data Handbook; Gearhart-Owen Industries, Inc., Fort Worth, Texas, p. 240.
- Glenn, W. E., and Hulen, J. B., 1979, A study of well logs from Roosevelt Hot Springs KGRA, Utah; SPWLA Twentieth Annual Logging Symposium, June

3-6, Tulsa, Oklahoma, Paper ZZ.

- Glenn, W. E. and Nelson, P. H., 1977, Borehole logging techniques applied to base metal ore deposits; EXPLORATION 77 Symposium, Ottawa, Canada, pub. in Econ. Geol. Rept. 31, p. 273-294, Geol. Surv. Canada, 1979.
- Goguel, J., 1976, Geothermics; McGraw-Hill Book Co., N.Y., p. 200.
- Goldman, L. H. and Marr, H. E., 1979, Application of high resolution gamma ray spectroscopy to well logging, SPWLA Twentieth Annual Logging Symposium, June 3-6, Tulsa, Oklahoma, Paper GG.
- Goudouin, M. Tixier, M. P. and Sinard, G. L., 1957, An experimental study on the influence of the chemical composition of electrolytes on the SP curve; Trans. AIME, Vol. 210, p. 58.
- Gunnick, R., 1978, Computer techniques used in the analysis of gamma-ray spectra; in Radiation Techniques in Industry, Transactions of American Nuclear Society 24th Annual Meeting.
- Guyod, H., 1946a, Temperature well logging, Part 3; The Oil Weekly, Nov. 4, 1946.
- _____, 1946b, Temperature well logging, Part 4; The Oil Weekly, Nov. 11, 1946.
- Hafen, P. L., Adams, S. S., and Secor, G. B., 1976, Application of magnetic susceptibility measurements to uranium exploration in sandstones; in Exploration for Uranium Ore Deposits, IAEA, Vienna, p. 367-378.
- Hallenburg, J. K., 1971, A resume of spontaneous potential measurements; SPWLA Twelfth Annual Logging Symp. Trans., May 2-5, Paper H.
- Hammer, S., 1950, Density determinations by underground gravity measurements; Geophysics, Vol. 15, (4), p. 637-652.
- Heydorn, K., 1978, Quality assurance of computer programs for photopeak integration in activation analysis; in Analytical and Mathematical Methods for Data Analysis, Trans. 24th Ann. Meeting, Nucl. Soc. Amer.
- Hill, H. J. and Anderson, A. E., 1959, Streaming potential phenomena in SP log interpretation; Petr. Trans., (216), p. 203.
- Hohmann, G. W., 1975, Three dimensional induced polarization and electromagnetic modeling; Geophysics, Vol. 40, (2), p. 309-324.
- Hohmann, G. W., Van Voorhis, G. V., and Nelson, P. H., 1978, A vector EM system and its field applications; Geophysics, Vol. 43, (7), p. 1418-1440.
- Hood, P. J., 1970, Magnetic surveying instrumentation; a review of recent

- advances; Proceedings of the Canadian Centennial Conference on Mining and Groundwater Geophysics, Niagara Falls, Oct. 22-27th, 1967; Mining and Groundwater Geophysics 1967, Editor L. W. Morley, Geol. Surv. Can., Econ. Geol. Sur., (26), p. 3-31.
- Hood, P. J., and Dyck, A. V., 1975, Magnetic drillhole measurements in numerical exploration; in Borehole Geophysics Applied to Metallic Mineral Prospecting, A review; Editor A. V. Dyck, Geol. Surv. Canada, Paper 75-31, p. 35-38.
- Howell, L. G., Heintz, K. O., and Barry, A., 1966, The development and use of a high precision downhole gravity meter; Geophysics, Vol. 31, (4), p. 764-772.
- Howell, E. P., Gant, Jr., O. J., and Crebs, T. J., 1978, Slim hole logging and analysis for uranium exploration; SPE of AIME paper 7434, 53rd Annual Fall Tech. Meeting, Houston, Texas.
- Hoyer, W. A., and Locke, G. A., 1972, Logging for copper by in situ neutron activation analysis; SME of AIME Transactions, Vol. 252, p. 409-417.
- IRT Corporation, 1976, Future research in borehole assaying technology, Volume I; prepared for U.S.B.M. Contract J0255018, March 8, 1976, p. 325.
- Jageler, A. H., 1976, Improved hydrocarbon reservoir evaluation through use of borehole-gravimeter data; J.P.T. June, 1976, p. 709-718.
- Jain, M., Close, D. A., and Evans, M. L., 1978, Gamma-spectral calculations for uranium well logging; in Advance in Nuclear Techniques for Uranium Exploration - II: Passive Methods, Transactions of Amer. Nucl. Soc. 24th Annual Meeting.
- Johnson, 1962, A history of well logging; Geophysics, Vol. 27, (4), p. 507-527.
- Jones, B. R., 1972, The use of downhole gravity data in formation evaluations; SPWLA Thirteenth Annual Logging Symposium, May 7-10, Tulsa, Oklahoma, Paper M.
- Keller, G. V., Grose, L. T., Murray, J. C., and Skokan, C. K., 1979, Results of an experimental drill hole at the summit of Kilauea volcano, Hawaii; Jour. Volc. and Geoth. Res., Vol. 5, (314), p. 345-385.
- Ketola, M., 1972, Some points of view concerning mise-a-la-masse measurements; Geoexploration, Vol. 10, p. 1-21.
- Keys, W. S., 1979, Borehole geophysics in igneous and metamorphic rocks; The Log Analyst, Vol. 20, (4), p. 14-28.

- Keys, W. S., and MacCary, L. M., 1971, Application of borehole geophysics to water-resources investigations; Techniques of Water-Resources Investigations of the U.S.G.S., Capter E2, Book 2, p. 126.
- Killeen, P. G., Conaway, J. G., and Bristow, Q., 1978, A gamma-ray spectral logging system including digital playback with recommendations for a new generation system; G.S.C. Paper 78-1A, Current Research, Part A., p. 235-241.
- Klein, J. D., and Shuey, R. T., 1978, Nonlinear impedance of mineral-electrolyte interfaces, Part I: Pyrite; and Part II: Galena, chacopyrite, and graphite; Geophysics, Vol. 43, (6), p. 1222-1249.
- Kakesh, F. P., Schwartz, R. J., Wall, W. B., and Morris, R. L., 1965, A new approach to sonic logging and other acoustic measurements; J.P.T., March, 1965, p. 282-286, and in SPWLA Reprint Volume, Acoustic Logging, March 1978, Paper G.
- Kosanke, K., 1978, Survey of uranium exploration and assessment technology; in Advances in Nuclear Techniques for Uranium Exploration -- I: Active Borehole Logging, Transactions of Amer. Nucl. Soc. 24th Annual Meeting.
- Kruse, H. H., 1978, Spectra processing with computer graphics; in Analytical and Mathematical Methods for Data Analysis - I, Trans. Amer. Nucl. Soc. 24th Annual Meeting.
- Lantto, V., 1973, Characteristic curves for interpretation of highly magnetic anomalies in borehole measurements; GeosExploration, Vol. 11, (2), p. 75-85.
- Levanto, A. E., 1959, A three component magnetometer for small drill-holes and its use in ore prospecting; Geophys. Prospecting, Vol. 7, (2), pp. 183-195.
- Lindseth, R. O., 1979, Synthetic sonic logs -- a process for stratigraphic interpretation; Geophysics, Vol. 44, (1), p. 3-26.
- Logn, Ø., and Bølviken, B., 1974, Self potentials at the Joma Pyrite Deposit, Norway; GeosExploration, Vol. 12, p. 11-28.
- Lyttle, R. J., Lain, E. F., Lager, D. L., and Davis, D. T., 1979, Cross-hole electromagnetic probing to locate high contrast anomalies; Geophysics, Vol. 44, (10), p. 1667-1675.
- McCulloh, T. H., 1965, A confirmation by gravity measurements of an underground density profile based on core densities; Geophysics, Vol. 30, (6), p. 1108-1132.
- McMurray, H. V., and Hoagland, A. D., 1956, Three dimensional applied potential studies at Austinville, Virginia; Bull. Geol. Soc. Amer.,

Vol. 67, p. 683-696.

- Merkel, R. H., and Alexander, S. S., 1971, Resistivity analysis for models of a sphere in a half-space with buried current sources; Geophys. Prosp., Vol. 19, (4).
- Mithisrud, G. C. and Summer, J. S., 1967, Underground I.P. surveying at Homestead Mine; Min. Cong. J., vol. 53, (3), p. 66-69.
- Moore, E. J., 1957, Application of borehole geophysics to mining exploration; Seventh Annual Drilling Symposium Exploration Drilling, University of Minnesota.
- Myklebust, R. L., and Firoi, C. E., 1978, A simplex method for fitting gaussian profiles to X-ray spectra obtained with an energy-dispersive detector; in Analytical and Mathematical Methods for Data Analysis-II, Trans. 24th Ann. Meeting, Amer.-Nucl. Soc.
- Myung, J. I., and Baltosser, R. W., 1972, Fracture evaluation by the borehole logging method; Proc. 13th Symp. Rock Mech., Urbana, p. 31-56.
- Myung, J. I., and Helander, D. P., 1972, Correlation of Elastic Moduli dynamically measured by in-situ and laboratory techniques, SPWLA Thirteenth Annual Logging Symp. Trans., May 7-10, Tulsa, Oklahoma, paper H.
- _____, 1973, Borehole investigation of rock quality and deformation using the 3-D velocity log; Birdwell Division Seismograph Service Corp., Tulsa, Oklahoma.
- Nargolwalla, S. S., 1973, Nuclear Technique for Borehole Logging of Geologic Materials; Scintrex Limited, Concord, Ontario, Canada, p. 23.
- Nelson, P. H., and Glenn, W. E., 1975, Influence of bound water on the neutron log in mineralized igneous rock, SPWLA Sixteenth Annual Logging Symp. Trans., June 4-7, New Orleans, Louisiana, Paper M.
- Mullens, H., and Van Espen, P., 1978, Nonlinear least-squares fitting for low-energy photon spectra; in Analytical and Mathematical Methods for Data Analysis - I, Trans. 24th Ann. Meeting Amer. Nucl. Soc.
- Oristaglio, M. L., 1978, Geophysical investigations of earth structure within the vicinity of boreholes; Ph.D. thesis, University of Oxford, England.
- Parr, R. M., Houtennans, H., and Schaerf, K., 1978, The IAEA intercomparison of methods for processing Ge(Li) gamma ray spectra; in Trans. 24th Annual Meeting of Amer. Nucl. Soc.
- Parasnis, D. S., 1974, Some present day problems and possibilities in

- mining geophysics, *Geoexploration* Vol. 12, p. 97-120.
- Pickett, G. R., 1960, The use of acoustic logs in the evaluation of sandstone reservoirs; *Geophysics*, Vol. 25, (1), p. 250-269.
- _____, 1970, Applications for borehole geophysics in geophysical exploration; *Geophysics*, Vol. 35, (1), p. 81-92.
- _____, 1973, Pattern recognition as a means of formation evaluation; *SPWLA Fourteenth Annual Logging Symp. Trans.*, Paper A.
- Pirson, S. J., and Wong, F. S., 1972, The neglected SP curve; in *SPWLA Thirteenth Annual Logging Symp. Trans.*, Paper C.
- Poupon, A., Hoyle, W. R., and Schmidt, A. W., 1970, Log Analysis of sand-shale sequences -- a systematic approach; *J. P.T.*, July 1970.
- Price, W. J., 1964, *Nuclear radiation detection*; McGraw-Hill Book Co., N.Y., p. 430.
- Randall, R., Hopkinson, E., and Youmans, A. H., 1978, A study of the effects of diffusion on pulsed neutron capture logs, *J.P.T.*, December, p. 1788-1794.
- Rasmussen, N.F., 1975, The successful use of the borehole gravity meter in northern Michigan; *The Log Analyst*, Vol. 16, (5), p. 3-10.
- Ritch, H. J., 1975, An open hole logging evaluation in metamorphic rocks; *SPWLA Sixteenth Annual Logging Symp. Trans.*, June 4-7, New Orleans, Louisiana, Paper V.
- Sanyal, S. K., Juprasert, S., and Jusboche, M., 1979, An evaluation of a rhyolite-basalt-volcanic ash sequence from well logs; *SPWLA Twentieth Annual Logging Symp.*
- Savre, W. C., 1963, Determinations of more accurate porosity and mineral composition in complex lithologies with the use of sonic, neutron and density surveys; *J.P.T.*, Sept.
- Schillinger, A. W., 1964, Calumet successfully uses I.P. probe underground to boost ore discoveries, *Min. Engr. Nov.*, pp. 83-88.
- Schlumberger, 1972, *Log Interpretation Volume I -- Principles*, Schlumberger Limited, N. Y., p. 112.
- Schneider, G. J., 1979, Personal communication, U.S.B.M., Denver, Colorado.
- Scintrex, 1978, *Advanced Electromagnetic Borehole Logging System*; Scintrex Limited, Concord, Ontario, Canada.
- Scott, J. H., 1963, Computer analyses of gamma-ray logs; *Geophysics*,

- Vol. 28, (3), p. 457-465.
- Scott, J. H., Dodd, P. H., Drouillard, R. F., and Mudra, P. J., 1961, Quantitative interpretation of gamma ray logs; *Geophysics*, Vol. 26, (2), pp. 182-191.
- Scott, J. H., and Tibbetts, B. L., 1974, Well logging techniques for mineral deposit evaluation : A review, U. S. Dept. Int. Bureau of Mines Information Circular 8627.
- Scott, J. H., Daniels, J. J. and Hasbrouck, W. P., 1975, Hole-to-Hole geophysical measurement research for mineral exploration; SPWLA Sixteenth Ann. Logging Symp. Trans., paper KK.
- Segesman, F., and Lui, O., 1971, "The excavation effect"; SPWLA Twelfth Annual Logging Symp. Trans., Paper N.
- Seigel, H. D., and Margolwalla, S. S., 1975, Nuclear logging system obtains 'bulk samples' from small boreholes, *E/MJ*, p. 101-103, August. 101-103.
- Senftle, F. E., Moore, H. D., Leep, D. B., El-Kady, A., and Duffey, D., 1971, Analytical sensitivities and energies of thermal neutron capture gamma rays II; *Nucl. Inst. and Methods*, Vol. 93, p. 425-459.
- Senftle, F. E., Wiggins, P. F., Duffey, D., and Philbin, P., 1971, Nickel exploration by neutron capture gamma rays; *Econ. Geol.*, Vol. 66, p. 583-590.
- Senftle, F. E., Moxham, R. M., Tanner, A. B., Philbin, P., Boynton, G. R., and Wager, R. E., 1977, Importance of neutron energy distribution in borehole activation analysis in relatively dry, low-porosity rocks; *Geoexploration*, Vol. 15, p. 121-135.
- Sherman, H., and Locke, S., 1975, Depth of Investigation of neutron and density sondes for 35 per cent porosity sand; SPWLA Sixteenth Annual Logging Symp. Trans., Paper Q.
- Silva, J. B. C., and Hohmann, G. W., 1979, Interpretation of three-component drill hole magnific data: 49th Ann. Inter. Meeting of Soc. Explo. Geophys., New Orleans.
- Smith, N. J., 1950, The case for gravity data from boreholes; *Geophysics*, Vol. 15, (4), p. 605-635.
- Smith, R. C. and Steffensen, R. J., 1970, Computer study of factors affecting temperature profiles in water injection wells; *JPT*, Nov., p. 1447-1458.
- Snyder, D. D., 1973, Characterization of porphyry copper deposits using well logs; *Geophysics*, Vol. 38, (6), p. 1221-1222, (Abstract).

- Snyder, D. D., 1973, Analytic models for the interpretation of electrical surveys using buried current electrodes, *Geophysics*, Vol. 35, (3), p. 513-529.
- Snyder, D. D., 1976, The borehole bouguer gravity anomaly -- application to interpreting borehole gravity surveys; SPWLA Seventeenth Annual Logging Symp. Trans., Paper AA.
- Snyder, D. D., Merkel, R. H., and Williams, J. T., 1977, Complex formation resistivity -- The forgotten half of the resistivity log, SPWLA Eighteenth Ann. Logging Symp. Trans., June 5-8, Paper Z.
- Stadukkin, V. D., 1963, The determination of the magnetic susceptibility of rocks and ores by measurement of the magnetic field intensity in artificially magnetized bore-holes for the purpose of location and evaluation of iron-ore deposits; *Bull. Izvestiya.*, No. 9, p. 1381-1385, p. 845-847 (Eng.)
- Stronwald, D. G., and Kosanke, K. L., 1979, Spectral gamma-ray logging I: Energy Stabilization methods; SPWLA Twentieth Ann. Logging Symp. Trans., Paper DD.
- Summers, G. C., and Broding, R. A., 1952, Continuous velocity logging, *Geophysics*, Vol. 17, (3), p. 598-614.
- Telford, W. M., Geldart, L. P., Sheriff, R. E., and Keys, D. A., 1976, *Applied Geophysics*, Cambridge University Press, N. Y., p. 860.
- Tittle, C. W., 1961, Theory of neutron logging I, *Geophysics*, Vol. 26, (1), p. 27-39.
- Tittman, J., Sherman, H., Nagel, W. A., and Alger, R. P., 1966, The sidewall epithermal neutron porosity log, *J.P.T.* Oct.
- Tittman, J., and Wahl, J. S., 1965, The physical foundations of formation density logging (gamma-gamma); *Geophysics*, Vol. 30, (2), p. 284-294.
- Tixier, M. P., Alger, R. P., and Doh, C. A., 1959, Sonic Logging, *J.P.T.*, May, also in SPWLA Reprint Vol., Acoustic Logging, 1978.
- Veneziani, I. I., Colombo, U., Pirson, S. J., and Broome, M. B., 1972, The redox log; SPWLA Thirteenth Ann. Logging Symp. Trans., Paper D.
- Wagg, D. M., and Seigel, H. O., 1963, Induced polarization in drill holes, *Can. Min. Jour.*, Vol. 84, p. 54-59.
- Wahl, J. S., Tittman, J., Johnstone, C. W., and Alger, R. P., 1964, The dual spacing formation density log; *J.P.T.* Dec.
- Ward, S. H., and Harvey, H. A., 1954, Electromagnetic surveying of diamond drill holes, *Can. Min. Manual*, Pub. by National Business Pub.,

Gardenvale, Quebec.

- Ward, S. H., Cambell, R., Corbett, J. D., Hohmann, G. w., Moss, C. K., and Wright, P. H., 1975, Workshop in Mining Geophysics, Univ. Utah publication for NSA, AER76-80802.
- Wilson, R. D., and Cosby, M., 1980, Field evaluation of active and passive direct uranium borehole logging methods; report in prep. Surbsurface Systems Dept., Bendix Field Engr. Corp. Grand Junction, Colorado.
- Wilson, R. D., Stromswold, D. C., Evans, M. L., Jain, M., and Close, D. A., 1979, Spectral Gamma-ray logging II and Spectral Gama-ray Logging III, papers EE and FF, SPWLA Twentieth Ann. Logging Symp. Trans.
- Woods, D. V., 1975, Model study of the CRONE borehole pulse electromagnetic (PEM) system; M. A. Thesis, Dept. of Geology, Queen's Univ., Ontario, Canada.
- Wyllie, M. R. J., Gregory, A. R., and Gardner, D. W., 1956, Elastic wave velocities in heterogeeous and porous media; Geophysics, Vol. 21, (1), p. 41-70.
- Wyllie, M. R. J., Gregory, A. R. and Gardner, G. H. F., 1958, An experimental investigation of factors affecting eleastic wave velocities in porous media, Geophysics, Vol. 23, (3), p. 459-493.
- Youmans, A. H., Hopkinson, E. C., Bergan, R. A., and Ochry, H. L., 1964, Neutron Lfitmie, A new nuclear log; J. P. T., March.
- Zablocki, G. J., 1966, Electric-properties of some iron formations and adjacent rocks in the Lake Superior region; Ming. Geophys., Soc. Expl. Geophys., (Vol. 1), p. 465-492.
- _____, 1974, Magnetic assays from magnetic susceptibility measurements taconite production blast holes, northern Minnesota, Geophysics, Vol. 39, (2), p. 174-189.
- Zablocki, G. J. and Keller, G. V., 1957, Borehole geophysical logging methods in the Lake Superior District; Seventh Ann. Drilling Symp. Explo. Drilling, University of Minnesota, October, p. 15-24.
- Zamensk, Jr., Glenn, E. E., Norton, L. J., and Caldewell, R. L., 1970, Formation evaluation by inspection with the borehole televiewer, Geophysics, Vol. 35, (2), p. 254-268.
- Zikovsky, L. and Schweikert, E. A., 1978, Use of computer-simulated gamma-ray spectra in activation analysis; in Analytical and Mathematical Methods for Data Analysis - I, Trans. Twenty-fourth Ann. Meeting, Amer. Nucl. Soc.

SECTION SIX - SEISMIC METHODS

Introduction

Seismic methods are just now finding routine application to metallic minerals exploration although they have been well developed for petroleum exploration and for determining details of the earth's interior. The two main reasons for the relative lack of use in mineral exploration seem to be the high relative cost of most seismic surveys and the difficulty, using present equipment and techniques, of getting good results in the structurally complex areas in which many mineral deposits are found. Nevertheless, there is agreement that seismic methods could contribute a great deal if some problems could be solved. This section will briefly review the principles of the method, data collection and reduction, problems in applying the method to mining, and applications. A good general reference is Dobrin (1976).

Principles

Seismic methods are concerned with the propagation of elastic waves in the earth. There are two types of body waves: compressional waves and shear waves. These two wave types are often called longitudinal and transverse or "P-waves" and "S-waves", respectively. Compressional waves are ordinary sound waves in rock with particle motion back and forth along the direction of wave propagation; shear waves consist of particle motion perpendicular to the direction of wave propagation. Because fluids do not support shear stresses, shear waves are propagated only in solids. Compressional waves propagate in both solids and fluids.

Seismic waves travel through rock at speeds that depend upon the elastic properties of the rock. This dependence is given in the following equations:

$$V_p = \sqrt{\frac{\lambda + 2\mu}{\rho}} \quad (6-1)$$

$$V_s = \sqrt{\frac{\mu}{\rho}} \quad , \text{ where} \quad (6-2)$$

V_p = P-wave velocity, V_s = S-wave velocity,

λ = a Lamé coefficient = $\frac{E}{(1 + \sigma)(1 - 2\sigma)}$,

μ = modulus of rigidity = $\frac{E}{2(1 + \sigma)}$,

ρ = density,

E = Young's modulus, and

σ = Poisson's ratio.

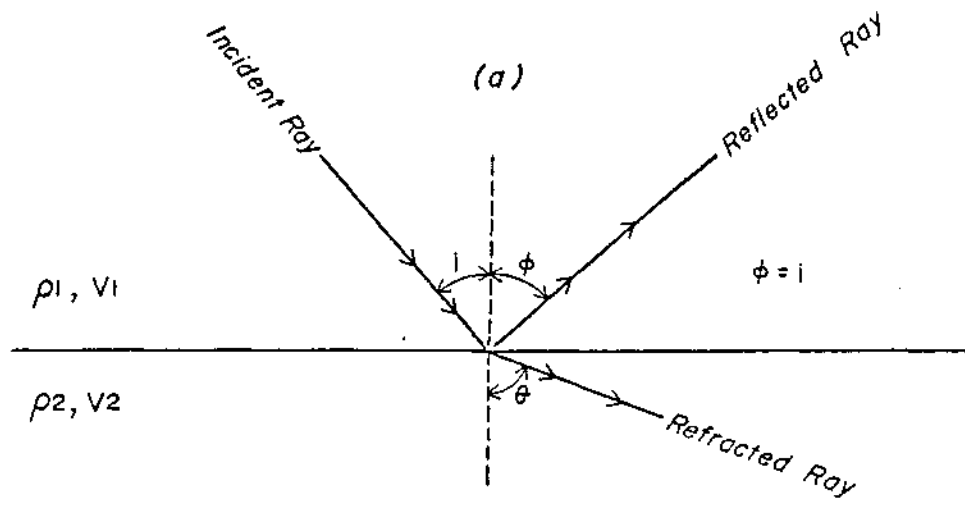
Typical values for these elastic parameters for well-indurated or crystalline rocks are $E=10^{12}$ dyne/cm², $\sigma =0.25$, and $\rho =2.67$ gm/cm³, so we can determine that $\lambda =4 \times 10^{11}$ dyne/cm², $\mu=4 \times 10^{11}$ dyne/cm², and typical seismic velocities in rock are $V_p =6.7$ x km/sec (22,000 ft/sec) and $V_s = 3.87$ x km/sec (12,700 ft/sec). Because σ can never exceed 1/2, λ is always positive. Thus, V_p is always greater than V_s . Table 6-1 lists general ranges for seismic velocities as a function of rock type.

TABLE 6-1
SEISMIC VELOCITIES OF ROCKS

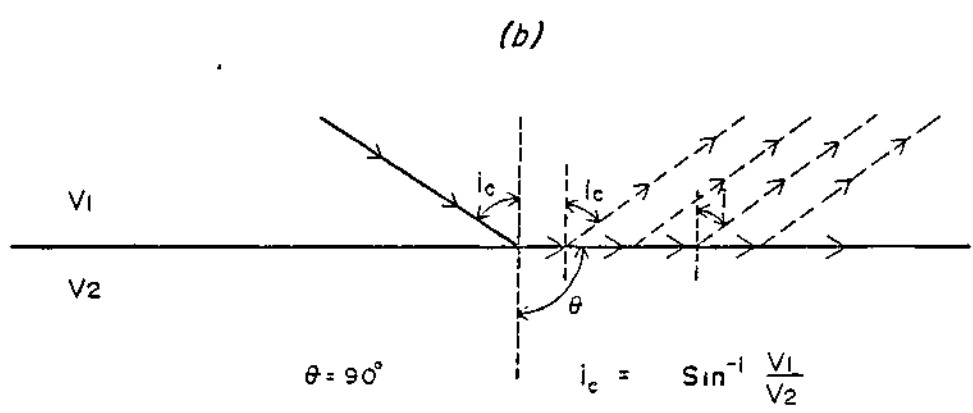
<u>MATERIAL</u>	SEISMIC VELOCITY, KM/SEC	
	<u>P</u>	<u>S</u>
Air	0.33	---
Water	1.46	---
Alluvium, Clay, Moraine	0.75-2.5	0.45-1.5
Sandstone and Shale	1.2 -3.7	0.75-2.0
Limestone and Dolomite	3.5 -6.5	1.5 -4.0
Metamorphic Rocks	3.5 -7.0	2.0 -4.0
Granite and other crystalline rocks	5.0 -7.0	2.5 -4.0
Basalt	3.5 -6.5	1.8 -3.9

In addition to P- and S-body waves, there are waves that propagate along the earth's surface. Raleigh waves and Love waves are two such surface waves. They travel at speeds slightly lower than S-waves. These surface waves are not used in prospecting, and indeed they cause ground roll that can obscure signals from depth.

Seismic waves in rocks are reflected and refracted, in the same way as light waves, when they intersect a boundary of physical property contrast. Figure 6-1 shows a seismic ray approaching a boundary between rocks of different acoustic impedance, $\rho_1 V_1$, at an angle of incidence, i . Part of the ray is reflected at the boundary and part is refracted, and the proportion of reflected to refracted energy depends on the acoustic impedances on each side of the boundary and the angle of incidence. In addition, a portion of the



Reflection Coefficient = $\frac{v_2 \rho_2 - v_1 \rho_1}{v_2 \rho_2 + v_1 \rho_1}$ $\sin \theta = \frac{v_2}{v_1} \sin i$

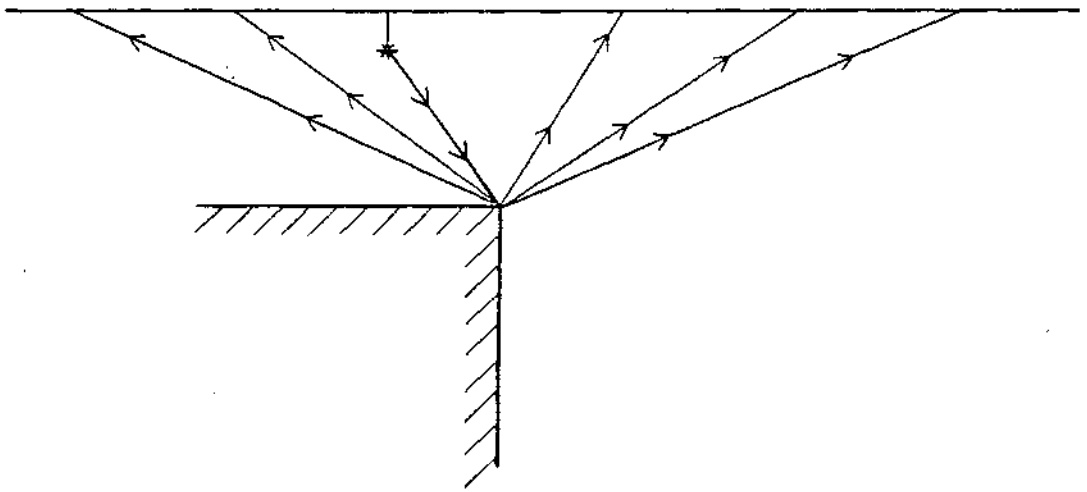


incident P-wave energy is converted to reflected and refracted S-wave energy, and incident S-wave energy is partly converted to reflected and refracted P-wave energy. The reflected portion travels upward at an angle of reflection, ϕ , that equals the angle of incidence, and the reflected wave can be detected when it reaches the surface, thereby forming the basis for detection of the interface by the seismic reflection method.

The refracted portion travels onward in the lower medium in accordance with Snell's law which states that the sines of the angles of refraction, θ , and incidence, i , are related to the velocity contrast as shown in Figure 6-1. Notice that $\theta > i$, if $V_2 > V_1$.

For each velocity contrast where $V_2 > V_1$ there is one angle of incidence at which the refracted wave travels along the boundary between V_1 and V_2 , i.e., $\theta = 90^\circ$ if $i_c = \sin^{-1} \frac{V_1}{V_2}$. In this case, the seismic wave travels at velocity V_2 , and the boundary becomes a continuous source of energy, some of which propagates back upward at angle i_c (Fig 6-1b). This refracted wave can return and be detected at the surface, again forming the basis for detecting the interface by the seismic refraction method. If $i > i_c$ for $V_2 > V_1$, there is total reflection, and no energy enters the lower medium. Both P- and S-waves are reflected and refracted, but P-waves are used in prospecting because they arrive back at surface detectors first due to their higher velocity. Arriving P-waves cause the seismic trace to move, and this often obscures S-wave arrivals.

Another wave often detected at the surface is a result of diffraction. Figure 6-2 shows an edge that has become a source of seismic radiation as a



result of seismic energy incident upon it. The diffracted arrivals at the surface often have characteristic hyperbolic patterns on the seismic record that allow them to be recognized and used to locate the edge.

For mineral exploration purposes seismic waves are generally man-made. Dynamite or primers exploded in blast holes 1 to 30 m deep are often employed. One-tenth to five pounds of 40 to 75 percent nitroglycerin are common shot sizes. Dynamite produces a signal consisting of a spectrum of frequencies. Small charges often are richer in high frequencies than one large charge. An alternative is to employ the Vibroseis¹ technique where one or more heavy, tractor- or truck-mounted vibrators are used to introduce a seismic signal into the ground. Vibroseis sources produce a signal that is swept through the frequency range of interest over a typical interval of 2 seconds and thus give more control on frequency. Another alternative is the type of energy source used with the Mini-Soise system.² Mini-Soise uses an ordinary earth tamper to introduce a long duration pseudorandom wave train into the ground. The signals detected by geophones are crosscorrelated with a reference signal produced by a sensor attached to the tamper. Signal stacking allows good, high resolution records to be produced even with the relatively weak tamper source.

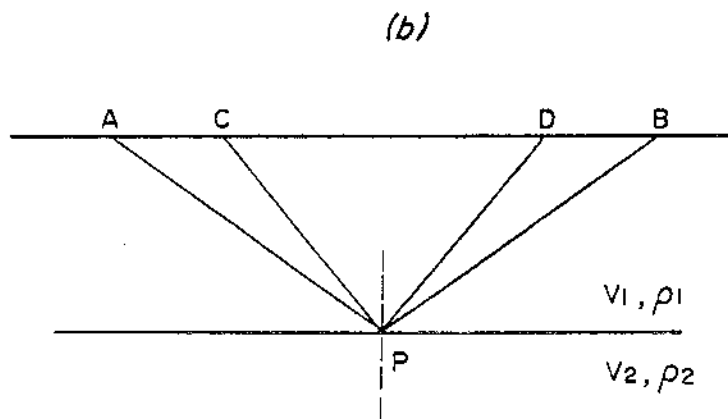
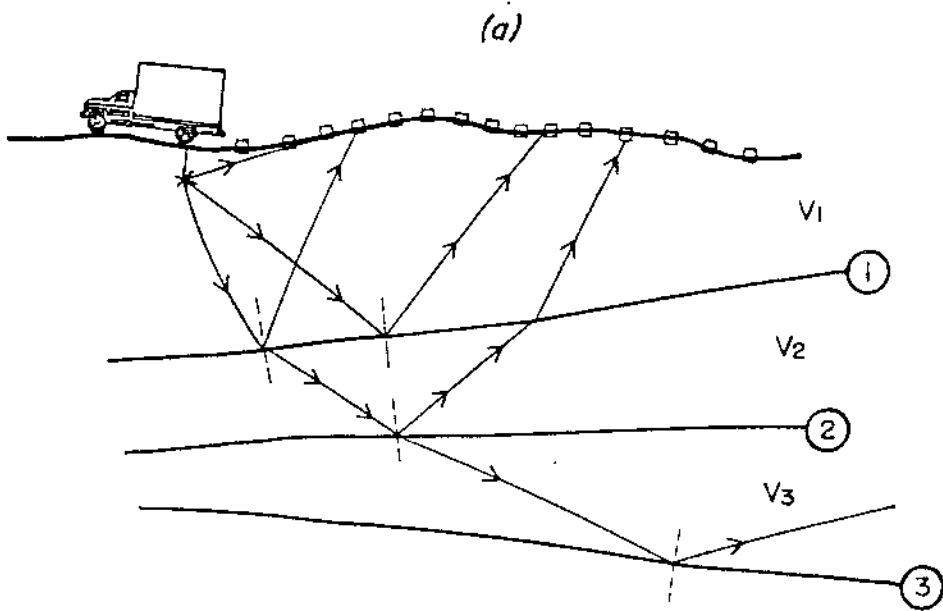
¹A trademark of Continental Oil Company.

²A trademark of Societe Nationale Elf-Aquitaine (Production).

When the signal arrives at the surface, it is detected by a series of seismometers or geophones that are positioned along a line. They are placed firmly in the soil so that vertical vibrations of the earth having displacements as small as 10^{-4} cm can be detected as a varying voltage created in a suspended coil system. The geophones send the electrical signals by multiconductor cable to a recording truck located along the line. Typical installations have 24 to 48 channels of information and record seismic signals along with precise shot time and other information on digital or FM magnetic tape.

The Seismic Reflection Method

Figure 6-3(a) shows a typical seismic reflection survey in an area where acoustic impedance contrasts are subhorizontal. The figure illustrates a few of the many reflected seismic ray paths. The reflection from interface 1 will be the first reflection detected. At later times, on each geophone, reflections from interfaces 2 and 3 will be detected. The reflection from interface 1 will arrive on a moving trace because the direct wave from shot to detector or a refracted wave, will usually constitute the first arrival at a geophone site. At some time late in the record, about 0.5-2 seconds, slow-traveling surface waves will be recorded at each geophone site. The total effect is that reflections early in the record, from reflectors shallower than about 500 to 1,000 feet (153 to 305m), will be difficult to detect because of geophone motion due to the first arrivals, and deep reflections late in the record will likewise be obscured as surface waves cause motion of the geophones. Between cessation of first arrival motion and onset of the surface wave motion there is a window in time that is optimum for recording reflections. One of the



challenges is to widen this time window through correct geophone deployment, filtering signals, using an array of sources, and/or controlling the frequencies so that both shallow and deep reflections can be more easily seen. Reliable detection of shallow reflectors is especially important in mining applications.

Once the seismic reflection data are recorded in the field, computer processing is required before interpretation of the seismic record sections can begin. A typical sequence of data processing might be (Shuey, et al., 1977): 1) demultiplex the field-recorded magnetic tapes, 2) edit sections of extraneous noise, 3) design stacking procedures and gather the data by common depth point, 4) initial static correction, 5) velocity analysis, 6) secondary static correction, 7) final velocity analysis, 8) normal movement correction and stacking, 9) deconvolution, and 10) band pass filtering and display. A brief description of some of this processing follows.

Common-depth-point (CDP) stacking refers to a method of increasing the ratio signal to noise (Figure 6-3(b)). Information from the interface at point P can be obtained by shooting at A and receiving with a geophone at B or by shooting at C and receiving at D. It is obvious that there are many other shot/geophone pairs that record energy reflected from P on the interface. In common survey practice, shot points and geophone stations are moved along the line in such a way that there is enough redundancy of data to obtain a number of reflections from specific parts of the interface. In the processing, each shot/geophone pair that has recorded information from a specific point on the interface is identified and the results are composited or stacked to increase

total signal. This survey and processing procedure is called *multifold surveying*, and geophysicists speak of a *6-fold CDP survey* or a *12-fold CDP survey* for example.

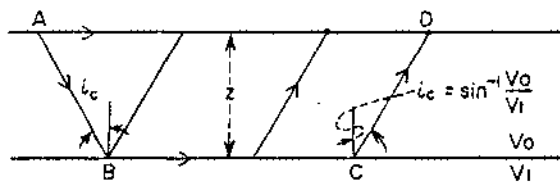
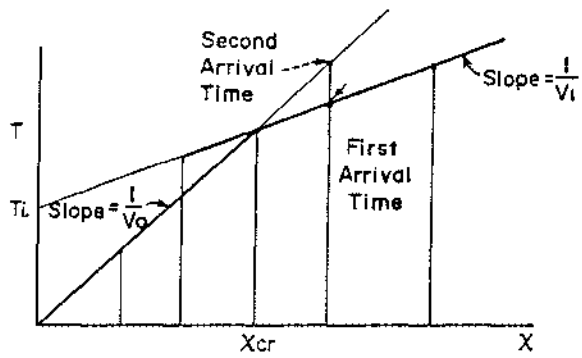
Static corrections refer to corrections that account for varying surface topography and for the effects of the low velocity weathering layer that always exists near the surface. The weathering layer consists of the weathered or unconsolidated near-surface material. It is usually variable in thickness and velocity. Determination of the thickness and velocity of the weathering layer along the survey line is important for reliable static corrections. Normal-moveout (NMO) corrections are made to account for the increasing slant path length for reflections from geophones at increasing distance from the shot. Obviously to make the static and normal movement corrections, the velocity section must be known. Velocities can be determined from the records themselves through sophisticated processing techniques or by observations in available drill holes. Drill hole observations can consist of acoustic velocity logging (see logging section) or by lowering a geophone progressively down a hole and measuring propagation time from a small shot on the surface near the hole. If drill holes are available, they should generally be used for velocity determination because this furnishes a source of data independent of the survey itself.

Complex and sophisticated computer programs have been devised by the petroleum exploration industry to apply the above corrections to seismic data. Proper application of these corrections is a skill and an art.

Once the corrections are applied and the seismic section is displayed, other processing techniques generally follow. In areas of complex geology where the dips of reflectors are not gentle, data migration must be done. Migration is the technique of locating the lateral positions of the reflecting points at depth. If dips are steeper than about 20° , migration may be required earlier in the processing. Consideration must also be given to whether or not a true depth section can be constructed from the record section which uses time for a vertical axis. If enough velocity information is at hand from deep drill holes, or if it can be derived from the survey data then the velocity section can be used to convert the time section to a depth section. Depths are important for certain applications, while velocity sections, which usually illustrate the structure well enough, are often sufficient.

The Seismic Refraction Method

In this method, use is made of the wave refracted along the boundary between media of different velocities. This wave travels at the speed of the lower medium. For geophones near the shot the first arrivals of seismic energy will be the direct wave from the shot as shown on Figure 6-4. But for geophones at a distance, the wave that travels down to the interface at velocity V_0 , along the interface at velocity V_1 , and then back to the surface at velocity V_0 will arrive first. By plotting the times after shot detonation of the first arrivals versus distance, a break in slope of the curve will be seen. The near segment will have a slope of $1/V_0$, whereas beyond a crossover



distance (X_{cr}) the slope will be $1/V_1$. The depth, Z , to the interface can be found from

$$Z = \frac{t_i}{2} \sqrt{\frac{V_1 V_0}{V_1^2 - V_0^2}} \quad (6-3)$$

or

$$Z = \frac{X_{cr}}{2} \sqrt{\frac{V_1 - V_0}{V_1 + V_0}} \quad (6-4)$$

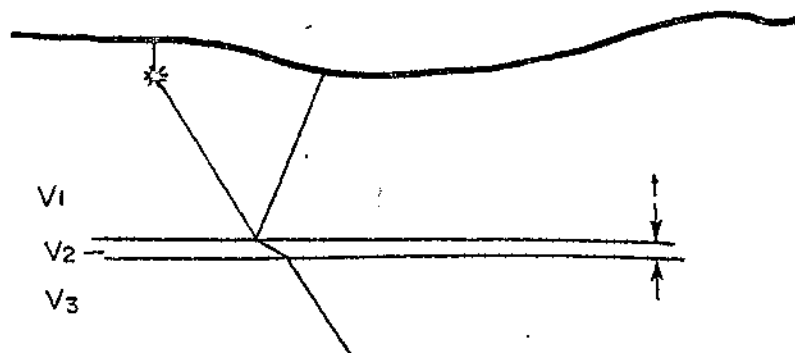
where t_i is the intercept time and 6-4) X_{cr} is the crossover distance (Figure 6-4).

The above explanation of the method can be extended to multilayer cases, to cases of dipping interfaces, and to mapping of faults. Dobrin's (1976) discussion of the method is recommended for more detail.

Problems in Mineral Application

In its present stage of development, most applications of the seismic method in the mining industry could be classed as shallow and relatively unsophisticated compared to uses of the method of the petroleum industry. The seismic method has a number of problems in its application to minerals exploration or mining. We will discuss some of these before giving two examples of application.

The wavelength of a seismic wave (λ), its frequency (f), and its velocity (V) are related as follows: $V = f\lambda$. From this relation we see that, for a particular velocity, longer wavelength waves have lower frequencies, and shorter wavelength waves have higher frequencies. Now whether a structure of the type shown in Figure 6-5 will produce a reflection or not is dependent



upon the thickness, t , of the structure relative to the wavelength of the seismic wave and upon the acoustic impedance contrast. If the thickness is less than about one-tenth of a wavelength, the seismic wave will be so little affected by V_2 that no detectable reflection will be produced. If $t \gg \lambda/6$, it may be possible to resolve the upper and lower boundaries. For a typical, well-indurated sedimentary rock or a crystalline rock of velocity 6.0 km/sec, we see that 10 Hz seismic waves have a wavelength of 600 m whereas 100 Hz seismic waves have a wavelength of 60 m. We conclude that planar features such as faults or discrete beds are not likely to be detected or resolved by seismic waves of frequency less than 100 Hz unless they are greater than about 6 m thick. In addition to detection, precise location of these features requires seismic waves that have short wavelength or high frequency. Thus, although most petroleum exploration is effectively accomplished using frequencies in the 10 Hz to 50 Hz range, the higher resolution necessary for most mining problems requires frequencies in the 50 Hz to 500 Hz range. Instrumentation for such high-resolution surveys is not universally available from seismic contractors.

The need for high frequencies creates other problems not generally encountered in petroleum work. The rate of attenuation of seismic signals as they travel through rock is a function of frequency as follows:

$$I = \frac{I_0 e^{-\beta r}}{r} \quad (6-5)$$

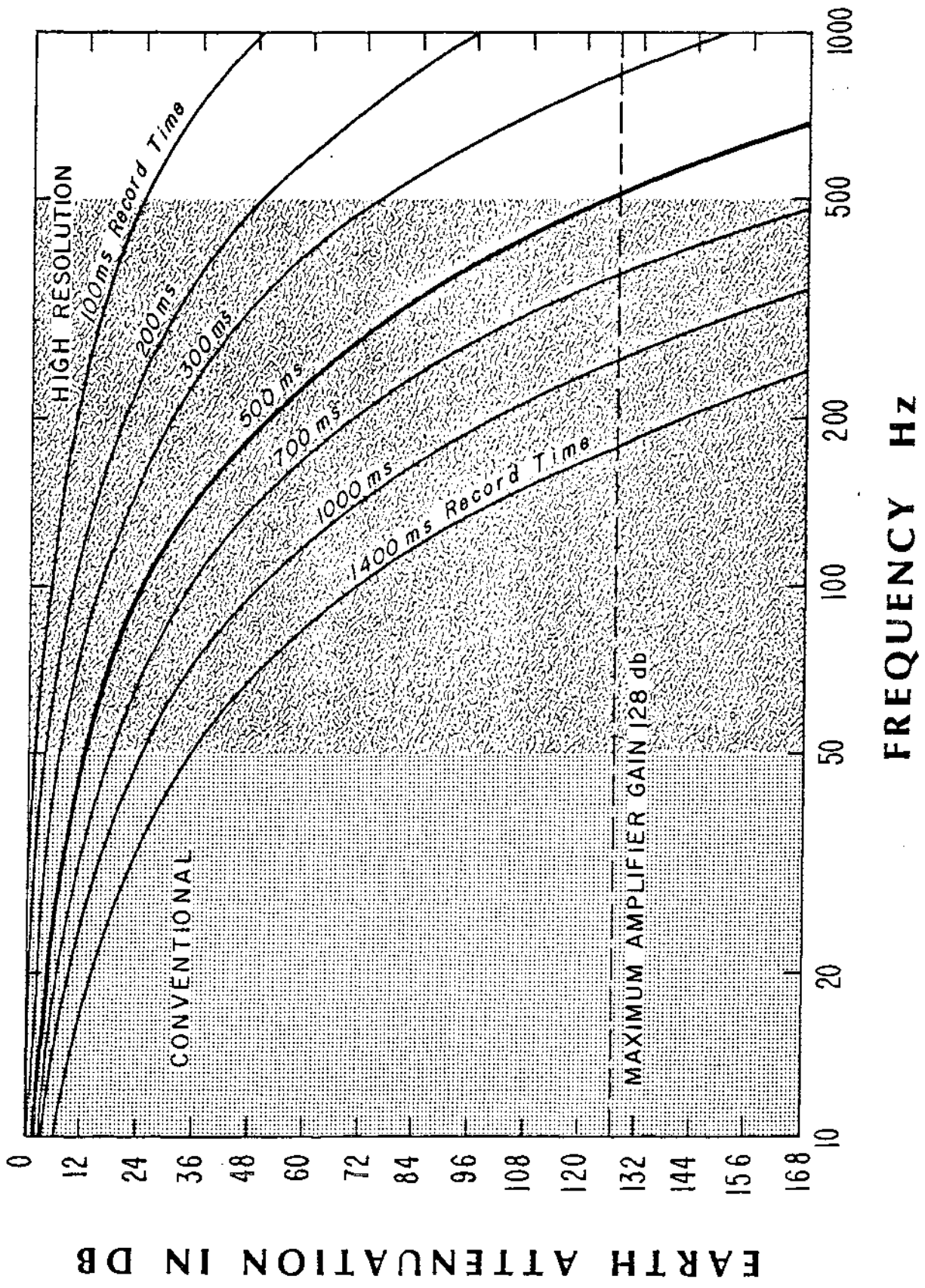
in which I = amplitude at distance r from source

I_0 = initial amplitude, and

β = absorption coefficient.

The $1/r$ dependence is caused by the spreading of a given initial amount of energy over larger and larger spherical surfaces as the wave moves outward from the source. The exponential decrease in signal amplitude with distance results from frictional dissipation in the medium. The absorption coefficient, β , depends upon the material, the signal frequency and the seismic velocity, such that β is larger for higher frequencies and for material of lower seismic velocity. Therefore, at the higher frequencies needed for high resolution, seismic signal strength attenuates faster than it would at lower frequencies. This attenuation is most severe in the weathered layer near the surface, where high frequency energy is very rapidly attenuated both in the downgoing wave and in the emerging wave. Figure 6-6 illustrates the way attenuation affects length of useable record as a function of frequency for one velocity and absorption coefficient. Note that at the frequencies needed for high resolution, the useable record time rapidly shortens as frequency increases. In some areas, a high-resolution survey may require placing either or both shot and geophones in holes that penetrate the weathering layer. This requirement will, of course, increase costs.

The high resolution commonly needed for mining problems has implications other than simply higher frequency. For one thing the spatial sampling rate, i.e., the geophone spacing, must be decreased so that horizontal resolution is nominally the same as vertical resolution. Whereas typical petroleum surveys use geophone spacings of 67 or 100 m high resolution surveys require spacings of 5.0 to 33.5 m. High resolution also requires closer timing of events and higher sampling rate for digital recording and processing. Many petroleum surveys are conducted with events timed to the nearest millisecond and a

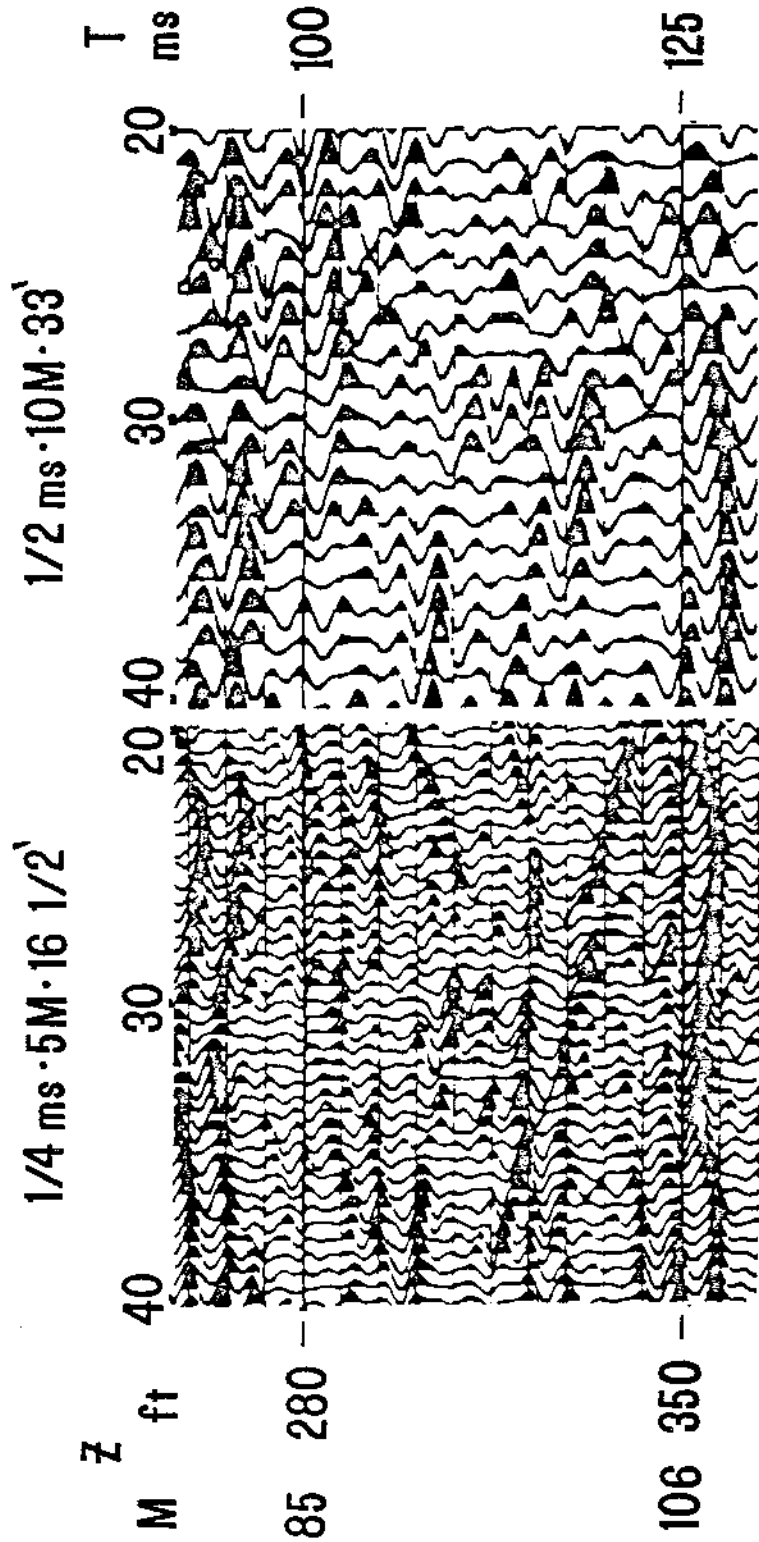


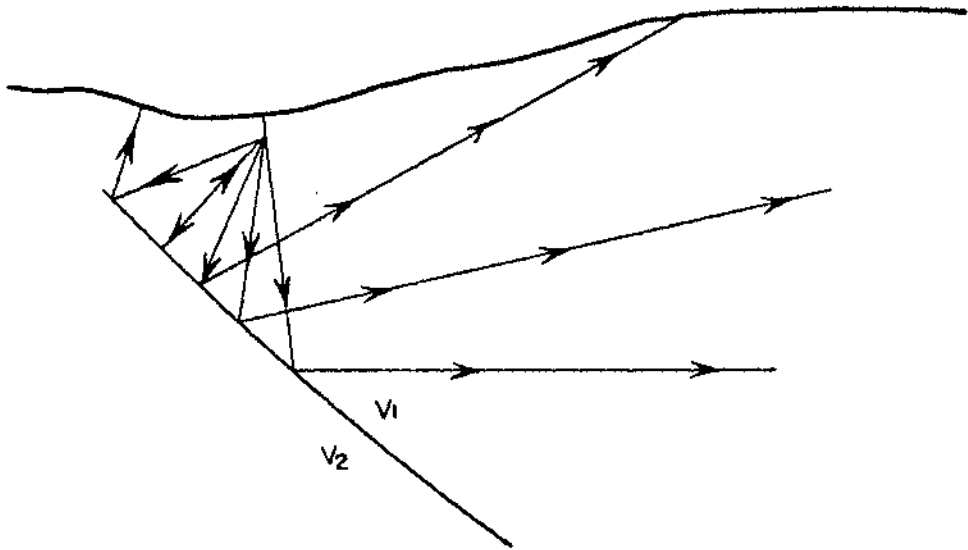
sampling rate of 2 milliseconds. For recording of high frequency signals, timing to 0.1 milliseconds and a sampling rate of 0.25 to 0.5 milliseconds is needed. Figure 6-7 shows the difference in level of detail obtained by using closer geophone spacing and shorter sampling time.

Figure 6-8 illustrates another of the problems in attempting to apply the reflection seismic method in areas of complex geology. Because of the steep dip of the interface only a relatively small portion of the interface is mapped with one shot. Reflections from deep on the interface do not return to the surface at a sufficiently close distance for a practical deployment of geophones to detect them. This problem is compounded somewhat by the fact that mining applications usually use close geophone spacings to increase resolution so that the entire array does not cover much distance.

One technique employed to diminish ground roll noise caused by surface waves in conventional surveying is to deploy a series of geophones in, say, a circular pattern at each receiving site. The radius of the circle is such that some geophones are moving upward while others are moving downward as the horizontally traveling surface waves pass. This produces cancellation of surface wave signal by the geophone array. But such an array discriminates against any horizontally travelling waves, including those from steep reflectors (Figure 6-8). Thus a compromise must be reached in geophone deployment; in certain cases it may be necessary to place the geophones in holes below the influence of surface waves.

Steeply dipping reflectors also can cause problems with the automatic data processing routines used in conventional seismic work. Migration may be





needed prior to stacking. Great care must be taken in data processing.

The main reason for dwelling on the problems of applying seismic surveys in mining is not to discourage use of the technique but simply to state the fact that good seismic equipment and techniques, applicable to mining problems, are just now being developed. Equipment and techniques developed for petroleum work are a good starting point, but great care must be taken in applying them directly to mining problems. Many geophysicists believe that mining industry-supported research and technique development for the seismic method would repay its cost multifold, but at the present time an insufficient amount of time and money are being spent to develop the technique in a reasonable time frame.

Applications

The seismic methods, particularly the reflection method, are effective at target depths beyond those appropriate for the electrical methods now dominant in much of the industry. In addition, smaller targets can often be detected. Consequently the potential cost-effectiveness of seismic techniques relative to other geophysical methods will increase as targets become smaller and deeper. The most cost-effective use of the technique at present may be in deposit delineation or mining exploitation, rather than in exploration.

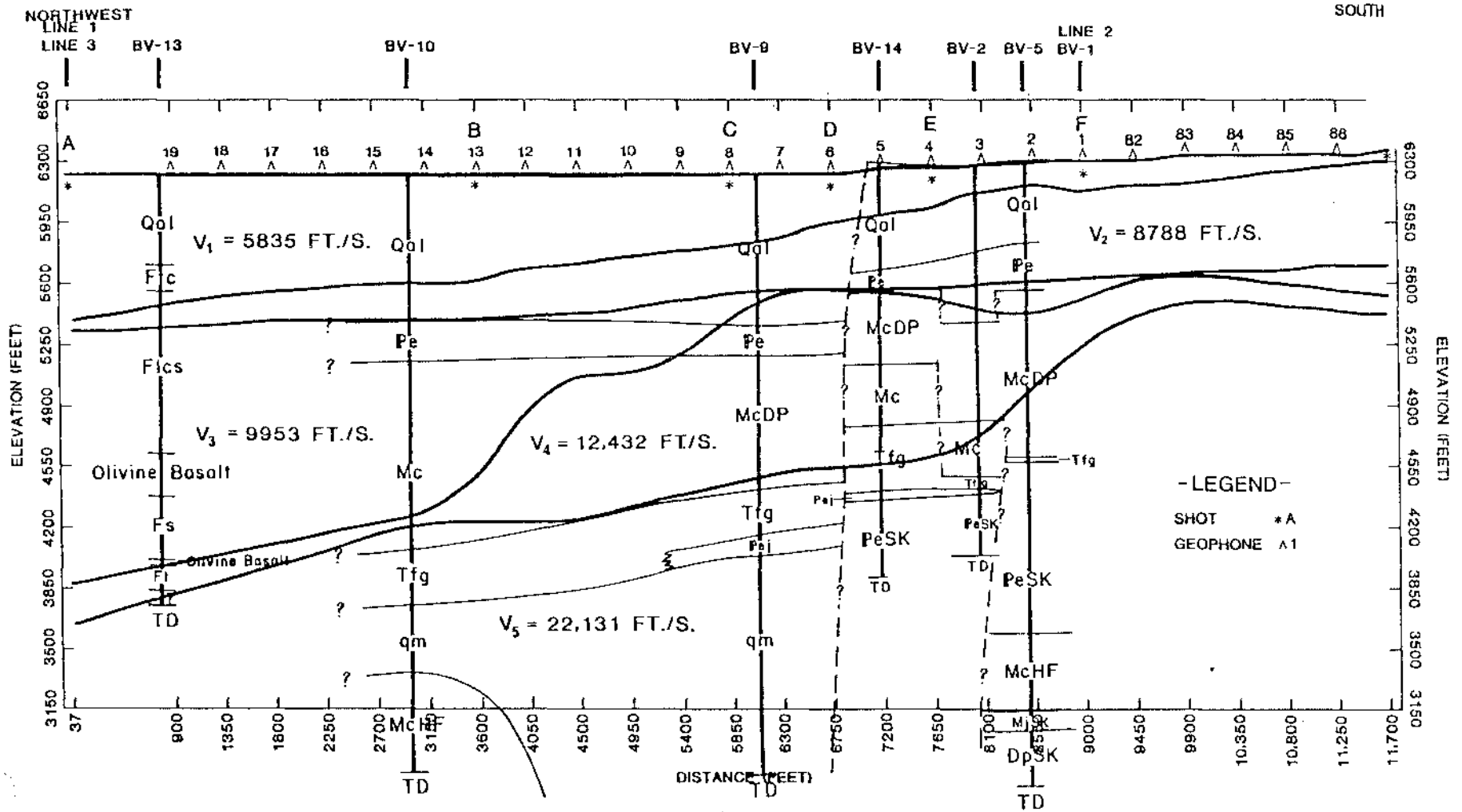
Refraction seismic techniques have been used in the mining industry for several decades. The main applications have been: 1) determination of depth to bedrock in placer mining and for other engineering reasons; 2) determination of thickness of the weathered zone or of overburden thickness for the purpose of correcting gravity data; 3) determination of rock quality in mining

and engineering problems where rock quality can be related to seismic velocity; and 4) study of sedimentary rocks in the search for mineralization or to determine structure where the section is subhorizontal and reasonably simple.

Figure 6-9 gives a good example of the use of the refraction method to study the Butte Valley, Nevada porphyry copper deposit. This deposit lies about 50 miles north of the Robinson District (near Ely) on the west side of the Cherry Creek range. It has been explored by several companies, including Cyprus Mines, Bear Creek Mining Company and, most recently, by Exxon Minerals. Gulf Science and Technology in cooperation with Bear Creek used the area as a test to determine the applicability of refraction and reflection to study of a deep, blind disseminated sulfide system. Some results of Gulf's work were reported by Fix in Shuey, et al. (1977).

At Butte Valley the prospect area is covered by 30 to 300 m of basin fill that overlays an unaltered, unmineralized Paleozoic sedimentary section. The Paleozoic rocks have apparently moved as a unit under the influence of gravity to cover an old, thin fanglomerate which overlies the sulfide system. Drilling therefore goes through the alluvium into fresh Paleozoic sedimentary rocks, through a fault zone into the fanglomerate, and then into mineralized rocks at a depth of about 610 m. Figure 6-9 shows several refracting horizons as detected by the Gulf survey and how the seismic interpretation fits the geology determined by logging several deep drill holes. Data interpretation in this case was from the refraction seismic inversion program developed by the U. S. Bureau of Mines (Scott, et al., 1970).

LINE 4 INVERSION MODEL AND DRILL HOLE LITHOLOGY



Several lines of reflection data were obtained at Butte Valley also. The survey was performed with standard petroleum instrumentation but with geophone spacings of 112.5 feet and six-fold coverage. Frequency content was between 16 Hz and about 75 Hz for most of the survey. Figure 6-10 shows the data for an east-west line over the prospect along with an interpretation. The seismic data reveal great structural complexity over the deposit, in the center section of the line. Numerous faults can be interpreted by noting restricted lateral extent of reflecting horizons. To the west, good reflections from the undisturbed, unaltered sedimentary section can be seen. It is evident that these seismic data are rich in detail that would be useful both in exploration and mining planning.

INTERSECTING LINES

DRILL HOLES

SHOT POINTS

LINE 3

LINE 4

6-36

5-30

6-25

6-20

BV-11

6-16

BV-9

5-10

BV-15

6-5

ELEVATION (FT)
8400
8300
8200

FOLD

0

0.1

0.2

0.3

0.4

0.6

0.8

0.7

0.6

0.8

1.0

0

0.1

0.2

0.3

0.4

0.6

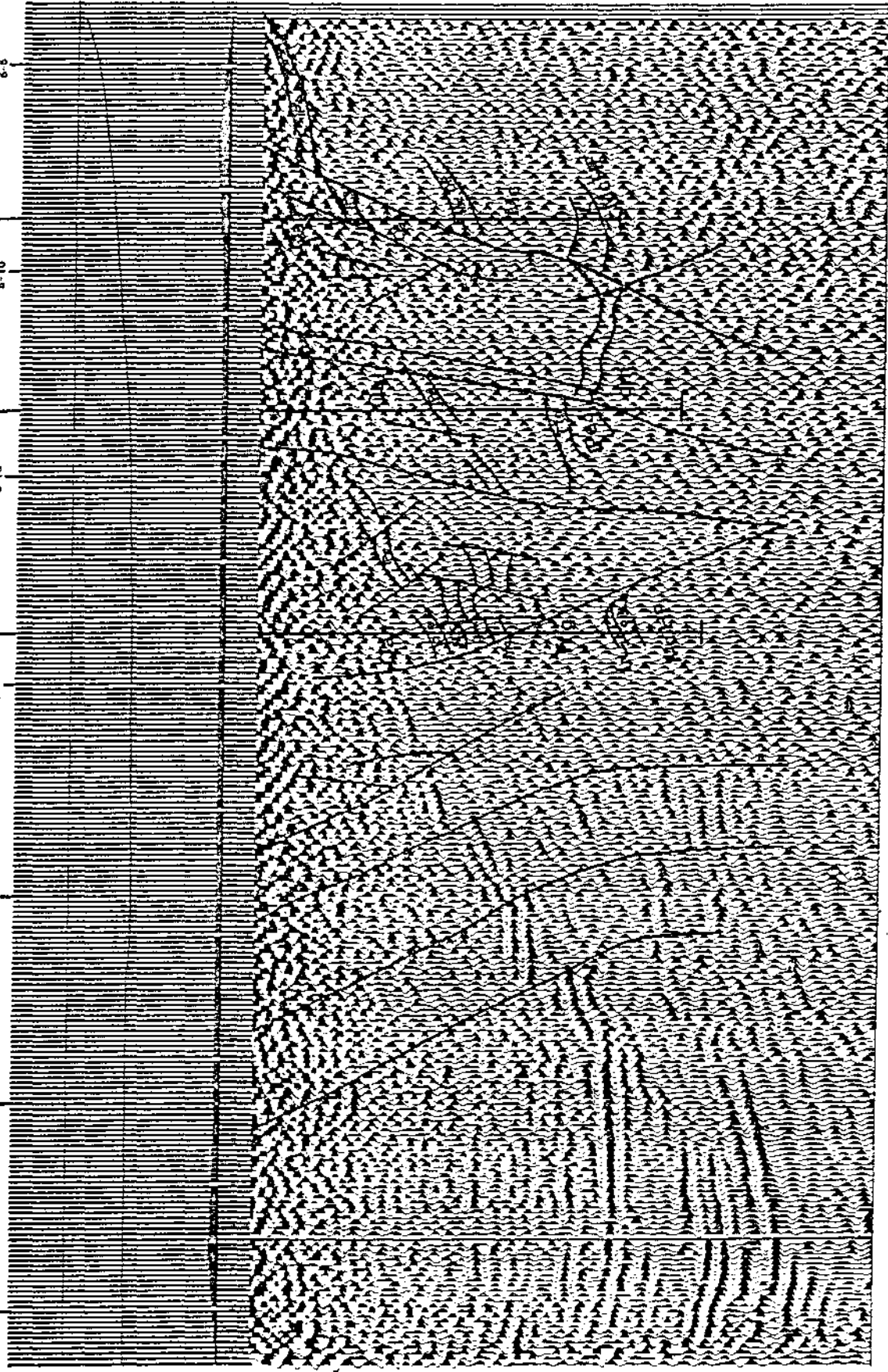
0.8

0.7

0.8

0.8

1.0



REFERENCES

- Dobrin, M. B., 1976, Introduction to geophysical prospecting; McGraw-Hill, Inc., 630 p.
- Scott, J. H., Tibbetts, B. L., and Burdick, R. G., 1970, Computer analyses of seismic refraction data: Rept. of Investig. 7595, Bur. Mines, U. S. Department of Interior, 95 p.
- Shuey, R. T., Farry, J., Fix, J., Omnes, G., and Rahsey, F., 1977, Seismic methods; in Workshop on Mining Geophysics, S. H. Ward, ed., University of Utah, Dept. of Geol. and Geoph.

SEISMIC METHODS - FIGURE CAPTIONS

- 6-1(a) Reflection and refraction of seismic rays.
- 6-1(b) Refraction along an interface.
- 6-2 Diffraction of seismic waves from an edge.
- 6-3(a) Illustration of typical seismic reflection survey.
- 6-3(b) Common depth point shooting.
- 6-4 Time-distance plot and ray path in a seismic refraction survey (after Dobrin, 1976).
- 6-5 Detection of a thin structure. Seismic waves of wavelength, , shorter than about $10t$ are needed for detection of a thin bed or fault.
- 6-6 Attenuation of seismic energy (after Shuey, et al., 1977).
- 6-7 Illustration of increase in detail obtained when data sampling time and geophone spacing are halved (after Shuey, et al., 1977).
- 6-8 Reflections from a steeply dipping interface.
- 6-9 Results of seismic refraction survey, Butte Valley, Nevada compared to drill hole lithology (after Shuey, et al., 1977).
- 6-10 Results of seismic reflection survey at Butte Valley, Nevada (after Shuey, et al., 1977).